

**Distributions of dissolved Iron and Zinc in the
Indian Ocean: Implications to their sources, sinks
and internal cycling**

A THESIS

**Submitted for the Award of Ph.D. degree of
MOHANLAL SUKHADIA UNIVERSITY**

**In the
Faculty of Science**

**by
Venkatesh Chinni**



**Under the Supervision of
Dr. Sunil Kumar Singh**

**PROFESSOR
GEOSCIENCES DIVISION**

**PHYSICAL RESEARCH LABORATORY
AHMEDABAD, INDIA**

**DEPARTMENT OF GEOLOGY
MOHANLAL SUKHADIA UNIVERSITY,
UDAIPUR (RAJASTHAN), INDIA**

Year of submission – 2018

DECLARATION

I, Mr. Venkatesh Chinni, S/o Mr. Srinivasa Rao Chinni, resident of E-204, PRL residences, Navrangpura, Ahmedabad – 380009, hereby declare that the research work incorporated in the present thesis entitled “**Distributions of Dissolved Iron and Zinc in the Indian Ocean: Implications to their sources, sinks and internal cycling**” is my own work and is original. This work (in part or in full) has not been submitted to any University for the award of a Degree or a Diploma.

I have properly acknowledged the material collected from secondary sources wherever required.

I solely own the responsibility for the originality of the entire content.

Place: Ahmedabad

Date:

(Venkatesh Chinni)

C E R T I F I C A T E

I feel great pleasure in certifying that the thesis entitled “**Distributions of dissolved Iron and Zinc in the Indian Ocean: Implications to their sources, sinks and internal cycling**” embodies a record of the results of investigations carried out by **Venkatesh Chinni** under my guidance.

He has completed the following requirements as per Ph.D. regulations of the University

- (a) Course work as per the university rules
- (b) Residential requirements of the university
- (c) Presented his work in the departmental committee
- (d) Published/accepted minimum of one research paper in a referred research journal.

I am satisfied with the analysis of data, interpretation of results and conclusions drawn.

I recommend the submission of thesis.

Date:

Name and designation of supervisor
Sunil Kumar Singh,
Professor

Countersigned by
Head of the Department

*Dedicated
To
My parents*

Smt. Venkata Ramalakshmi (Late) &
Sri. Srinivasarao Chinni

ACKNOWLEDGEMENTS

I am thankful to many people for meeting the stated objectives in my PhD work successfully and completing the thesis. This work would not have been completed without the support and encouragement of several individuals directly or indirectly.

Primarily, I would like to thank my supervisor, Prof. Sunil Kumar Singh, for introducing me to the field of “Trace metal biogeochemistry in seawater”. His supervision, advice, guidance and presenting skills from the early stage of this research and imparting me extraordinary experiences throughout the work were helpful for development as a researcher. A little discussion with him on any aspect related to experimental work, scientific discussion is always a fruitful. He always keeps me motivating and rejuvenates on the research topic chosen. I admire him for his guidance, support and encouragement right from my joining in the PRL.

I also express my sincerest gratitude towards Prof. (Late) S. Krishnaswami for his inspiration. It gives me great pleasure in acknowledging the support and guidance of Prof. M. M. Sarin during my thesis work. His systematic approach towards scientific problems and meticulous ways of handling the scientific instruments with perfection have been very encouraging to me. I thank to Drs. Ravi Bhushan, Rengarajan, Neeraj Rastogi and Mr. A. K. Sudheer for the support and motivation throughout my PhD time.

I am enormously grateful to Prof. Anil Bharadwaj, Director, Prof. P. Janardhan, Dean and Dr. Bhushit Vaishnav, Head Academic Services, Physical Research Laboratory for providing me support and facilities throughout the thesis work. I thank the members of Academic Committee for reviewing my work from time to time and providing their constructive inputs. My sincere thanks to Profs. K. P. Subramanian, J. Banerji, D. Banerjee, P. Venkatakrishnan, Drs. R. D. Deshpande, M. G. Yadava, L. K. Sahu, D. Chakraborty, N. M. Ashok, K. K. Marhas, Amit Basu, V. K. Rai, D. Ray, J. Pabari and Bhas Bapat for their informative lectures during the course work.

I would like to thank Department of Space (DOS) for the scholarship and support for the research. Thanks are due to MoES, Government of India for financial and logistic supports provided to GEOTRACES (India) programme. My thesis is part of this programme. I thank NCAOR and NORINCO for resourceful help during the ocean expeditions. I thank the Captains, Crew, Norinco team and all the scientific participants of

SK - 304, SK - 311, SK - 312, SK - 324, SK - 325 and SK - 338 for their help and joint sampling.

I am thankful to the all staff members of Library, Computer centre, workshop, Administration, Dispensary and maintenance section for their assistance during my PhD. Special thanks for the Mr. Waghale and Mr. Pramod bhai (Work shop) for the patience in making the Teflon columns of desired shape and length required for my experimental work. I also express my sincere gratitude to Mr. Manan Shah and Mr. Lakan singh for the automation of the FIAS by providing the LabVIEW software and their timely response if something goes wrong with the software.

I express my gratitude to all my friends at PRL. I would like to thank my batch mates (JRF – 2012), Apurv, Ashim, Bivin, Chandana, Deepak, Dipti, Jinia, Newton, Pankaj, Rahul. I thank my seniors Srinivas Bikkina, Vineet Goswami, Satinderpal Singh, Gyana Ranjan Tripathy and Jayati Chatterjee for their suggestions during my initial time of Ph.D. Thanks are also due to all my Chemistry lab friends Deka, Upasana, Sneha, Damu, Satish, Subbu, Jaldhi, Ramsha, Payal, Mahesh, Utsav, Chinmay, Prabhuti, Rahul, Shivam, Ankur, Akshay, Aswathy, Abhishek, Priyanka, Naman, Rupali, Nitesh, Balaji, Batuk, Harsh Raj, Nisha, Muruga, Anil, Preksha, Atinder, Sanjukta, Dipika, Romi and Pravin bhai for their unconditional support. I thank my Telugu friends Gangi Reddy, Aslam, Aditya Peketi, Kiran, Prasad Neelam, Deepthi, JK, Malai, Sekhar, Srinivas A, Sameer, Ejaz for creating home environment. I thank my hostel mates Manu George, Avdesh, Girish kumar, Guru Prasad Kadam, Saweeta, Ikshu, Anirban, Shraddha, Pradeep, Aman, Niharika, Ila, Vishnu and Nijil for the pleasant stay.

Finally, I would like to thank my wife (Bhargavi Devi), who is always there to share my feelings during good and odd times. Last but not the least; I thank my Father (Srinivasarao Chinni) and Sister (Nalini Devi) for supporting, believing and encouraging me with their best wishes. I strongly believe that the blessings of my mother are always with me and that drove me to complete the thesis work.

LIST OF ABBREVIATIONS

AABW	Antarctica bottom waters
AAIW	Antarctic Intermediate waters
AS	Arabian Sea
ASHSW	Arabian Sea high saline waters
AOU	Apparent Oxygen Utilization
BoB	Bay of Bengal
BoBLSW	Bay of Bengal less saline waters
CH ₄	Methane
CO ₂	Carbondioxide
Co	Cobalt
Cd	Cadmium
CLIVAR	Climate variability and predictability
CIR	Central Indian Ridge
Cu	Copper
DFe	Dissolved Iron
DZn	Dissolved Zinc
DO	Dissolved Oxygen
EICC	East Indian Coastal Current
Eq/ml	Equivalents per milli litre
Fe-FIS	Iron Flow injection system
Fe	Iron
GS	Geotraces surface
GD	Geotraces deep
He	Helium
HNLC	High Nutrient Low Chlorophyll
HDPE	High Density Polyethylene
ITW	Indonesian throughflow waters
IDP	Intermediate data product
IIW	Indonesian Intermediate waters
IW	Indonesian waters
LDPE	Low density Polyethylene
MQ	Milli Q

MNADW	Modified North Atlantic Deep Water
NASS	Seawater reference material for trace metals
Ni	Nickel
NICW	North Indian Central Waters
NIDW	North Indian deep waters
NIO	Northern Indian Ocean
OMZ	Oxygen Minimum Zone
ORV	Oceanic Research Vessel
PRL	Physical Research Laboratory
PTFE	Polytetrafluoroethylene
PGW	Persian Gulf waters
QD	Quartz distilled
RSW	Red sea waters
SAFe	Sampling and analysis for Iron
SK	Sagar Kanya
SRP	Soluble Reactive Phosphate
SSH	Sea Surface Height
SWIR	South Western Indian Ridge
TD	Teflon distilled
TEIs	Trace elements and Isotopes
Zn-FIS	Zinc Flow injection system
Zn	Zinc

ABSTRACT

The work addressed in the thesis deals with the contemporary spatial distributions of biolimiting key trace elements Iron (Fe) and Zinc (Zn) in the Indian Ocean to understand their sources, sinks and internal cycling. The results give us a primary level of understanding with new and startling information on the internal cycling of Fe and Zn in the Indian Ocean. Clean sampling techniques and measurement protocols to analyze DFe and DZn were established in India. The surface DFe concentrations in the Northern Indian Ocean display a clear increasing gradient as moving from oligotrophic waters of Indian Ocean. Atmospheric deposition, seasonal monsoonal winds and corresponding biology seems to be controlling the surface DFe concentrations in the Northern Indian Ocean comprises of the Bay of Bengal and the Arabian Sea. Subsurface maximum in the depth interval of 100 – 1000 m in the Bay of Bengal is due to the remineralization of particulate organic matter and Fe-Mn oxyhydroxide particles from the rivers situated at the north of the bay. A significant amount of laterally advected (Thousands of kilometers) hydrothermally derived DFe input is seen in the deeper waters of the Indian Ocean situated around the Carlsberg ridge and Central Indian Ridge. Further, a unique source for DFe in the deeper waters with a DFe concentration of ~2.7 nM (Higher by a factor of 4 compared to global deep ocean water concentrations for DFe) along the Java trench region is identified. Scavenging of DFe is dominant in the deeper waters (> 1000 m) of the Bay of Bengal where as organic complexation in the deeper waters of the Arabian Sea seems to be minimizing the Fe removal. Zn profiles display a typical nutrient type behavior in the study region. Overall, Zn concentrations range from 0.23 to 14.89 nM in the Indian Ocean. A strong correlation between Zn and Si consistent to the contemporary relation of DZn vs. Si in the global ocean is observed. The relation between DZn and Si, $DZn = (0.058 \pm 0.001) * Si$, $r=0.96$, $n=141$, observed for the subtropical Indian Ocean (Equator to 15° S) is similar to the global Zn vs. Si ratio (0.059) whereas $DZn = (0.047) * Si$, $r=0.94$, $n=589$ for the Northern Indian Ocean (North of Equator) is significantly lower compared to global average ratio. In the oxygen minimum zone waters, DZn/Si ratio is lower compared to surface and deeper waters. Results indicate loss of DZn in the oxygen minimum zone in the Northern Indian Ocean.

TABLE OF CONTENTS

Contents	Page
List of Tables	xix
List of Figures	xxi
Chapter 1	
<i>Introduction</i>	1
1.1 Introduction	3
1.1.1 Iron in seawater	4
1.1.2 Zinc in seawater	5
1.2 Geotraces and the Indian Ocean	7
1.3 Trace elements (Fe and Zn) in the study region	9
1.4 Objectives of the Thesis	10
1.5 Outline of the Thesis	10
Chapter 2	
<i>Materials and Methods</i>	13
2.1 Study Area	15
2.1.1 The Bay of Bengal	16
2.1.2 The Arabian Sea	16
2.1.3 The Andaman Sea	16
2.1.4 The Indian Ocean	17
2.2 Sampling and Filtration	17
2.2.1 Sampling	22
2.2.2 Protocol for cleaning the sampling bottles	23
2.3 Analytical Protocols	26
2.3.1 Determination of dissolved Iron in seawater	27
2.3.1.1 Iron analysis method details	27
2.3.1.2 Column description	31
2.3.1.3 Instrumentation block diagram	33
2.3.1.4 Hardware description	33
2.3.1.5 Software Interface	34
2.3.1.6 Iron calibration	36
2.3.1.7 Inter and Intra comparison of DFe data	38
2.3.1.8 Accuracy and precision of the method	39
2.3.2 Determination of dissolved Zinc in seawater	43
2.3.2.1 Zinc analysis method details	43
2.3.2.2 Software Interface	46
2.3.2.3 Cadmium interference	47
2.3.2.4 Zinc calibration	49
2.3.2.5 Nobias PA-1 resin description	50
2.3.2.6 Intercomparison of DZn data	51

2.3.2.7	Accuracy and precision of the measurement	53
2.3.3	Determination of basic hydrographic parameters	57
2.3.3.1	Dissolved Oxygen	57
2.3.3.2	Major nutrients	57
2.4	Conclusions	60
Chapter 3		
	<i>Distributions of Dissolved Iron in the Indian Ocean</i>	63
3.1	Introduction	65
3.2	Dissolved Iron in marginal and open ocean waters of the Northern, equatorial and eastern subtropical Indian Ocean	66
3.2.1	Results	67
3.2.1.1	Hydrographic and major nutrients	67
3.2.1.2	DFe distributions	77
3.2.2	Discussion	81
3.2.2.1	Fluorescence and DFe	81
3.2.2.2	DFe in the Bay of Bengal	83
3.2.2.3	DFe in the Andaman Sea	86
3.2.2.4	DFe from the equatorial and eastern subtropical Indian Ocean	86
3.2.2.5	DFe along Java trench region	88
3.2.2.6	Fe:C remineralization rates in the Bay of Bengal, the Andaman Sea and the eastern subtropical Indian Ocean	90
3.2.2.7	DFe as a limiting nutrient	93
3.3	Dissolved Iron distributions in the Arabian Sea and the western subtropical Indian Ocean	96
3.3.1	Results and discussion	97
3.3.1.1	T-S distribution during spring inter monsoon	97
3.3.1.2	T-S distribution in the Arabian Sea and the Western Subtropical Indian Ocean	99
3.3.1.3	Water mass structure	100
3.3.1.4	Dissolved Oxygen	102
3.3.1.5	Nutrient distribution during spring inter monsoon	104
3.3.1.6	Nutrient distribution during late southwest monsoon	105
3.3.2	Dissolved Iron concentrations in the Arabian Sea and the Subtropical Indian Ocean waters	109
3.3.2.1	Surface DFe in spring inter monsoon period	109
3.3.2.2	Surface DFe in late southwest monsoon period	110
3.3.2.3	Vertical profiles in the central Arabian Sea and subtropical Indian Ocean	111
3.3.2.4	Vertical profiles in the western Arabian Sea and over Carlsberg Ridge	115

3.3.2.5	Fluorescence and DFe	118
3.3.2.6	AOU vs. Major/Minor nutrients and Fe:C rates	119
3.3.2.7	Fe as a limiting nutrient in the Arabian Sea and The subtropical Indian Ocean	123
3.4	Dissolved Iron distributions - The Bay of Bengal vs. The Arabian Sea	125
3.5	Dissolved Iron cycling comparison in the Indian Ocean with the Atlantic and the Pacific Oceans	126
3.6	Summary and conclusions	128
Chapter 4		
	<i>Distributions of Dissolved Zinc in the Indian Ocean</i>	171
4.1	Introduction	173
4.2	Results	175
4.2.1	Hydrographic and major nutrients	175
4.2.2	DZn distributions	179
4.2.3	Zinc vs. Major nutrients Relationship	198
4.3	Discussion	199
4.3.1	DZn in surface and intermediate waters	199
4.3.2	DZn in deep waters	201
4.3.3	DZn and Silicate Relationship	204
4.3.3.1	Northeastern Indian Ocean	204
4.3.3.2	Northwestern Indian Ocean	205
4.3.4	Comparison of Zn-Si relationship in the Indian Ocean with global ocean	206
4.3.5	Zn vs. Si in the oxygen minimum zone waters of the Northern Indian Ocean	208
4.3.6	Effect of oxygen minimum zone on the Zinc cycle	210
4.3.7	Zn and Si in the deeper waters of Northern Indian Ocean	212
4.3.8	DZn and P in the Indian Ocean	213
4.3.9	Comparison of Zn distributions in the Indian Ocean with the Atlantic and the Pacific Oceans	214
4.4	Summary and Conclusions	215
Chapter 5		
	<i>Synthesis and Future Perspectives</i>	217
5.1	Summary	219
5.1.1	Establishment of clean sampling and flow injection methods	219
5.1.2	Sources/sinks influencing the DFe and DZn cycling	220
5.1.2.1	Distributions of DFe and DZn in the Northern Indian Ocean	220
5.1.2.2	Distributions of DFe and DZn in the subtropical Indian Ocean	222

5.2 Future Perspectives	222
<i>References</i>	226
<i>List of Publications/Conference proceedings</i>	248

LIST OF TABLES

Table	Caption	Page
2.1	Details of SK-304 sampling in the Indian Ocean	19
2.2	Details of SK-311 sampling in the Indian Ocean	20
2.3	Details of SK-312 sampling in the Indian Ocean	20
2.4	Details of SK-324 sampling in the Indian Ocean	21
2.5	Details of SK-338 sampling in the Indian Ocean	21
2.6	The valve operation during one analytical cycle of DFe	29
2.7	The Photon counting head H-8259-01 specifications	29
2.8	Valve position and timings during one analytical cycle	45
3.1	Fe:C rates in the Indian Ocean and present study	92
4.1	DZn data in the BoB	180
4.2	DZn data in the Andaman Sea	186
4.3	DZn data in the Arabian Sea	187
4.4	DZn data in the Indian Ocean	194

LIST OF FIGURES

Figure	Caption	Page
1.1	Geotraces section cruises over the global oceans	7
1.2	Unique features of the Indian Ocean	8
2.1	Cruises conducted under GEOTRACES-India programme	18
2.2	Expeditions done onboard ORV Sagar Kanya	19
2.3	Trace metal CTD connected to Kevlar cable	24
2.4	Winch van containing 8000 m long Kevlar cable	24
2.5	Class-1000 clean van for sub sampling of seawater	25
2.6	Seawater sampling inside class-1000 clean van	26
2.7	Schematic diagram for rinse step to remove seawater matrix	30
2.8	Schematic diagram for retention of analyte during loading	30
2.9	Schematic diagram for elution of analyte	31
2.10	Analysis of DFe onboard ORV Sagar Kanya	31
2.11	Functional group of AF Chelate 650 M	32
2.12	Six port valves with custom made Teflon column	32
2.13	Block diagram of the main control unit and PMT interface	33
2.14	Data acquisition and instrument control tab	36
2.15	Standard additions of Iron to the low iron seawater	37
2.16	Vertical profile for DFe during SK - 324.	37
2.17	Inter and Intra comparison of DFe data	39
2.18	Locations for SAFe and GEOTRACES reference standards	40
2.19	Reported values for reference standards for DFe	42
2.20	Structure of p-TAQ and Zn-pTAQ	44
2.21	Schematic diagram for Zinc flow injection method	45
2.22	Zinc flow injection system	46
2.23	Zinc flow injection system software and data control windows	47
2.24	Cd vs. P relationship in the seawater	48
2.25	Calibration graph for the Zinc in the seawater	50
2.26	Structure of Nobias resin	51

2.27	Comparison of DZn with neighboring stations in the BoB	52
2.28	Inter comparison of DZn	53
2.29	Reported values for reference standards for DZn	56
2.30	Inter comparison of major nutrients with crossover station	60
3.1	Sampling locations of SK-304 and SK-311	67
3.2	Water mass structure in the Northeastern Indian Ocean	69
3.3	Section plots of basic parameters along SK-304	71
3.4	Section plots of basic parameters along SK-311	74
3.5	SSH information along SK-311	75
3.6	Surface DFe concentrations along SK-304 and SK-311	78
3.7	Vertical profiles of DFe along SK-304 and SK-311	81
3.8	Section plots of DFe with overlaid fluorescence	82
3.9	Section profiles of DFe along SK-304 and SK-311	83
3.10	Fe:C remineralization rates	91
3.11	Section plot of Fe* along the basin	94
3.12	DFe vs. P in the study region	95
3.13	Map showing SK-312 and SK-324	97
3.14	Salinity and Temperature along SK-312	98
3.15	Salinity and Temperature along SK-324	99
3.16	Water masses along SK-312 and SK-324	100
3.17	Section plot of DO along SK-312	102
3.18	Section plot of DO along SK-324	103
3.19	AOU section plot along SK-324	103
3.20	Vertical profiles of DO in SK-324	104
3.21	Section plots of major nutrients along SK-312	105
3.22	Vertical profiles of nutrients in SK-324	106
3.23	Section plots of major nutrients along SK-324	108
3.24	Surface DFe concentrations during spring inter monsoon period	109
3.25	Surface DFe concentrations along SK-324	110
3.26	Vertical profiles of DFe in SK-312	110
3.27	Section plot of DFe along SK-312	114
3.28	Comparison of SK-312/11 with ER-9 Station	115

3.29	Vertical profiles of DFe along SK-324	116
3.30	Section profile of DFe along SK-324	117
3.31	DFe and Fluorescence section plot	119
3.32	AOU and major nutrient scatter plots in Arabian Sea	120
3.33	AOU and DFe scatter plot in western subtropical Indian Ocean	121
3.34	AOU and DFe scatter plot in the Arabian Sea	122
3.35	DFe vs. P scatter plot in the Arabian Sea	124
3.36	Section plot of Fe* in the SK-312 and SK-324	125
4.1	DZn analyzed stations in the Indian Ocean	174
4.2	Water masses in the Indian Ocean	176
4.3	DO vertical profiles in the Indian Ocean	177
4.4	Vertical profiles of Phosphate in the Indian Ocean	177
4.5	Vertical profiles of Silicate in the Indian Ocean	178
4.6	Vertical profiles of Zinc in the Indian Ocean	179
4.7	Section plots of DZn along SK-304, SK-324 and SK-338	202
4.8	Scatter plot for Si and DZn in the Northeastern Indian Ocean	204
4.9	Scatter plot for Si and DZn in the Northwestern Indian Ocean	205
4.10	DZn and Si comparison in the region with the global ocean	206
4.11	Linear correlation for Si and DZn in the Indian Ocean	207
4.12	Scatter plot for Si and DZn in the OMZ waters of the BoB	209
4.13	DZn vs. Si in the OMZ waters of the Arabian Sea	210
4.14	DZn vs. Si in the OMZ waters of the Northern Indian Ocean	211
4.15	Zn vs. Si scatter plot in deeper waters of Northern Indian Ocean	212
4.16	Scatter plot of Zn vs. P in the Indian Ocean	213

Chapter 1
Introduction

1.1 Introduction

Trace metals in seawater play an integral role in regulating the oceanic primary production by acting as catalysts in several metabolic processes (Bruland et al., 1991; Bruland et al., 2013; Clough et al., 2016; Morel et al., 1991; Morel and Price, 2003) like Carbon fixation, N₂ fixation, Silica uptake etc. Primary production is termed as conversion of inorganic carbon (atmospheric carbon dioxide (CO₂)) into organic carbon through photosynthesis. Certain trace metals play a key role in the biological pump (export of carbon from the surface of ocean to sea floor through primary production). This biological pump has direct implications to the global carbon cycle (Riebesell et al., 2007; Sarmiento et al., 1998) and hence the distributions of trace elements and behavior are linked to carbon cycle. In addition, trace elements act as tracers for paleo-climate, redox and paleo-oceanographic proxies (Tribovillard et al., 2006). Understanding the contemporary biogeochemical cycles of these trace metals vis-à-vis carbon cycle may help us to better decipher the past oceanic processes, which in turn can predict the future response of the global climate (GEOTRACES Science plan, 2005).

The vital role of trace metals in controlling the ocean productivity was recognized through iron hypothesis. In early 1930's Gran (1931) and Hart (1934) proposed that some parts of the surface ocean productivity might be limited by the availability of micronutrient, Iron (Fe). Later these regions were termed as High Nutrient Low Chlorophyll (HNLC) regions (Martin et al., 1989). In these surface oceanic regions, ample amount of major nutrients viz. Nitrate (NO₃), Phosphate (P) and Silicate (Si) which are primary burners for primary productivity in addition to sunlight, are available but phytoplankton biomass is very low compared to other regions. Along with the Southern Ocean, the Equatorial Pacific, Subarctic Pacific Oceans and the western Arabian Sea also possess the HNLC regions. It was proposed that productivity could be limited due to lack of dissolved Fe (DFe) in the seawater. This hypothesis was tested by Prof. John Martin in the lab as well as in the open ocean waters of the Southern Ocean and confirmed that small additions of trace element, Fe in the HNLC regions increases the primary production (Martin et al., 1989, 1990, 1991). So far, 12 mesoscale Fe

experiments have been done in the HNLC regions between the year 1993 and 2005. The results suggest that Fe is the most important limiting nutrient in the seawater for the primary production (Boyd et al., 2007, 2000; Tsuda et al., 2003).

The HNLC regions consist of 40% of the world oceans and it is now recognized that productivity in these regions are limited by the availability of trace elements. These regions include the Southern Ocean, the North Pacific Ocean, the Equatorial Pacific Ocean and the Sub Arctic Ocean. Among all the bioactive trace metals in seawater, Fe and Zn have gained more importance due to their crucial involvement in several metabolic processes.

Despite the significant importance of these trace elements in controlling the primary productivity, ecosystem dynamics and hence carbon cycle, their studies in various oceanic basins are very limited. Their sources, sinks and internal cycling are poorly understood. Such studies on trace elements (Fe and Zn) particularly in the Indian Ocean are very limited. Non-availability of clean sampling systems and protocols to collect and analyze seawater for Fe and Zn without any contamination have hampered their studies in the field of oceanography. GEOTRACES programme was initiated a few years ago to fill these voids in the global ocean. In this thesis, an effort has been made to understand the distributions of Fe and Zn in the Indian Ocean waters by knowing their sources, sinks and internal cycling in the water column.

1.1.1 Iron in seawater

Fe is the fourth most abundant element in the Earth's crust (Wedepohl 1995), in spite its concentration in the seawater is very low. It is a crucial element for chlorophyll production and nitrogen assimilation in all the living organisms (Boyd et al., 2007; Moore et al., 2009; Rueler and Ades 1987). Generally, Fe exists in two oxidation states +2 and +3. Thermodynamically Fe in +2 oxidation state is more soluble and it is most favorable oxidation state, but in the oxygenated seawater, Fe (+2) reacts immediately with oxygen and forms Fe (+3) in the seawater (Rose and Waite, 2002). At circum neutral pH of seawater, Fe readily hydrolyzes with the oxygen and forms stable oxy-hydroxides which are insoluble in the seawater and rapidly gets removed from the water column (Liu

and Millero, 2002). The observed concentrations of Fe in the seawater is more than its solubility due to the dominance of organic complexation (99% of Fe in the seawater complexes with the organic ligands) which is compensating the removal of Fe from the water column (Gledhill and Buck, 2012; Vandenberg, 1995). The most assimilated form of Fe in the marine organisms is Fe in +2 forms (Sunda, 2012). Studies suggest that small amounts of Fe in +2 form can be sustained in the surface waters and in the oxygen minimum zone (OMZ) either by direct or indirect photochemical reaction of Fe (+3) complexes and also by biological remineralization process in the OMZ regions (Barbeau et al., 2001, 2006; Bruland et al., 2013; Croot and Laan, 2002; Croot et al., 2001, 2005; Maldonado and Price, 2001; Moffett et al., 2007; Rijkenberg et al., 2006; Sarthou et al., 2008; Shaked et al., 2004).

It was believed that atmospheric deposition is the main and a major external source of Fe in the surface waters of the oceans (Duce and Tindale, 1991; Grand et al., 2015; Jickells et al., 2005). However, with the advent of measurement of dissolved Fe all over the global ocean throughout the water column it is now recognized that in addition to the atmospheric dust other sources also play a key role in the marine Fe cycle. Resing et al. (2015) have shown that the DFe can advect laterally to several thousands of kilometers from hydrothermal vent sources without any scavenging. Until this study, it was believed that most of the Fe is removed from the water column due to the formation of Fe-oxyhydroxide complexes once it releases in to the oxygenated seawater in the deeper waters. In addition, studies have shown that sediment resuspension, continental shelves, margins and sea ice are crucial sources of DFe (Elrod et al., 2008; Hurst et al., 2010; Johnson et al., 1999; Lam et al., 2006, 2012; Lohan and Bruland., 2008; Nishioka et al., 2007, 2017; Tagliabue et al., 2014; Wu et al., 2009).

1.1.2 Zinc in seawater

Zinc (Zn) is the 22nd abundant element in the Earth's crust (Wedepohl 1995) however, in the open ocean waters, it exist in nanomolar (nM) levels. In general, Zn concentrations are low in surface waters and continuously increase

with respect to the depth. It occurs in the range of 0.1 nM to ~12 nM in the seawater. Its concentration varies in the world ocean with the lower concentrations observed in the Atlantic Ocean as compared to the Indian and the Pacific Oceans (Bermin et al., 2006; Bruland and Lohan., 2003). High values in the deeper waters of the Pacific Ocean have been observed which are mainly due to the aging of water masses.

Zn shows the nutrient type distribution in the oceans. Zn is a co-factor for almost 300 enzymes such as carbonic anhydrase, alkaline phosphatase etc., and it is an essential metal for microorganism growth (Morel et al., 1994; Sinoir et al., 2012; Shaked et al., 2006). Lower Zn concentrations in picomolar (pM) levels in the surface open ocean waters may limit the primary production and CO₂ uptake (Anderson et al., 1978; Ibrahim et al., 2008; Lane and Morel, 2000; Morel et al., 1994; Price and Morel, 1990). Unlike Fe, there are no open ocean experimental studies to conclude the Zn limitation for the productivity (Coale et al., 2003; Crawford et al., 2003; Jakuba et al., 2012; Lohan et al., 2005). Further, Zn in the seawater shows strong correlation with silicate (Bruland, 1980) suggesting similar behavior. Vance et al. (2017) suggested that strong correlation of Zn and Si can be explained by their coupled biogeochemical cycles through southern ocean. In the contemporary oceans, the strong relation between Zn and Si is still an enigma. Studies (Ellwood and Hunter, 2000; Thamatrakoln and Hildebrand, 2008), suggest that Zn involvement in the biogenic opal is very less compared to total uptake of Zn.

Zn mostly exists in +2 state and its speciation is dominated by the organic complexation. More than 95% of Zn in the seawater is organically complexed (Donat and Bruland, 1990; Jakuba et al., 2012; Kim et al., 2015) and reduces the bioavailable form (Free Zn⁺² ions) to 1 pM levels (Bruland et al., 1989; Ellwood and Vanderberg, 2000). Speciation studies are important to characterize the fraction of Zn freely available for biology. The distribution of the total dissolved concentrations of Zn in the seawater is required to assess its bioavailability. In the contemporary oceans, the data for the dissolved Zn is sparse. Zn is the most notorious element, which is more prone for the contamination in the seawater. Researchers are developing the electrochemical methods to study their

physicochemical characteristics in the oceans to study its availability in order to understand its biogeochemical cycle in seawater.

1.2 GEOTRACES and the Indian Ocean

The GEOTRACES is an international programme to study global marine biogeochemical cycles of trace elements and their isotopes. The main objectives of GEOTRACES are to map the global oceans for trace elements, isotopes distributions and understand their internal cycling. The initiation of this programme led researchers to cover globally unexplored areas to unravel the role of trace elements on oceanic biogeochemistry. There are 35 countries and more than 900 researchers are involved in this international project for the global coverage of trace elements and their isotopic distributions in the oceans.

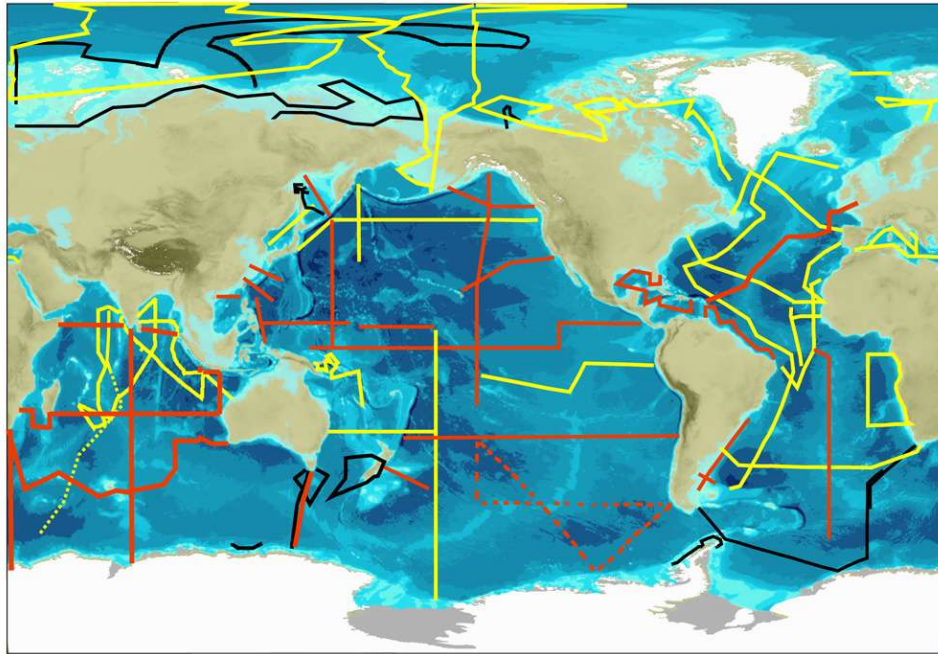


Figure 1.1: GEOTRACES section cruises over the global oceans. Yellow color lines (including dotted yellow lines) indicate completed cruises. Red lines (including dotted red lines) indicate proposed cruises while the black lines indicate completed cruises for which the data has been submitted to IDP (Intermediate data product). Map source - GEOTRACES website.

The ultimate goal of this programme is to predict the future climatic conditions by understanding the past and the present systematic with the help of these biogeochemical cycles.

Indian Ocean: Indian Ocean is unique basin and act as conduit between the Atlantic and the Pacific Oceans.

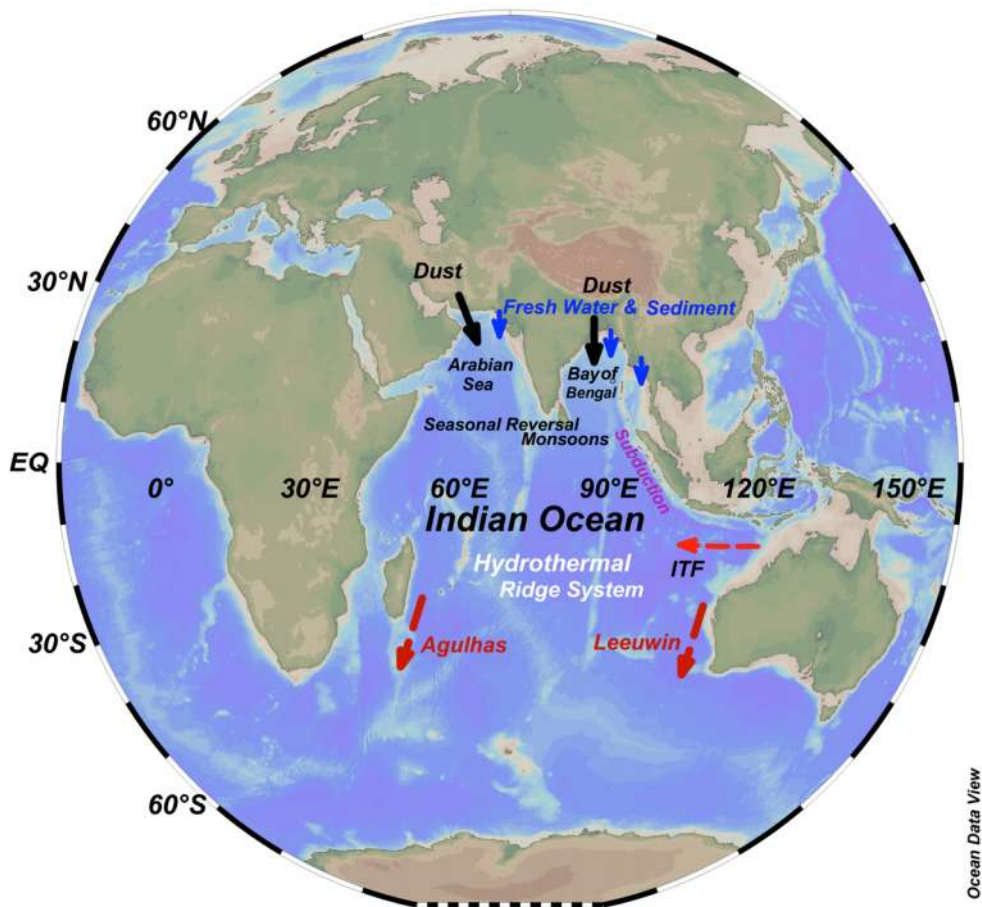


Figure 1.2: Indian Ocean and its unique features impacting the biogeochemistry of the basin.

Unlike the Atlantic and the Pacific Oceans, the Indian Ocean has low-latitude land boundary to the north. It is characterized by low and high latitude water exchange through the Indonesian Through Flow (ITF) and the Agulhas current. The Indian Ocean is criss-crossed with three meridional ridges and a triple junction of three spreading centers. It is influenced by strong monsoonal wind forcing that reverses

seasonally. The boundary currents reverse seasonally with monsoon, impacting biogeochemical cycles and ecosystem response of the basin. Like subtropical gyres in the other oceans, it has large gyres, which are the basic drivers for the surface circulation. The Indian Ocean has two basins, the Arabian Sea and the Bay of Bengal which are characterized by high productivity resulting in the formation of a major denitrification/suboxic basin and a natural laboratory of river-ocean interactions respectively. Western Indian Ocean is impacted by the dust input from nearby arid land-masses whereas its eastern counterpart is impacted by volcanism. Indian plate is subducting under Burmese plate along the Java trench in the basin. The geography of the basin and the oceanographic processes operating in the Indian Ocean influences the biogeochemistry of the global oceans and makes it important to study the biogeochemistry of the Indian Ocean.

The basic objectives of this study are to study the distribution and internal cycling of DFe and DZn in the Indian Ocean. This study is part of the GEOTRACES programme and carried out under the GEOTRACES-INDIA programme in the Indian Ocean.

1.3 Trace elements (Fe and Zn) in the Study Region

The Indian Ocean is the least explored basin for the trace elements and their isotopic studies. The first vertical profile of Fe in the Indian Ocean was reported by Saager et al. (1989). With the advent of new clean sampling system and measurement protocols for dissolved trace elements in the ocean, subsequent studies continued to investigate the DFe distributions in the Indian Ocean (Grand et al., 2015a, 2015b; Kondo and Moffett, 2013; Measures and Vink, 1995; Moffett et al., 2007; Nishioka et al., 2013; Takeda et al., 1995; Vu and Sohrin, 2013). The existing data for dissolved Zinc (DZn) is even more sparse in the Indian Ocean compared to DFe data. Saager et al. (1991) produced first data set for trace metals in the Indian Ocean. First reliable data on Zn in the Southwestern Indian Ocean was produced by Morley et al. (1993) with six full vertical profiles. Recently, Gosnell et al. (2012); Vu and Sohrin, (2013) and Kim et al. (2015) measured dissolved Zn in few profiles in the Indian Ocean by following the GEOTRACES protocols.

In the present thesis, DFe concentrations (> 1000 data points) and total dissolved Zn concentrations (~ 800 data points) are reported from the Indian Ocean. The data comprises measurements from the Bay of Bengal (BoB), the Andaman Sea, the Arabian Sea (AS) and the Indian Ocean (South of equator) with an unprecedented resolution.

1.4 Objectives of the Thesis

The primary objectives of the thesis are to establish and understand:

1. Clean sampling system in India onboard ORV Sagar Kanya
2. The sensitive flow injection method to measure (pM) to nanomolar (nM) level concentrations of DFe in the seawater based on chemiluminescence detection.
3. The sensitive flow injection method to measure sub nanomolar level concentrations of dissolved Zinc (DZn) in the seawater by fluorometric detection.
4. The distributions of DFe in the Indian Ocean waters with implications to their sources, sinks and internal cycling in the water column.
5. The distributions of DZn in the Indian Ocean waters: Implications to their sources, sinks and internal cycling in the water column.

1.5 Outline of the Thesis

Chapter 1: Introduction

This chapter provides a basic introduction of trace elements in seawater, their importance as micro-nutrients for ocean productivity and as tracers to study various paleo-redox and paleo-oceanographic processes. Further, this chapter provides the aim of the study and highlights the research gap in the contemporary understanding of selected bioactive trace elements in the least explored Indian Ocean waters.

Chapter 2: Material and Methods

This chapter briefly explains the sampling and analytical protocols established in the lab to achieve the stated objectives. The trace metal clean sampling and measurement of DFe and DZn protocols and methods presented in the thesis are first of its kind. Accurate and precise determination of Fe and Zn in

the seawater by chemiluminescence and fluorometric detection are also briefly described. The validation of these established methods were cross checked with the available reference standards and comparing with the previously published results from cross-over stations. Inter-comparison is a must for the GEOTRACES programme for validating the data and it is accomplished in this work and discussed in the chapter.

Chapter 3: Distributions of dissolved Iron in the Indian Ocean

In this chapter, detailed description of the distributions of DFe in the Indian Ocean is discussed. Based on the hydrographic parameters and for the sake of simplicity this chapter is divided into sub-sections and basin wise explanation is presented. A huge spatial variability is observed in the vertical profiles for Fe. Potential sources of Fe such as Aeolian dust, continental sediments, continental margins, converging and diverging plate boundaries as significant source contributors in the Indian Ocean are discussed. The distinct Fe:C remineralization rates in the basin with its implications are stated. Stoichiometric relation with the major nutrients and its implications and Fe limitation are also discussed in the chapter.

Chapter 4: Distributions of dissolved Zinc in the Indian Ocean

This chapter presents the distributions of dissolved Zinc in the water column of the Indian Ocean. Spatial variability and internal cycling of Zn is explained basin wise, using the hydrographic parameter dataset. Tight correlation of Zn and Si in the Indian Ocean is observed in the basin. This strong correlation and ratios are compared with other oceanic basins to understand the Zn cycle in the basin.

Chapter 5: Synthesis and Future Perspectives

In this chapter, major outcomes of the thesis are summarized and insights for the future perspectives are mentioned.

Chapter 2
Materials and Methods

The main objective of this thesis is to understand the distributions of bioactive trace elements, Fe and Zn in the water column of the Indian Ocean waters, which involves finding their sources, sinks and internal cycling. This objective falls in the ultimate goal of the GEOTRACES, an international programme initiated in 2005 to understand the global wide distributions of trace elements and their isotopes to better characterize the role of trace elements in controlling the various oceanic processes. This study gives a primary understanding of the distributions of Fe and Zn in the least explored Indian Ocean.

To achieve these objectives, seawater samples from the Indian Ocean and sensitive analytical methods were required. Clean sampling protocols have been adopted to collect and store the samples to avoid contamination. Flow injection systems for Iron (Fe-FIS) and Zinc (Zn-FIS) were also established for onboard as well as offshore analysis of Fe and Zn in the seawater. The following sections briefly explain the clean sampling methods implemented to sample the seawater and analytical protocols established in the lab to measure such low level concentrations of Fe and Zn.

2.1 Study Area

This study has been carried out in the Indian Ocean, between latitude 28° S and 20° N and longitude 55° E and 110° E. The Indian Ocean is the third largest ocean after Pacific and Atlantic Oceans. The Indian Ocean is locked by landmass in the northern side. The northern Indian Ocean is marked with the presence of seasonal reversal of monsoonal winds and surface currents. In general, the northern Indian Ocean is more productive compared to the equatorial and subtropical Indian Ocean due to reversal of winds and currents that brings sub-surface waters to the surface, which enhances the productivity. The two adjacent basins of the northern Indian Ocean, the Bay of Bengal (BoB) and the Arabian Sea (AS, Figure 2.1) are characterized by the presence of the oxygen minimum zone (OMZ) in the intermediate waters due to freshwater stratification and higher productivity respectively. The presence of hydrothermal vents, atmospheric dust input from adjacent arid landmasses and water exchanges with the Pacific and the Atlantic Oceans could influence the biogeochemistry of the Indian Ocean.

2.1.1 The Bay of Bengal

The BoB, spanning between latitudes 5 – 21° N and 80 – 90° E, experiences both summer and winter monsoons every year during the periods June – September and November – January, respectively, which bring changes to the surface circulation and local hydrography. A number of rivers, the Ganga, the Brahmaputra, the Godavari, the Krishna etc., drain into the BoB and supply $\sim 1.6 \times 10^{12} \text{ m}^3$ freshwater (UNESCO, 1993) and $\sim 1.4 \times 10^9$ tons of suspended load annually making it one of the oceanic basins receiving very high flux of continental materials (Basu et al., 2001; Galy and France - Lanord, 1999, 2001; Milliman and Mead, 1983; Sarin et al., 1989; Singh et al., 2008) leading to fresh water stratification in the surface BoB (Gopalakrishna et al., 2002; Madhupratap et al., 2003; Prasanna Kumar et al., 2002; Shetye et al., 1996) inhibiting vertical mixing. However, the stratification is often shattered by the formation of eddies (Prasanna kumar et al., 2002; Sarma et al., 2016).

2.1.2 The Arabian Sea

The AS is also situated at the same geographical latitude location as of the BoB and shares similar atmospheric forcing and seasonal reversal of monsoons in the northwestern part of the Indian Ocean. The AS is one of the most productive regions and receives $\sim 1.7 \times 10^{11} \text{ m}^3$ of water and $\sim 5 \times 10^8$ tons (pre-damming) of sediments annually from rivers along with a huge supply of atmospheric mineral dust ($\sim 1 \times 10^8$ tons) from nearby deserts (Goldberg and Griffin, 1970; Goswamiet al., 2012; Kolla et al., 1976; Ramaswamy and Nair, 1994; Sirocko and Sarnthein, 1989). AS is characterized by the occurrence of intense oxygen minimum zone (OMZ) in the intermediate water column where as anoxic conditions can also be seen along the west coast of India during late summer and autumn (Bange et al., 2005; Naqvi et al., 1994, 2006).

2.1.3 The Andaman Sea

Andaman Sea is located in the northeastern part of Indian Ocean extending from Myanmar in the north to Sumatra in the south and Andaman-Nicobar Islands in the west to the Malay Peninsula in the east. The average water column depth of the Andaman Sea is ~ 1100 m. In the north, the basin receives fresh water supply from the Irrawaddy and the Salween rivers. Horizontal ventilation of the

Andaman Sea is restricted from BoB by the Andaman-Nicobar Islands. The exchange of water from BoB is mainly through Ten degree channel with a sill depth of ~800 m and through the Great Channel in the south with a sill depth of ~1400 m (Gupta et al., 1981; Nozaki and Alibo 2003; Raju et al., 2004). Biogeochemistry in this basin could be influenced by active subduction zone (Khan et al., 2005) and submarine volcanoes (Sheth et al., 2009).

2.1.4 The equatorial and southern Indian Ocean

Compared to the AS and the BoB, the equatorial and southern Indian Ocean is oligotrophic in nature due to less/negligible supply of nutrients from atmospheric deposition, rivers and no influence of seasonal reversal of monsoonal winds. Additionally, the Indian Ocean receives Pacific Ocean waters by the Indonesian Through Flow (ITF), (You and Tomczak, 1993) between 5° S to 15° S latitude along the Indonesian Islands and transports the surface water to the southern Atlantic Ocean through Agulhas current (Beal et al., 2011). The Indian Ocean region south of equator does not receive atmospheric dust and riverine input as much compared to the northern Indian Ocean, but the presence of ridges like the Central Indian Ridge, Southwest Indian Ridge, and the Carlsberg Ridge makes the Indian Ocean a huge inventory for trace metals in the deeper waters. The region contains several hydrothermal active vent fields (Van Dover et al., 2001). A recent study found the input from hydrothermal vent fields in the deep waters of the Indian Ocean for the bioactive trace metals like Fe and Mn (Nishioka et al., 2013).

2.2 Sampling and filtration

Samples for trace metal analysis were collected from six GEOTRACES-INDIA cruises (details listed in Tables 2.1 - 2.5) aboard the oceanographic research vessel *ORV Sagar Kanya* in Indian Ocean comprising of the Bay of Bengal, the Arabian Sea and the Andaman Sea. The primary challenge here was sampling and storage of seawater samples for trace metal analysis without any contamination. Because, these trace elements, Fe and Zn, exists in the sub nanomolar (10^{-9}) to picomolar (10^{-12}) concentrations in the seawater. The regularly available hydrographic CTD and sampling protocols are found not suitable for sampling the bioactive trace metals. A factor of 4-5 higher

concentrations was observed in the trace metal data in the samples collected using regular CTD in our work. Regular CTDs are deployed by connecting the frame to a hydrographic cable made of metals and they apply grease to the metallic wire regularly to avoid rusting which is not suitable/recommended for collecting samples for trace metals analyses. Therefore, a rapid and non-contaminating sampling system and systematic protocols were needed for sampling seawater for analysis of the bio-essential metals for reliable data. The data shown for the samples produced in this thesis were collected using trace metal CTD.

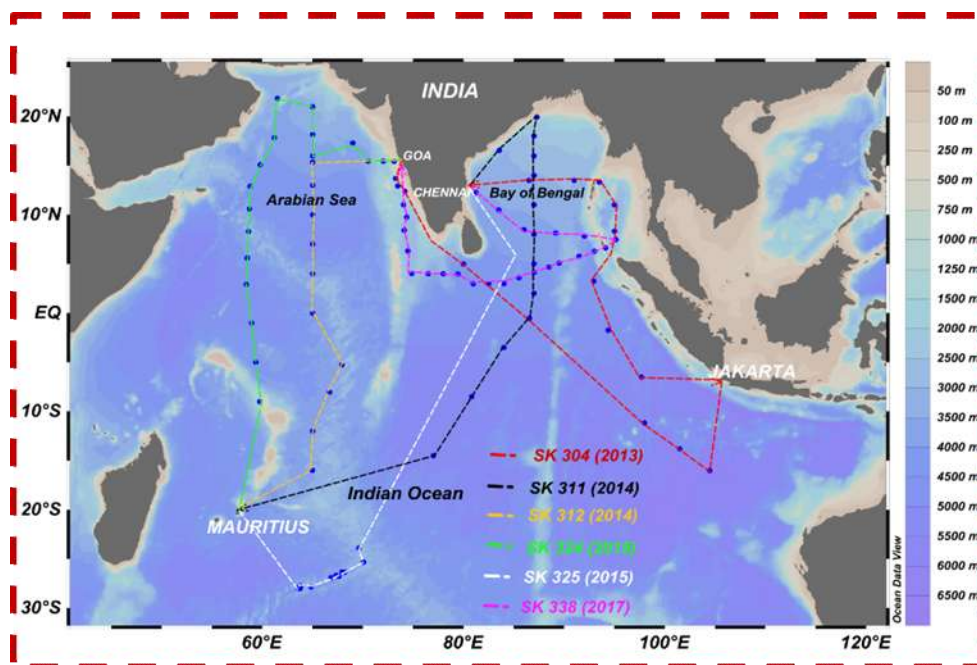


Figure 2.1: Cruises conducted in the Indian Ocean to study the biogeochemical cycles of Fe and Zn.



Figure2.2: All GEOTRACES-INDIA expeditions were carried out onboard ORV Sagar Kanya.

Table 2.1: Details of sampling in the Bay of Bengal, the Arabian Sea, the Andaman Sea and the equatorial and southern Indian Ocean during SK-304 cruise in March to May 2013

Station	Latitude* (N)	Longitude* (E)	Sampling depth (m)
SK304A-1	13.706	73.263	800
SK304A-2	12.395	74.159	710
SK304A-4	5.001	79.998	4327
SK304A-6	-0.530	86.560	4687
SK304A-8	-11.161	97.986	5127
SK304A-9	-13.818	101.493	5072
SK304A-10	-16.026	104.463	5860
SK304B-11	-6.503	97.666	5401
SK304B-13	-1.757	94.367	4798
SK304B-14	3.246	92.934	4511
SK304B-16	8.334	95.002	2902
SK304B-17	11.004	95.003	3466
SK304B-20	13.331	93.496	1889
SK304B-21	13.498	91.002	3023
SK304B-22	13.500	86.503	3213

*Latitude and Longitude are mentioned in decimal degree units.

Table 2.2: Details of sampling in the Bay of Bengal and Indian Ocean during SK-311 cruise in March to April 2014

Station	Latitude (N)	Longitude (E)	Sampling depth (m)
SK311-1	16.534	83.567	2983
SK311-2	19.944	87.296	1079
SK311-3	18.015	87.001	2502
SK311-4	16.003	87.000	2816
SK311-5	14.003	87.001	3094
SK311-6	11.013	87.000	3450
SK311-7	8.017	86.999	3768
SK311-8	5.009	86.996	4106
SK311-9	2.006	87.001	4449
SK311-10	-3.501	84.000	5005
SK311-11	-8.498	80.802	5281
SK311-12	-14.491	76.993	5281
SK311-16	-25.319	70.040	2442

Table 2.3: Details of sampling in the Arabian Sea and Indian Ocean during SK-312 cruise in April to May 2014

Station	Latitude (N)	Longitude (E)	Sampling depth (m)
SK312-8	-15.999	64.985	3182
SK312-9	-12.001	64.999	3449
SK312-10	-8.017	66.691	4161
SK312-11	-5.267	67.900	3000
SK312-12	-0.007	65.005	3900
SK312-13	3.997	65.000	3800
SK312-14	6.998	64.999	4858
SK312-15	9.999	64.999	4543
SK312-16	12.999	64.999	4203
SK312-17	15.999	64.999	3797

Table 2.4: Details of sampling in the Indian Ocean during SK-324 cruise in September 2015

Station	Latitude (N)	Longitude (E)	Sampling depth (m)
SK324-1	15.430	73.100	100
SK324-2	15.460	72.030	1946
SK324-3	15.450	70.499	3344
SK324-4	17.300	68.999	3345
SK324-5	15.350	64.999	3795
SK324-6	18.175	64.999	3400
SK324-7	21.000	64.999	2956
SK324-8	21.850	61.499	3160
SK324-9	17.850	61.200	3800
SK324-10	15.100	59.799	4090
SK324-11	12.900	58.799	4380
SK324-12	10.600	58.699	3600
SK324-13	8.300	58.630	2650
SK324-14	5.600	58.500	3850
SK324-15	2.900	58.400	4500
SK324-16	-1.000	58.950	4580
SK324-17	-5.000	59.350	4070
SK324-18	-9.000	59.750	850

Table 2.5: Details of sampling in the Northern Indian Ocean during SK-338 cruise in January to March 2017

Station	Latitude (N)	Longitude (E)	Sampling depth (m)
Sk338-1	12.266	81.250	3417
Sk338-2	10.483	83.499	3566
Sk338-3	8.500	86.000	3669
Sk338-4	8.148	89.148	3577
Sk338-5	7.833	91.997	3435
Sk338-6	7.489	95.131	2579
Sk338-7	6.648	94.113	2007
Sk338-8	6.283	92.999	1787
Sk338-9	5.781	91.496	3812
Sk338-10	5.084	89.499	3380
Sk338-11	4.699	88.500	4005

Sk338-12	4.149	86.998	3900
Sk338-13	3.601	85.498	4177
Sk338-14	3.001	83.999	4264
Sk338-17	3.974	79.434	4301
Sk338-18	3.999	77.993	2959
Sk338-19	4.000	76.493	3158
Sk338-20	4.027	74.843	2618
Sk338-21	6.322	74.467	2752
Sk338-22	8.436	74.102	2759
Sk338-24	11.030	74.033	2070

2.2.1 Sampling

Trace metal CTD was used during the expeditions for seawater sampling for trace elemental measurements. Samples for basic parameters like nutrients, dissolved oxygen (DO) etc., were also collected using trace metal CTD hydrocasts. Trace metal clean CTD consists of 24 Teflon coated 12 L Niskin bottles (General Oceanics Inc.) mounted on aluminum powder coated frame. This Al powder coated frame was connected to the Kevlar cable through a pulley to lower from surface to bottom of the ocean floor to collect seawater. Clean winch system procured from Le Bus Co. was used for entire sampling. Kevlar cable was pooled on non-metallic drum of this winch (Figure 2.4). Upon recovery, Niskin bottles were taken inside of the clean van (Figure 2.5) for subsampling. This clean van (SILHOUETTE STEEL LTD.) is used to control the contamination. Inside the clean room (Figure 2.6), samples were filtered by passing seawater through 0.2 μm pore size PALL ACROPAK filters for dissolved fraction of the trace metals. The filters used for filtering the seawater are highly sterile and made of synthetic polymer to avoid any protein bond formation with the particles in the seawater. Sufficient amount, $\sim 200\text{ml}$ of seawater was passed through this filter and discarded before collecting the sample in to the respective pre cleaned bottles. The seawater aliquots were rinsed repeatedly before collecting the sample to avoid cross contamination. Hence, the reported data for Fe and Zn in this thesis are for the dissolved fraction. Seawater was filtered under zero gas at 1.5 atm pressure to speed up the filtration process. The gravity filtration consumes a huge time. LDPE bottles (1L), which were precleaned by following the GEOTRACES protocol

(Section 2.1.2), were used for collection. Each sample bottle was cleaned with sufficient amount of seawater before collecting the respective depth sample to ensure the homogeneity of the sample. Conc. HCl (Sea star chemicals, Fisher scientific) was added to the sample collected after filtration under a class-100 laminar flow bench (Air clean systems) to maintain a pH of ~ 1.7 and packed in double bagged zip lock bags for further analysis (Figure 2.6). 1.2 ml Conc. HCl was added to one liter of seawater and 0.1 ml was added to 60 ml of sample bottles to bring seawater pH of ~ 1.7 from ~ 8.2 . The small volume (~ 60 ml) of seawater samples was collected during collection of 1L bottles for onboard analysis of Fe and Zn by flow injection systems.

2.2.2 Protocol followed for cleaning the sampling bottles

Prior to collection, LDPE bottles used were cleaned as following:

Step-1: Rinsed bottles with Milli-Q water filled with 5% Extran (Fisher scientific) concentrated detergent.

Step-2: Cleaned 3 times with MQ water.

Step-3: Bottles were completely filled with 3N HCl (obtained by Teflon distilling the commercially available AR grade HCl) for 7 days. This acid was used for 6-7 cycles.

Step-4: Clean with MQ water.

Step-5: Bottles were filled with 1N HNO₃ (Teflon distilled/Sea star chemicals (Fisher scientific) for 3 days. This acid was used for 6-7 cycles.

Step-6: Clean with MQ.

The above-mentioned steps were also followed for 60 ml LDPE bottles used for storing seawater samples used for measuring DFe onboard.



Figure 2.3: Trace metal CTD with 24 x 12 L Niskin bottles mounted on an aluminum powdered rosette (Left), CTD frame connected to a Kevlar cable through a Teflon pulley (Right).



Figure 2.4: Winch van containing 8000 m long Kevlar cable.



Figure 2.5: Class-1000 clean van on board ORV Sagar Kanya for sub sampling of the seawater.



Figure 2.6: Seawater filtration, collection, acidifying and packing onboard ORV Sagar Kanya.

2.3 Analytical Protocols

The data reported for the dissolved concentrations of Fe and Zn in the present thesis were analyzed using flow injection systems. For the determination of low-level concentrations of Fe and Zn, a highly sensitive chemiluminescence and fluorometric methods were established in the laboratory for the first time. Flow injection is a method of introducing sample into the continuous flow of reagents through the detector. These flow injection techniques are inexpensive, reliable, less prone for contamination, and it is easy to transport. These flow injection instruments can be operated both offshore as well as onshore. The advantage of these systems compared to other available techniques (GFAAS- Graphite furnace atomic absorption spectrophotometer, ICP-MS Inductively coupled plasma mass spectrometers) is that in-situ determination of trace metals

immediately after collecting samples which reduces the contamination effects during storage and transportation.

Within the flow injection systems, different methods are available for determination of trace metals. For example, Fe determination can be done either using chemiluminescence or spectrophotometric detection. In this thesis work, Fe flow injection system by chemiluminescence method (Fe-FIS) to measure sub nanomolar to picomolar level concentrations of DFe in seawater and a Zn flow injection system by fluorometric detection is established to measure sub nanomolar level concentration of DZn in the seawater.

The following sections briefly discuss the methods for determination of Fe and Zn in seawater.

2.3.1 Determination of dissolved Iron by flow injection system using chemiluminescence method

The instrument consists of a miniature low power (5V) photomultiplier tube (PMT), micro-electric and solenoid actuated valves and processing electronics. The developed software allows full control of all flow injection components, processing and analyzing of data from the PMT. Moreover, a low-cost and innovative auto sampler using robotic arm is developed to perform the contamination free handling of liquid samples, which can intake 42 samples in one sequence without any user intervention. This miniature instrument is ideally suitable for shipboard measurements.

Seawater is preconcentrated on commercially available Toyopearl AF Chelate 650M resin. The instrument was successfully tested onboard ORV Sagar Kanya during the cruise SK-324 in 2015. The detection limit which is taken 3 times the standard deviation of MQ water for 2 minutes loading time is 20 pM. The precision of the system is < 5%.

2.3.1.1 Iron analysis method details

All bottles used for making standards and reagents were made of Teflon (NALGENE). Initially bottles were cleaned with 5% EXTRAN solution followed by soaking with 2N HCl and 1N HNO₃ for several days with cleaning in between bottles with ultra-high pure water (UHP) of resistance $R > 18.2 \text{ M}\Omega$. The acid

used for soaking the bottles were purified by distilling the quartz distilled acid in Savillex-1000 DST system. All reagents and standards were handled in the class-100 non-metallic horizontal laminar flow bench (CHEMETRON). A GILSON MINIPULS peristaltic pump was used for passing all the reagents and seawater sample. Two low-pressure six-port injection valves with two position microelectronic actuation for changing the direction of flow in between the analysis were used. Valve position details were shown in the Table 2.6. The schematics of the method details of the Fe system are displayed in the Figures, 2.7, 2.8 and 2.9. All manifold tubing used was PVC from Fisher Brand. Flow rates were mentioned in the flow diagram. For HCl, NH₄OH, luminol and H₂O₂ PVC tubing coded white-white was used. For seawater sample and rinse solutions tubing coded violet – violet was used and for sample buffer tubing coded yellow – orange was used. All PVC tubing was replaced regularly after every 72 hours of continuous usage. Temperature controlled water bath (COLE-PARMER) with a precision of ± 0.1 °C was used for maintaining the reaction temperature. High purity MQ was used for rinsing the column after loading of seawater sample to remove any interfering ions in the preconcentration column. Seawater was preconcentrated at a pH $\sim 3.9 \pm 0.1$ to retain Fe in the solution. To bring seawater pH to desired range, an ammonium acetate buffer solution of 0.12 M was prepared by mixing ultrapure acetic acid and ammonium hydroxide from Fisher scientific chemicals. A tapered inline column of length 1 cm (Global FIAS) was used in buffer line to remove any blank from the buffer line. To ensure all Fe in +3 form, 60 μ l of 1% H₂O₂ was added to the samples 1 hour before starting the analysis. Fe from the column was eluted using 0.4 N HCl diluted from ultrapure hydrochloric acid from fisher scientific. The released Fe mixes successively with 0.96 M NH₄OH (prepared from 25% Suprapure ammonium hydroxide MERCK chemicals), working luminol and 0.35 M H₂O₂ (From Suprapure 30% H₂O₂ solution MERCK chemicals) to produce a chemiluminescence signal at a constantly maintained temperature of 35 °C in water bath. The reaction coil in the water bath is 5m length and knitted as described by Selavka et al. (1987). Working luminol was prepared by taking 3 ml of stock luminol in 1000 ml MQ by adding 60 μ l of TETA solution. Working luminol is prepared 24 hrs before the

start of the analysis. Stock luminol is prepared by adding 270 mg of luminol and 540 mg KOH in 30 ml MQ. Stock luminol is prepared every 4 days. The intensity of the chemiluminescence signal is measured using the Hamamatsu photon counting head H8259-01. One analytical cycle took 500 S. The details of the photon counting head are given in Table 2.7. The complete set up of Fe Flow injection system is displayed in Figure 2.10.

Table 2.6: The valve operation during one analytical cycle of DFe

Cycle	Time	Valve Position 0	Valve Position 1	Operation
T0	0 to 10	A	B	Acid wash (Start of cycle)
T1	11 to 40	A	A	Conditioning
T2	41 to 160	B	A	Sample loading
T3	161 to 220	A	A	Rinse
T4	221 to 450	A	B	Elution (End of cycle)

Table 2.7: The Photon counting head H-8259-01 specifications

Specifications	
Photocathode area size	4 × 20 mm
Wavelength (Short and long)	185 nm and 850 nm
Input voltage	+4.5 V to +5.5 V
Count linearity	$2.5 \times 10^6 \text{ S}^{-1}$
Dark count Typ.	80 S^{-1}
Dark Count Max.	200 S^{-1}
Operating ambient temperature	+5 °C to +40°C

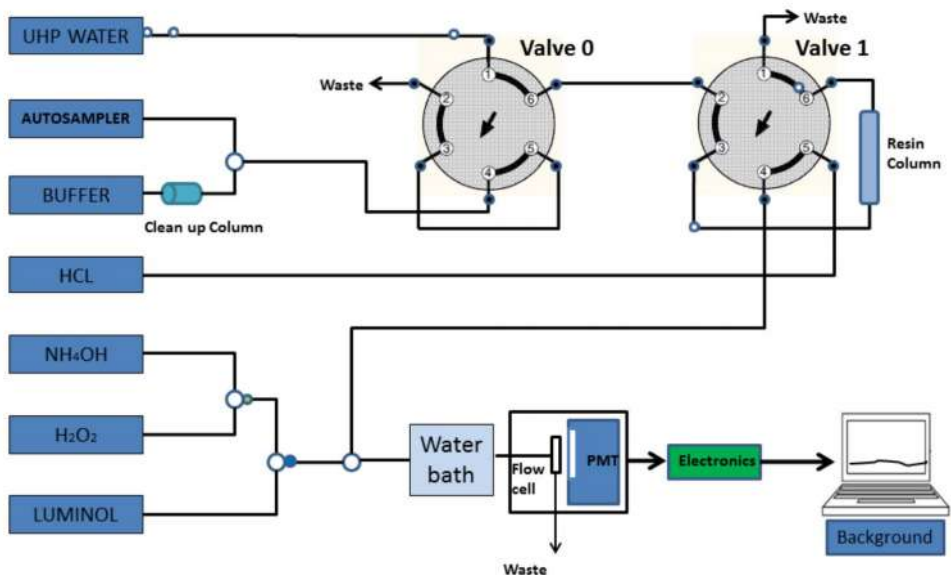


Figure 2.7: Schematic diagram for the rinse step to remove seawater matrix.

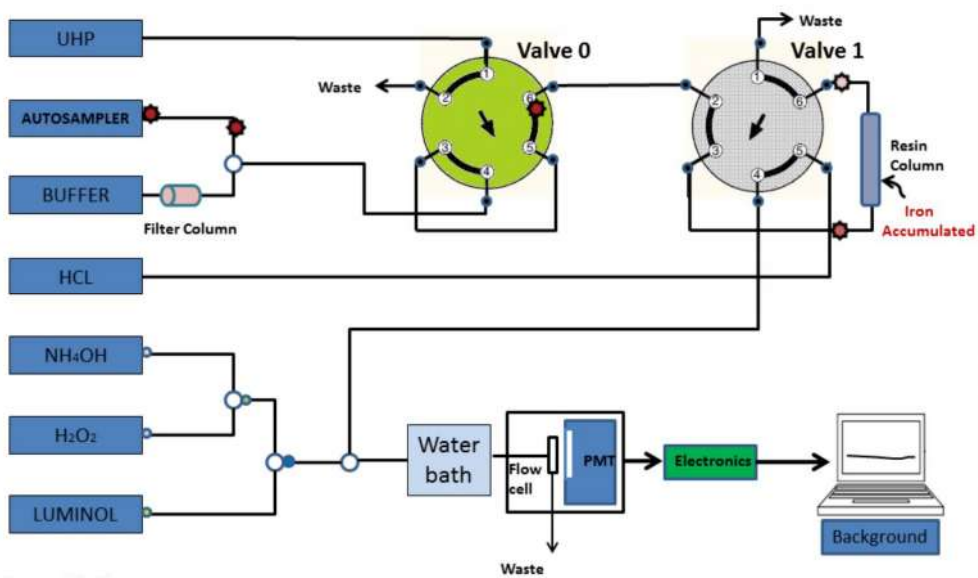


Figure 2.8: Schematic diagram for the retention of analyte during loading of the sample on column. Analyte is shown in circles.

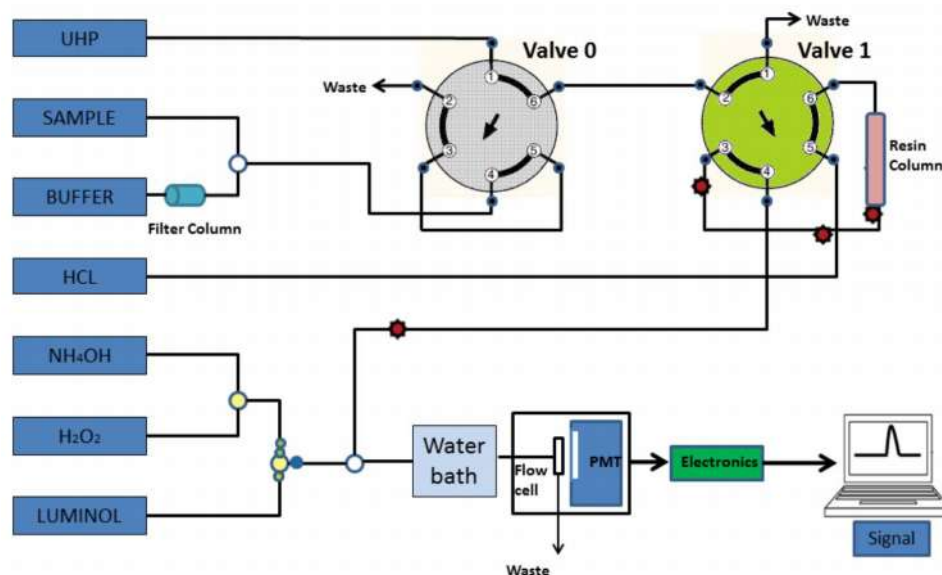


Figure 2.9: Schematic diagram for the elution of analyte from the column.

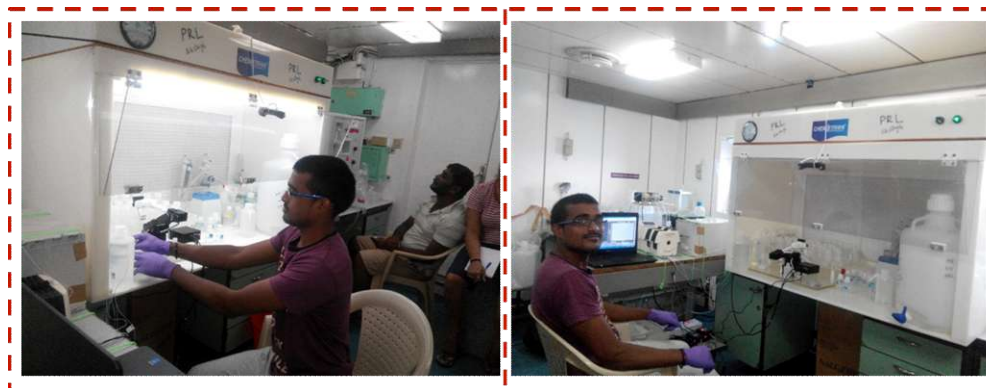


Figure 2.10: Analyzing DFe during SK - 324 cruise onboard ORV Sagar Kanya using Fe-Flow injection system.

2.3.1.2 Column Description

A Teflon column of length 6 cm with an inner diameter of 2.5 mm was used for pre-concentrating the Fe in the seawater sample. The resin used was Toyopearl AF Chelate 650M. A maximum volume of ~ 200 μ l of IDA (Iminodiacetate) resin is packed in the column. This resin is derivatized with iminodiacetic acid for immobilized metal affinity chromatography. The structure of the resin is shown in Figure 2.11 along with the image of column, which was made in-house. This resin has a ligand density of 25 - 45 μ eq/ml with an

adsorption capacity of ≥ 60 mg/ml. The in-house made Teflon column is shown in the Figure 2.12.

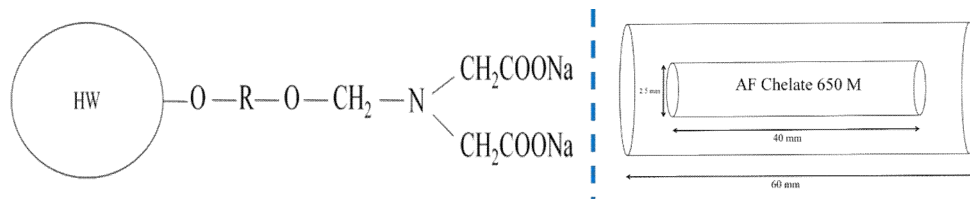


Figure 2.11: Showing the functional group of the Toyopearl AF Chelate 650M resin (left) and Teflon column dimensions (Right).

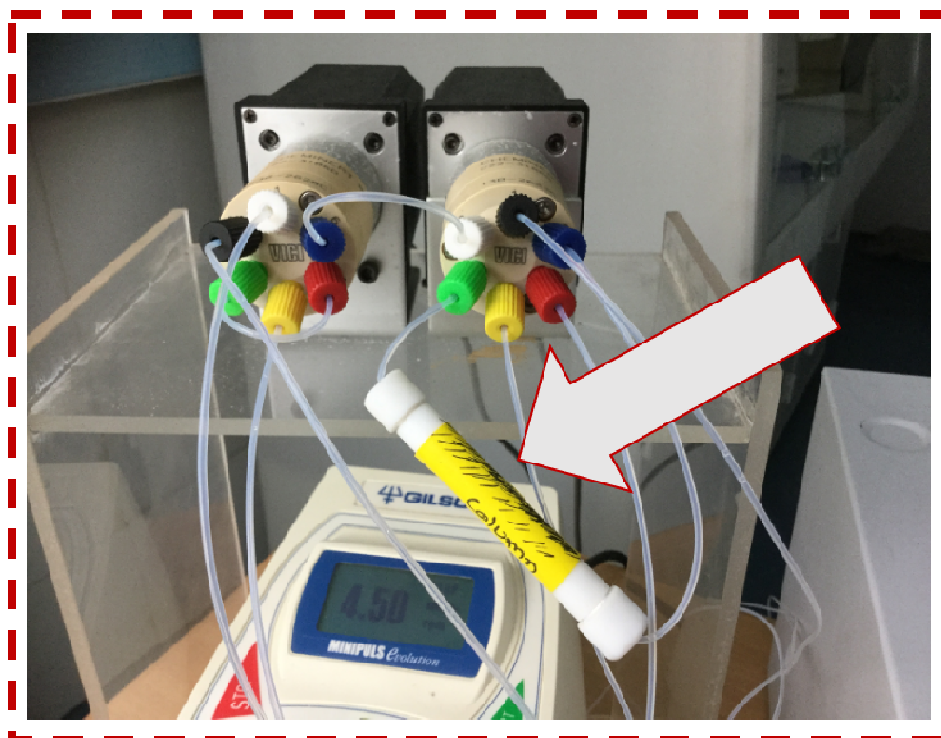


Figure 2.12: The two six port valves along with the 4 cm Teflon column (White arrow) used for preconcentrating DFe from the seawater sample.

2.3.1.3 Instrumentation

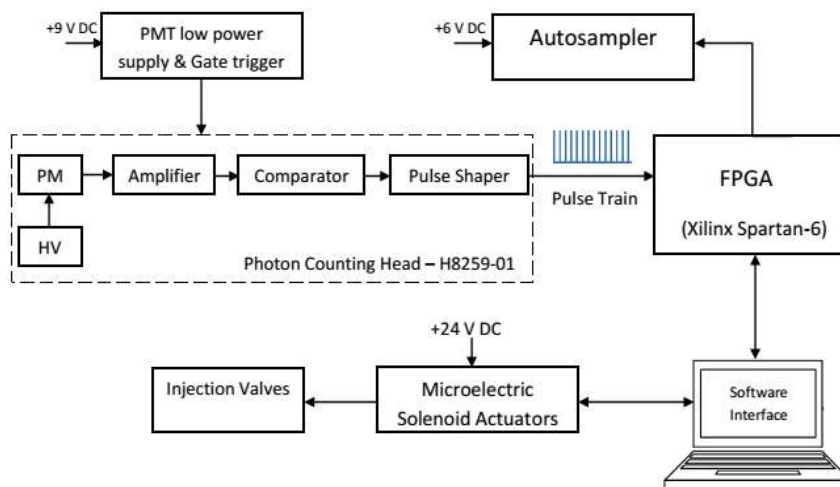


Figure 2.13: Block diagram of the main control unit and PMT interface of the instrument.

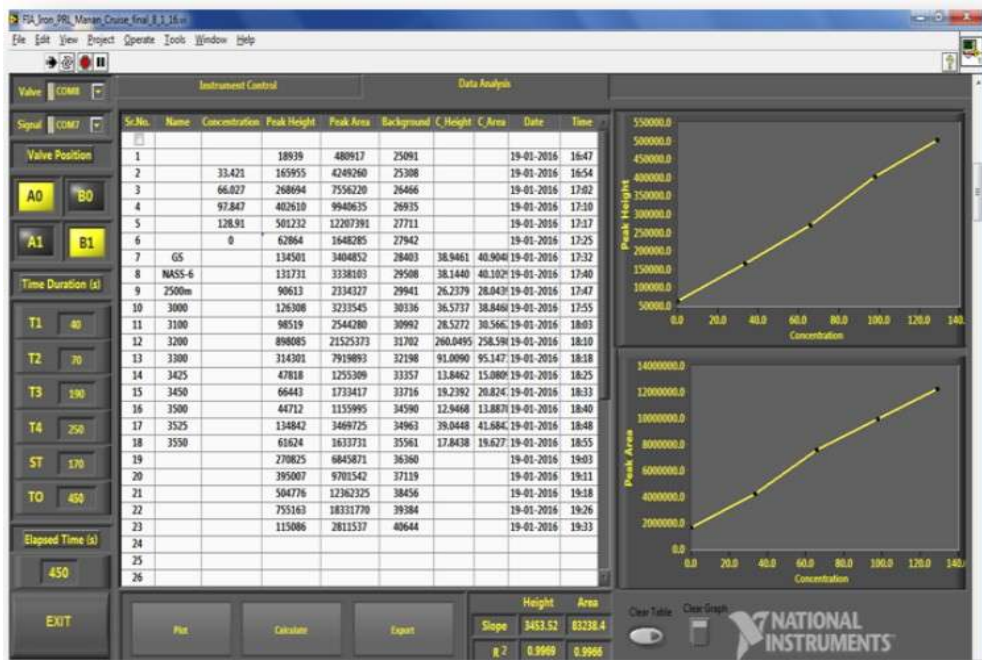
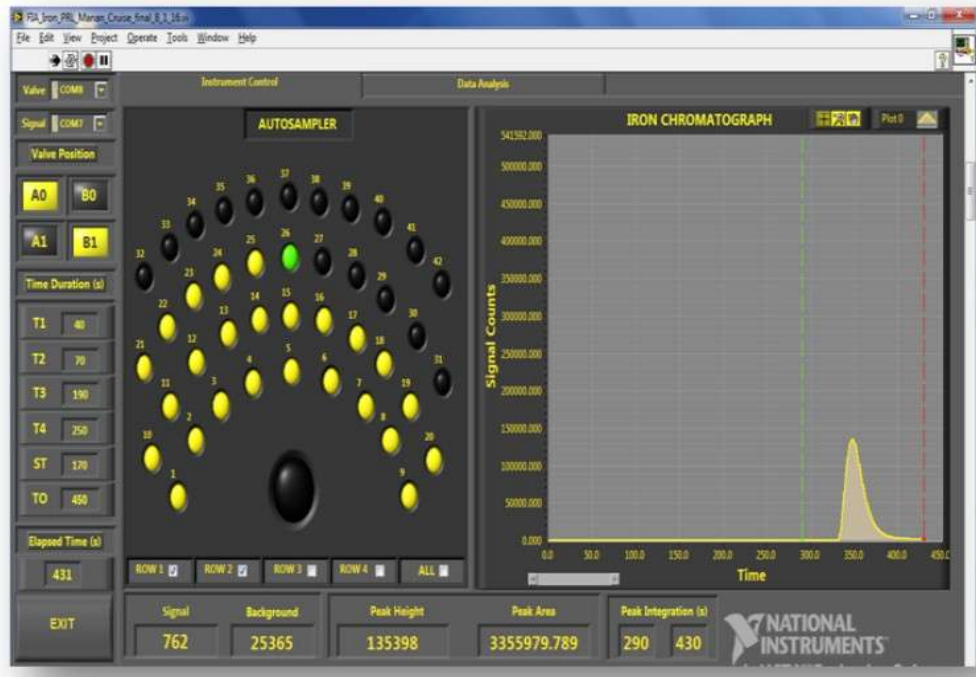
2.3.1.4 Hardware description

The instrument control (Figure 2.13) is mainly divided into three categories: PMT interface, control of auto sampler and injection valves. The control firmware is programmed into FPGA (Xilinx Spartan-6), which is an essential part of the system-hardware. It can operate at very high speed (100 MHz) and performs all the independent tasks concurrently. The photon counting head (H8259-01) operates at low power (5V) and can be remotely controlled by a gate trigger circuit. The signal from the PMT is amplified and shaped into positive logic pulses. These pulses are integrated by the FPGA through a 28-bit high-frequency counter generated in the firmware. The pulse integration time is selected from the range of 1 millisecond to 1 second as per the requirement. The 6-port two-state injection valves are operated with the help of micro-electric solenoid actuators by serial commands from the developed operating software. The switching time for a single operation is less than 150 milliseconds. The auto sampler is a very handy tool for contamination-free handling of samples, especially when there are large numbers of samples to be analyzed. A novel and inexpensive auto-sampler, using

a robotic arm, was developed to automate the sample sequence. In this approach, a robotic arm reaches to sample bottles as per the user determined sequence and a sampling tube attached to its arm gripper is inserted into the sample bottles for suction. The other end of a sampling tube is connected to the sample inlet via peristaltic pump. The sampling inlet has a diameter of 0.8 mm and is made of PTFE. The arm movement calculations are based on inverse kinematics approach. The design of the sample tray structure has provision of handling 42 samples in a single run. This auto sampler can be integrated with any analytical instrument making it useful for various liquid sampling applications. The robotic arm and sample stand are completely free of metals to avoid any contamination.

2.3.1.5 Software Interface

The instrument software called Virtual Instrument (VI) was written in LabVIEW version 2011. It facilitates user to control, monitor and analyze every element of the instrument. The software front panel (Figure 2.14) consists of two tabs Instrument control and data analysis. The communication interface has two units (USB-serial), one for controlling valves and one for PMT signal processing and for operating auto-sampler. The timing sequence (T1 to T4) for one sample analytical cycle is adjusted as per the requirement of chemiluminescence method and valve position is monitored on the panel. Individual sample or multiple samples can be selected from autosampler section. Instrument analyzes the selected samples in ascending order consecutively. Predefining the peak starting time and peak ending time is needed for calculating respective peak height and peak areas. At the end of each sample analysis, software calculates signal peak height, peak area in the predefined mentioned time (Where generally peak can be seen) and saves it for data analysis. The Fe Chromatograph of the each analyzed sample is saved to the predefined location in the computer storage. The standard calibration curve and slope-regression values are obtained just by a single click button. The unknown concentration of each sample is also calculated similarly using calibration curve. Every element in the front panel is connected in the wiring diagram (Figure 2.14) which includes functions for control operations, signal processing and data management.



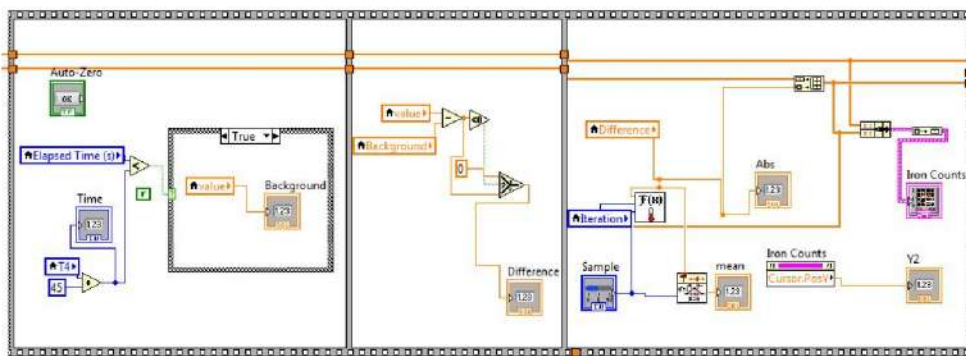


Figure 2.14: Software interface Instrument control tab and data analysis tab (Above) and partial graphical code for the instrument control and data acquisition (Below).

2.3.1.6 Calibration

A 1000 ppm Fe ICP single element standard traceable to SRM from NIST Fe (NO₃)₃ in 2-3% HNO₃ solution (MERCK) was used for making primary standards. Primary standards were prepared in UHP water by keeping pH 1.7. Ultrapure HCl was added to the precisely weighed MQ water to bring a pH of ~1.7. Working standards were prepared in seawater containing low Fe (or) prepared seawater by passing through the columns containing IDA resin. This seawater was prepared in bulk, about 500 ml every time during the seawater sample analysis. The working standards were made fresh every day during the analysis in low Fe seawater (LFeSW). A known amount of primary standard was added to the LFeSW to prepare working standards of 0.6, 1.2, 1.8 and 2.4 nM. LFeSW was taken by default as a 0 nM. The procedural blank was measured by passing UHP water in to the system as a sample for 120 seconds and this procedural blank was found to be less than <60 pM. During the course of one analytical cycle a total of ~40 samples were analyzed which includes 5 working standards, blanks, reference standards, seawater samples and repeats.

The Fe flow injection system was operated onboard SK-324 cruise during September – October 2015 and the analyses were completed successfully without any interruption. A total of 18 full vertical profiles were measured during 40 days of the cruise. Figure 2.16 shows the vertical profile of DFe measured onboard at station-4 in Arabian Sea collected at 15.35° N, 65° E. The profile matches with the typical open ocean profile for DFe in the seawater.

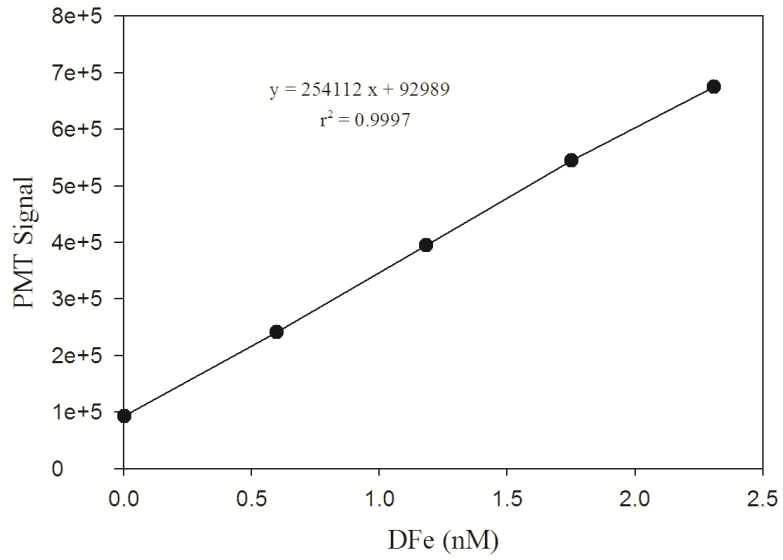


Figure 2.15: Standard additions of Fe to the low Fe seawater.

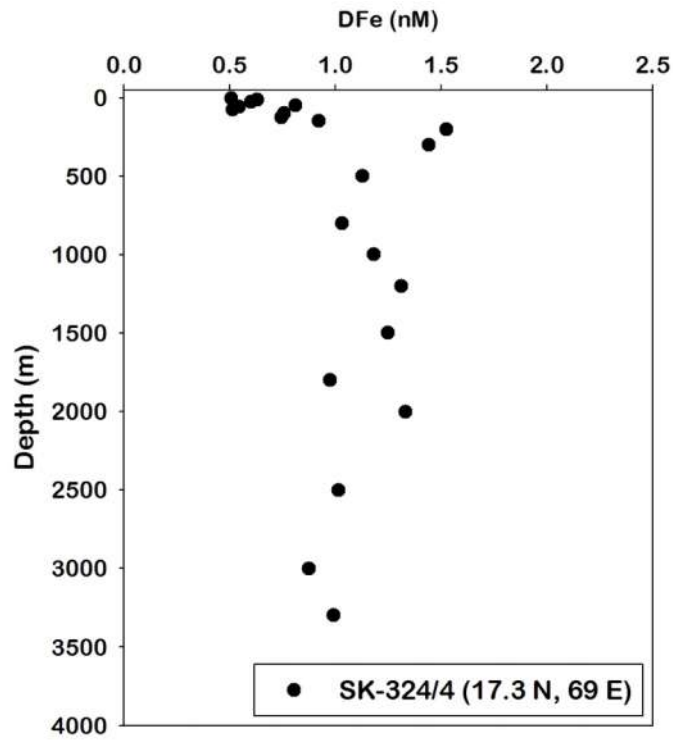
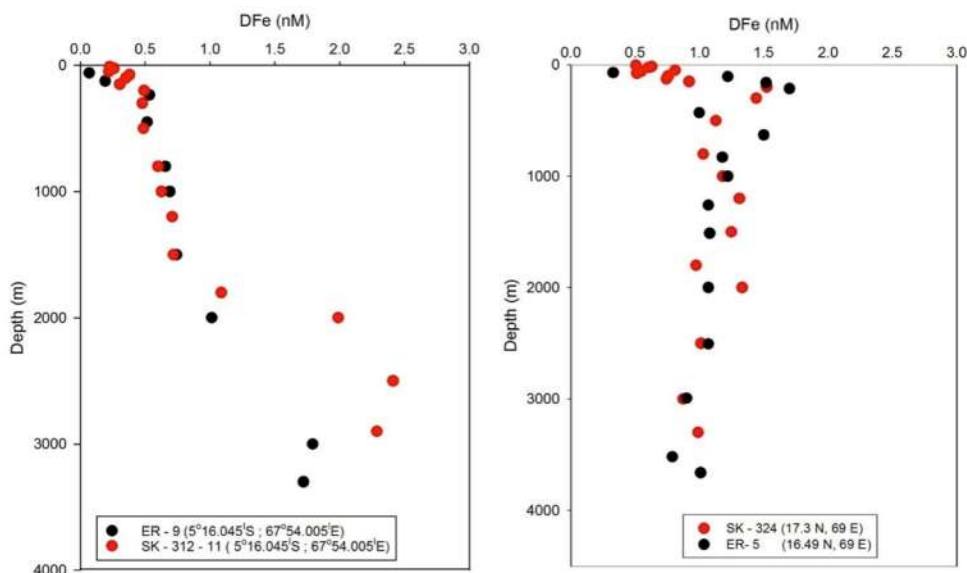


Figure 2.16: Vertical profile for DFe during SK - 324.

2.3.1.7 Inter and intra comparison of DFe data

Cross-over stations have to be occupied for checking sampling and measurement quality between groups to establish a homogenous platform for maintaining the data quality. Especially, these comparisons are required for the trace metal determination in seawater (Johnson et al, 2007). In view of this, we occupied two stations in Arabian Sea during SK 324 and SK 312 cruises, where sampling and analysis for DFe was done earlier by Nishioka et al. (2013) under JAPANESE-GEOTRACES programme. The sampling period of Japanese group was November 2009 to January 2010. The SK 312 and SK 324 cruises sampling was done during May 2014 and September 2015. The data reported for DFe were produced using FIA chemiluminescence detection based on Obata et al., (1993). The results obtained in this study show very consistent and reliable with respect to the published work of Nishioka et al. (2013). During the cruise SK-311, we have sampled SK-311/5 station close to our previous cruise station SK-304/22. We have compared these two stations to check consistency in the sampling. The comparison of vertical profiles of DFe measured by both the laboratories and intra comparison between our own cruises is shown in Figure 2.17.



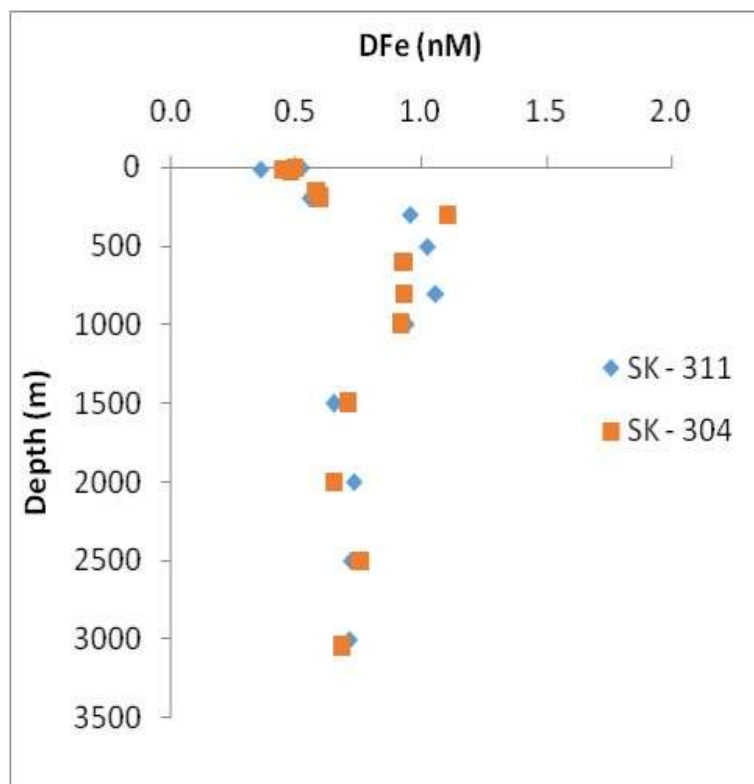


Figure 2.17: Comparison of DFe data between GEOTRACES-JAPANESE group and GEOTRACES-INDIA group at the same location (Above), DFe data from the same location sampled during two different cruises under GEOTRACES-INDIA.

2.3.1.8 Accuracy and precision of the method

The accuracy and precision of the established method were checked by measuring available reference standards for the trace metals during the analysis of reference seawater samples. These reference samples were provided by Prof. Kenneth Bruland and Dr. Smith (California University, Santa Cruz). Figure 2.18, shows the locations of these reference materials, which were collected in North Atlantic and North Pacific oceans. The certified value for GS, SAFe D1, SAFe D2, GD are 0.54 ± 0.04 (nM), 0.67 ± 0.04 (nM), 0.93 ± 0.17 (nM), 1.00 ± 0.10 (nM) (Johnson et al., 2007, Bruland Research Lab). The mentioned errors are 66% standard deviation (1 Sigma). In addition to these reference materials, NASS-6 standard procured from National Research Council of Canada is analyzed whose certified value is 0.495 ± 0.046 $\mu\text{g/L}$. The reported values for above stated reference standards are shown in Figure 2.19. The consensus value for the NASS-6

is beyond the linear range of the currently established method. The current method calibration was done up to 2.7 nM of DFe concentration. The NASS-6 values reported in the Figure 2.18 (E) were 15 times diluted with MQ. The reported value after correcting dilution factor is $0.484 \pm 0.090 \mu\text{g/L}$ ($n=27$) which agrees very well with the consensus value given by the Canadian research council.

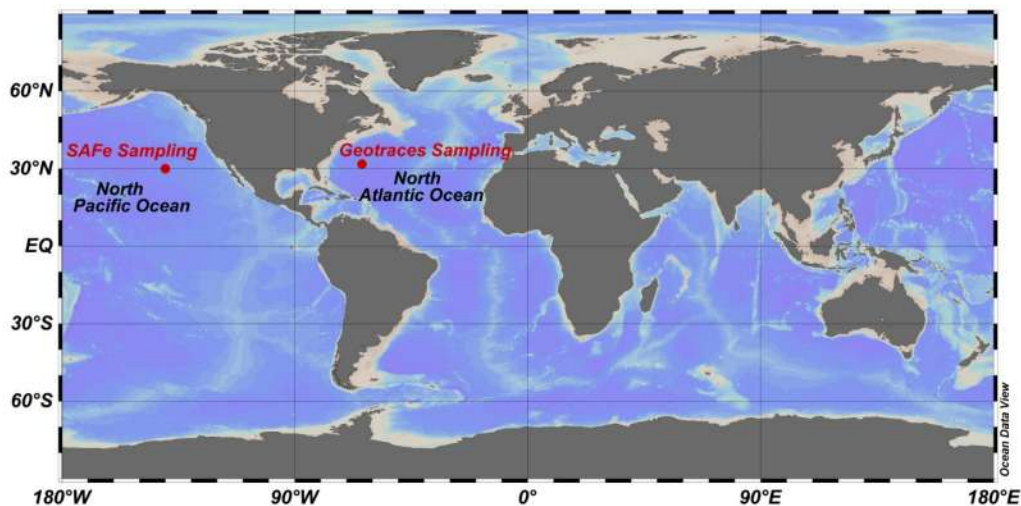
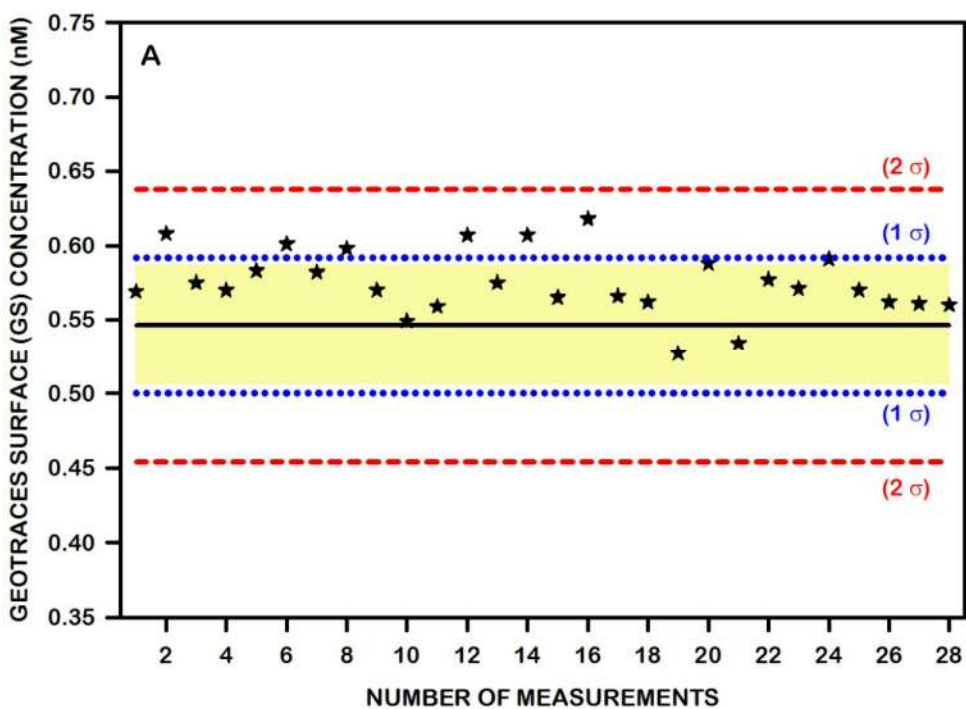
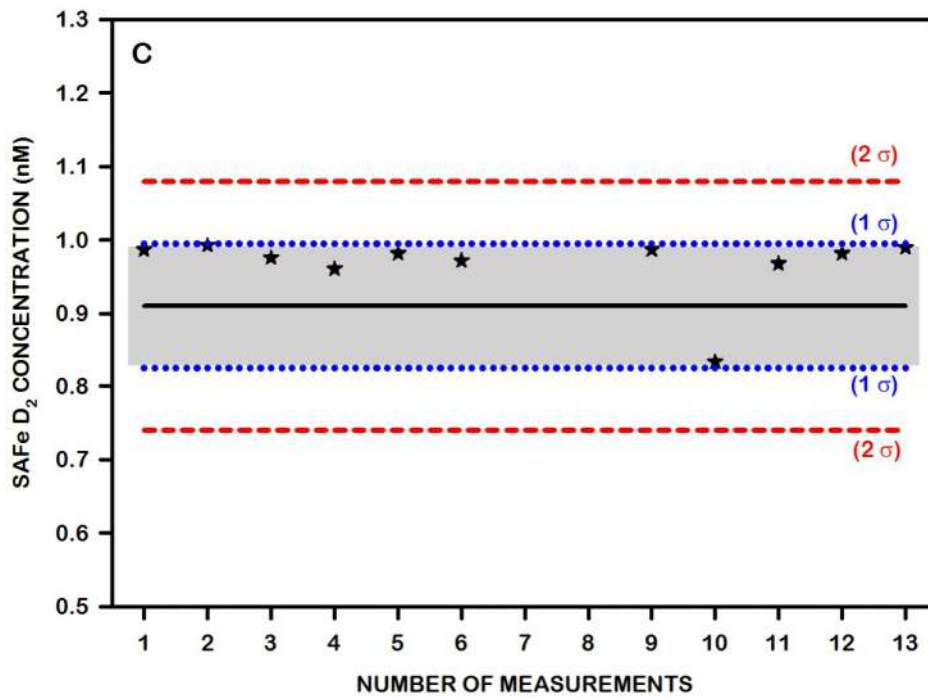
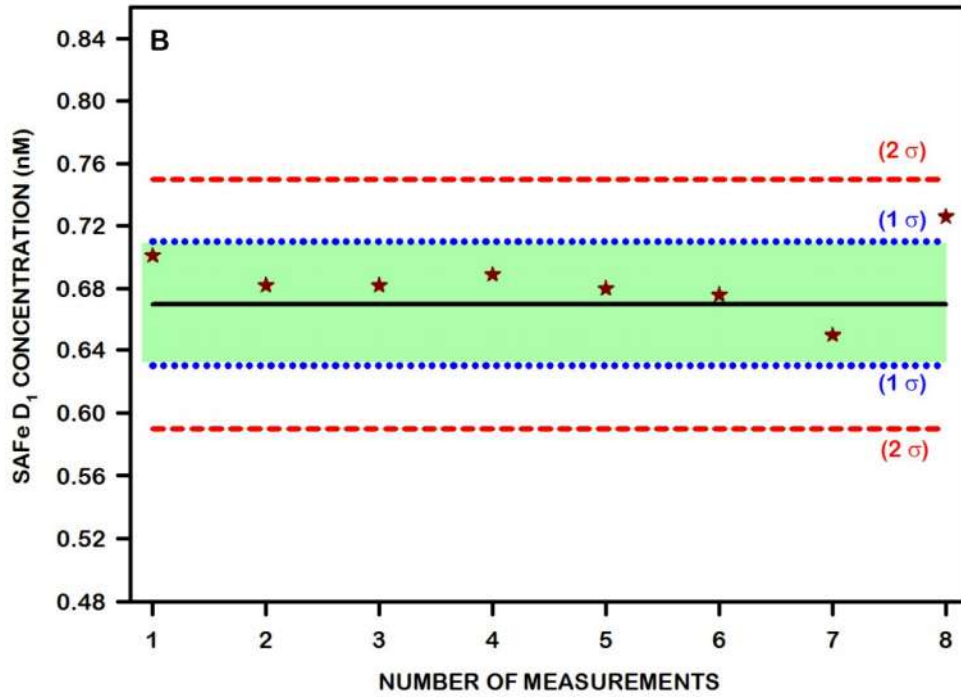


Figure 2.18: Locations for the Reference standard materials for SAFE and GEOTRACES standards.





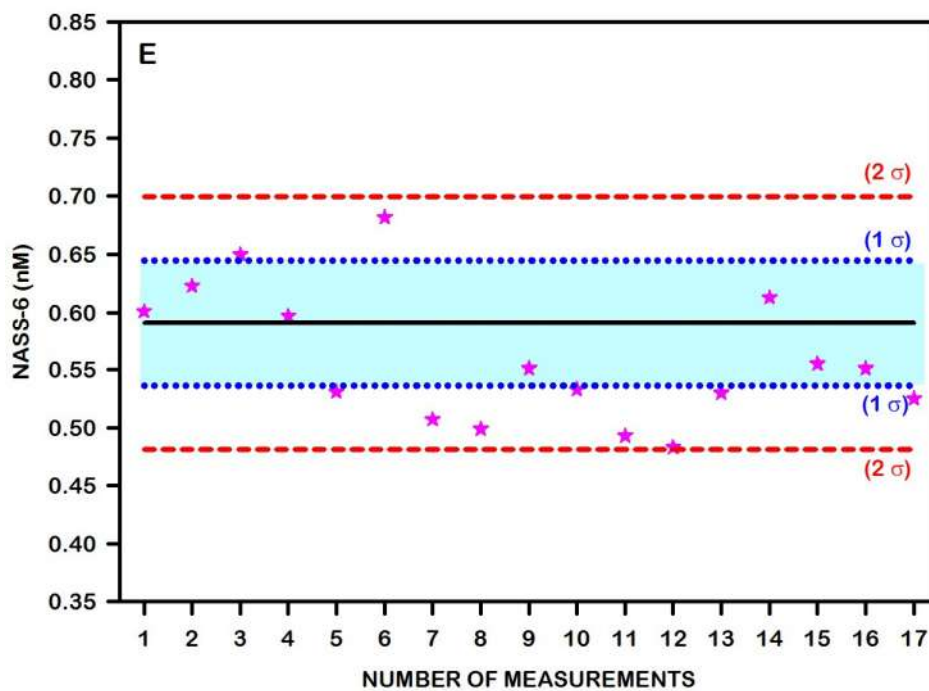
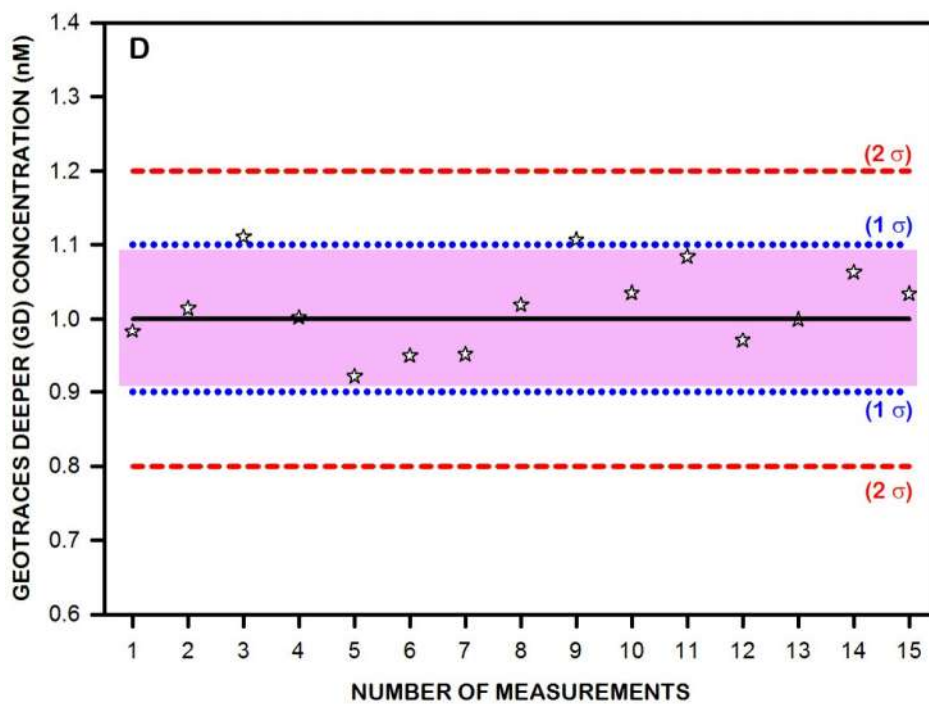


Figure 2.19: Reported values for reference standards. **(A)** GEOTRACES Surface sample (GS), **(B)** Sampling and analysis for Iron deeper sample (SAFe D1), **(C)** Sampling and analysis for Iron deeper sample (SAFe D2), **(D)** Geotraces deeper sample (GD), **(E)** Seawater reference material for trace metals by National Research Council Canada. The solid black line represents the average value of the reference standard. Blue dotted lines represent the 1σ deviation. Red lines shows the 2σ variation in the samples. The colored region represents 1σ standard deviation from the average reported value. The reported values are **(A)**, GS – 0.57 ± 0.02 nM (n=28), **(B)** D1 – 0.68 ± 0.02 nM (n=8), **(C)** D2 – 1.01 ± 0.13 nM (n=13), **(D)**. GD – 1.01 ± 0.05 nM (n=15), **(E)**. NASS-6 – 0.57 ± 0.10 nM (n=27).

2.3.2 Determination of dissolved Zinc by flow injection system using fluorescence method

DZn data documented in the thesis is generated using Zn flow injection system based on fluorometric detection. The Zn flow injection system consists of peristaltic pump, Fluorescence detector, two 6 port positioned valves and a robotic arm (Figure 2.20). The complete details on the Zn method, precision and accuracy are described in the following sections.

2.3.2.1 Zinc analysis method details

Samples were analyzed for Zn using a flow injection system by fluorescence detection (Nowicki et al., 1994; and Gosnell et al., 2012). Samples were buffered offline at a pH $\sim 5.1 \pm 0.1$ and preconcentrated on AF Chelate 650M iminodiacetate resin for 2 minutes. Samples were buffered using 2M ammonium acetate buffer. 1ml of this sample buffer was added to a 30 ml of pH 1.7 seawater samples to bring the final pH of the sample to the range of 5.1 to 5.2. Buffering of the samples was done one hour before the start of the analysis. After loading, the column is rinsed for 90S with 0.16M NH_4Ac and successively column is eluted with 0.08M HCl to remove Zn from the column. The eluted Zn mixes with the pTAQ reagent to give the fluorescent signal. Zn forms a stable complex with Para Tosyl Amino quinoline (p-TAQ) which is a critical reagent in this method. The structure of p-TAQ and its complex with the Zn is shown in the Figure 2.20. The fluorescence was measured using RF20A Shimadzu Fluorescence detector at 365 nm excitation and 500nm emission wavelengths. At the end of the analysis column is cleaned with 1N HCl for 20S. Columns

containing Nobias PA1 resin were placed in line to rinse and pTAQ channels to reduce the blank contribution.

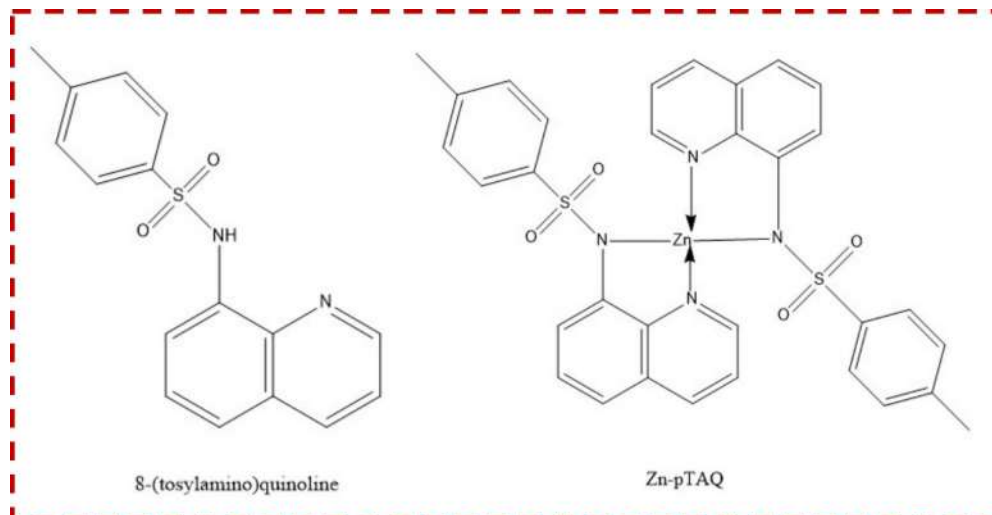


Figure 2.20: Structure of p-TAQ and Zn-pTAQ

GILSON minipuls peristaltic pump was used for pumping the reagents. PVC manifold tubing coded Blue – Yellow is used for sample, rinse and pTAQ working reagents and PVC tubing coded Grey – Grey is used for HCl. The manifold tubings used were procured from Fisher brand scientific chemicals. All the other tubings used were made of PTFE (Fisher scientific) of internal diameter 0.8 mm.

All reagents were prepared in clean Teflon bottles. A 2M ammonium acetate sample buffer is prepared by mixing the ultrapure acetic acid (Fisher scientific) and ultrapure ammonium hydroxide (Fisher scientific) in the ultrapure water (18.2 MΩ cm). A stock solution of pTAQ is prepared by mixing 0.291 g of pTAQ in 20ml triton and the solution is stirred for 24 hrs. The stock solution was prepared 2 months before of its use for preparing working solution of pTAQ. The working solution of pTAQ was prepared by mixing 100 ml of 1M boric acid, 25 ml of 2M NaOH in 1000 ml ultrapure water by adding 800 μl of stock pTAQ solution. 1M boric acid is prepared by mixing 31g boric acid (Supra pure, Merck chemicals) in 500 ml ultra-sonicated pure water. 2M NaOH is prepared by mixing

2g NaOH (trace metal grade, Sigma Aldrich) in 25 ml pure water. All reagents were prepared freshly every time. One analytical cycle took 10 minutes.

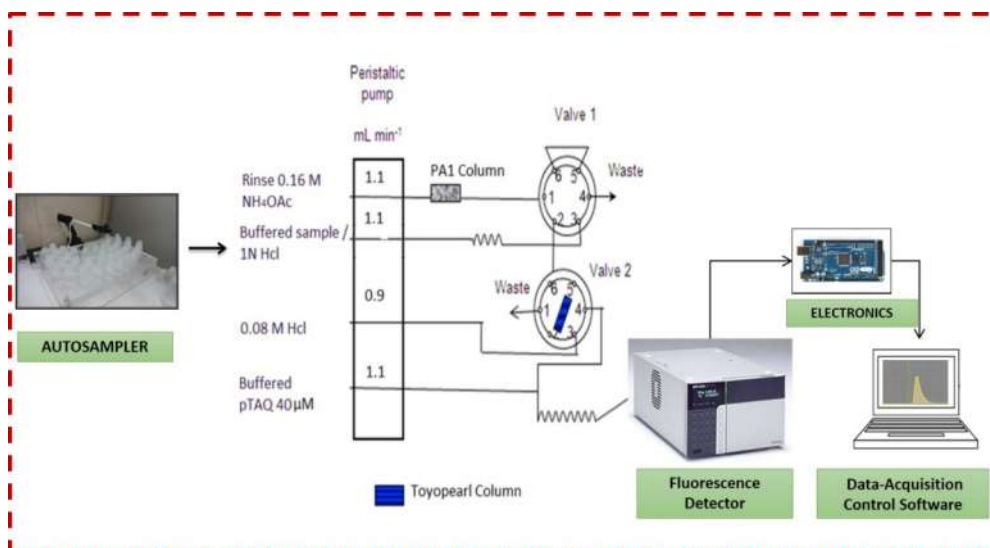


Figure 2.21: Schematic diagram for Zn flow injection method and system components.

The operation and valve position during a single analytical run was mentioned in the Table 2.8. The starting and ending positions of the valve are in AB mode. In this mode, 0.08 M HCl passes through the column and makes it sure that no Zn is retained in the column. To make sure that no memory effect is there, the ending and opening modes were kept AB mode. The Zn flow injection system is displayed in the Figure 2.22. Software for the flow injection system was developed in the LAB view software and front panels of the auto sampler and chromatograph windows are shown in the Figure 2.23.

Table 2.8: Valve position and timings during one analytical cycle.

Position	Valve Time (s)	Mode	Reagents
AB	0-110	Elution	0.08 HCl
BA	110-350	Loading	Sample
AA	351-430	Rinse	0.16M NH ₄ Ac
AB	431-500	Elution	0.08 HCl
BA	501-520	Cleaning	1M HCl
AB	540	Cycle Ends	

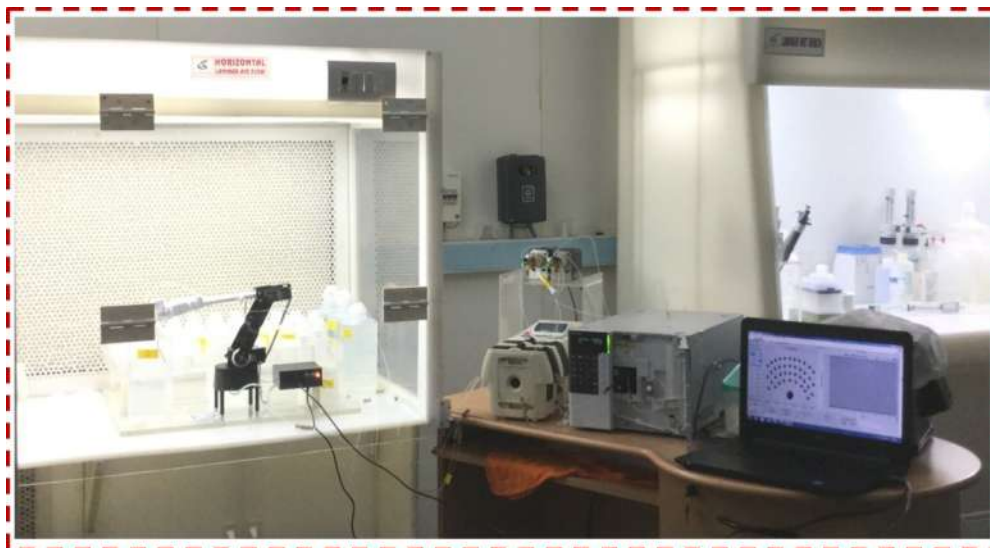


Figure 2.22: Zinc flow injection system.

2.3.2.2 Software interface

The interface is made in the LAB view (National Instruments) software to control the valve operation without any user interference. Figure 2.23 displays the front panel of the instrument and Chromatograph control tabs. The front panel of the developed software mainly shows three tabs namely (1) Instrument control tab, (2) Data Analysis tab and (3) Chromatograph tab. As previously described, in a single operation there is a feasibility of running 42 samples continuously. There is a possibility of choosing any sample at any point of time and it can be done by directly clicking on the numbers displayed in the instrument control tab. Once the sample analysis is done the data is automatically displayed in the corresponding numbers of the data analysis tab. The peak tailing and shape of the particular sample can be seen from the chromatograph tab.

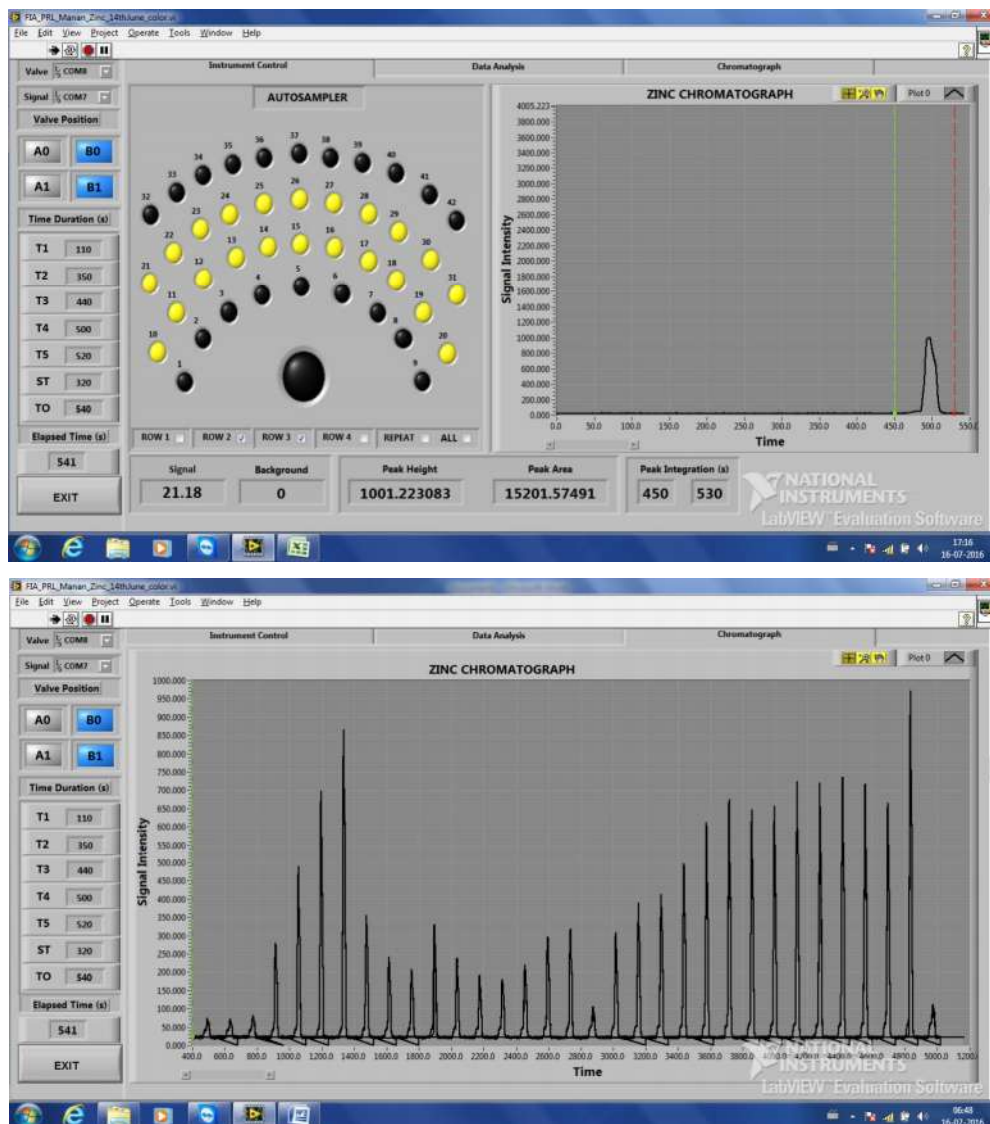


Figure 2.23: Zn flow injection system software and data control windows.

2.3.2.3 Cadmium interference

The flow injection method established for Zn determination by fluorescence detection is having an interference with Cadmium, but still this method gives promising results during offshore as well as onboard. Cadmium also forms stable complexes with the pTAQ (Para tosyl amino quinoline). This study found 70% interference with Cd in this method consistent to the previously published work(Nowicki et al., 1994) with 70% interference, 67% interference

signal (Wyatt et al., 2014). The interference found in this study is much higher compared to 30% interference signal reported by Gosnell et al. (2012). Zn concentrations were measured by correcting 70% interference signal from the Cadmium (Cd) concentrations. Cd concentrations were estimated using the global Cd:PO₄⁻³ relationship given by Boyle, 1988. Gosnell et al. (2012) preconcentrated the sample at pH ~ 5.05 ± 0.05 using HQ resin whereas Wyatt et al., (2014) preconcentrated seawater at a pH of 5.2 using IDA resin. The recent work of Janssen and Cullen (2015) has overcome the problem of interference with the Cadmium by using the NTA resin at a pH of 4.3. A change in the preconcentration pH of IDA resin may differentiate both Zn and Cd. This needs to be confirmed by conducting detailed experiment. In this work, Zn is preconcentrated using IDA resin at a pH of 5.1 ± 0.1.

Boyle, (1988) observed a significant relation between Cd and Phosphate in the oceans (Figure 2.24). The data used to establish the relation between Cd and Phosphate was from North east Pacific Ocean, North West Atlantic Ocean, North Atlantic Ocean, Gulf of Mexico and Arctic Ocean.

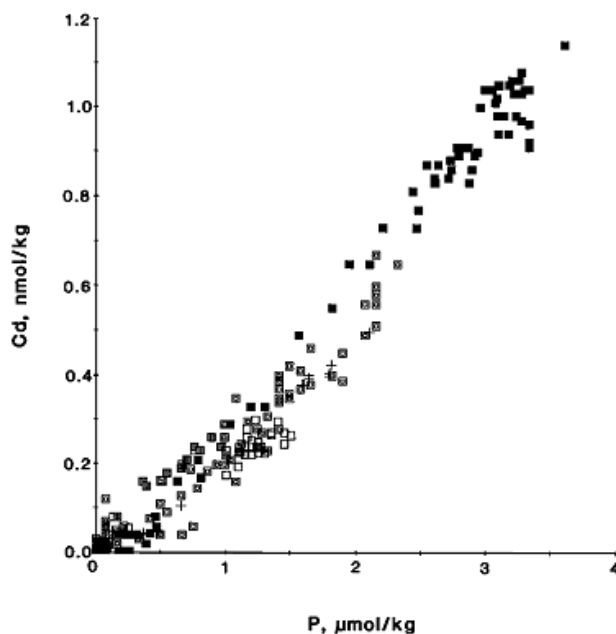


Figure 2.24: Cd vs. P relationship in the seawater taken from Boyle (1988).

Boyle, 1988 observed a kink between Cd and P at 1.3 μM of Phosphate concentration. He observed two significant slopes between Cd and P for Phosphate concentrations. The observed slopes are

$$\text{Cd (nM)} = (0.21) (\text{Phosphate } (\mu\text{M})) \text{ [For Phosphate } < 1.3 \mu\text{M}] \text{ and}$$

$$\text{Cd (nM)} = (0.40) (\text{Phosphate } (\mu\text{M})) \text{ [For Phosphate } \geq 1.3 \mu\text{M}]$$

The above equations are used to correct the Zn concentrations obtained by the Zn flow injection method. In general, in the open oceans the Cd concentrations reaches up to a maximum of 1 nM in the deeper samples, whereas Zn reaches to a maximum of 10-12 nM. Therefore, 70% of the Cd signal in the open ocean is around 0.7 nM (if it is deeper sample) which is about 7% of the total signal. This 7% signal has been corrected based on global relation of Cd and P (Boyle,1988) which is very reliable.

2.3.2.4 Calibration

A 1000 ppm Zn ICP single element standard traceable to SRM from NIST Fe $(\text{NO}_3)_3$ in 2-3% HNO_3 solution (MERCK) was used for making primary standards. Primary standards were prepared in UHP water by keeping pH~1.7. Ultrapure HCl was added to the precisely weighed MQ water to bring a pH of ~1.7. Working standards were prepared in seawater containing low Zn, which is prepared by passing the seawater through the PA-1 cartridge. This seawater is prepared in bulk, about ~500 ml every time during the seawater analysis. Fresh working standards were made every day during the analysis time in low Zinc seawater (LZnSW). The instrument was successfully checked onboard during the cruise SK-338. Calibration was done by collecting the surface sample (This sample was collected at Fluorescence maxima). This sample collected for LZnSW was brought immediately to a pH of 5.0 ± 0.1 and passed through PA-1 resin to remove the Zn in the sample and the column passed solution was used for making the working standards. A known amount of primary standard was added to the LZnSW to prepare working standards of 0, 3, 6, 9 and 12 nM. LZnSW was taken by default as a zero nM.

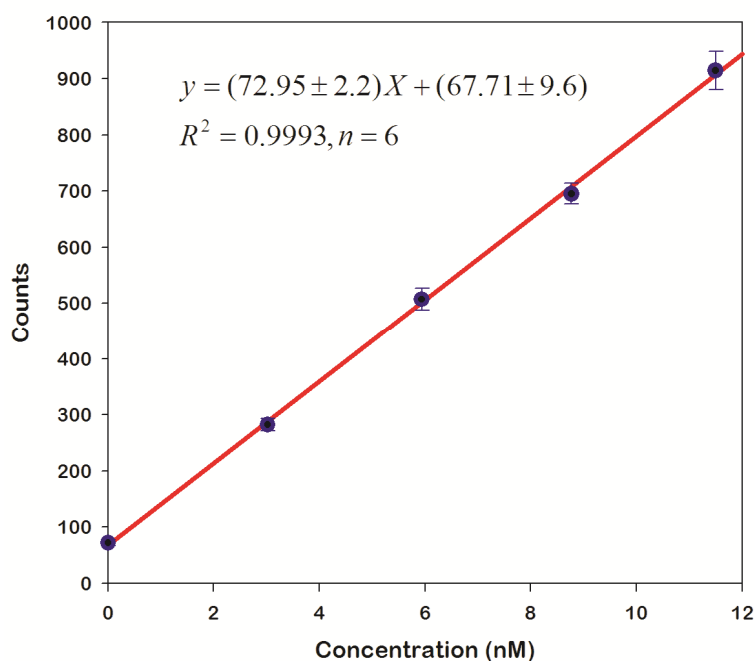


Figure 2.25: Calibration graph for the Zinc in the seawater.

The zero nM working standard was considered as a blank for the system. This blank found to be around 0.8 nM. During the course of one analytical cycle ~40 samples were analyzed, which includes 5 working standards, blanks, reference standards, seawater samples and repeats. The Figure 2.25 shows the calibration produced for determining the Zn concentrations in the seawater by the standard addition method.

2.3.2.5 PA-1 resin description

PA-1 resin is also called Nobias chelating resin. This resin is highly selective for the trace metals in the seawater. This is the combination of the EDTA (Ethylene diamine tetra acetate) and IDA (Imino diacetate resin). Due to this combination the resin is more selective for trace metals with the increase of the pH range for pre concentration of trace metals. Researchers analyzing trace metals on ICP-MS are widely using PA-1 resin due to its broader range of pH for holding trace metals and more tendencies for metal binding. The structure of PA-1 is given in Figure 2.26 that shows forming chelating bonds with the Nickel and Copper.

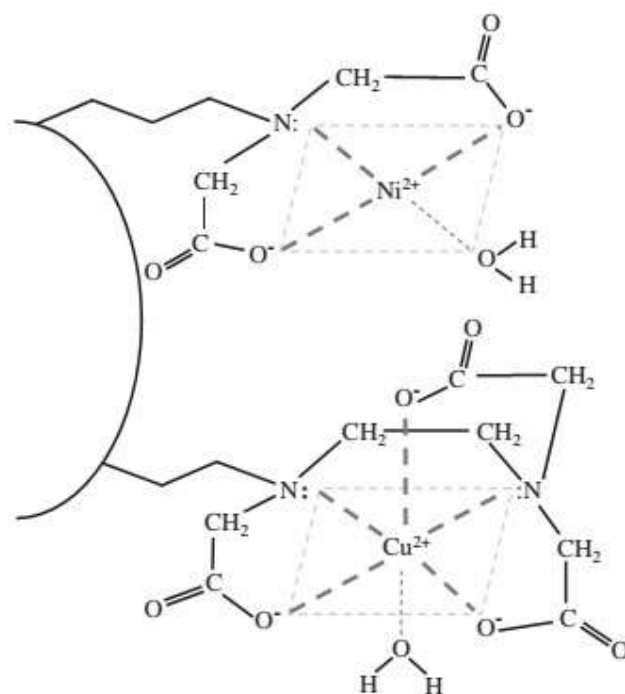


Figure 2.26: Structure of Nobias resin chelating with the Nickel and Copper trace metals.

2.3.2.6 *Inter-comparison*

Sampling the same location by two different groups in same/different times and comparing the results is the strict protocol to check the quality of data in the GEOTRACES programme to achieve and to know the quality of the sampling and analytical precision. In the Northeastern Indian Ocean, there exist very scarce studies for the distributions of DZn in the water column. Studies so far reported were Vu and Sohrin, (2013) restricted to only one full vertical profile in the BoB and Kim et al, (2015) with one profile in the BoB and the remaining stations in the Andaman Sea. We compared the DZn data obtained in this study with the DZn profiles reported by the Vu and Sohrin. (2013) and Kim et al. (2015). The profile trend is in good agreement with the published data of this region. The data for DZn reported in Vu and Sohrin. (2013) and Kim et al. (2015) were obtained from the published research articles and GEOTRACES IDP 2014 data. Vu and Sohrin (2013) measured samples for DZn using HR-ICP-MS and Kim et al. (2015) data for DZn profiles were obtained using Cathodic stripping voltammetry. In the

present study, DZn data was produced using Flow injection system by fluorometric detection.

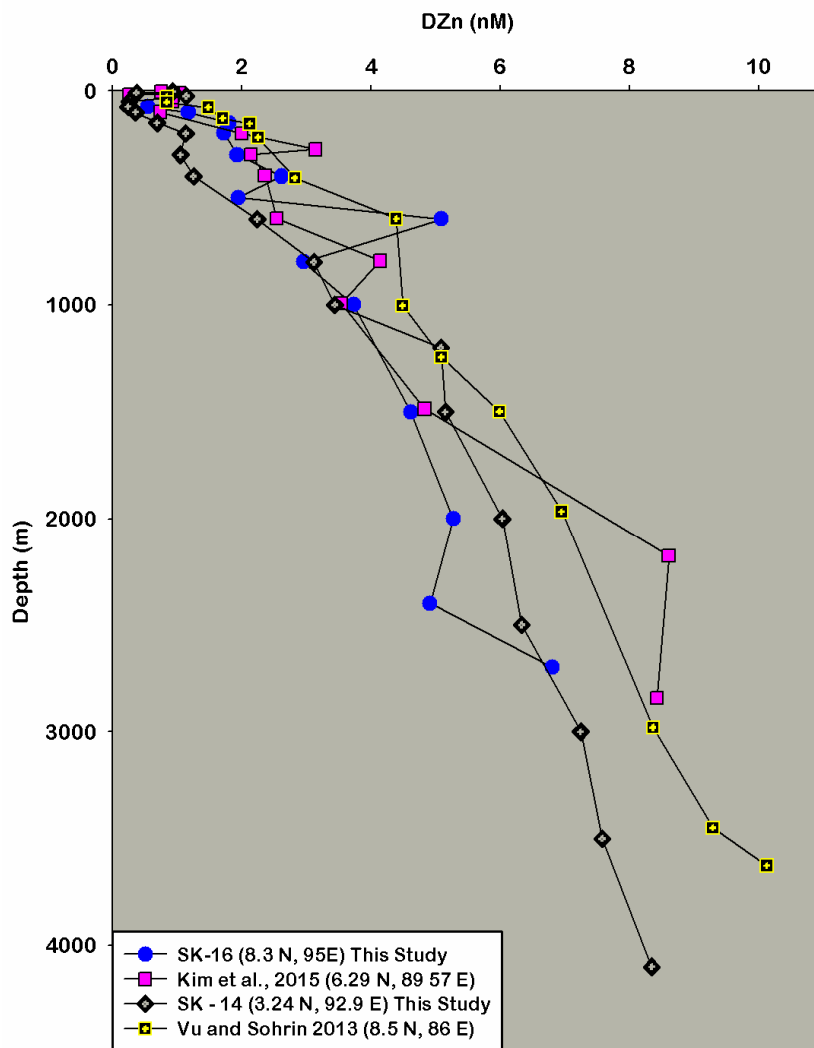


Figure 2.27: Comparison of vertical profile of DZn analysed during SK 304 with other existing data in the BoB.

During GEOTRACES GI-10 cruise, we re-occupied a station in the Bay of Bengal, where GEOTRACES Japanese group sampled earlier and where DZn data was reported. The data obtained during both the cruises are compared (Figure 2.28) which displays a very good similarity. DZn is measured onboard using flow

injection system during GI-10 cruise. The Japanese group analyzed DZn data by using High Resolution Inductively coupled plasma Mass Spectrometry (HR-ICP-MS).

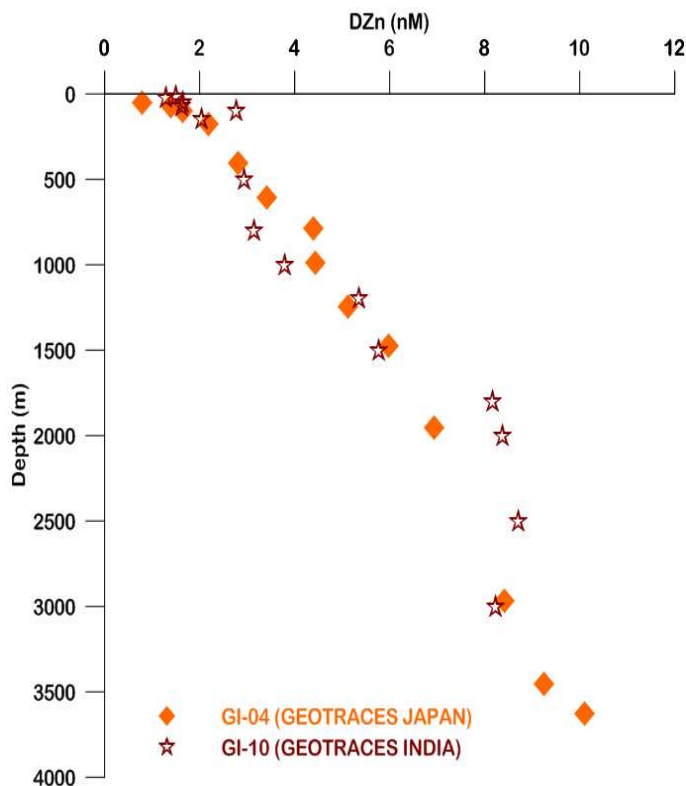
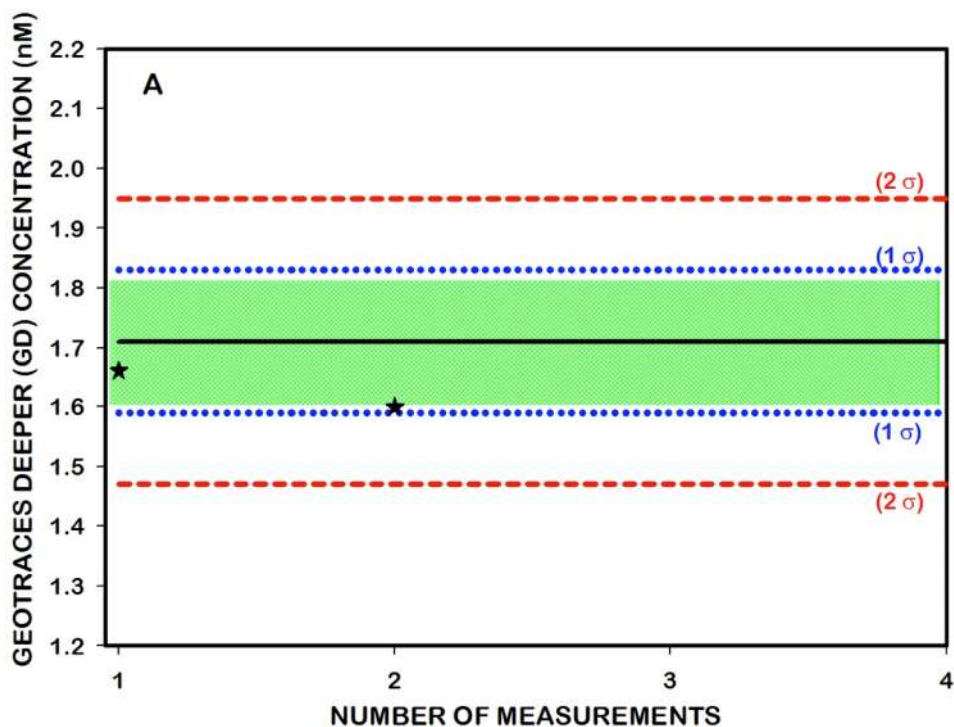


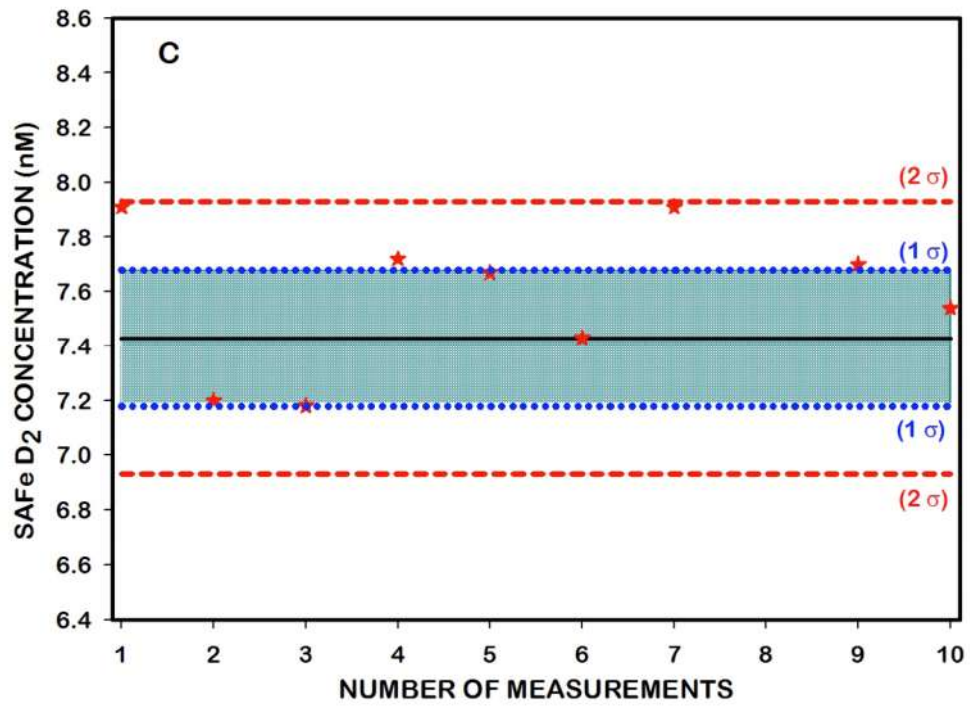
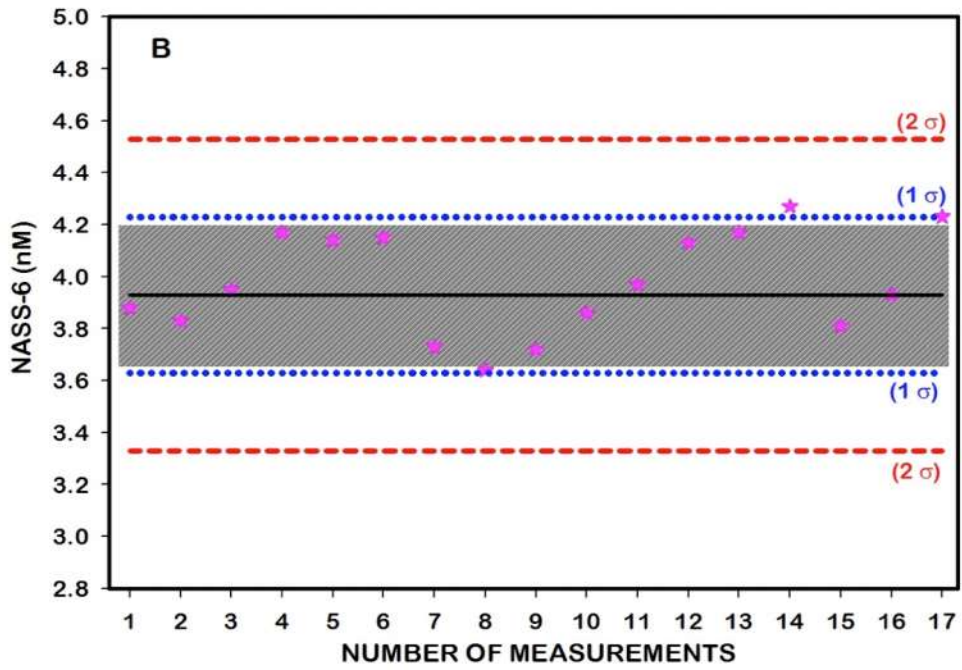
Figure 2.28: Comparison of vertical profile of DZn acquired during SK-338 Cruise with those of the Japanese data in the BoB.

2.3.2.7 Accuracy and precision of the measurement

Accuracy and precision of the method for the measurement of Zn in seawater by fluorometric detection are checked by measuring available reference standards for the trace metals during the analysis of seawater samples. These reference samples were provided by Prof. Kenneth Bruland and Dr. Smith (California University, Santa Cruz). These reference material were collected as a part of Sampling and Analysis for Iron in seawater programme. Figure 2.17, shows the location for these reference materials, which were collected in North Atlantic and North Pacific oceans. The certified values for SAFe S, SAFe D1, SAFe D2 and GD are 0.069 ± 0.010 (nM), 7.40 ± 0.35 (nM), 7.43 ± 0.25 (nM) and 1.71 ± 0.12 (nM), respectively (Johnson et al., 2007), (Bruland research Lab).

These certified values are reported by averaging the values reported by many laboratories during ascertaining the values for this reference material. In addition to these reference materials, NASS-6 standard, procured from National Research Council, Canada is analyzed whose certified value is 3.93 ± 0.30 nM. The reported values for above stated reference standards are shown in Figure 2.29. In the literature the Zn measurement by fluorometric detection were found linear up to 500 nM (Nowiciki et al., 1994). In the seawater, the maximum Zn concentrations reported is up to 12 nM. Hence, linearity range was not an issue and was not verified here. The NASS-6 values which were reported in $\mu\text{g/L}$ unit were converted to nM in the Figure 2.29 B. The solid line in the Figure represents the mean value of the GEOTRACES deeper consensus value. The blue and red dotted lines above and below the solid lines mentions the 1σ and 2σ range for the consensus values.





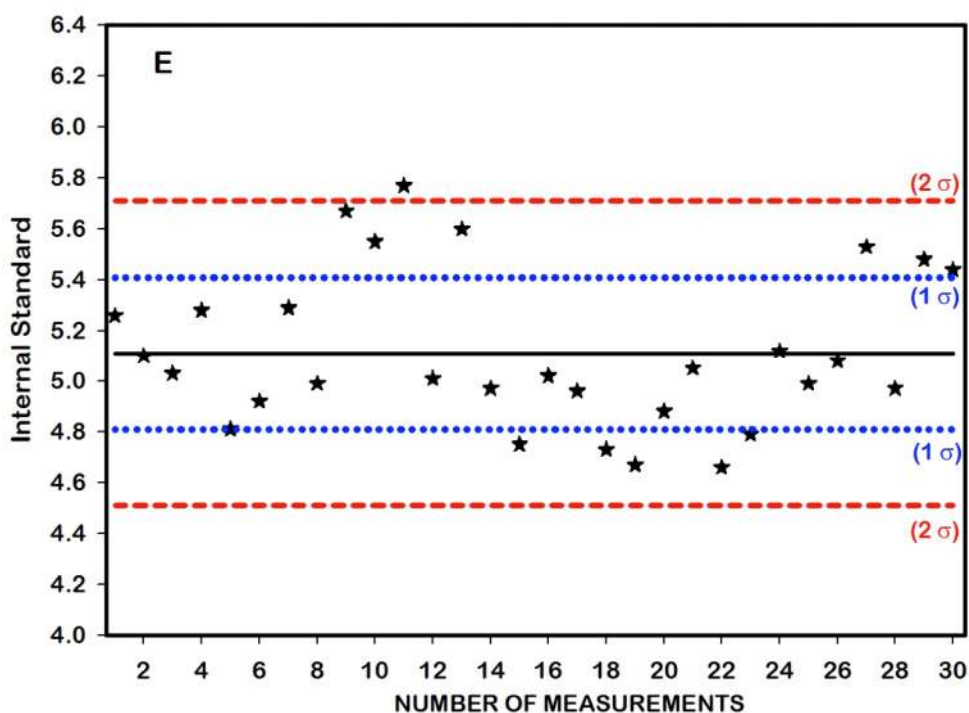
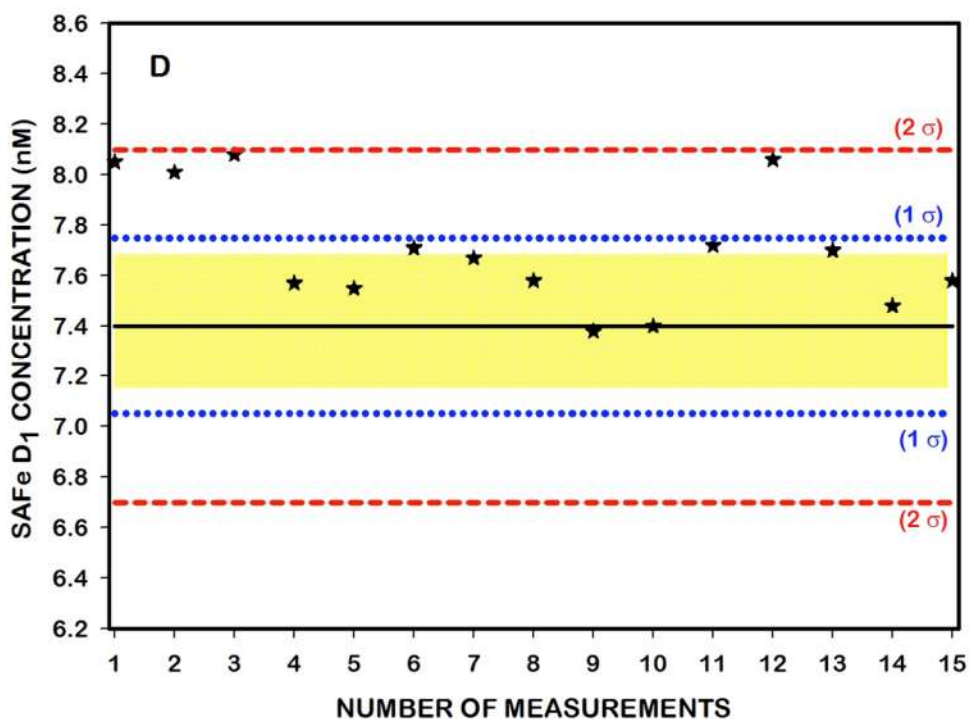


Figure 2.29: Reported values for reference standards. (A) Geotraces Surface sample (GS), (B) Sampling and analysis for Iron deeper sample (SAFE D1), (C)

Sampling and analysis for Iron deeper sample (SAFe D2), **(D)** GEOTRACES deeper sample (GD), **(E)** Seawater reference material for trace metals by National Research council Canada. The solid black line represents the average value of the reference standard. Blue dots represent the 1σ deviation. Red lines shows the 2σ variation in the samples. The colored region represents 1σ standard deviation from the average reported value. The reported values are **(A)** GD – 1.71 ± 0.12 nM (n=2), **(B)** NASS-6 – 3.97 ± 0.19 nM (n=17), **(C)** D2 – 7.58 ± 0.27 nM (n=9), **(D)** D1 – 7.70 ± 0.23 nM (n=15), **(E)** Internal standard – 5.11 ± 0.30 nM (n=27).

2.3.3 Determination of dissolved oxygen and major nutrients (Nitrate, Nitrite, Silicate and Phosphate)

The data shown in the thesis work for dissolved oxygen were measured by Winkler's titration whereas major nutrients Nitrate, Nitrite, Silicate and Phosphate were measured using spectrophotometric procedures. The protocols followed are briefly discussed below.

2.3.3.1 Dissolved oxygen determination

Unfiltered seawater samples from the trace metal clean CTD was collected in glass bottles without any entrainment of air bubbles in to the collected sample. DO was measured using Winkler's method which is an iodometric titration. Dissolved oxygen present in the seawater does not directly oxidizes the iodide ion to iodine, a multi-step oxidation was performed using manganese as a transfer medium. DO in water reacts with manganous (II) hydroxide in strongly alkaline medium forming manganese (III) hydroxide (precipitate). When acidified to pH less than 2.5, the manganese (III) hydroxide is dissolved to liberate manganese, which is a strong oxidizing agent in acidic media. It reacts with iodide ions (previously added), liberating equivalent amount of free iodine, which is titrated against a standard thiosulphate solution. The precision of the measurement was within 10%.

2.3.3.2 Major nutrients determination

The biological productivity of seawater depends on the available nutrients and organic matter. The primary producers predominantly utilize all the inorganic nutrients Nitrate, Nitrite, Silicate and Phosphate. Unfiltered seawater sample from the 12 L Niskin bottles where trace metal sampling was done were collected for the major nutrient analysis. Samples were collected in 250 ml PP bottles and kept

inside of the refrigerator at 4 °C until determination. Analysis was done within 24 hrs of the sample collection.

Phosphate in seawater was allowed to react with acid Ammonium molybdate, forming a phosphomolybdate complex, which is reduced by ascorbic acid, in the presence of antimony ions to a blue coloured complex containing 1: 1 atomic ratio of phosphate and antimony ions. The blue colour forming through the reaction was measured at 880 nm using 1 cm cell (cuvette) in Spectrophotometer (Skalar/Shimadzu - 1800 Model). The inorganic phosphate ions in seawater react with the acidified molybdate reagent to yield phosphomolybdate complex, which is reduced to molybdenum blue. The colour was measured spectrophotometrically at 880 nm. Ammonium molybdate in sulphuric acid, containing antimony in the bivalent state is the mixed reagent, which was added to the sample. The presence of antimony ions leads to a rapid reaction resulting in the formation of phosphor antimony molybdate complex (P: Sb as 1:1), which yields a heteropoly blue complex on reduction.

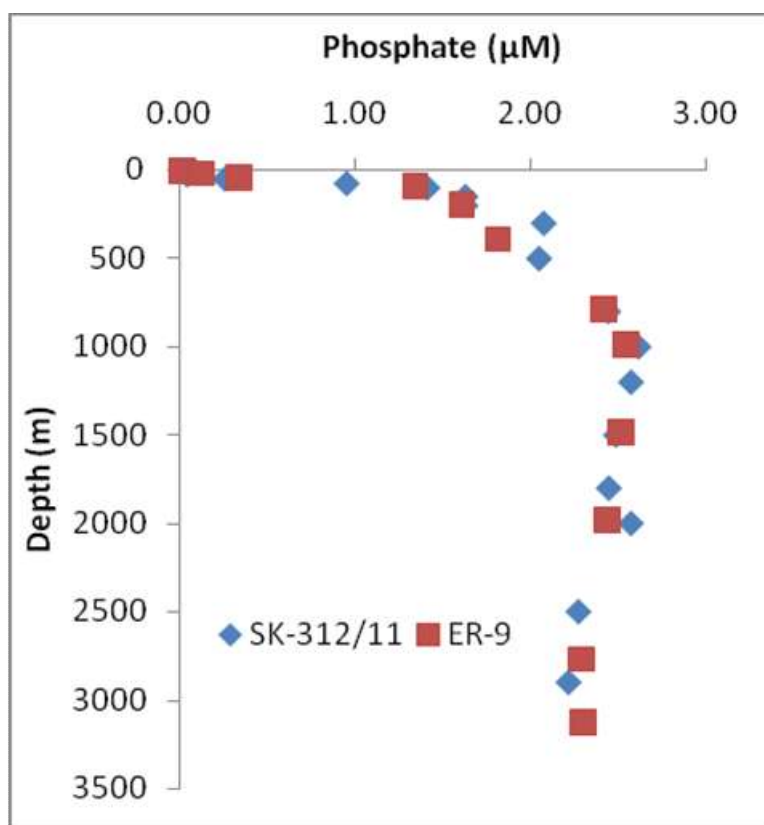
The seawater sample is allowed to react with molybdate under conditions which result in the formation of silicomolybdate, phosphomolybdate and arsenomolybdate complexes. A reducing solution, containing metol and oxalic acid, is then added which reduces the silicomolybdate complex to give a blue reduction compound and simultaneously decomposes the phosphomolybdate or arsenomolybdate eliminates the phosphate and arsenate interference. The colour is measured spectrophotometrically at 810 nm in Skalar/Shimadzu Spectrophotometer

The Nitrite in seawater is diazotized with Sulphanilamide at pH 1.5 to 2.0 and then resulting diazo compound is coupled with N – (1- naphthyl) – Ethylene diamine to form a highly coloured azo dye with absorption maxima at 540nm. Absorption is noted from the Spectrophotometer.

Nitrate in seawater is quantitatively reduced to nitrite by heterogeneous reduction involving copper – cadmium granules. Nitrite thus produced was determined by diazotizing with Sulphanilamide and coupling with N – (1- naphthyl) – Ethylene diamine through the column without change. The absolute values of Nitrate was determined by subtracting the Nitrite values. Blanks were

quantified using MQ as a sample. The values obtained for the MQ was subtracted from the samples. The precision of the Nutrients analysis was $0.02 \mu\text{mol/L}$.

During the analysis of the major nutrients reference material was not measured for the accuracy check. Instead, the nutrient data analyzed was cross checked with the cross-over station of the GEOTRACES Japanese station sampled in the Arabian Sea during 2009. The SK-312/11 station sampled during our GEOTRACES-India cruise is exactly the same location where Japanese group has done sampling. For the accuracy check of the nutrients in the present thesis work, comparison was done and it is displayed in the Figure 2.30.



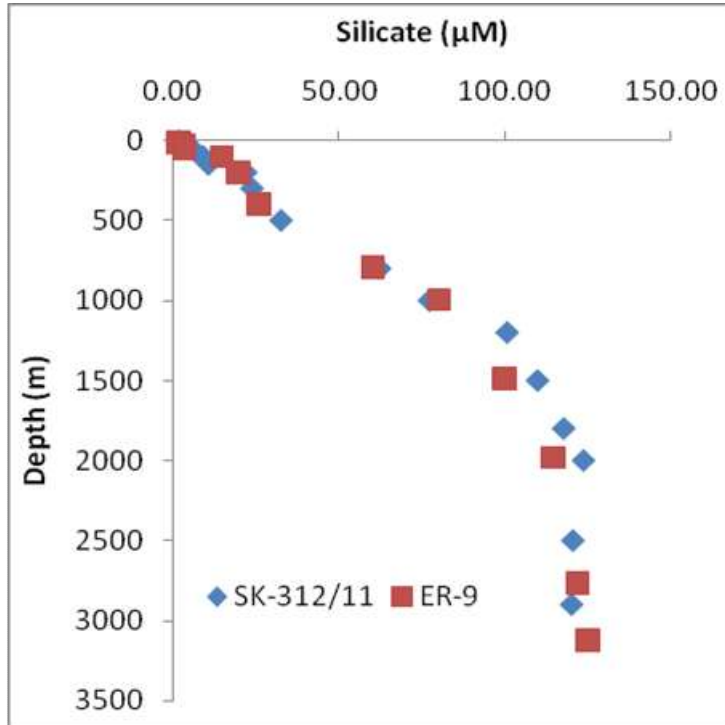


Figure 2.30: Comparison of nutrients (Phosphate and Silicate) of crossover station between SK-312/9(GI-02) and GEOTRACES-Japanese station (ER-9; Vu and Sohrin 2013).

2.4 Conclusions

Trace metal clean sampling system alongwith measurement protocols of dissolved Fe and Zn in seawater with great accuracy and precision were established. Thousands of seawater samples during six cruises were collected in the Indian Ocean for analysis of trace elements in them.

Chapter 3

Distributions of dissolved Iron in the Indian Ocean

3.1 Introduction

The trace elements, Iron (Fe), Manganese (Mn), Zinc (Zn), Cobalt (Co), Nickel (Ni), and Copper (Cu) are vital for microorganisms in seawater. The knowledge of sources, sinks and processes governing their distributions in the contemporary oceans are very important to understand their impact on the carbon cycle and global climate (GEOTRACES Science plan, 2006). These elements act as co-enzymes in numerous biological processes (Bruland et al., 1991) and are involved in number of biological processes (Bruland et al., 1991) such as nitrogen fixation. Among the essential trace metals, Iron (Fe) gained more importance owing to its low concentrations in seawater limiting primary productivity in many parts of the oceans (Martin and Fitzwater, 1988; Martin et al., 1988; Martin et al., 1989; Martin, 1990; Martin et al., 1991; Sunda et al., 1995). Fe is the most studied bioactive trace element in seawater since trace metals recognized as metal enzymes and also as a co-factor in several metabolic reactions. Availability of Fe in the surface seawater controls the ocean primary productivity and modulates the atmospheric CO₂. Fe also regulates the Nitrogen Fixation in oligotrophic waters (Falkowski et al., 1997; Boyd et al., 2007; Moore et al., 2007). Primary production in surface waters of HNLC (High Nutrient Low Chlorophyll) regions which accounts for about 40% of world oceans is limited by Fe availability (Coale et al., 1996; Martin and Fitzwater, 1988; Martin et al., 1988, 1989, 1990, 1991; Sunda et al., 1995). It is believed that nano-molar additions of Fe to the remote southern surface ocean during glacial period through atmospheric deposition resulted in stimulating the algal photosynthesis and successive reduction in atmospheric CO₂ (Martin et al., 1990; Boyd et al., 2000; Watson et al., 2000). Iron exists in two redox states; +2 and +3. In general, iron favours the +2 oxidation state, in the oxygenated seawater. At circum neutral pH of seawater, Fe forms oxyhydroxides which is thermodynamically unstable and gets removed from the water column (Turner et al., 2001; Liu and Millero, 2002). However, organic complexation (~99%) of Fe in seawater increases its solubility (Kuma et al., 1996; Gledhill et al., 2012).

The global biogeochemical cycle of Fe can be better understood by improving the ocean-wide sampling and evaluating its distribution in terms of sources, sinks

and internal cycling. These studies will be helpful in assessing the role of Fe cycle on global carbon cycle by incorporating the information in geochemical models (Parekh et al., 2004; Tagliabue et al., 2014a; Aumont et al., 2015; Volker & Tagliabue et al., 2015; Frants et al., 2016). Under the international GEOTRACES programme, the Atlantic and the Pacific Oceans have been sampled and studied in detail for dissolved trace elements biogeochemistry. Such study in the Indian Ocean is limited to few depth profiles and surface sampling, restricting the understanding of their sources, sinks and internal cycling in this part of the globe. Saager et al. (1989) report the first vertical profile of Iron in the Indian Ocean. With the advent of new clean sampling system and measurement protocols for dissolved trace elements in the ocean, limited data of DFe in the Indian Ocean are reported by Takeda et al. (1995); Measures and Vink, (1999); Moffett et al. (2007); Kondo and Moffett (2013); Nishioka et al. (2013); Vu and Sohrin, (2013); Grand et al. (2015a, 2015b); Moffett et al. (2015). Measurements of DFe reported by Grand et al. (2015b) are restricted to upper 1000m of seawater with an unprecedented resolution of 1° interval under U.S. CLIVAR CO₂ repeat hydrography along the line IO9N. Vu and Sohrin (2013) reported few full vertical profiles in the Indian Ocean and few other available studies are limited to the oxygen minimum zone of the Arabian Sea (Measures et al., 1999; Moffett et al., 2015). As a part of GEOTRACES – India programme, a total of 55 full vertical profiles were sampled and analyzed for DFe altogether in the BoB, AS, Andaman Sea and the Indian Ocean to understand the biogeochemistry of DFe in the Indian Ocean.

This chapter is further sub-divided into two sections to explain the DFe internal cycling in the entire Indian Ocean including marginal seas in the Northern Indian Ocean.

3.2 Distributions of dissolved Iron in the marginal and open ocean waters of the Northern, Equatorial and eastern subtropical Indian Ocean

This part deals mostly with north and northeastern part of the Indian Ocean, mainly the Bay of Bengal, the Andaman Sea and the Indian Ocean south of

equator. For comparison, two stations in the Arabian Sea are also considered (Figure 3.1)

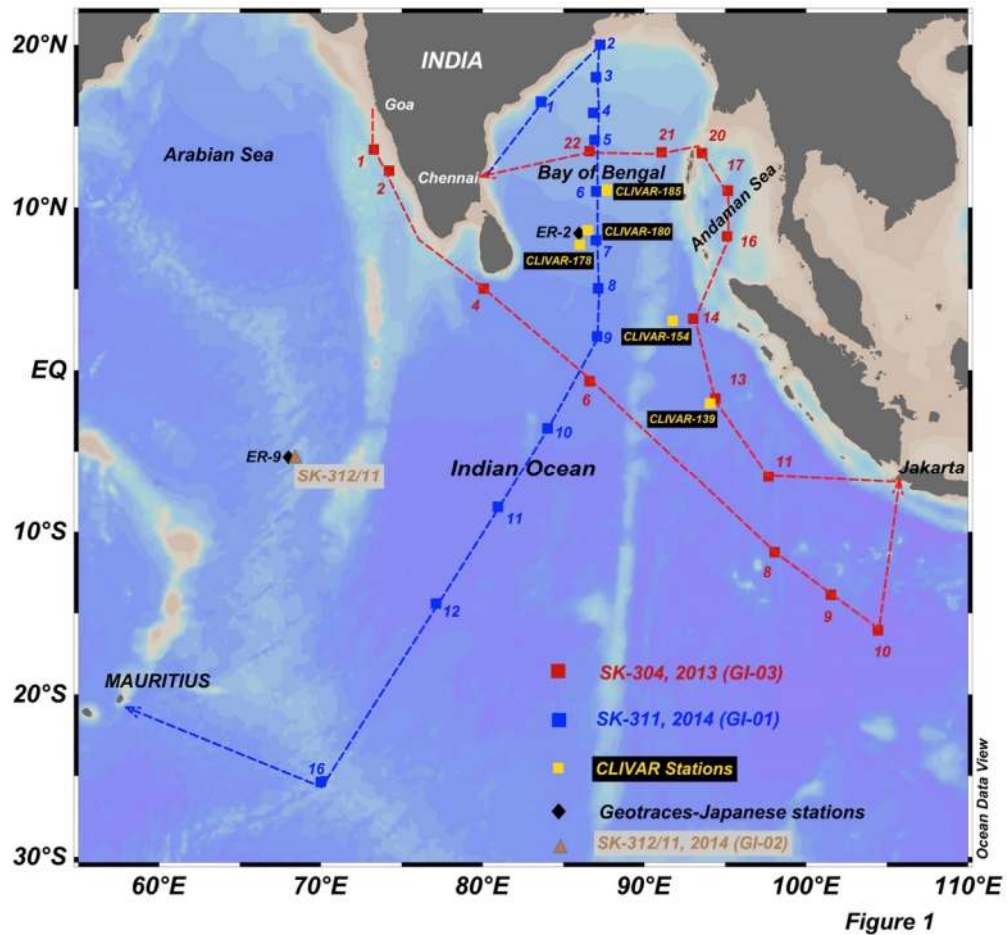


Figure 3.1: Map showing the sampling locations in the Indian Ocean during SK-304 (GI-03) in 2013 and SK-311 (GI-01) in 2014 as part of GEOTRACES-INDIA programme onboard ORV Sagar Kanya. For comparison, selected stations of the Japanese GEOTRACES ER-9 and ER-2 sampled in 2009, CLIVAR stations 139,154,178,180,185 sampled in 2007 and GEOTRACES-India station SK-312/11 (GI-02) sampled in 2014 in the Indian Ocean are also shown in the figure. Oceanic data view 4 software is used for plotting all the color contours in this and successive figures (Schlitzer, 2017).

3.2.1 Results

3.2.1.1 Hydrographic and major nutrient distributions

The results of DFe obtained in this study have been discussed by dividing the area into four basins based on the geography of the basins and the physical parameters. Figure 3.2 displays different water masses present in the (i) BoB, (ii)

Andaman Sea and (iii) Indian Ocean (south of equator). Numerous studies were carried out in the Indian Ocean to characterize the water masses and their circulation pattern (Wyrski, 1973; Sastry et al., 1985; Murty et al., 1992; Kumar and Li, 1996; Rao et al., 1996; Varkey et al., 1996; You and Tomczak, 1993, You, 1997, 1998, 2000; Tomczak and Godfrey, 2003; Schott, 2001; Frank et al., 2006; Singh et al., 2012; Goswami et al., 2014). The Antarctic Bottom Water (AABW) occupies the bottom layers in the Indian Ocean, which may extend up to north BoB and the AS. In the northern Indian Ocean, the bottom waters are termed as Circumpolar Deep Waters (CDW) mainly due to the mixing of deep and bottom waters while intruding into the BoB and AS (You and Tomczak, 1993). Above these bottom waters, Indian deep waters (IDW) occupy the depth range of 1500 – 3000 m at the Equator and the northern Indian Ocean. The Indian Ocean also receives upper ocean waters from the Pacific Ocean waters through the Indonesian Through Flow (ITF) (Qian et al., 2004). These ITF waters are modified while crossing across the Indonesian Islands and can be traced between 10° S and 15° S (Frank et al., 2006; Clemens et al., 2016), and further move along the equator towards the Somali basin and enter in to the AS along the Somali current during the onset of southwest monsoon. The Antarctic Intermediate Waters (AAIW) originated in the Antarctic region that is relatively less saline compared to its over and underlying waters and occupies the water column at the depth range of 800-1100 m (You 1998).

The salinity of surface waters in the northern BoB is generally low due to a large fresh water influx from the Ganga-Brahmaputra river system. These waters are termed as Bay of Bengal Less Saline Waters (BBSW). In contrast, salinity of the surface waters of AS are higher compared to surface salinity of BoB due to excess evaporation over precipitation and less riverine supply. The upper surface layers in the AS are termed as Arabian Sea High Salinity Waters (ASHSW). In addition, the AS contains high saline waters in the depth range between 300 and 800 m originating from marginal seas, the Persian Gulf Waters (PGW) and the Red Sea Waters (RSW). The seasonal reversal of monsoonal winds bring high saline surface waters into the BoB during summer monsoon and less saline waters from the BoB to the AS during winter monsoon. The surface waters of the

Andaman Sea are less saline due to large fresh water supply from the Irrawaddy and the Salween rivers. Deeper depths of the Andaman Sea are occupied with central waters of the BoB flowing across the Ten Degree channel.

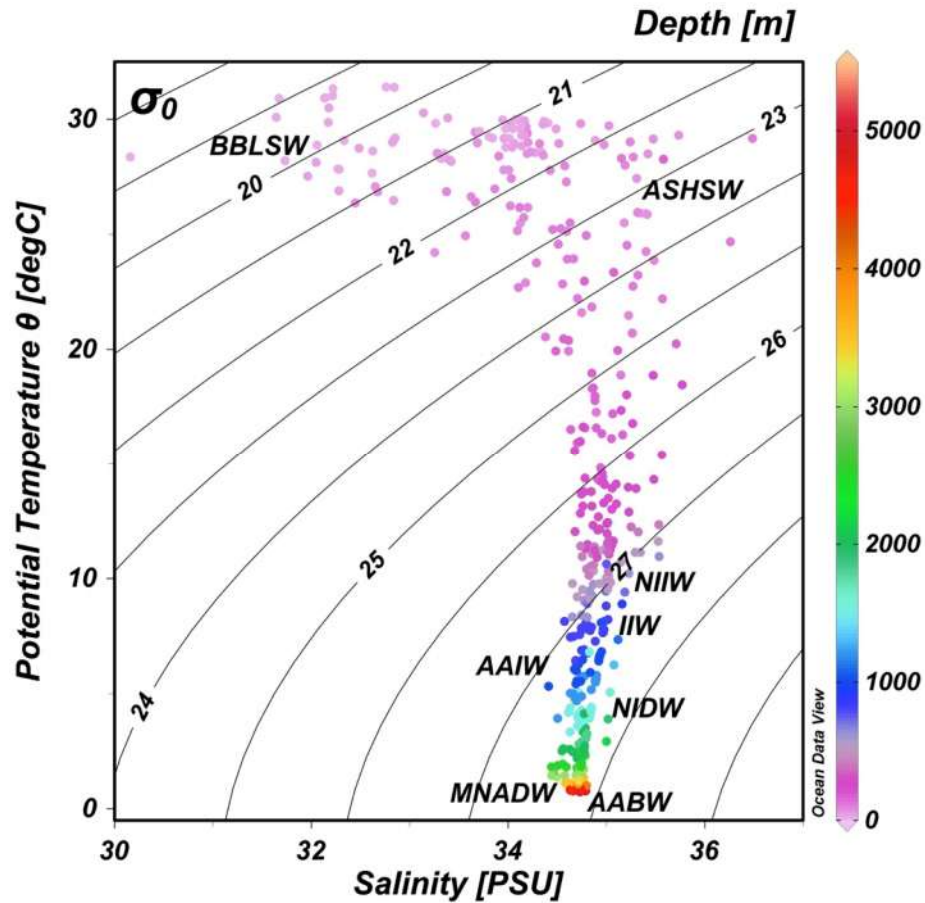
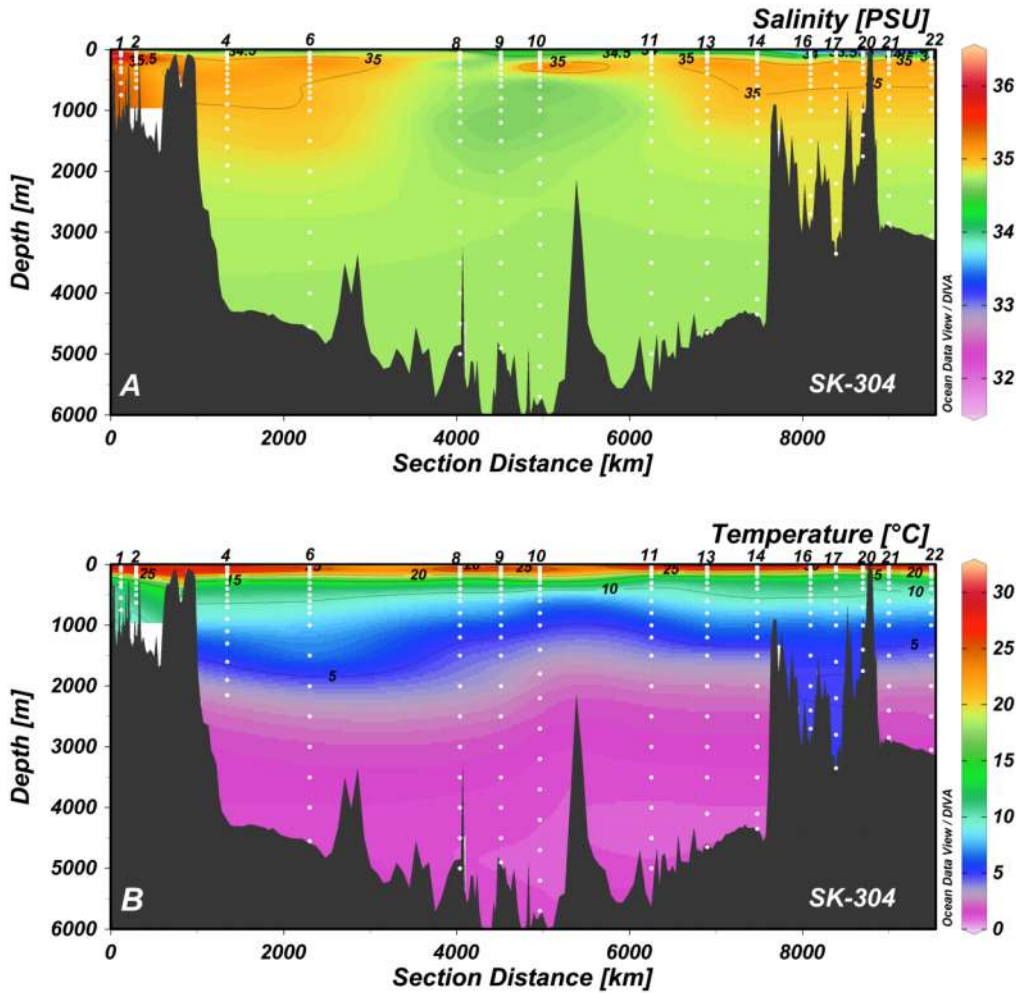


Figure 3.2: Salinity vs. Potential temperature with Isopycnal lines for all the stations of SK – 304 and SK-311. BBLSW – Bay of Bengal less saline waters, ASHSW- Arabian Sea high saline waters, NIIW – North Indian Intermediate waters, IIW – Indonesian Intermediate through flow waters, AAIW – Antarctic intermediate waters, NIDW – North Indian deep waters, AABW – Antarctic bottom waters and MNADW – Modified north Atlantic deep waters.

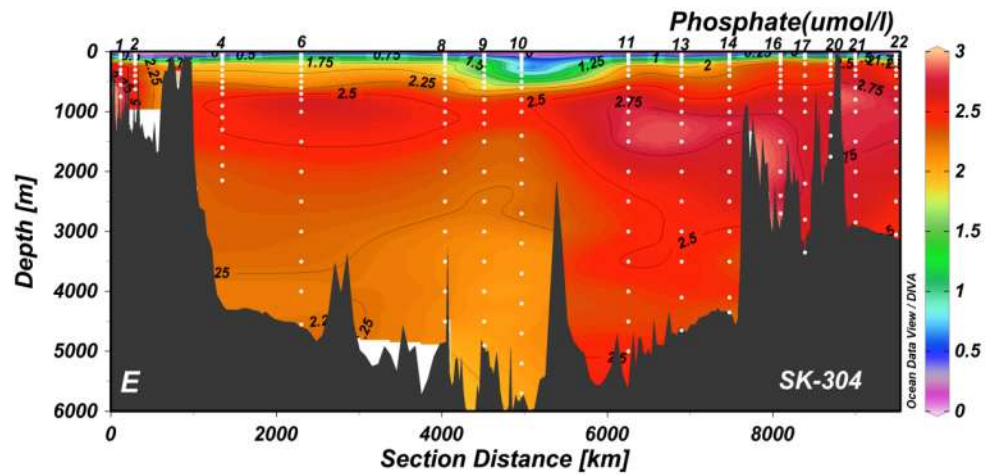
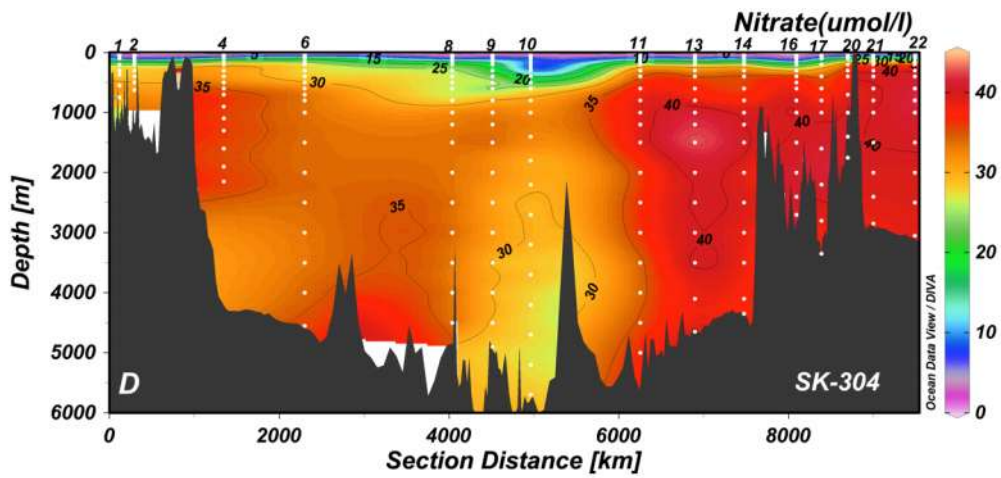
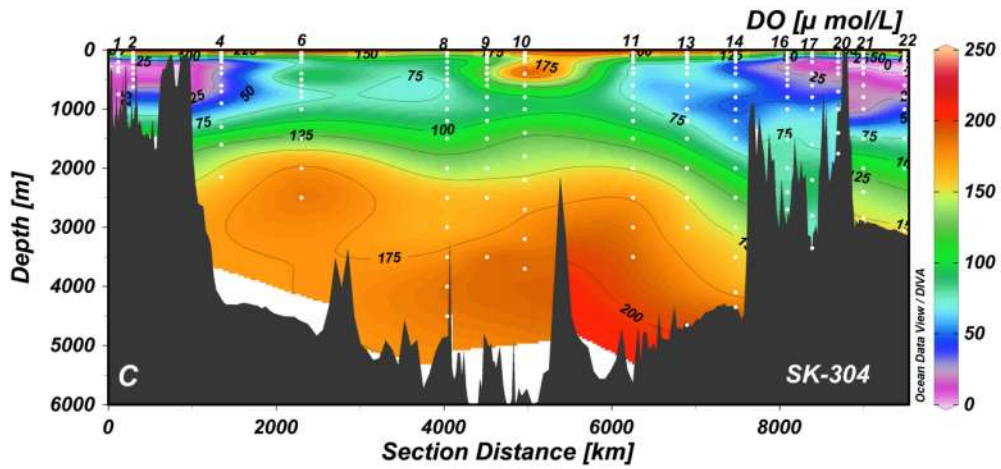
The basic parameters salinity, temperature, dissolved oxygen (DO), and major nutrients nitrate, phosphate and silicate for the Northeastern Indian Ocean region are shown in the Figures (3.3 and 3.4).

(i) The Bay of Bengal

The SK-304/21-22 and SK-311/1 to 8 were sampled in BoB. Contrasting surface salinities is observed in the BoB (Figure 3.4A) compared to the two coastal stations of AS. Due to the monsoonal currents, characteristics of Arabian Sea High Saline Waters in the BoB and low saline waters of BoB in AS can be seen in respective summer and winter monsoons (Shankar et al., 2002).



Distributions of dissolved Iron in the Indian Ocean



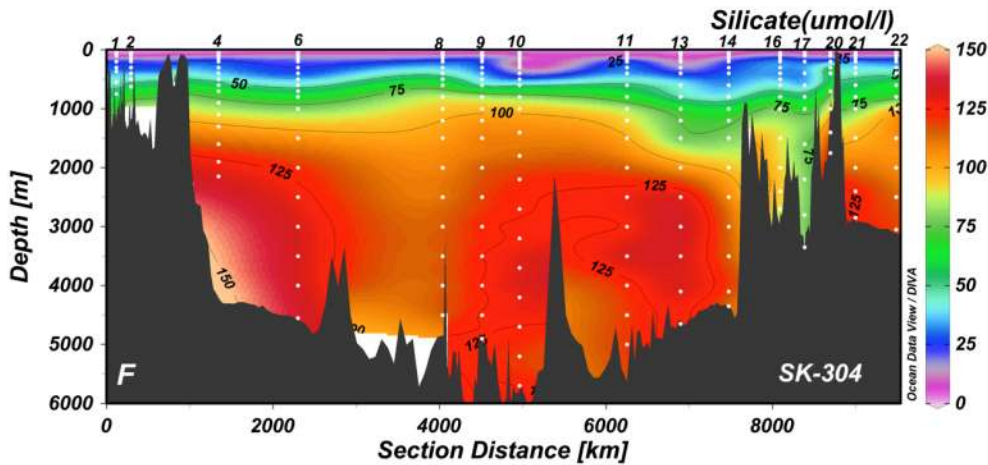
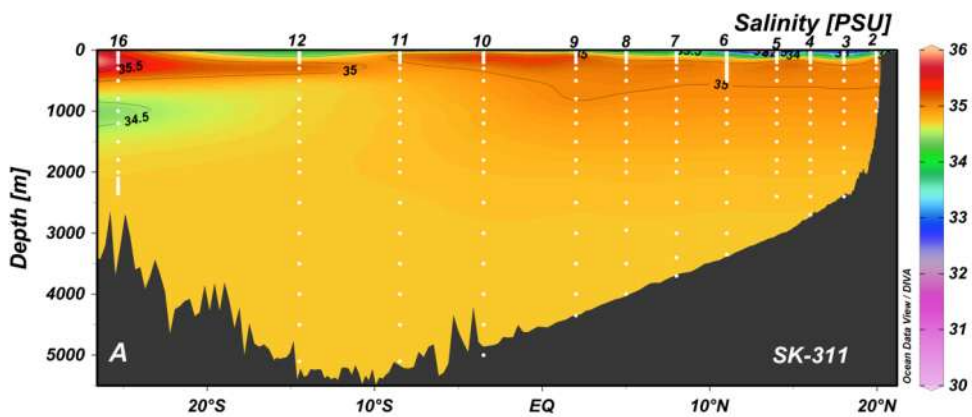
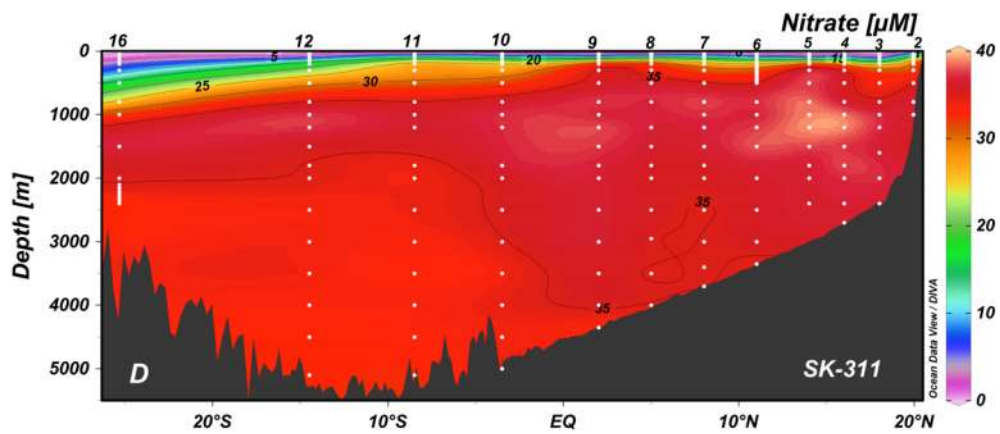
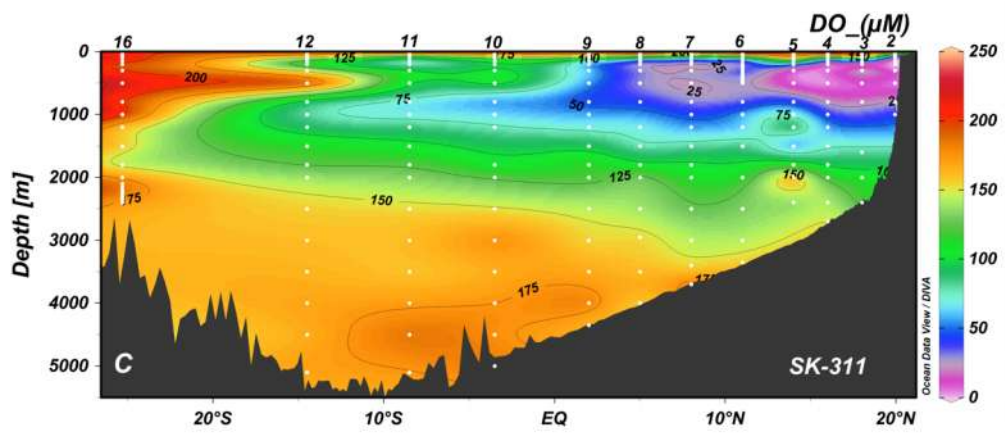
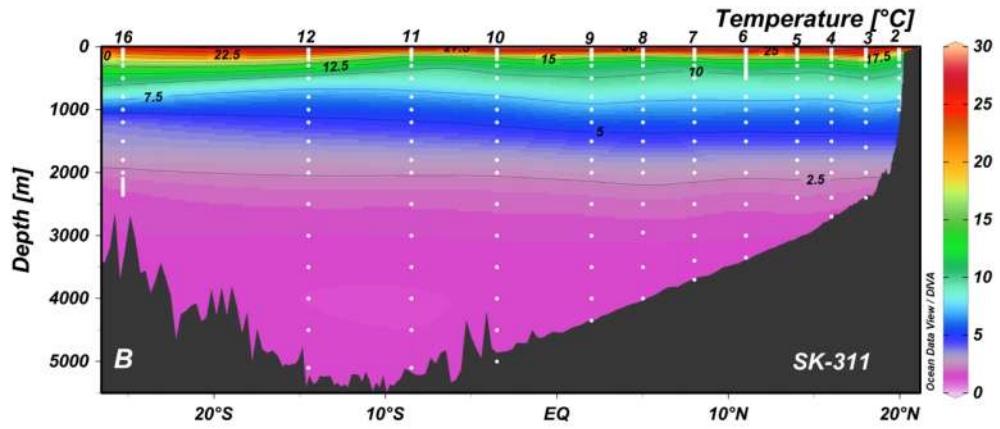


Figure 3.3: Section plots for hydrographic parameters in the SK-304 cruise. (A) Salinity, (B) Temperature, (C) Dissolved Oxygen, (D) Nitrate (E) Phosphate, and (F) Silicate. Station numbers are represented at the top of the figure.

The observed surface salinities of stations sampled in the BOB are significantly low due to the large fresh water influx from rivers and Ganga-Brahmaputra, which causes the stratification in the upper layers (50 m) (Gopalakrishna et al., 2002; Sengupta et al., 2006). These less saline waters and stratification are more pronounced in the stations north of 10° N. The dissolved oxygen values are higher in the surface in all the stations of BoB without any surface gradient. Below 100 m, oxygen minimum zone is observed in the BoB (Figure 3.4C).



Distributions of dissolved Iron in the Indian Ocean



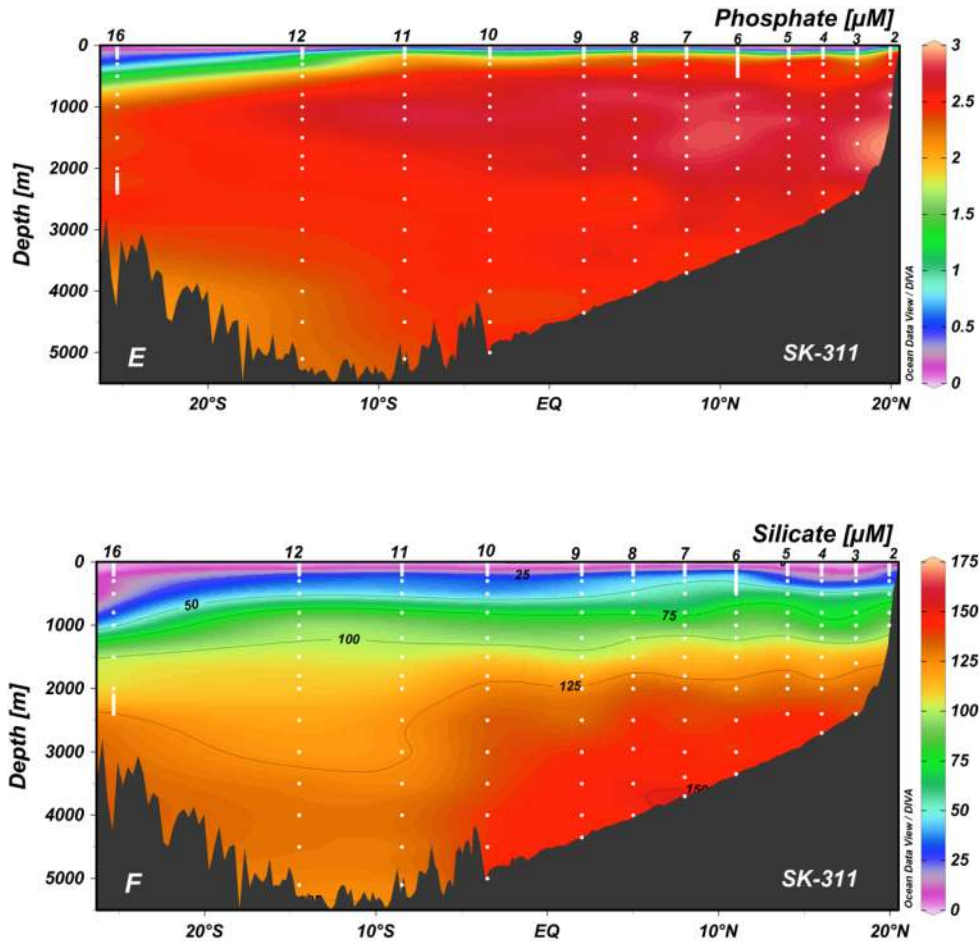


Figure 3.4: Section plots for hydrographic parameters in the SK-311 cruise. (A) Salinity, (B) Temperature, (C) Dissolved Oxygen, (D) Nitrate (E) Phosphate, and (F) Silicate. Station numbers are represented at the top of the figure.

The primary factors controlling the OMZ in the BOB are the stratification, minimizing the ventilation (Sarma, 2002) which gets intensified in the northern BoB due to high fluvial input (Sarma et al., 2013; Singh et al., 2012). The OMZ in the intermediate water columns of the BoB is observed north of 5° N. Thermocline in the northern bay is shallower compared to southern bay. Deepening of thermocline at SK-311/3 is observed compared to neighboring stations otherwise, it follows a north-south increasing trend.

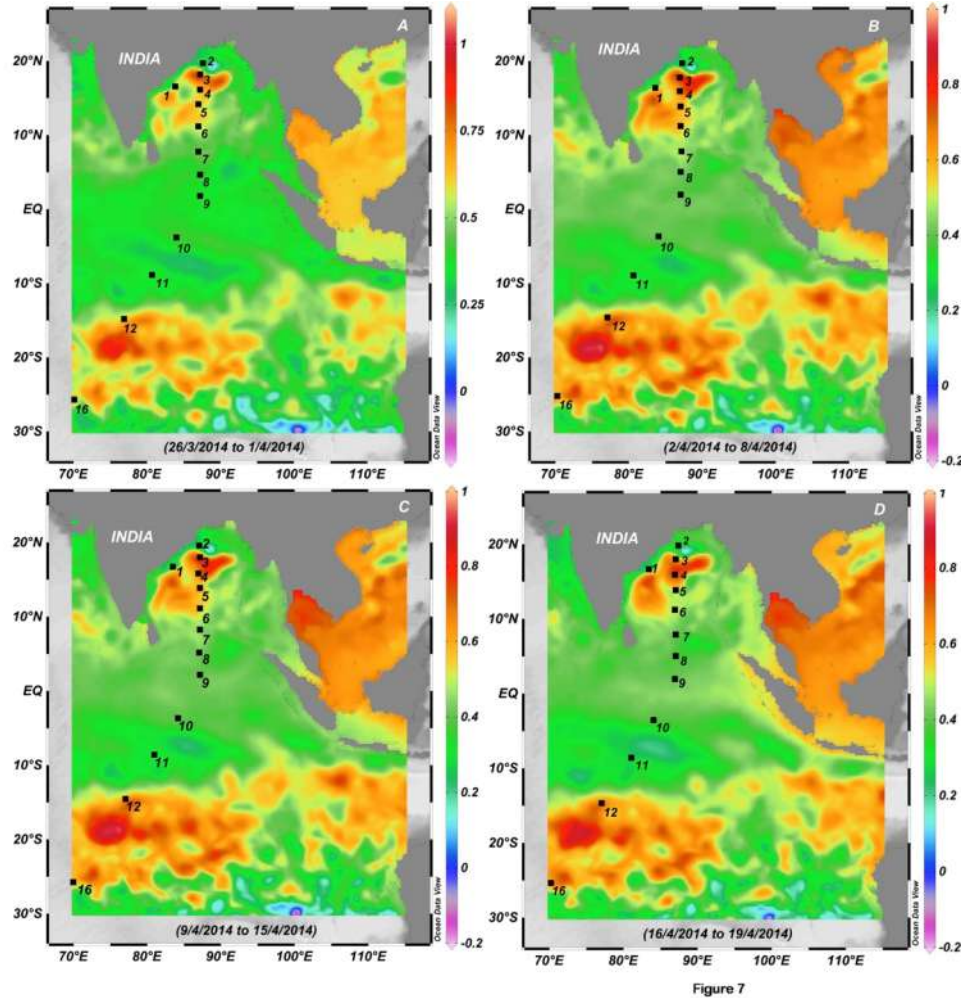


Figure 3.5: Sea surface height (SSH) plots during SK-311 sampling period. Data reveals the presence of Eddy in the BoB close to 18°N. SSH data was obtained from CMEMS (COPERNICUS MARINE ENVIRONMENT MONITORING SERVICE).

The Sea Surface Height (SSH) plots for SK-311 (Figure 3.5) indicate the presence of mesoscale anticyclonic eddy in the BoB during sampling period of 2014. Station SK-311/3 is impacted by eddy (Figure 3.5). The nitrate and phosphate concentrations are very low in the top 50 m of the BoB (Figures 3.4 D and 3.4 E) where as silicate concentrations are relatively higher (Figure 3.4F). The Ganga – Brahmaputra alone supply 133×10^9 mol/yr dissolved silica to the bay which accounts ~2% of total supply to world oceans by riverine input (Sarin et al.,

1989; Singh et al., 2015). Silicate concentrations observed are generally high in the surface of the BoB due to the large fresh water influx (Singh et al., 2015).

(ii). The Andaman Sea

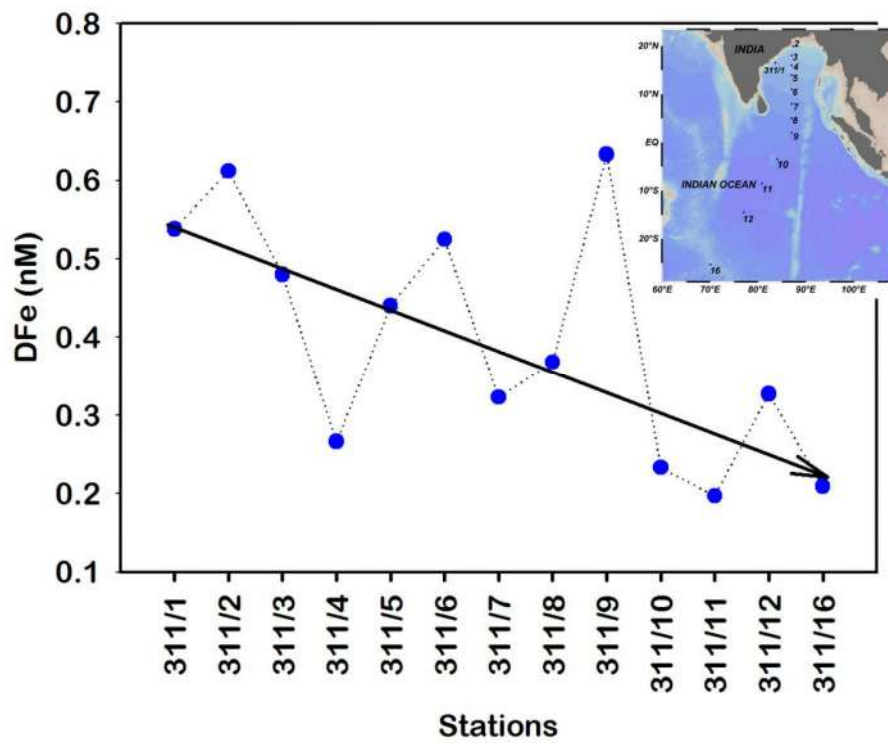
The stations SK-304/16, 17 and 20 were sampled in Andaman Sea. The Andaman Sea is separated from the BoB by the Andaman-Nicobar Islands preventing the horizontal ventilation. The surface salinity in the basin is quite low (< 33) due to the presence of the Irrawady/Salween rivers in the northern side of Andaman stations. Observed Nitrate and Phosphate concentrations are low in the surface compared to the silicate values. The nutricline starts at 45 m. Below oxycline, DO values decreased with depth and was observed even lower than 25 μM . Intense OMZ (Oxygen \sim below detection limits) has not observed in these stations. The basic parameters data in the waters below 1200 m depth are constant and these deeper values coincide with the values of BoB in the depth interval of 1000 – 1200 m. The Andaman Sea exchanges its deeper waters with the intermediate waters of BoB through 10° channel (Nozaki et al., 2003). High rapid vertical mixing rates are observed in the deeper waters of Andaman Sea (Dutta et al., 2007). Kim et al. (2015) reported similar features in the basic parameters.

(iii). Equatorial and subtropical Indian Ocean

The Indian Ocean (around and south of Equator) is an oligotrophic region and primary production is low compared to the Northern Indian Ocean (Subha et al., 2017). The surface salinity was 33.975 (SK-311/10) at station near equatorial Indian Ocean and increases further towards south 35.197 (SK-311/16). The salinity contours indicate the intrusion of Pacific Ocean waters through Indonesian Through Flow at the stations SK-304/08, 09 and 10 (Figure 3.3A). Higher saline waters are observed from surface to 300 m (35.197 at surface to 35.566 at 300 m) in the Indian Ocean at 25.3° S. Below 300 m, Antarctic Intermediate Water (AAIW) with lower salinity (34.967 to 34.413) is observed in the depth range of 500 to 1000 m (Figure 3.2). OMZ is not observed in the Indian Ocean stations south of equator. The influence of water mass with higher oxygen can be seen up to 13° S. Deepening of the nutricline (Figures 3.4 D, 3.4 E and 3.4 F) is observed south of equator.

3.2.1.2 Dissolved Iron distributions

The surface (average of ≤ 10 m) concentrations of dissolved iron (DFe) in the Indian Ocean are given in Annexure 1 and displayed in the Figures 3.6, 3.7 and 3.9. Surface DFe in the BoB displays a north – south gradient with relatively higher concentrations in the north with exception at stations SK-311/4, 6 and 9. Similar N-S gradient in surface DFe in the part of BoB is also reported by Grand et al. (2015b). Anomalous DFe at station SK-311/4 could be due to the impact of the anticyclonic eddy as discussed in the earlier section. Further, higher concentration in surface DFe at two stations SK-311/9 near equator could be due to equatorial upwelling bringing deeper water with higher concentration of DFe at the surface which is also reflected at station SK-304/6.



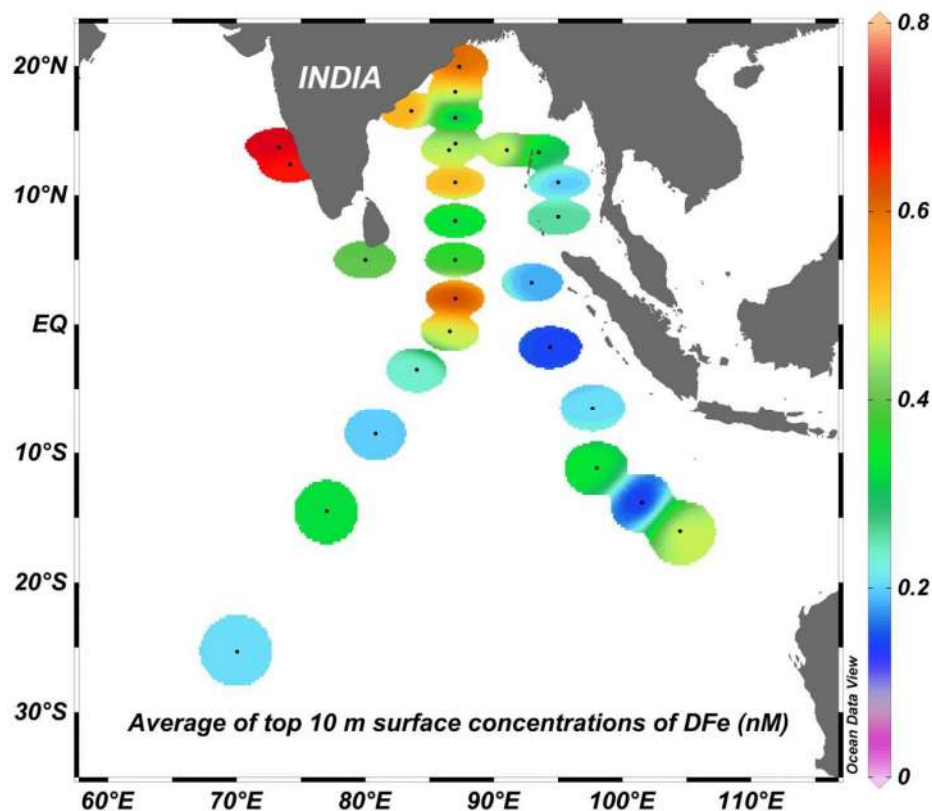
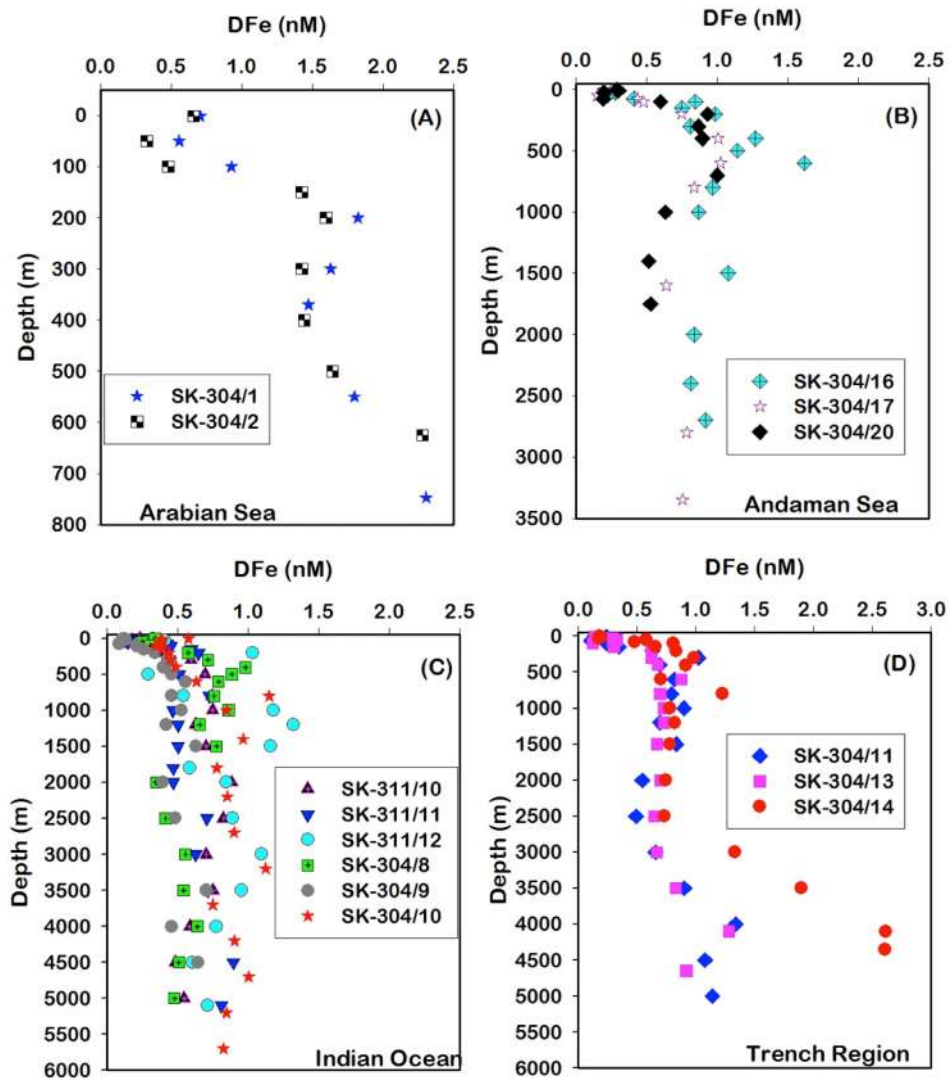


Figure 3.6: The surface (Average of top 10 m) dissolved Iron concentrations in the study region (SK-304 and SK-311). BoB reports relatively high surface concentrations compared to Andaman and Southern stations. N-S decreasing trend in DFe (SK – 311) values can be seen in the BoB.

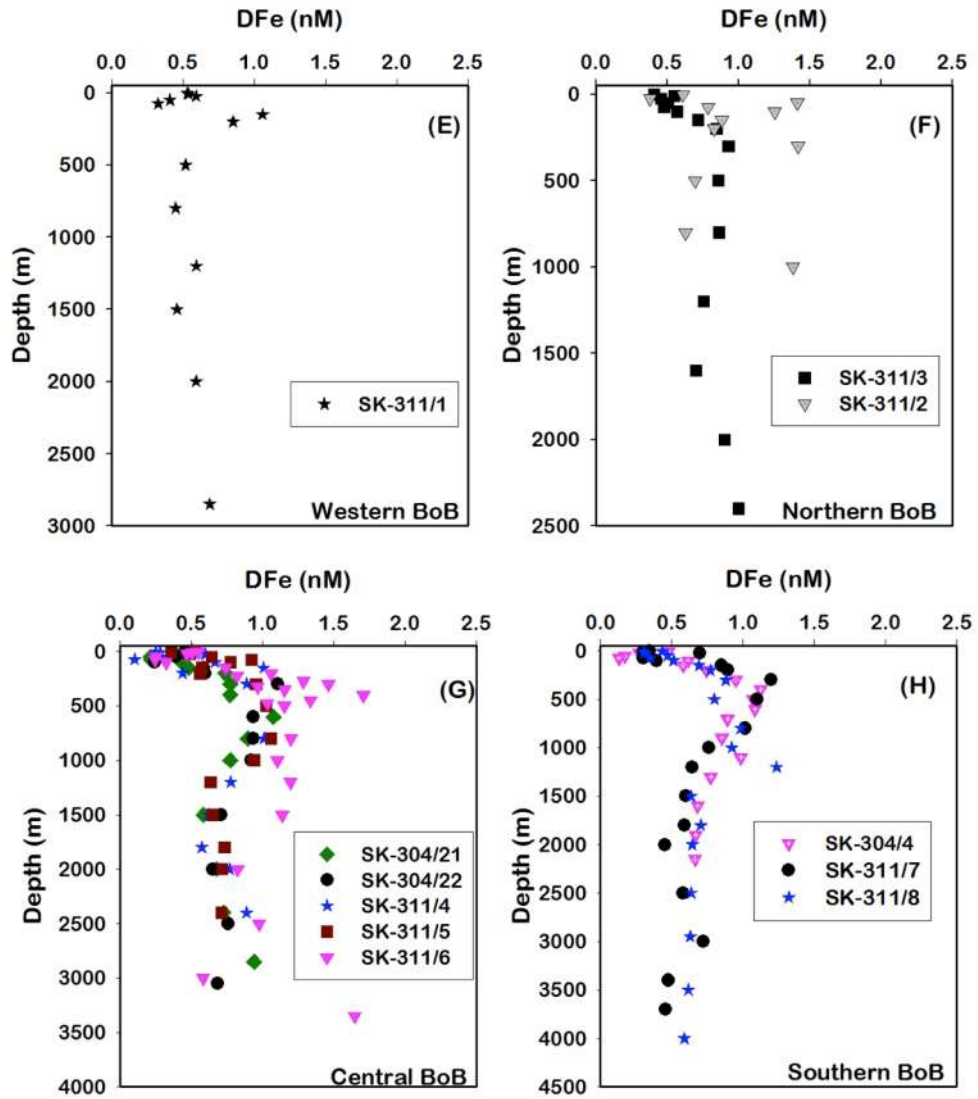
Intermediate waters in between 200 – 1000 m of water depth of BoB up to 5°N are rich in DFe (Figures 3.7 and 3.9). This sub-surface enrichment is also seen by Grand et al. (2015b) and Vu and Sohrin, (2013). Sub-surface maxima have also been seen in the Andaman Sea stations. This enrichment is not seen in the stations south of 5 °N. The DFe in the intermediate waters in depth range of 100 -1000 m average 0.95 ± 0.22 (n=76) for BoB, 0.90 ± 0.24 (n=21) for Andaman Sea, 0.61 ± 0.28 (n=79) for the Indian Ocean south of equator respectively. The overall DFe concentrations in this study range from 0.11 nM to 2.61 nM with a mean value of 0.69 ± 0.37 nM (n=499) and compares with the DFe concentrations in the west Atlantic Ocean averaging 0.55 ± 0.36 nM (n=1407; Rijkenberg et al., 2014). This average concentration of DFe given for present study does not contain deeper sample data of the SK-311/16 as this station is impacted by the hydrothermal

activity with very high DFe (see the later discussion). In general, vertical profiles of DFe show nutrient type behavior in the Indian Ocean with surface minima increasing with depth except in the coastal stations.

DFe profile in the coastal waters and in the northern most water columns of the BoB deviates from nutrient-type profile. The average concentrations of DFe for the deeper waters (>1000 m) are 0.77 ± 0.24 (n=66) in the BoB, 0.83 ± 0.27 (n=11) in the Andaman Sea and 0.75 ± 0.23 (n=78) in the Indian Ocean (Excluding the high value of deeper sample at SK-311/16).



Distributions of dissolved Iron in the Indian Ocean



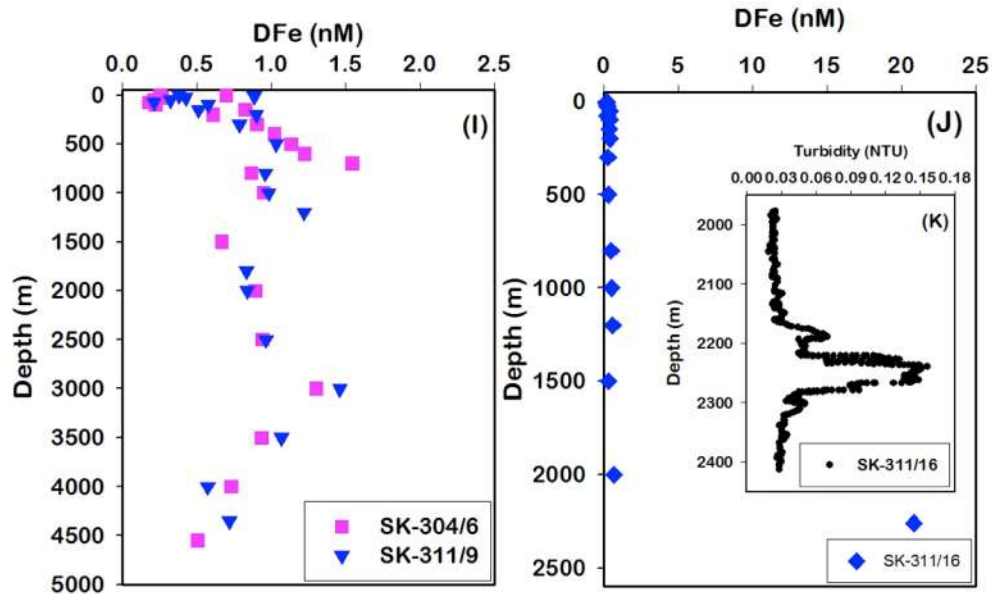


Figure 10

Figure 3.7: Vertical profiles of DFe from the study region. To avoid the clutter, the plots are arranged basin wide. (A) Arabian Sea, (B) Andaman Sea, (C) Indian Ocean, (D) Java Trench Region, (E) Northwestern Bay of Bengal, (F) Northern Bay of Bengal, (G) Central Bay of Bengal, (H) Southern Bay of Bengal, (I) Near Equator stations, (J) SK-311/16 sampled at Triple junction region and (K) Turbidity signal at station SK-311/16 indicating hydrothermal plume between 2200 and 2300 m depth interval. Turbidity data obtained from Regular CTD.

3.2.2 Discussion

3.2.2.1 Fluorescence and DFe

Depth of fluorescence maximum increased (Figure 3.8) from north to south BoB following the thermocline. The depth of fluorescence maximum observed at northern bay is ~50 m while at southern bay is ~90 m. Further deepening of the fluorescence peak observed moving from equator to southern stations (75 m to 120 m). The DFe and fluorescence section profiles for top 200 m are shown in the Figure 3.8. The fluorescence peak region is coinciding with lower DFe concentrations depicting the biological uptake of Fe by organism vis-à-vis biological production. Similar observation has not been found near the coastal stations, fluorescence peaks are associated with higher DFe in the coastal region, which could be due to more than ample supply of DFe in these regions from multiple sources.

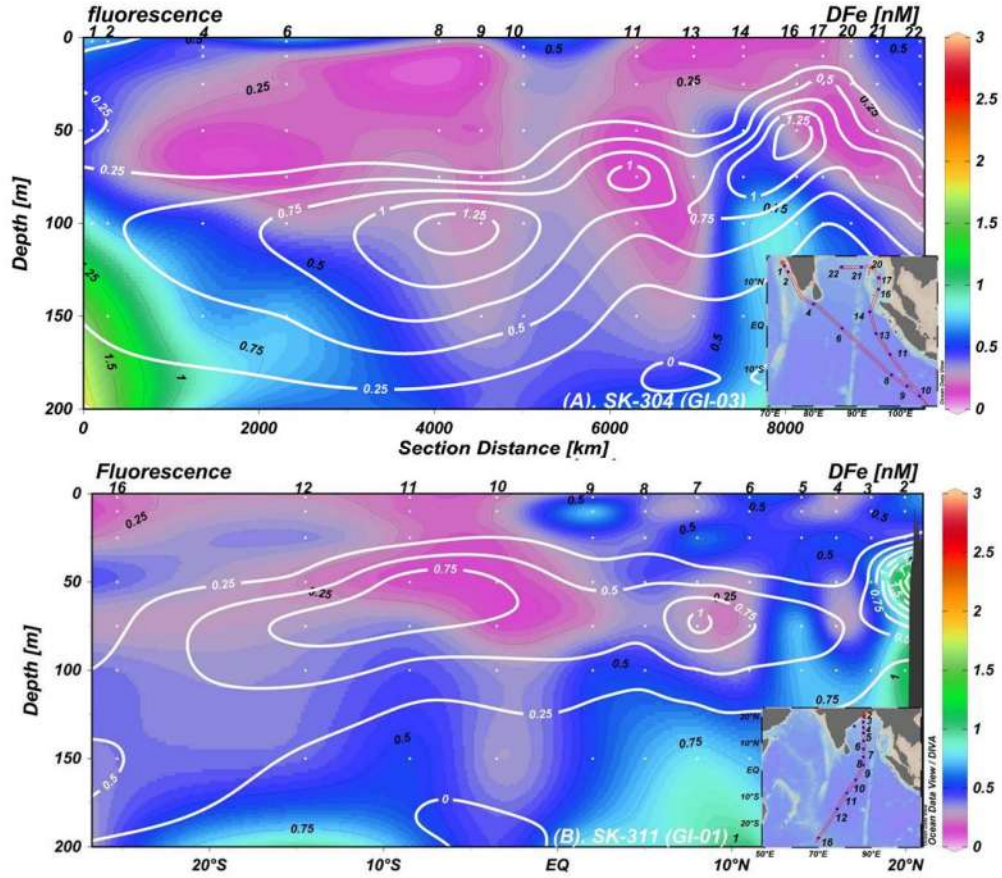


Figure 3.8: Section plots for top 200 m for Fluorescence and DFe in the SK-304 and SK-311. Deepening of Fluorescence peak can be seen as moving from north to south. Fluorescence peak corresponds to DFe minima due to biological consumption.

DFe distributions

The section profiles of DFe for both cruises SK-304 and SK-311 are shown in the Figure 3.9. Following the basic parameters, the DFe data is also explained on basin wise: (i) The BoB, (ii) The Andaman Sea and (iii) The Indian Ocean. In addition to the different water masses present in the respective basins, processes such as re-mineralization of organic matter, dissolution of atmospheric dust and of Fe-Mn oxyhydroxides coated on the riverine particles along with hydrothermal activities seem to control the distribution of DFe in the Indian Ocean. Part of the DFe distribution in the Indian Ocean is being controlled by its

utilization by biological productivity. Higher productivity (high Fluorescence) in parts of the Indian Ocean (Figure 3.8) is associated with low DFe indicating consumption of Fe by productivity. Coastal region of the AS and the BoB are marked with higher DFe despite higher productivity (Figure 3.8) which could be due to its multiple sources in these regions.

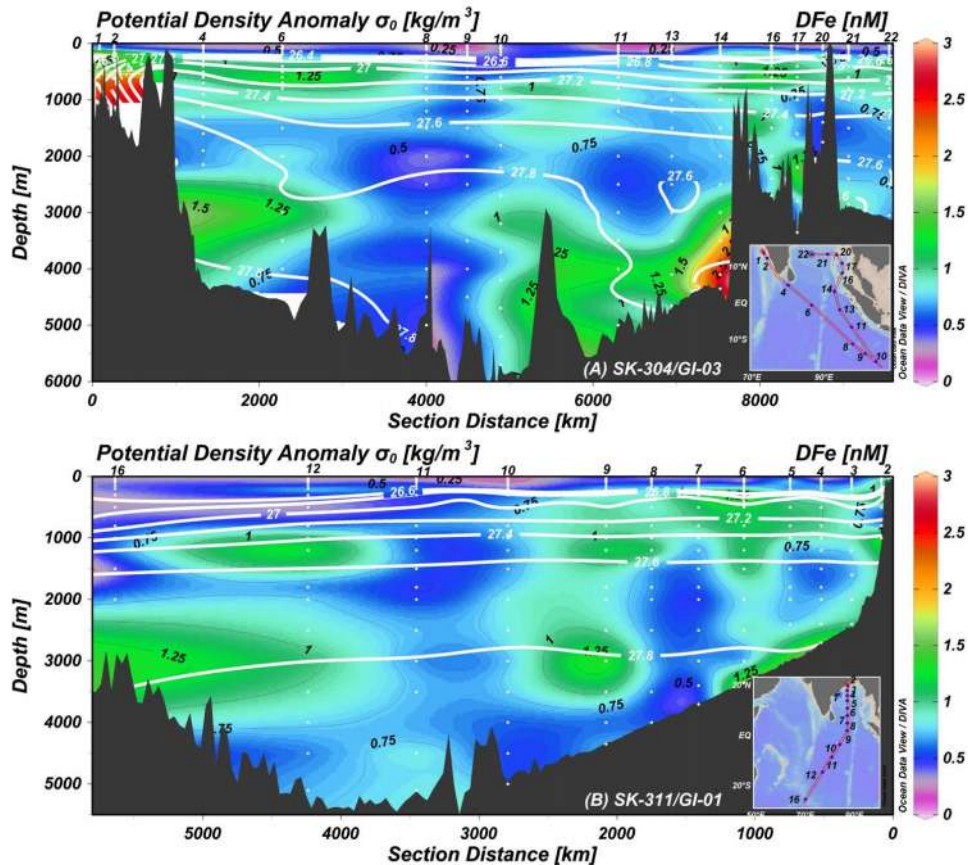


Figure 3.9: Section profiles of DFe from SK-304 and SK-311 cruises. High concentrations are found in the intermediate waters of BoB, Andaman Sea and deeper samples near Java trench region.

3.2.2.2 Dissolved Iron in the BoB

The vertical profiles of DFe in the BoB region are shown in the Figures (3.7 E, 3.7 F, 3.7 G and 3.7 H). The DFe concentrations in the surface waters of BoB displaying decreasing trend in N-S direction (Figure 3.6). High concentration (~ 0.615 nM) of DFe in the surface waters is observed at SK-311/2, which is located at northern side close to the mouth of Ganga-Brahmaputra River. In

contrast, relatively low concentration of DFe (~ 0.344 nM) is observed in the surface waters at the southern station of BoB (SK-311/7). The atmospheric mineral dust could be the major source of DFe to the surface waters of the open oceans (Jickells et al., 2005). Previous studies emphasized that surface waters of BoB receive more soluble Fe through anthropogenic processed mineral dust from nearby arid landmasses during continental outflow (Kumar et al., 2010; Srinivas et al., 2011). Overall, surface DFe concentrations in the North of Equator are relatively high compared to oligotrophic waters of Indian Ocean (South of equator, Figure 3.6). The high surface DFe values in the north of equator is also consistent with the previous study (Grand et al., 2015b) compared to oligotrophic waters of Indian Ocean. The correlation observed between surface DFe and DA1 in the BoB indicates the role of atmospheric deposition and/or riverine sediments in controlling their abundances in north of equator (Grand et al., 2015 b). The clear decreasing trend of surface DFe could not be seen in the present study as well as in the Grand et al. (2015b) which may be due to the presence of eddies in the BoB (Figure 3.5). A detailed study is needed to infer the role of eddies on micro-nutrients in BoB.

The sub-surface enrichment of DFe observed in this study has also been reported previously by Grand et al. (2015b) and Vu and Sohrin, (2013). Sub-surface maxima in DFe at station SK-311/1 is not that prominent as seen in the other locations of the BoB. The high export flux was observed at this location with lower primary production. Subha Anand et al. (2017) observed high POC values during the same cruise (SK-311-1/GI-01). The magnitude of riverine particles received at SK-311/2 is higher compared to the station SK-311/1. The station SK-311/2 is situated at the mouth of Ganga-Brahmaputra river system whereas SK-311/1 is situated in the northwestern BoB and at the proximity of monsoonal rivers Godavari, Krishna etc. The river discharge during the sampling time of SK-311/1 is low from Godavari, Krishna etc., compared to discharge received by SK-311/2 at Ganga-Brahmaputra river system. The SK-311/2 is the northern most station located very near to the mouth of the Ganga-Brahmaputra River. The Ganga – Brahmaputra alone supply 133×10^9 mol/yr dissolved silica to the bay which accounts $\sim 2\%$ of total supply to world oceans by riverine input

(Sarin et al., 1989; Singh et al., 2015). Silicate concentrations are generally high in the surface waters of the BoB due to the large fresh water influx (Singh et al., 2015). The high export of particulate organic carbon at this location indicates that DFe may be getting scavenged from the water column. The internal cycling of DFe in the northern coastal BoB stations could be affected by processes like huge suspended/particulate matter discharging from the rivers/re-mineralization in OMZ zone/scavenging and East Indian Coastal current (EICC) (Sarin et al., 1989; McCreary et al., 1996; Shankar et al., 2002; Singh et al., 2012; Goswami et al., 2014; Yu et al., 2017). Relatively high concentrations of DFe is observed in the northern BoB compared to the central and the southern BoB. Large flux of terrestrial sediments coated with Fe-Mn hydroxide supplied by the Ganga-Brahmaputra river system could be an important source of DFe to northern BoB waters. Low DO values ($\leq 25 \mu\text{M}$) has been observed at a station 5°N in the BoB, in depth range between 150 – 1000m. Such low oxygen levels were not observed at southern stations in the BoB. The poor ventilation of waters in this region associated with the surface stratification in the upper layer makes DO low in the intermediate waters of BoB (Sarma, 2002; Sarma et al., 2016). The section plots of DFe in the BoB (Figure 3.9) display high concentration of DFe in the intermediate waters (between 100 to 1000 m) of the BoB which are associated with low DO levels. Such high DFe concentrations are not seen in the stations with higher concentration of oxygen. These observations emphasize that re-mineralization of organic matter along with dissolution of Fe-Mn hydroxide in the water columns with low oxygen are the main sources for high DFe in the intermediate waters of BoB. Singh et al. (2012) have revealed that Antarctica Bottom Water (AABW) dominates the bottom waters of BoB. The average DFe concentrations for the AABW in the BoB for depths greater than 2700 m is $0.83 \pm 0.38 \text{ nM}$ ($n=16$). These bottom waters are overlaid by Northern Indian Deep Water (NIDW) and Modified North Atlantic deep waters MNADW in the depth range of 1200 to ~ 2500 m. The average DFe concentrations of NIDW and MNADW in BoB is $0.75 \pm 0.18 \text{ nM}$ ($n=50$).

3.2.2.3 DFe in the Andaman Sea

Vertical profiles of DFe in the Andaman Sea show typical nutrient type behavior (Figure 3.7 B) with a surface minimum and increases with depth. The DFe concentrations of top 25 m in the Andaman Sea average $\sim 0.24 \pm 0.04$ nM (n=8). Sub-surface enrichment in the DFe level has been observed in the intermediate waters between 100-1000 m with an average concentration of 0.90 ± 0.24 nM (n=21). This sub-surface enrichment is attributed to remineralization process in the water column. The Andaman Sea receives huge amount of sediments with organic matter from the Irrawaddy and Salween rivers (Bird et al., 2008; Ramaswamy et al., 2008; Damodararao et al., 2016). The average DFe concentration in the Andaman basin below 1200 m water depth is 0.83 ± 0.27 nM (n=10). The monotonous behavior in the hydrographic parameter such as salinity, temperature, DO, silicate, phosphate (Figures 3.3) has been observed in the deeper waters of the Andaman basin. Andaman Sea exchanges waters with BoB mainly through the Ten degree channel, which is deeper relative to the Preparis channel in the north side with a sill depth of ~ 250 m (Varkey et al., 1996). The vertical mixing time estimated for the deeper waters of the Andaman Sea is ~ 5 y (Dutta et al., 2007; Okubo et al., 2004). The vertical profiles at SK304/17 and SK304/16, located at the core of the Andaman basin, display a monotonous DFe values below 1800m. This observation suggests the low scavenging rates for Fe in deeper waters attributed to organic complexation. Since the deeper waters of Andaman Sea are rapidly exchanged with the intermediate waters of BoB, the similar organic complexation occurring in the depth interval of 800-1200 m of BoB should reflect in the deeper waters of Andaman Sea. There exists no study from the BoB and the Andaman Sea focusing on organic complexation of DFe. However, our inference is based only on five data points of DFe values (*i.e.*, below 1500 m) in the Andaman Sea; high resolution data sets are required for further understanding.

3.2.2.4 DFe from the equatorial and eastern subtropical Indian Ocean

The DFe at stations sampled in the equatorial and subtropical Indian Ocean (below 5°N) during SK-304 and SK-311 are shown in Figures (3.7 C and

3.7 I). The concentrations are significantly lower in these regions compared to the stations in the Northern Indian Ocean. Sub-surface maxima were not observed at these stations. Interestingly, high concentration of DFe (20.87 nM) is observed at depth 2260 m at station SK-311/16 (Figure 3.7 J), which is sourced from the hydrothermal vents from nearby ridge system confirmed by the turbidity maxima at same depth (Figure 3.7 K). The very high concentration of DFe at station SK-311/16 is not included in the section plot (Figure 3.9). Along the central Indian ridge and south-west Indian ridge, presence of several hydrothermal vents is reported (Van Dover et al., 2001; Tao et al., 2004; Statham et al., 2005; Kawagucci et al., 2008; Ray et al., 2012; Nishioka et al., 2013). An active hydrothermal vent is identified over the central Indian ridge segment 12 miles north of the triple junction region (Gamo et al., 2001, 1996). The sampled location in this study is well known for the hydrothermal activity and was identified earlier as Kairie vent field (Rudnicki et al., 2002; Gallant et al., 2006; Kumagai et al., 2008). Rudnicki et al. (2002) have observed DFe maxima in the plume particles between 2150 to 2350 m of water depth and clear water below 2400 m. Higher DFe concentration observed in this study along with those reported by Japanese GEOTRACES (Nishioka et al., 2013) in this region suggest significant supply of DFe into the deeper waters of Indian Ocean from the hydrothermal vents present along the Central Indian Ridge and south-western Indian Ridge. The lateral advection of DFe from the Kairie vent site may be the reason for the observed high concentrations of DFe at SK-311/12 between water depth of 2000 and 3000 m (Figure 3.7 C). The DFe profiles at stations located nearer to equatorial region SK-304/6 and SK-311/9 are shown in the Figure 3.7 I. This location lies in the region where high DO containing waters from the southern Indian Ocean mixes with the poorly ventilated low DO containing waters. These two stations are sampled in the same season but in the successive years. In the depth interval of 2500 – 3000 m, increasing DFe is seen in the both SK-304/6 and SK-311/9 along the density anomaly of 27.8 Kg m^{-3} (Figures 3.9 A and 3.9 B) which could be sourced from nearby subduction zone characterized by high DFe (discussed in later section). High DFe is unlikely to be attributed to the sediment resuspension as concentrations of DFe are decreasing towards bottom. The average DFe

concentrations of AABW (depths greater than 3000 m) in the Indian Ocean is 0.77 ± 0.24 nM (n=26). Study of Singh et al. (2014) showed that 80-90% of the waters in the depth greater than 3000 m is dominated by AABW in the northern Indian Ocean and this dominant feature is seen up to 12° N.

3.2.2.5 Dissolved Iron along the Java Trench

During SK-304B (Second leg of SK-304), three water profiles (SK-304/11, 13, 14) were sampled along the Java Trench (Figure 3.1), from Eastern to Northern Indian Ocean before entering into the Andaman Sea. The vertical profiles of DFe for these three stations are shown in the Figure (3.7 D). The surface concentrations are very low in this area compared to other stations in the Indian Ocean. The sub-surface maxima were not observed in these stations unlike in the Northern Indian Ocean stations. These locations are characterized neither by OMZ nor by river-borne particle fluxes. The average DFe concentration (0.87 ± 0.19 nM, n=7) in the depth range between 100 and 1000 m at station SK-304/14, matches quite well with that of the Andaman Sea (0.90 ± 0.24) indicating intermediate waters of Andaman Sea passes through Great Channel in the southern direction (Varkey et al., 1996) in to the equatorial and northeastern Indian Ocean. The station SK-304/14 is located close to the Great Channel may receive the DFe signal from 100 – 1000 m depth of Andaman Sea. The hydrographic parameters (T and S) at depth range 100-1000 m at SK-304/14, SK-304/16 and SK-304/17 were compared and found consistent. DFe concentrations at these stations are invariant between depths 1000-2500 m and sudden increment in DFe values are observed below 2500 m. The increasing trend in the DFe values below 2500 m is also seen in SK-304/11 and SK-304/13 with the highest concentrations (2.61 nM) observed at SK-304/14. A discernible increase in the DFe concentrations in the deeper layers has been observed in between 3000–4500m water depth (Figures 3.9 A and 3.7 D). The DFe concentration at SK304/14 (~2.61 nM) is higher by a factor of 4 compared to DFe in deeper waters of global oceans (Martin et al., 1989; Johnson et al., 2007; Rijkenberge et al., 2014; Worsfold et al., 2014; Nishioka et al., 2013; Abadie et al., 2017) and the bottom/deep waters in this area (section 4.2). The lateral advection of higher DFe from station SK-304/14 could be responsible for high DFe at deeper depth at

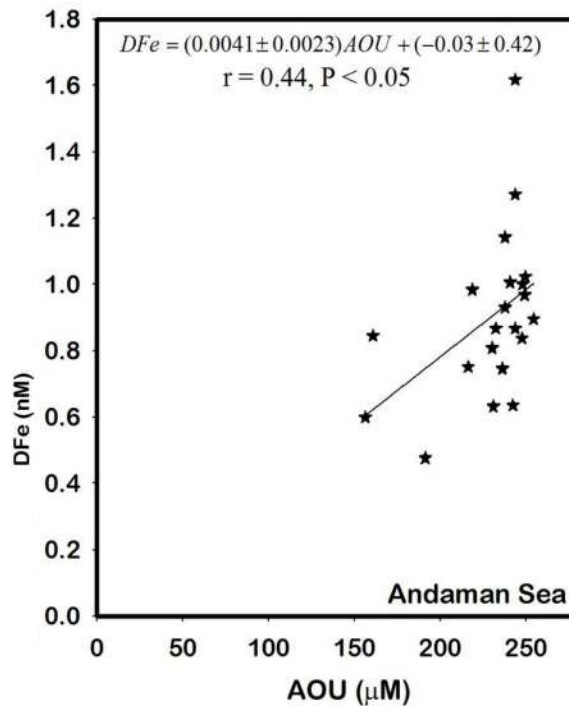
station SK-311/9. This transport of DFe could be mediated by the northwestward transport of AABW along the east of the Ninety Degree East Ridge (NER), (Frank et al., 2006, Clemens et al., 2016). Finger-printing of bottom ventilation at the NER is still poorly understood. As suggested by Frank et al. (2006), there may be a possibility of AABW flowing to western direction across the sills of NER which may carry the high DFe water from SK-304/14 to the SK-311/9. The density anomaly observed at depth having high DFe values at station SK-304/14 is $27.6 - 27.8 \text{ Kg m}^{-3}$ (Figure 3.9 A) which is quite similar to that observed at the station SK-311/9 at depth with high DFe suggesting advection of water with high DFe from SK-304/14 (Figure 3.9A) to the SK-311/9 (Figure 3.9 B) across the sills. This high DFe is also observed in the deeper depths of stations SK-304/11 and SK-304/13 suggesting the impact of Fe derived from subduction zone. These observations seem to suggest that the subduction related DFe is getting advected more than 1000 km distance.

High DFe in the deeper water at the station SK-304/14 is associated with the subduction boundary along the Java Trench. This is first report of high DFe sourced from a subduction zone. The high DFe is observed very close to the trench near subduction boundary (Figures 3.1 & 3.9). This region is seismically very active and faces frequent earthquakes due to the convergence of Indian plate with the Indonesian plate. This convergent plate boundary represents an active continental margin where oceanic lithosphere is being subducted beneath the continental lithosphere without a marine basin behind the volcanic arc; rather the arc is built directly on the adjacent continent (Frisch, 2014). This highlights the interaction of the fault systems present in this region during the convergence of continental plates which could serve as a source for DFe. Subduction of oceanic lithosphere along with sediments containing Fe-Mn nodules/oxy hydroxides could interact with subduction fluids to supply DFe in these regions. Fe-Mn nodules are present abundantly in the seafloor of the equatorial Indian Ocean (Cronan and Tooms, 1969; Nagender Nath et al., 1992; Shyam Prasad, 2007). Presence of high DFe in the subduction zone is also associated with higher abundances of dissolved REEs in this region (our unpublished results). Fault system could interact with subducting water and could act as a source of DFe in subduction zones. Similar to

diverging plate boundary, converging boundaries seems to act as a source for DFe to the seawater. The obtained feature in the deeper waters of Indian Ocean along the trench region needs a thorough investigation to understand the supply mechanism of DFe along this region.

3.2.2.6 *Fe:C remineralization rates in the BoB, the Andaman Sea and the subtropical Indian Ocean*

Re-mineralization of organic matter is the major source for DFe in sub-surface waters of the world oceans. The extent of re-mineralization in the depth interval of 100 – 1000 m is calculated using the linear regression correlations between AOU and DFe (Figure 3.10).



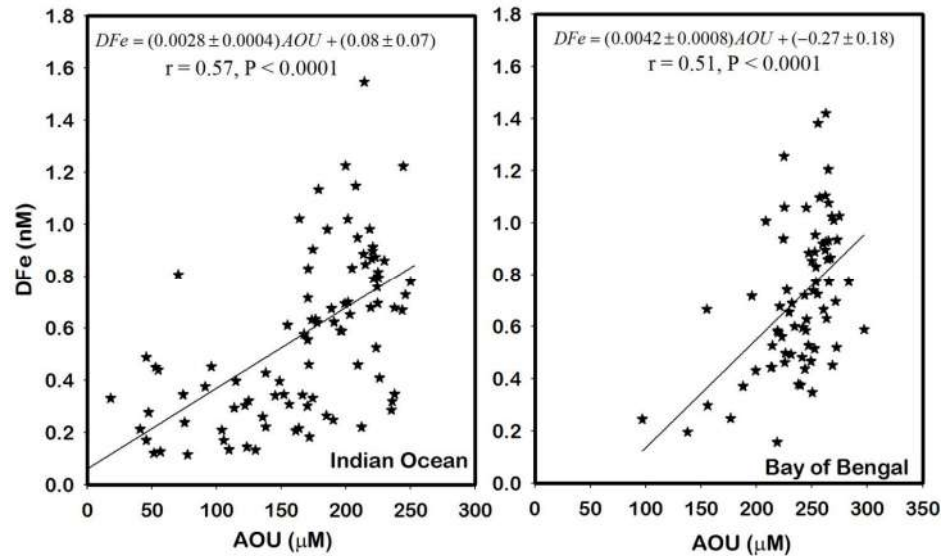


Figure 3.10: Fe:C remineralisation rates for DFe in the Andaman Sea, Bay of Bengal, and the subtropical Indian Ocean. The significant relation between AOU and DFe in the water depths between 100 to 1000 m shows that remineralization in the intermediate water is the significant sources for DFe. These ratios have been used to calculate Fe:C rates.

Fe:C regeneration ratios estimated from the present data set is based on AOU measurements and an $O_2: C_{org}$ ratio of 1.4 ± 0.1 (Laws, 1991; Anderson, 1995). Apparent oxygen utilization (AOU) represents the extent of remineralization in the oceans i.e., amount of oxygen consumed by the bacteria to degrade the organic matter. AOU is measured by subtracting measured oxygen values from saturated oxygen values. Saturated oxygen values are determined using temperature and salinity values in the water column. These Fe:C estimations are valid only in the regions where water masses with low scavenging rates are present. Using this qualitative parameter, Fe:C regeneration rates were calculated in oceanic basins (Bergquist and Boyle, 2006; Rijkenberg et al., 2014; Grand et al., 2015b and references there in). It is suggested in the studies of Witter et al. (2000), Hopkinson and Barbeau, (2007) and Boyd et al. (2010) that in OMZs enhanced DFe is due to the organic matter remineralization, which is stabilized simultaneously by Fe binding ligands in the solution. In the present study region, there exists OMZ in the depth range of 100-1000 m in the north of equator where corresponding maxima in DFe values suggest dominant remineralization process

without being scavenging. Therefore, it can be assumed that scavenging is quite low in the OMZ waters of the Northern Indian Ocean. NIIW occupies the majority of thermocline in the northern Indian Ocean (You and Tomczak, 1993; You, 1997) which is an aged form of Indian Central Water. The thermocline of the BoB contains the oldest central water of the north Indian Ocean (You and Tomczak, 1993).

Therefore, apparent Fe:C rates are estimated using relationships of DFe:AOU and Redfield ratio for O₂: C_{org} value 1.4 ± 0.1 (Laws, 1991; Anderson, 1995). DFe and AOU in the depth range of 100 to 1000 m are correlated in this work to calculate Fe:C rates. The significant relationship between DFe and AOU (Figure 3.10) is observed in all the regions of the study area (*i.e.*, BoB, AS, Andaman Sea and Indian Ocean). The AOU derived Fe:C rates estimated are 5.88 ± 2.65 $\mu\text{mol/mol}$, 5.74 ± 3.06 $\mu\text{mol/mol}$, 8.96 ± 3.85 $\mu\text{mol/mol}$ and 3.92 ± 0.83 $\mu\text{mol/mol}$ for the BoB, Andaman Sea, AS and equatorial/south of equator Indian Ocean, respectively. Significant positive intercepts are found at the stations other than equatorial/south of equator Indian Ocean, suggesting its contribution from additional sources such as shelf sediments/riverine particle flux in addition to *in-situ* remineralization (Singh et al., 2012; Yu et al., 2017). The estimated Fe:C ratios in the sinking organic matter from the euphotic zone of the Indian Ocean, BoB, AS and the Andaman Sea implies an overall spatial/regional difference in the uptake ratios of phytoplankton community. These qualitative Fe:C rates in the present study are shown in Table 3.1 along with the rates for other oceanic basins calculated similarly. Higher Fe:C in the northern Indian Ocean indicate the higher availability of DFe in these regions.

Table 3.1: Apparent Fe:C remineralization rates in the study region

S.No.	Location	Fe:C($\mu\text{mol/mol}$)	Study
1	Andaman sea	5.74 ± 3.06	Present study
2	Bay of Bengal	5.88 ± 2.65	Present study
3	Equatorial and Subtropical Indian Ocean	3.92 ± 0.83	Present study

3.2.2.7 Dissolved Iron as a limiting nutrient

Fe* is defined by Parekh et al, (2005) as $Fe^* = [DFe] - R_{Fe:P}[PO_4^{-3}]$ where $R_{Fe:P}$ implies the average biological uptake ratio of Fe over Phosphate. Fe* has been used in oceanic basins like tropical and subtropical Atlantic Oceans (Bergquist and Boyle 2006), West Atlantic Ocean (Rijkenberg et al., 2014), tropical and subtropical southeastern Pacific Ocean (Blain et al., 2008), western and central subarctic Pacific Oceans (Nishioka and Obata, 2017). These studies have used Fe* to identify the potentially growth limiting concentrations of DFe over phosphate and also to find the external sources for Fe other than organic matter remineralization. The value $R_{Fe:P}$ may vary significantly depending on the regional differences and phytoplankton community structure (Sunda and Huntsman, 1995; Twining and Baines, 2013). The term $R_{Fe:P}[PO_4^{-3}]$ gives the organic matter remineralization contribution in the water column. The Phosphate values in the regeneration length scale are a good indicator for remineralization process. The phosphate values in the water column of depth 100 – 1000 m are correlated against AOU to know the extent of remineralization in the study region.

The AOU vs. phosphate are correlated very well with a significant correlation coefficient of $R^2=0.82$ inclusive of both OMZ and non-OMZ samples. This strong correlation ($R^2=0.82$) suggests that remineralization is the dominant process in the intermediate waters and phosphate values in this region can be used as a tracer for the remineralization process. The scavenging of DFe in the OMZ is less due to the high re-mineralization/excess organic ligands (Witter et al., 2000; Hopkinson and Barbeau, 2007; Boyd et al., 2010). The DFe and phosphate in the depth range of 100 - 1000 m are compared on basin-wise and the correlations are shown in the Figure 3.12. A $R_{Fe:P}$ values of 0.28 ± 0.05 observed for BoB & Andaman Sea together with an intercept of 0.23 ± 0.13 and the Indian Ocean (equatorial/south of equator) samples are observed with the slope of 0.26 ± 0.03 with an intercept of 0.16 ± 0.06 . The positive intercept indicates excess DFe concentrations other than remineralization of organic matter. The obtained $R_{Fe:P}$ values of 0.28 ± 0.05 and 0.26 ± 0.03 in the BoB &

Andaman Sea and the Indian Ocean respectively are used in the above-mentioned Fe^* equation to identify the positive and negative Fe^* values in the study region.

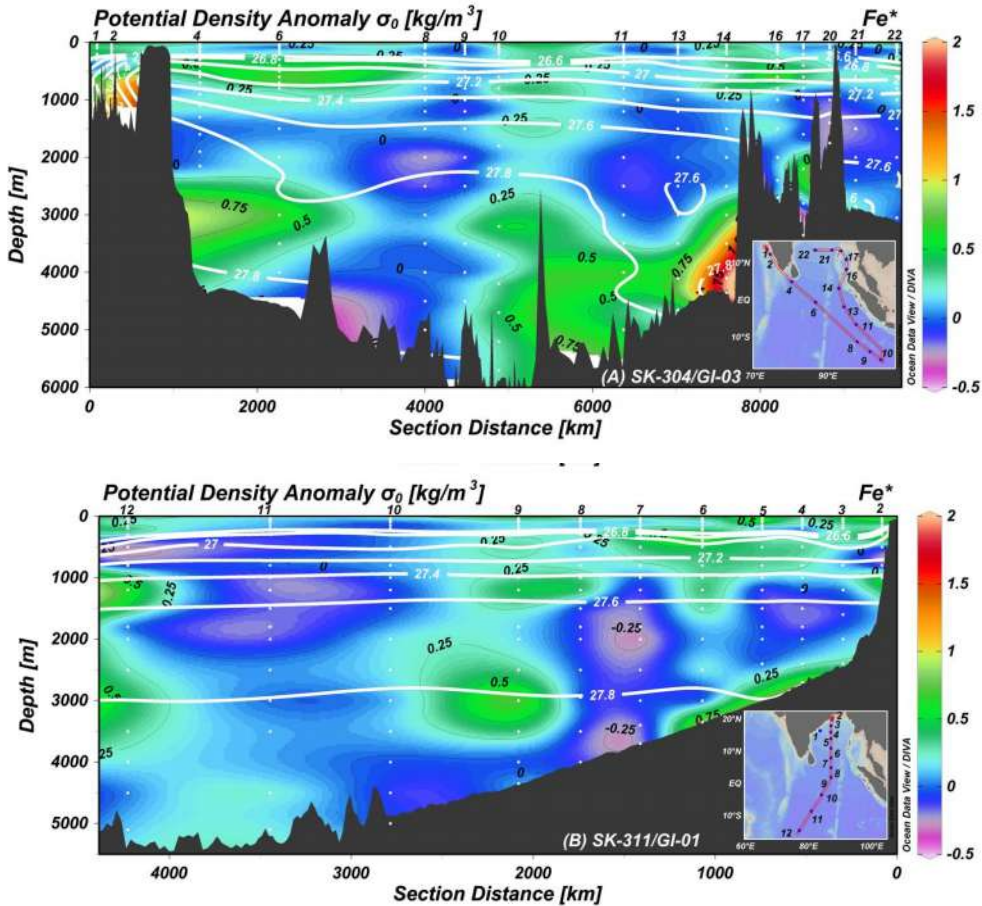


Figure 3.11:Section plots of Fe^* for (A) SK-304 and (B) SK-311 cruises. The contour line of zero separating the positive Fe^* from negative Fe^* for both the SK304 and SK311.

The $R_{Fe:P}$ for the previously published study of Grand et al. (2015a) data is also calculated to compare with the present study $R_{Fe:P}$ values and it yielded a ratio of 0.32 ± 0.07 with an intercept of 0.22 ± 0.18 for BoB and a ratio of 0.30 ± 0.06 with an intercept of 0.09 ± 0.13 for the Indian Ocean similar to the range of $R_{Fe:P}$ values estimated in present study. $Fe^* > 0$ represents the region having excess DFe over phosphate whereas $Fe^* < 0$ indicates regions having DFe deficiency

over phosphate. A zero-contour line (Figure 3.11 A and B) differentiates the excess vs. deficient DFe over phosphate regions. Positive Fe^* values are observed in the intermediate waters of Northern Indian Ocean suggesting additional source for DFe in these waters other than in-situ remineralization. The positive Fe^* values are mostly observed in the isopycnal lines of $26.4 - 27.2 \text{ Kg m}^{-3}$ which are mostly NIIW (white contour lines of Figures 3.11 A and 3.11 B). Negative Fe^* values in the same density interval of $26.4-27.2 \text{ Kg m}^{-3}$ (Figure 3.11 B) is observed in the south of equator suggesting the scavenging is more dominant in the oxygen rich waters of oligotrophic Indian Ocean stations.

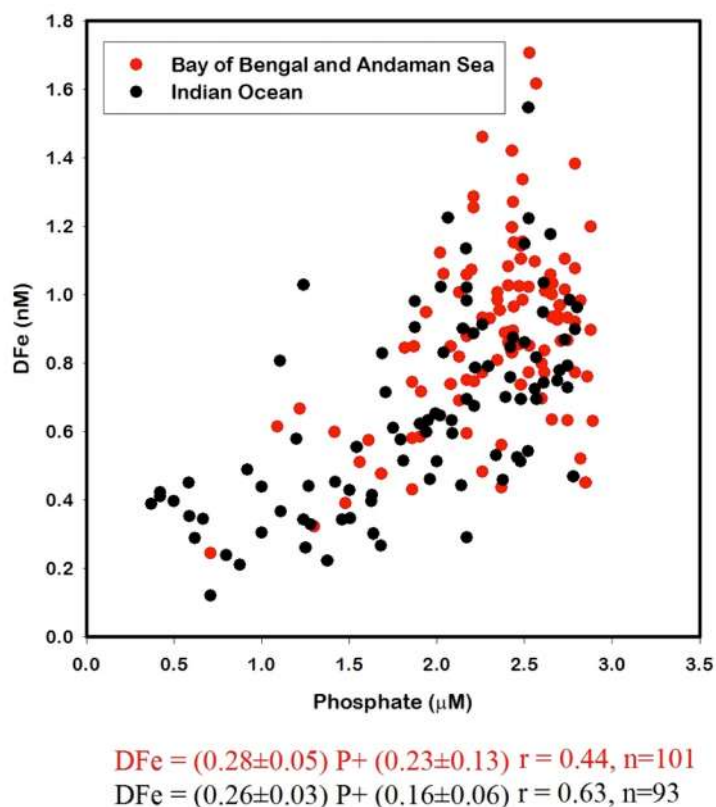


Figure 3.12: Correlation between DFe and Phosphate in the water column of 100 – 1000 m in the regions of BoB - Andaman Sea and eastern subtropical Indian Ocean.

The high particulate fluxes from rivers and shelf sediments could be important sources of the additional DFe in the intermediate waters of northern Indian

Ocean. In addition to high particle flux and shelf sediments, positive Fe* values in the region could also be attributed to external sources such as hydrothermal vents and subduction regions as discussed earlier. Interestingly, negative Fe* values are observed in the waters of northern Indian Ocean below 1200 m.

Recent study of Subha Anand et al. (2017) mentioned that export fluxes are very low in the BoB due to remineralization in the sub-surface waters based on particle reactive ^{234}Th measurements of sinking organic matter. Since the export of organic carbon is less due to remineralization (which generally happens between 100–1000 m) in the BoB, export of DFe from the surface water to intermediate/deep waters may also be low. Therefore, negative Fe* values (Figures 3.11 A and 3.11 B) observed in the deeper waters of northern Indian Ocean could be due to less Fe export from the intermediate waters and scavenging of preformed Fe in the deeper water column.

3.3 Dissolved Iron distributions in the Arabian Sea and western subtropical Indian Ocean

This section describes the distributions of DFe in the Arabian Sea and the western subtropical Indian Ocean collected during spring inter-monsoon period of 2014 and post southwest monsoon period of 2015. The study region is sampled onboard ORV Sagar Kanya (SK–312 and 324 cruises; See chapter 2) as a part of GEOTRACES-India section study. Twenty-eight stations were sampled following clean sampling protocol and were analyzed for DFe. During SK-324 cruise of the late southwest monsoon time DFe was measured onboard without any interruption. All station samples were analyzed using flow injection system under non metallic laminar flow bench. SK-312 samples were analyzed after the cruise completion in the laboratory under non metallic class-100 flow bench. During these cruises we have covered central, western regions of Arabian Sea with high resolution and the subtropical Indian Ocean. These cruises are part of GEOTRACES-India programme.

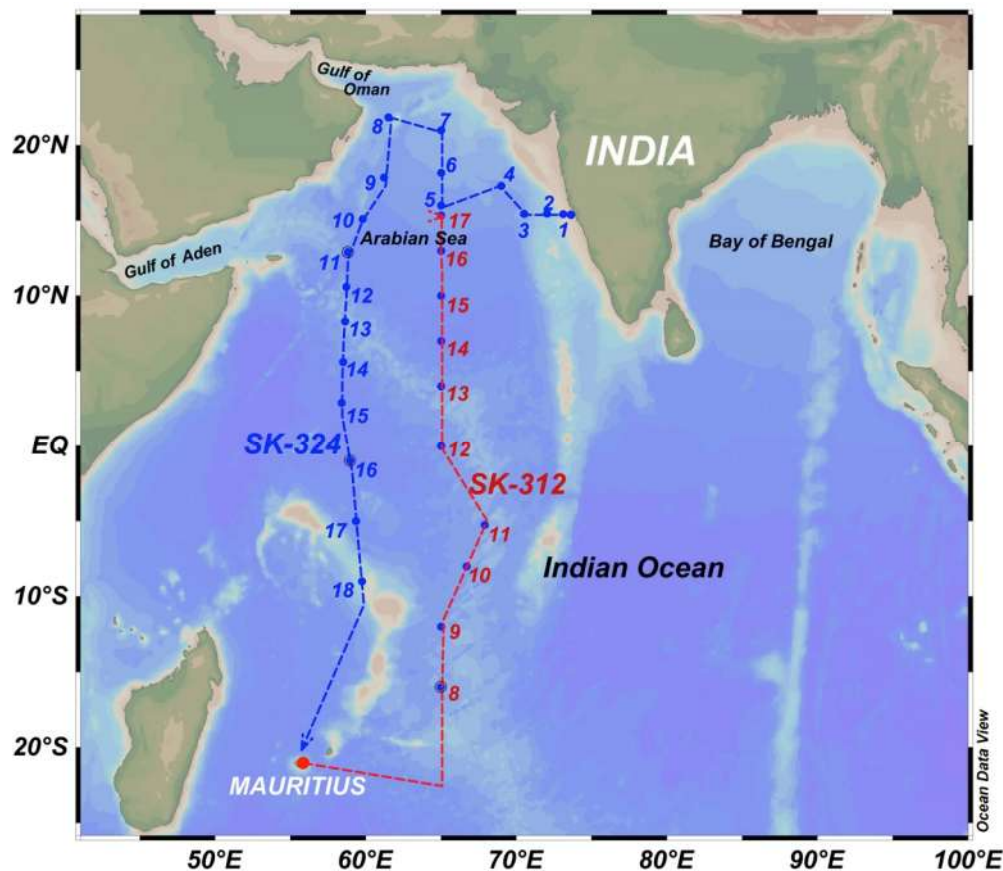


Figure 3.13: Map showing the sampling locations during SK-312 and SK-324 cruises. Cruise started from Mauritius and ended at Goa during SK-312 and vice-versa during SK-324 cruise.

Cruise SK-312 was started from Mauritius towards North and completed at SK-312/17 before reaching to Goa during SK-312. During SK-324, cruise started from Goa and sampled in eastern, central, western Arabian Sea and Somali basin before reaching to Mauritius. Sampling locations of the SK-312 and SK-324 cruises are displayed in the Figure 3.13. The sampling collection and analysis for DFe are discussed in the Chapter 2. DFe data are given in annexure 1.

3.3.1 Results and Discussion

3.3.1.1 Temperature-Salinity distributions during spring inter-monsoon

The general settings of the basic parameters salinity and temperature along the study region is shown in the Figure 3.14. High salinity waters are visible in the

surface waters north of stations SK – 312/14 (above 5 °N). In addition to this intermediate waters of stations sampled in the Arabian Sea are highly saline compared to stations sampled below equator.

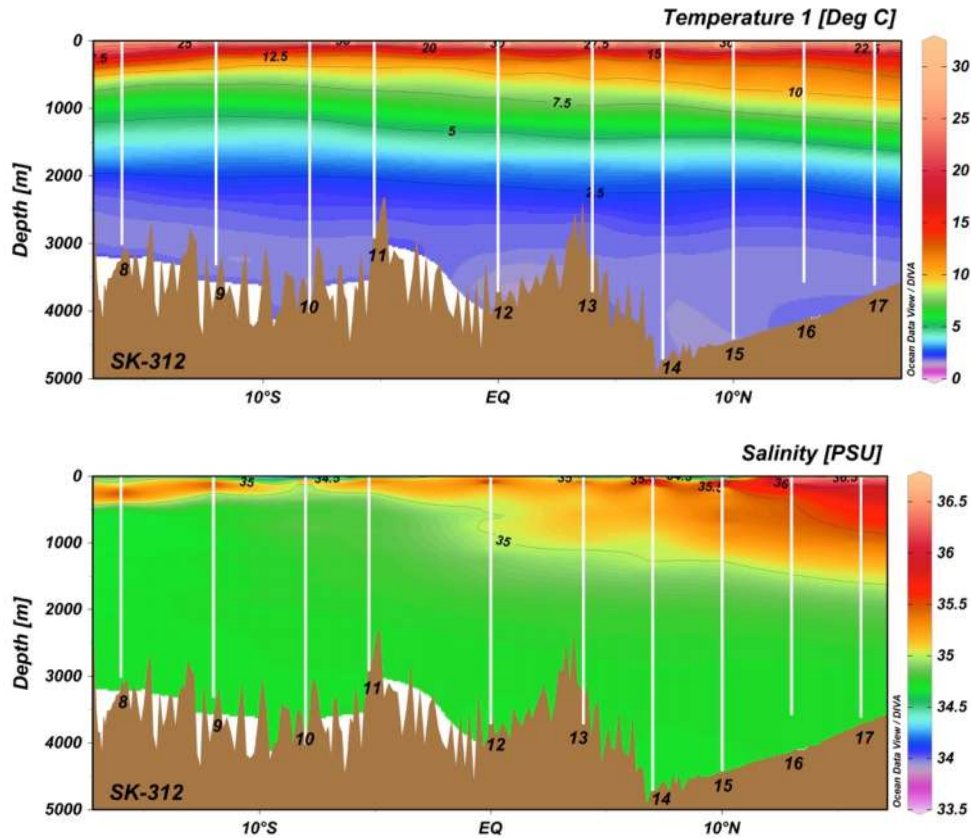


Figure 3.14: General behavior of Salinity and Temperature along the cruise SK - 312.

Relatively lower surface salinity values are seen in the remaining stations (south of 5° N) of the region compared to stations of AS. Sub-surface waters at stations SK-312/8 and SK-312/9 have higher salinity that is consistent with salinity values in the Indian Ocean sampled in cruise (SK-311). The high surface salinity values in the AS are due to the excess evaporation over precipitation. The sub-surface waters of AS is also highly saline due to the mixing of marginal waters, the Red Sea waters (RSW) and the Persian Gulf waters (PGW) which make sub-surface waters highly saline compared to underlying waters.

3.3.1.2 Temperature-Salinity during SK-324 cruise in the western Arabian Sea, eastern Arabian Sea and the western subtropical Indian Ocean

The Figures 3.15 and 3.16 shows the general temperature, salinity distributions and water masses (based on potential temperature vs. salinity) in the present study area. The high salinity value of 36.5 is seen up to station SK-324/12 in the salinity plot. These surface waters are nothing but ASHSW that typically forms in the Arabian Sea due to the convective mixing of waters during winter monsoon (Kumar and Prasad, 1999). It is also observed that intermediate waters have high salinity until station 12 (Figure 3.15) due to the presence of the PGW (Persian Gulf waters) and RSW (Red Sea waters).

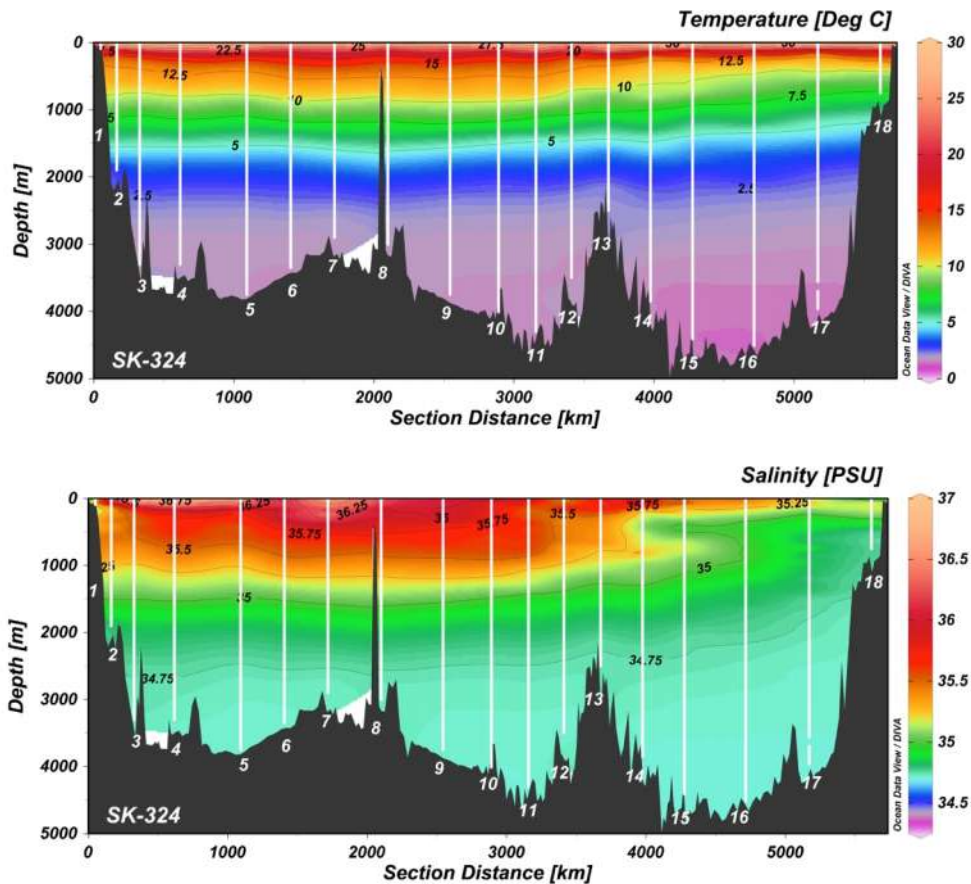


Figure 3.15: Section plot for Temperature and Salinity along the section SK-324.

The Arabian Sea waters show well-stratified layers in the surface with higher temperatures (Figure 3.15). Below 10 °N, the signatures of PGW and RSW

(high salinity values) have not been observed. The thermocline of the Arabian Sea waters mainly composed of ASHSW, RSW and PGW.

3.3.1.3 Water masses in the study region based on Temperature-Salinity plot with overlying isopycnal lines

The water mass structure of Arabian Sea and Indian Ocean is well characterized (Wyrтки, 1973; Shenoi et al., 1993; Dileep kumar and Li, 1996; You, 2000; Schott and McCreary, 2001, You and Tomczak, 1993; Goswami et al., 2014). Using potential temperature and salinity over isopycnal lines comprehensive list of water masses contributing to the region is listed in Figure 3.16. As discussed, surface and sub-surface waters are dominated by ASHSW, PGW and RSW.

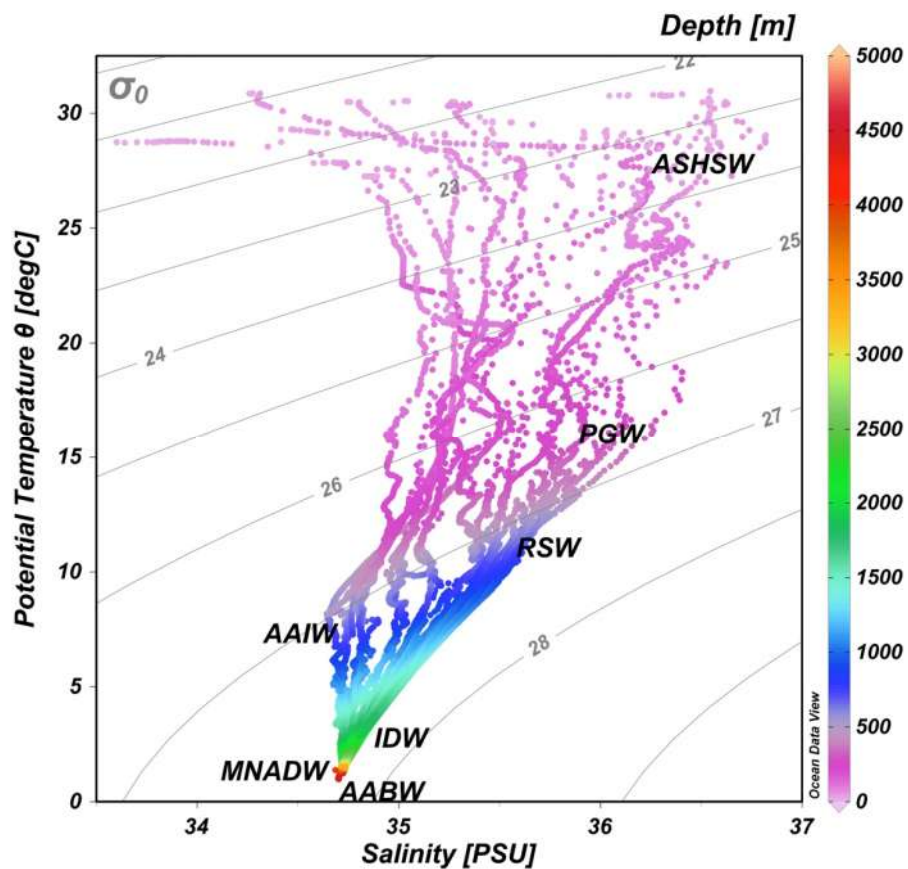


Figure 3.16: Potential temperature vs. salinity with isopycnal lines to characterize the different water masses in the study region.

These water masses occupy top 1000 m of the AS. Deeper waters are occupied by the NADW, which are modified during their transit from southern Indian Ocean towards northern side of the region, and these are mostly termed as MNADW in the AS. Bottom waters are dominated by the AABW in the region (Goswami et al., 2014). The high saline ASHSW are seen in the stations SK-312/14, 15, 16 and 17 with salinity values ranges from 35.4 to 36.7 with potential temperature range from 27 ± 3 °C (Figure 3.14). The surface salinities for remaining stations fall below 35.4. The PGW and RSW originate from Persian Gulf and Gulf of Oman and occupy the depth below ASHSW. As the PGW, progresses further southern AS from Oman region salinity values decreases. This is evident on TS plot. At stations SK-312/16 and 17 at a depth of 300-400 m the salinity is $\sim 35.6 - 35.8$ and at stations SK-312/14 and 15 salinity is about 35 with the potential temperature ranging between 12 °C to 14 °C.

At the origin, PGW has a salinity of 36.8 with potential temperature of 18 °C (Shenoi et al., 1993). The RSW which are originating from the Gulf of Aden occupies in the depth range of ~ 600 m of the Arabian Sea water column with the salinity of ~ 36 and similar to PGW the salinity values decrease to ~ 35 with potential temperature of ~ 10 °C. The MNADW and AABW occupy the deeper and bottom water layers respectively of the study region. The NADW, which forms at the North Atlantic, mixes with the Weddell Sea deep waters (WSDW) at south Atlantic and becomes denser and this denser modified water is generally termed as MNADW in the Indian Ocean. The AABW which forms at the polar region is denser than this MNADW and occupies below. The AABW bifurcates at the polar region and part of it moves towards Indian Ocean and to Pacific Ocean. The NADW and AABW in these deep and bottom waters further progresses northward through southwest Indian ridge (SWIR; Warren, 1978). These waters move towards Amirante Passage (Johnson and Damuth, 1979; Johnson et al., 1991; Dileep kumar and Li, 1996; Goswami et al., 2014) and Somali basin before entering into the AS (Mantyla and Reid, 1995). The Indonesian waters originates between 10° S and 15° S from the Northeastern Indian Ocean are relatively less saline and warmer (Jeandel, 1998). The less surface saline (33.8) waters observed at the station SK-312/10 could be due to these Indonesian surface waters from the

northeastern side. AAIW which forms at the Antarctic region can be traced at the stations of Indian Ocean with the depth interval of ~800-1100 m with potential temperature of ~8 °C.

3.3.1.4 Dissolved Oxygen

Section plot of dissolved oxygen is shown in the Figure 3.17. Intense oxygen minimum zone with DO values ~25 μM is seen in the AS waters in between 100 to 1000 m water column. This OMZ is slowly faded out as moving towards southern stations. Deeper waters of AS having relatively low DO values compared to stations in the southern side. The DO values with 50 μM are seen up to equator. The vertical profiles of dissolved oxygen are shown in the Figure 3.20. The salient feature seen here is dissolved oxygen values in between 100 to 1200 m (Figure 3.18) are very low in the stations from 1 to 14. The values go down to 25 μM in the most of the area and even anoxic conditions (DO – below detection limits) are observed. This feature is not observed in the remaining stations (15 to 18). These low values in the DO are the perennial feature of Arabian Sea attributed to the high productivity and bacterial remineralization in this area.

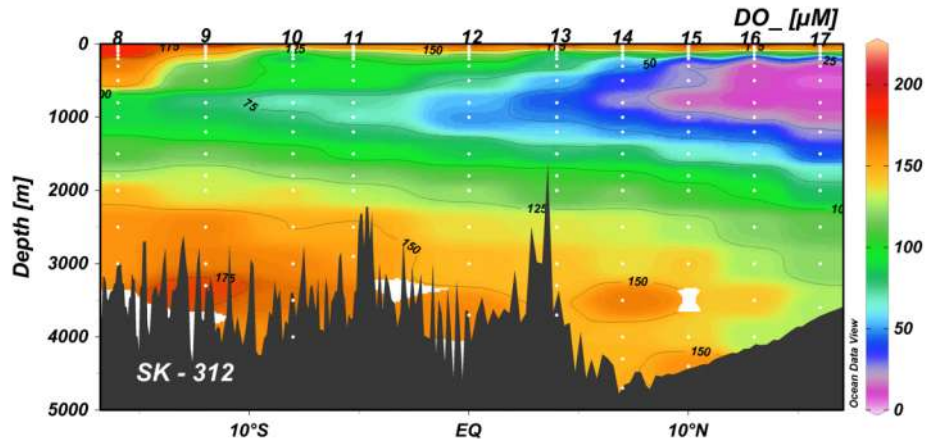


Figure 3.17: Section plot for DO. OMZ is noticed in the intermediate water column of Arabian Sea waters and western subtropical Indian Ocean.

AOU (Apparent oxygen utilization) is the parameter used to represent the extent of respiration in the water column. The high values of AOU observed in the intermediate waters (100 to 1200 m; Figure 3.18) indicate high bacterial respiration in this region.

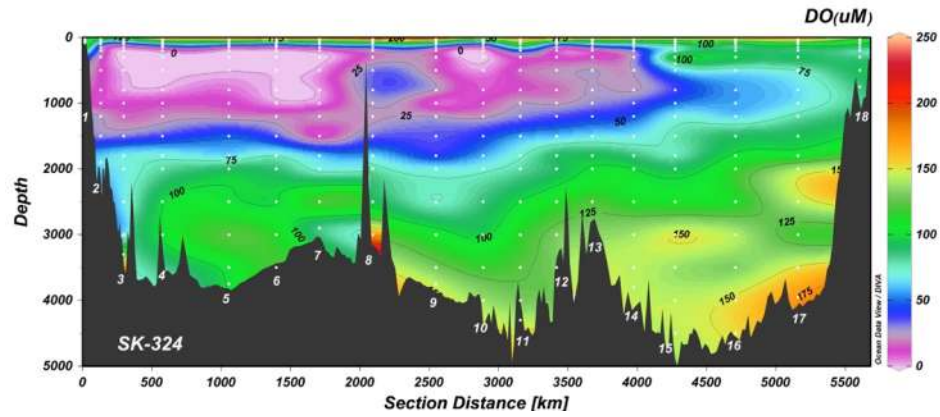


Figure 3.18: Dissolved oxygen section profile from the present study area.

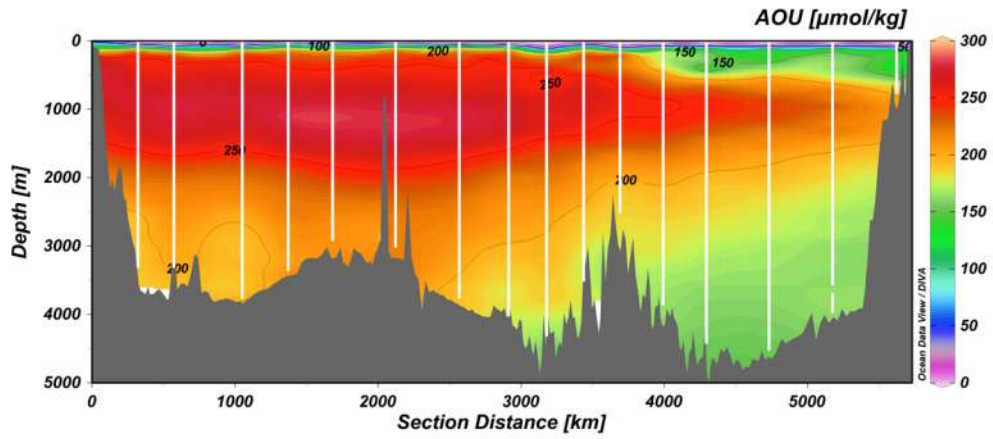


Figure 3.19: Apparent oxygen utilization (AOU) section profile from the study area.

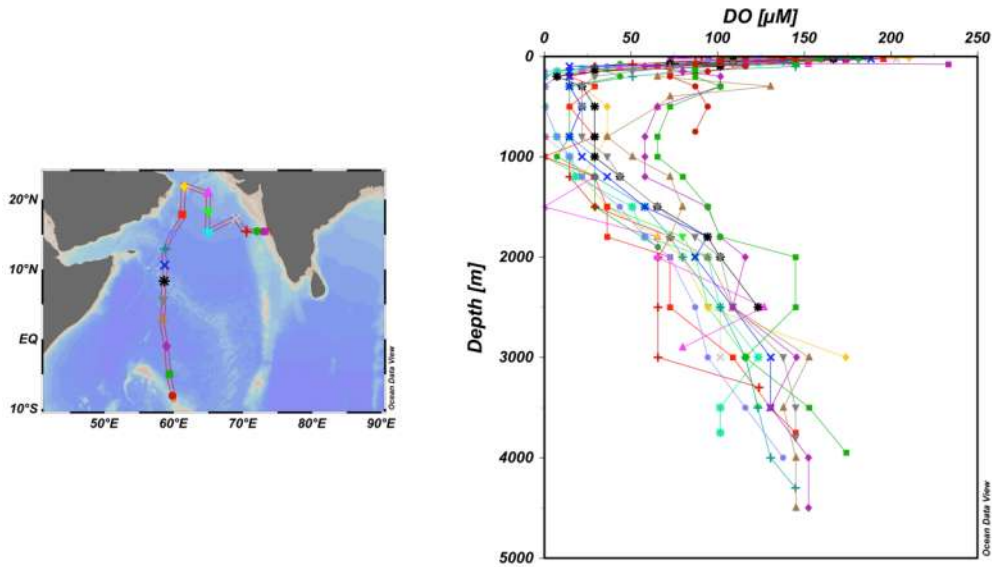


Figure 3.20: Vertical profiles of Dissolved oxygen (DO) in the SK-324 section.

3.3.1.5 Major nutrients distribution during spring inter monsoon

The measurement protocols of major nutrients are detailed in Chapter 2 of this thesis. The Figure 3.21 displays the distributions of nutrients in the AS and Indian Ocean during spring inter monsoon period. The profiles obtained in the study are oceanographically consistent. In the deeper waters starting from 5 °N, the silicate concentrations reaches up to ~150 μM and south of 5 °N, Si concentrations observed are ~125 μM (Figure 3.21 C). The regeneration length scale for Si as moving from the AS to Indian Ocean is increased. High concentrations of phosphate (~2.75 μM) is observed between 1000 to ~1500 m in the AS waters and that contour line can be traced up to equator. Phosphate reaches up to ~2.5 μM in deeper waters of the AS which builds up to ~2.25 μM in deeper waters below equator (Figure 3.21 B). Nitrate behavior is also similar to the Phosphate. High concentrations of nitrate (~35 μM) are observed in deeper waters of the AS and relatively less in the Indian Ocean stations. High nitrate concentrations are observed in between 1000 to ~1800 m.

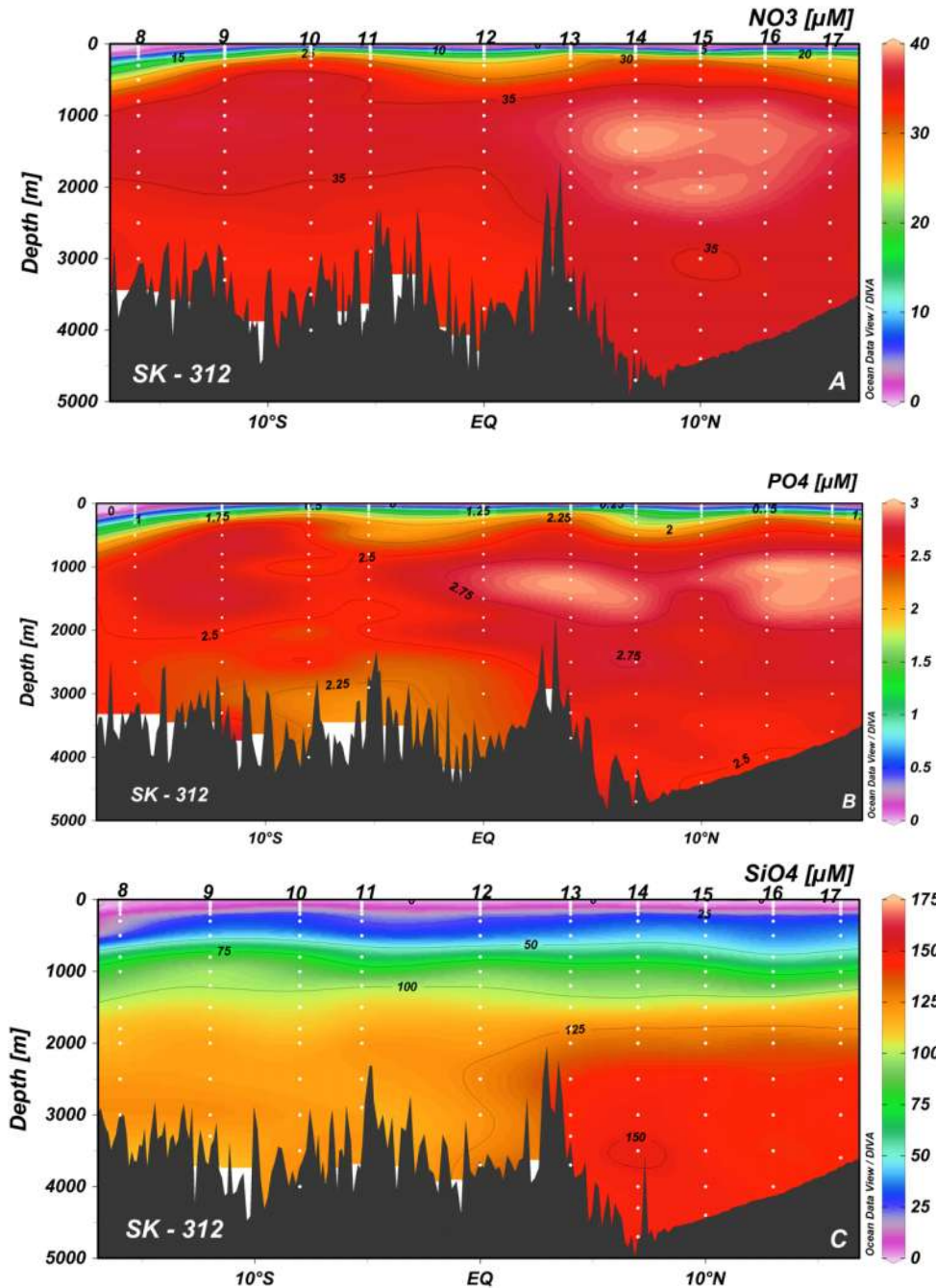


Figure 3.21: General distributions of major nutrients (A) Nitrate, (B) Phosphate and (C) Silicate along the cruise section SK-312.

3.3.1.6 Major nutrients during post southwest monsoon

The major nutrients silicate and phosphate profiles are shown in the Figure 3.22. The profiles are oceanographically consistent with surface low and increment with respect to the depth indicating their involvement in the biology.

Silicate reaches maximum of up to 150 μM in the deeper bottom waters and Phosphate reaches a maximum of 3.5 μM in the intermediate depths. Except in the station 16 the remaining stations, silicate and phosphate is almost consistent.

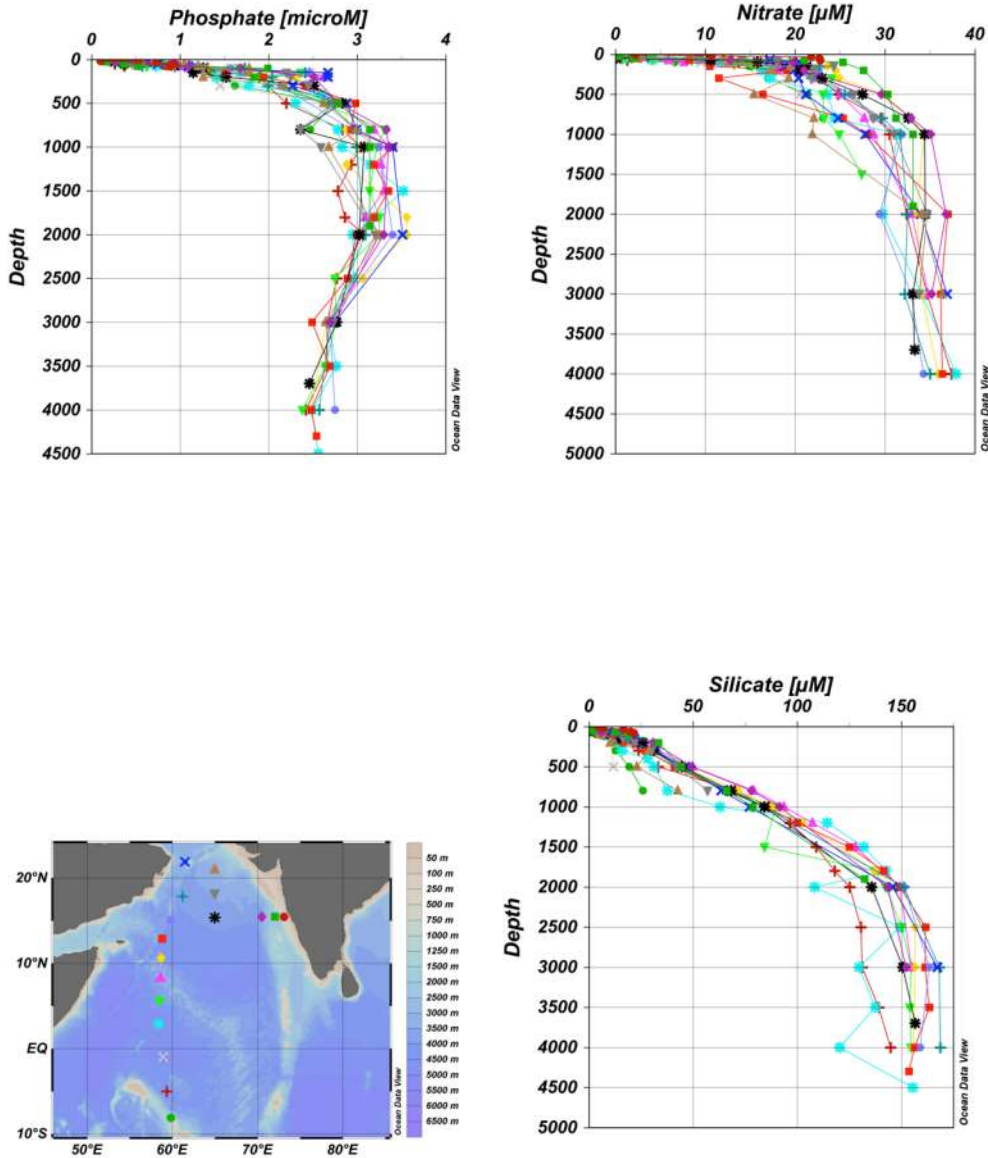


Figure 3.22: The vertical profiles for major nutrients nitrate, phosphate and silicate with the marked stations.

The values of silicate and phosphate at deeper depth at station 16 are relatively low compared to the other stations. Figure 3.22 shows the overall distributions of major nutrients in the section. Maximum concentrations of nitrate are observed in deeper waters with $\leq 35 \mu\text{M}$ and low values are observed in the surface. Maximum concentrations of phosphate are observed in the intermediate depths. Remineralisation process brings the phosphate back to water column in the intermediate depths due to high remineralisation/respiration. Silicate shows maximum in the deeper waters. North of equator the Si concentrations in the deep waters reaches to $150 \mu\text{M}$ where as south of equator stations the Si concentrations noticed were $125 \mu\text{M}$. The observed regeneration length scales are also different among N, P and Si. N and P show similar regeneration length scales but not the Si. Si regenerates little deeper compared to N and P. As N and P involves in the organic tissues its surface regeneration is expected whereas the Si involves in the hard body tissues, regenerating in the little deeper depth compared to N and P. The regeneration for N and P happens at 50 m for the nitrate and phosphate. Silicate regenerates at 200 m.

Distributions of dissolved Iron in the Indian Ocean

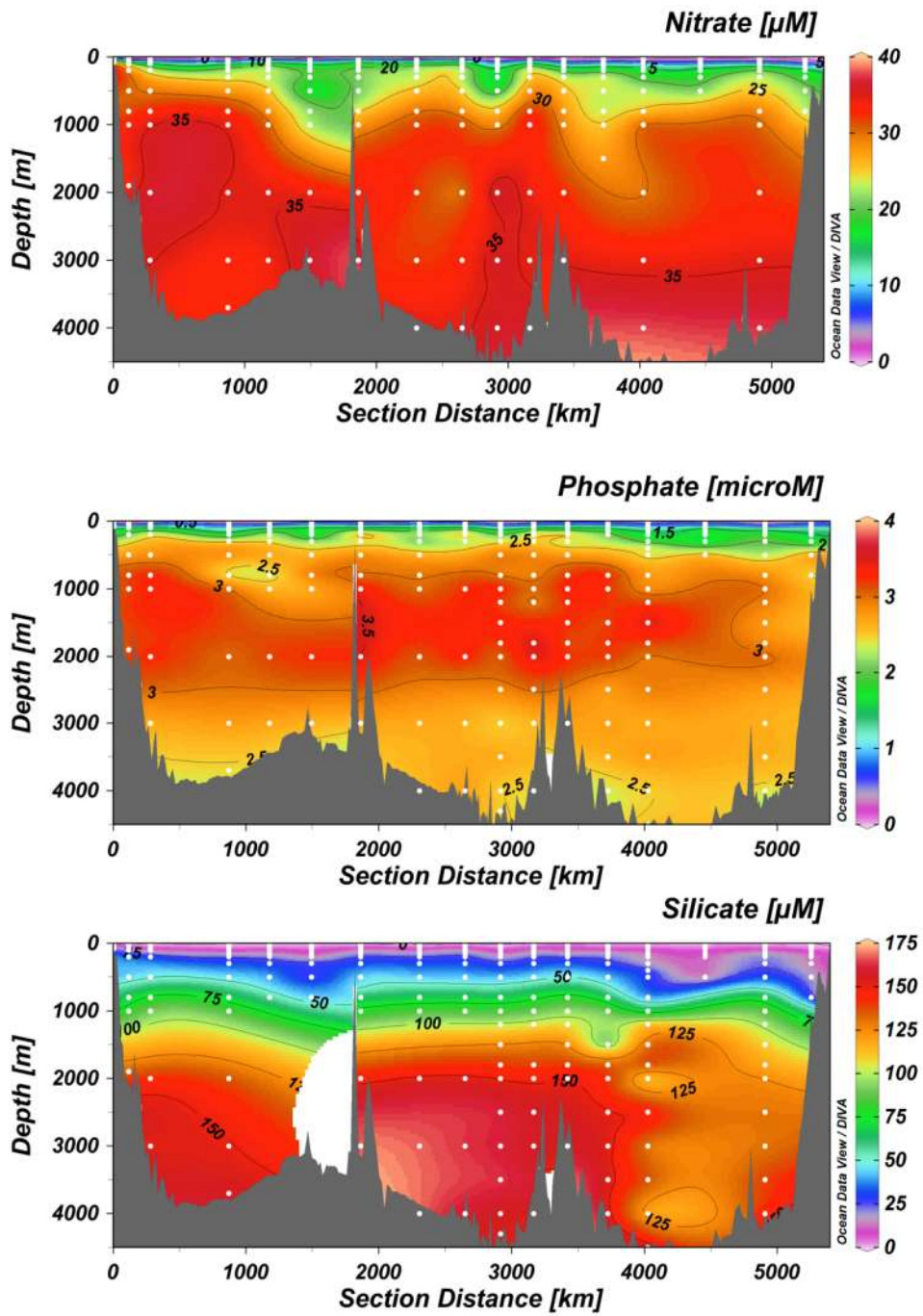


Figure 3.23: Section profile for nitrate, phosphate and silicate.

3.3.2 Surface dissolved Iron concentrations in the Arabian Sea and the subtropical Indian Ocean waters

3.3.2.1 Spring inter-monsoon period

The surface concentrations of DFe in the study region are shown in the Figure 3.24. Low concentrations of < 0.4 nM are reported during the spring inter-monsoon period, March 7-April 4, 1995. Except Measures and Vink, (1999), the results obtained in the study region in this work are consistent to other workers. Lower concentrations in the surface waters of the AS are observed in spring inter monsoon period compared to post southwest monsoon. The general trend observed in the surface waters during this season is decreasing from Northern Arabian Sea to as moving towards southern stations in the Indian Ocean suggesting crucial role played by atmospheric deposition emanating from nearby landmasses.

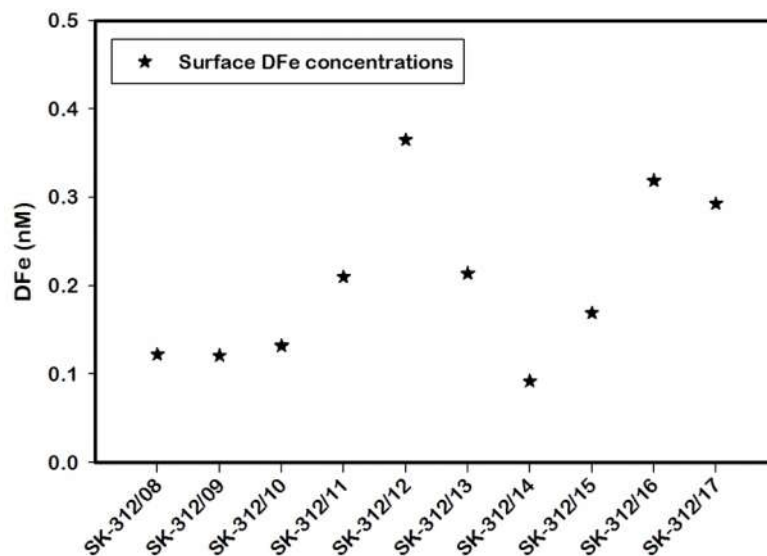


Figure 3.24: DFe concentrations in the surface waters (≤ 5 m) of SK-312 stations.

High primary production observed in the AS stations (Subha Anand et al., 2018) during this season may be the reason for observed low DFe values relative to the post southwest monsoon season. In addition, a factor of 3 lower primary production values in the Indian Ocean compared to AS stations was observed (Subha Anand et al., 2018). The stations with low primary production has very low DFe values (< 0.15 nM) and which may be the reason for a factor 3 difference

in the primary production values in the northern and southern stations. These southern Indian Ocean stations may be shortage of bioavailable Fe due to lack of sources like atmospheric deposition as in the AS. At station SK-312/12, relatively high DFe concentrations are noted compared to remaining stations of the sampled section.

3.3.2.2 Post southwest monsoon period

The DFe concentrations for post southwest monsoon period in the surface waters of the study region are shown in the Figure 3.25. The values range from 0.204 nM to 1.327 nM. There is a clear difference in the surface DFe values in the stations sampled near to the coast and Open Ocean. The two stations SK-324/2 and SK-324/3, which are close to the proximity of west coast of India, contain high surface DFe concentrations. In the open ocean stations observed surface DFe values are low (Factor of ~ 3) compared to the coastal stations.

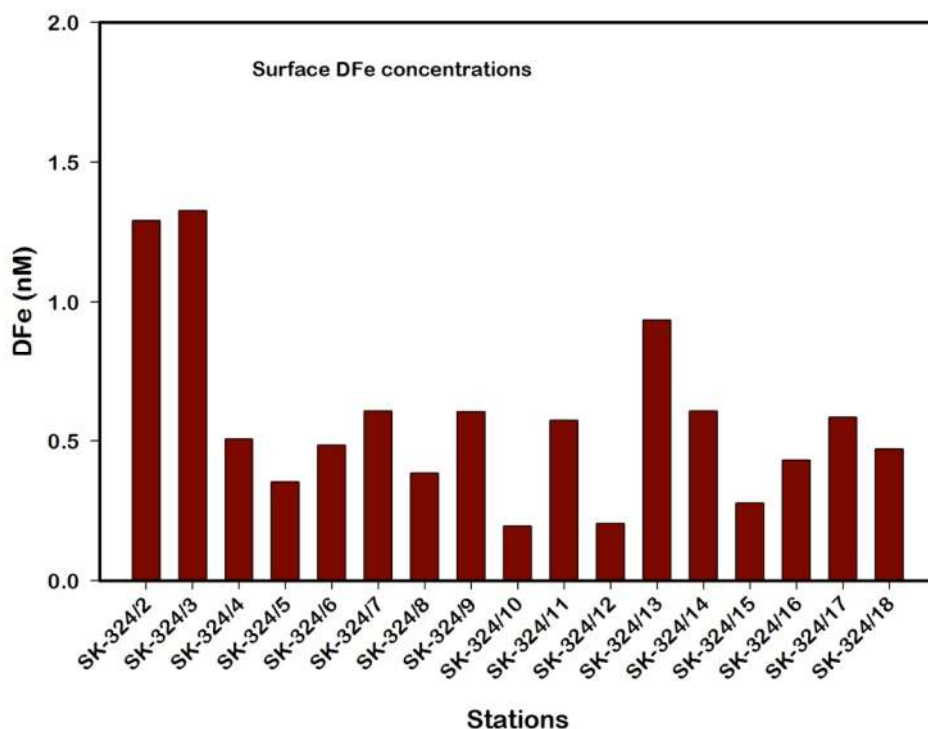


Figure 3.25: DFe in the surface waters of Arabian Sea and Indian Ocean during Post southwest monsoon period.

During late southwest monsoon surface DFe concentrations reported in the AS were in the range of 1.0 ± 0.2 nM (Northern section of AS) and 0.8 ± 0.2 nM (Southern section of AS; Measures and Vink, 1999) and during early northeast monsoon surface Fe values in the region were 0.8 – 1.2 nM. The DFe in the present study are lower by a factor of ~ 3 compared to the published data except at SK-324/2 and SK-324/3. Significant change in the surface DFe values are seen compared to the SK-312 cruise (Figure 3.24) sampled in the AS during April – May period. Measures and Vink. (1999) also reported seasonal variation in the surface DFe values in the AS but the values reported by those workers are considerably higher compared to our reported values in both the sampling periods. The atmospheric dust deposition is the major source for Fe in the open oceans (Duce and Tindale, 1991). During southwest monsoon, atmospheric deposition of mineral dust is the major source of DFe for surface waters of AS (Chester et al., 1991; Kumar et al., 2008). In addition to dust deposition, the monsoon currents bring cold nutrient rich waters to the surface by upwelling along the northwestern Arabian Sea and west coast of India (Banse, 1959; Madhupratap et al., 1990; Shetye et al., 1990; Smitha et al., 2008). The observed high concentrations in DFe in the Arabian Sea during September - October 2015 compared to the low values during April - May 2014 could be attributed to the atmospheric deposition during monsoon period and up-welled waters which can bring Fe rich water to the surface.

3.3.2.3 DFe vertical profiles in the central Arabian Sea and subtropical Indian Ocean

The vertical profiles for DFe show nutrient type behavior (Figure 3.26) with low concentrations at surface and increase with depth. The section plot of DFe (Figure 3.27) shows the influence of different sources on the Fe cycle in the region. The distributions of surface concentrations of DFe are discussed in earlier section (Figure 3.24). Lower concentrations of DFe in the southern stations are attributed to its biological uptake by phytoplankton and gradual increase observed in the DFe concentrations in the northern Arabian Sea could be due to atmospheric dust deposition. The vertical profiles in the Figure 3.26 clearly show

two different types of internal cycling. The Fe profiles in the Arabian Sea are clearly different from the

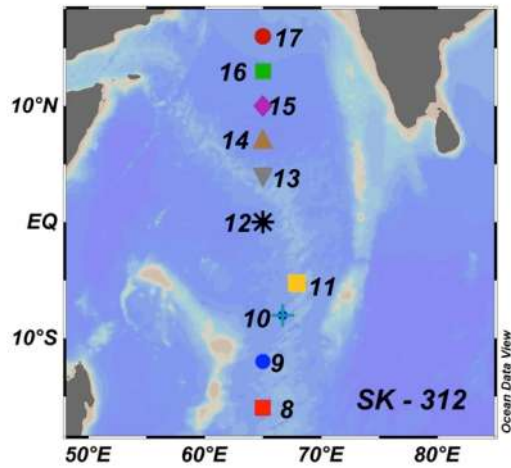
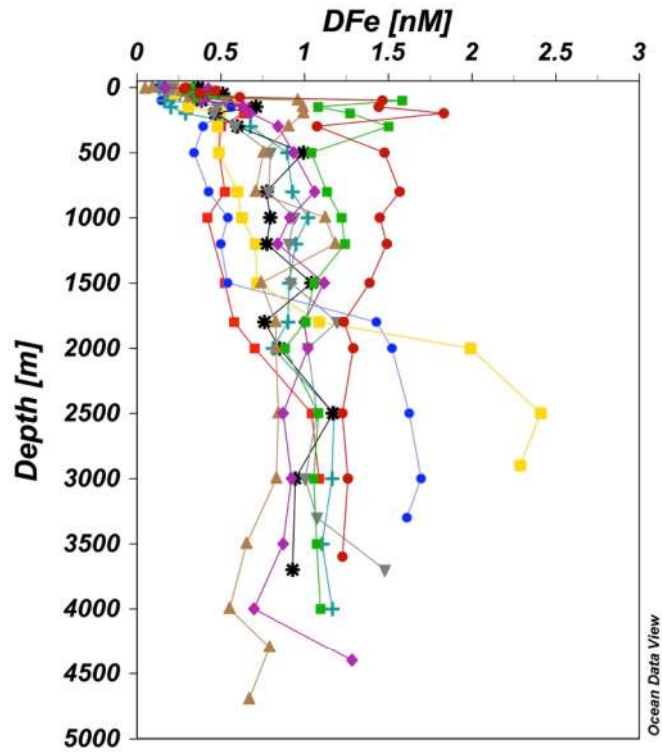


Figure 3.26: Vertical profiles for DFe in the Arabian Sea and Indian Ocean region sampled onboard Sagar Kanya during the cruise SK-312.

profiles of the subtropical Indian Ocean. In sub-surface waters, DFe concentrations increase sharply in the Arabian Sea stations. Such sharp increase in the subtropical Indian Ocean stations has not been observed.

The stations sampled in the northern Arabian Sea (SK-312/16 and 17) have very high concentrations of DFe in the depth interval of 75 m just below the surface waters. At these two stations in the northern Arabian Sea, DFe are invariant in almost entire depth of the water column with high concentrations (~1.6 nM) noted in the intermediate depths. As moving towards the southern Arabian Sea, DFe concentrations gradually decreased. Intense OMZ is observed in the stations SK-312/16 and SK-312/17 and the high DFe coincided with the low DO in these waters. The observed enrichment of DFe in the intermediate waters where DO values fall to suboxic levels is attributed to the intense remineralization (Discussed later). Earlier studies (Witter et al., 2000, Moffett et al., 2007) have reported higher DFe in OMZ water column of AS. Witter et al. (2000) studied organic complexation in the water column of AS and found excess ligand concentrations, 20 times higher in the deeper waters than overlying surface waters which could increase the bioavailability of Fe in the water column. In addition, Moffett et al. (2007) found 50% of total DFe in +2 form and suggested Fe reduction as a plausible source in the suboxic waters of AS. Similar enrichment in DFe is not seen in the other stations due to the absence of suboxic conditions. The deeper stations of Indian Ocean stations show enriched DFe in the water below 2000 m (Figure 3.26). The section plot (Figure 3.27) shows the lateral transportation of DFe in the deeper waters in between 2000-3500 m. This advected signal can be seen between 4° N and 15° S. Nishioka et al. (2013), which has highlighted the role of hydrothermal vents as a significant source, also see such enrichment in the Indian Ocean. In this study also, it is confirmed that deeper waters of Indian Ocean along the section (65° E) has a significant contribution from hydrothermal sources. Along with the DFe data, Nishioka et al., (2013) has found similar enrichments in the Manganese (Mn), Helium (He) and Methane etc. in these locations, which are the tracers to confirm the hydrothermal signal. Numerous studies (Von Dover et al., 2001; Statham et al., 2005; Kawagucci et al.,

2008; Ray et al., 2012; Tao et al., 2012) have highlighted the possibility of hydrothermal vents along the CIR and SWIR.

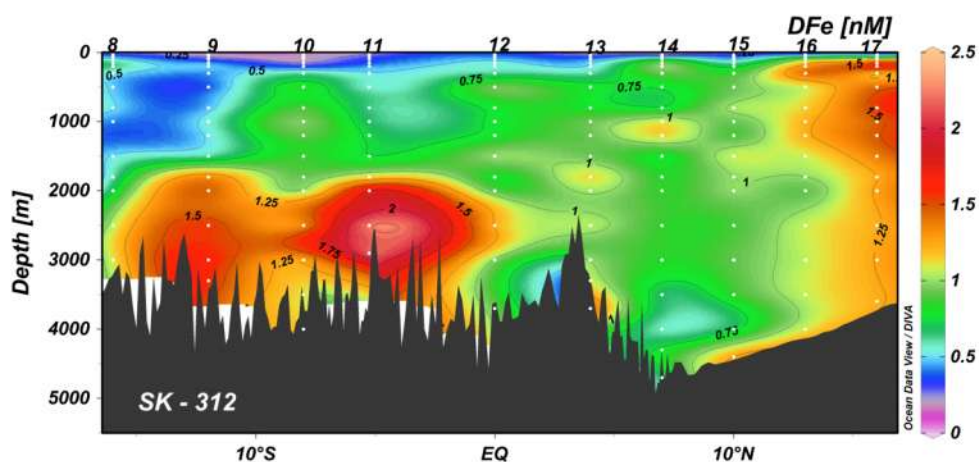


Figure 3.27: Section plot for DFe in the Arabian Sea and Indian Ocean. Station numbers are mentioned corresponding to the sampled location. Colour bar represents the concentrations of DFe.

Similar to Nishioka et al. (2013), light transmission and temperature anomalies are not seen in the deeper layers where DFe enrichment is seen. Srinivasan et al., (2004) found high He values in the deeper waters of Indian Ocean at 8° S, 60-65° E and 5-25° S, 80° E. Recent studies (Resing et al., 2015) also highlighted the advected signal of DFe from vent sources to several thousands of kilometers. These enriched signals in the deeper waters are due to the vent sources situated along the CIR, SWIR and Carlsberg ridges. Carlsberg ridge also seems to contain significant unknown hydrothermal vents which could contribute to DFe inventory (Discussed in later section). We have reoccupied the Japanese station ER-9 of Nishioka et al. (2013) during our cruise (SK-312/11) to compare the DFe data. The profile matches well (Figure 3.28) with the published data of Nishioka et al. (2013) except in the deeper depths where the DFe values are impacted by the hydrothermal vent signal. It is evident from the Figure 3.28 that temporal variation also could bring the changes in the Fe signal. The difference in DFe at deeper depth observed during both the sampling period could result if there is temporal variation in the water masses. However, this is negated based on the basic parameter data suggesting similar water masses during both sampling period.

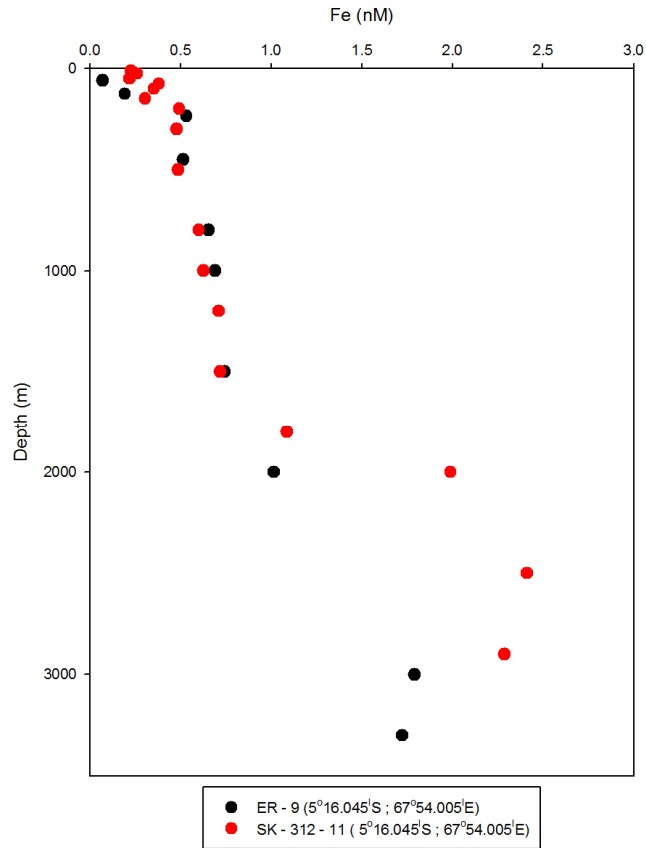


Figure 3.28: Comparison of SK-312/11(This study) and ER-9 (Nishioka et al., 2013).

This observed temporal variation depends on the flux and strength of the buoyant plumes. The hydrothermal vents as a significant source contributor for DFe inventory is recently identified and studies in this basin are required to decipher the impact of vent sources in the deeper waters of Indian Ocean.

3.3.2.4 Vertical profiles of DFe in the western Arabian Sea and over Carlsberg ridge

The DFe profiles in the Figure 3.29 shows the typical nutrient type profile with the surface low and increase with depth. Lower DFe concentrations in the surface waters of top 50 m display the biological consumption. At greater depths concentrations increases reaching a values > 1 nM consistent to lower DO values

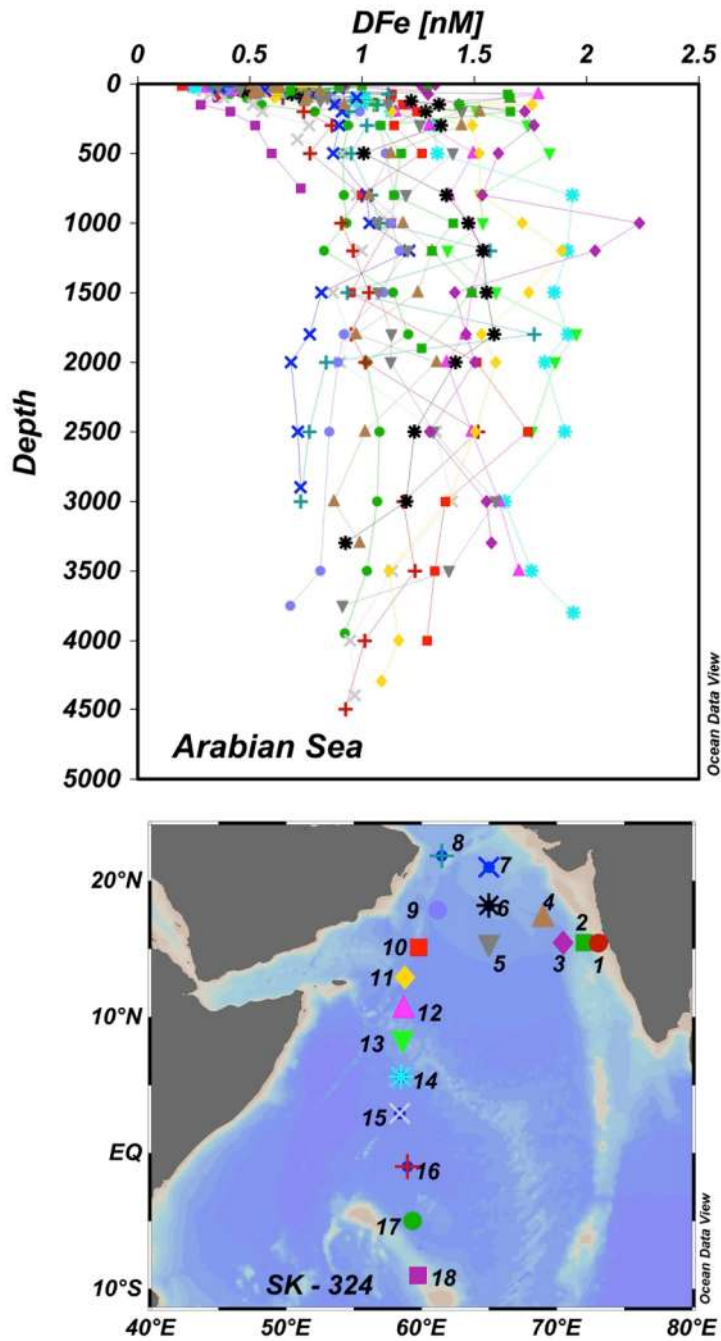


Figure 3.29: Vertical profiles of DFe along SK-324 cruise in the Arabian Sea and the Indian Ocean.

suggesting the intense remineralization in the intermediate waters of the Arabian Sea consistent with results obtained during the spring inter-monsoon period. However, DFe concentrations observed in the intermediate waters near to the

Oman basin, northwestern part of the Arabian Sea (Stations 7, 8 and 9) are relatively lower compared to that in the intermediate waters the central and eastern Arabian Sea (Figure 3.29). Earlier studies (Measures et al., 2005) mentioned that, AS could be a HNLC region during post southwest monsoon. The relatively lower concentrations compared with the central AS, eastern AS and during spring inter-monsoon strengthening the fact that after southwest monsoon season western AS might act as a HNLC region. The vertical distributions of DFe along the section agree with those reported during spring inter-monsoon below photic zone. The observed large-scale horizontal transport of DFe along the central Indian ridge over thousands of kilometers signature has not found in the present section.

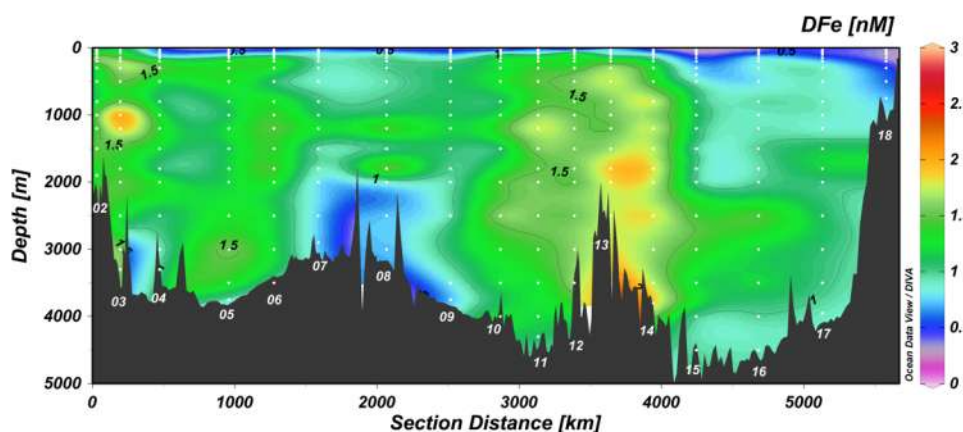


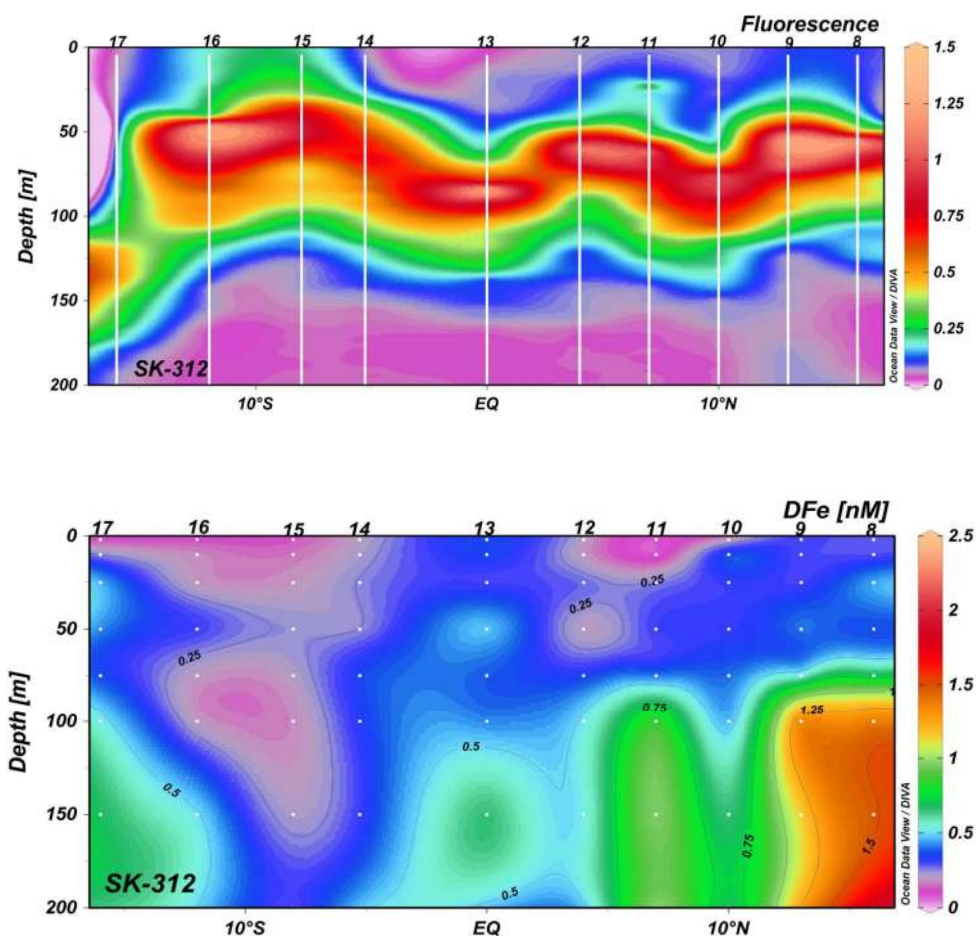
Figure 3.30: Section profile of DFe in the Northwestern Indian Ocean.

Nevertheless, the stations sampled over Carlsberg ridge has found rich in DFe concentrations. Recent studies (Rijkenberg et al., 2017) also found that magnitude of plume distribution is depends on the ridge spreading rate. The tracer ^3He , CH_4 and Mn are the best to identify the signal from the hydrothermal vent sources. If the source signal is from the ridge activity then the observed signal is stabilized against the removal from the oxic waters. Studies showed that hydrothermally derived DFe signal escapes from the precipitation, aggregation and scavenging by the formation of organic complexes (Fitzsimmons et al., 2017; Tagliabue et al., 2010; Yucel et al., 2011). However, the study region is least explored for the organic complexation other than the study of Witter et al. (2000) in the central AS. High concentrations of DFe are observed along the Carlsberg ridge (Figure

3.30) and Central Arabian Sea as well as close to west coast of India. Further studies are required for complete understanding of the source of high DFe signal over the Carlsberg ridge.

3.3.2.5 Fluorescence and DFe

The fluorescence maxima show significant depth differences within the region. The coastal stations have shown maxima in between surface to 50 m and fluorescence maxima depth shifts from 50 to 100 m as moving towards open ocean (Figure 3.31). In the central AS stations maxima is observed in between 25 to 50 m depth range and further increases as moving towards south direction. The coastal upwelling along the west coast of India brings the nutrient rich water to surface further enhancing the productivity. Except in the coastal stations, low concentrations of DFe are observed with respect to the fluorescence maxima showing its biological utilization.



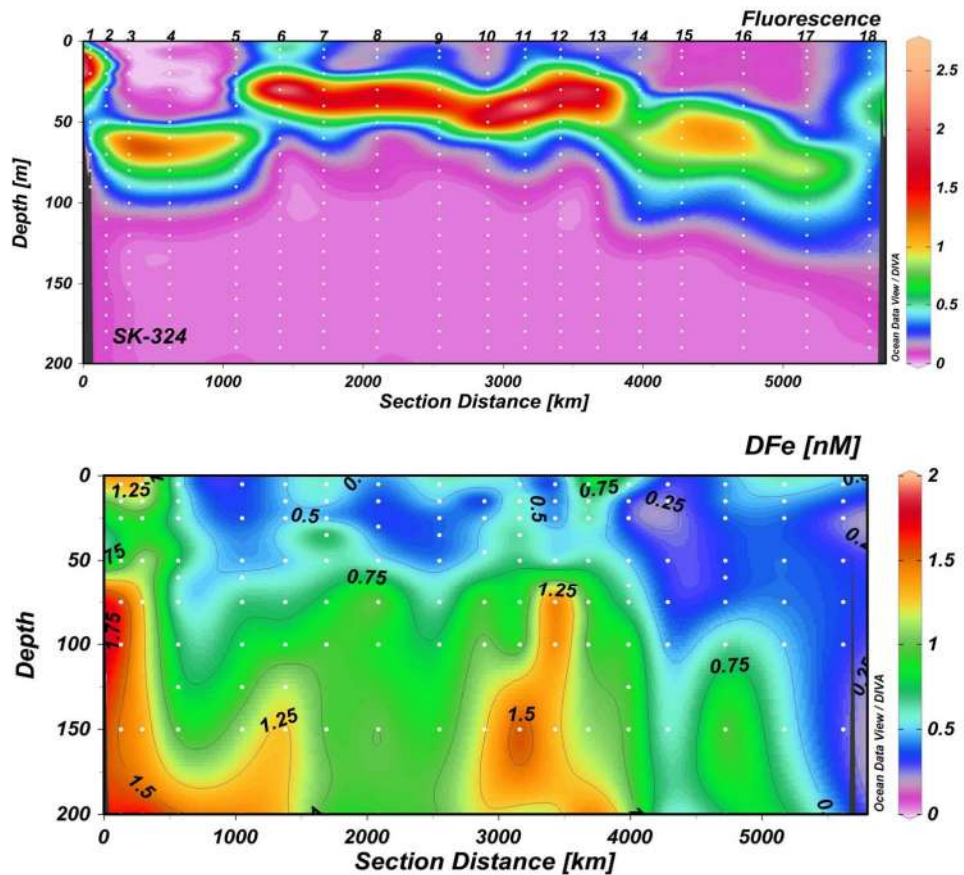


Figure 3.31: Fluorescence and DFe section profiles for the top 200 m in the AS during spring inter-monsoon (Above). Fluorescence and DFe section profiles for the top 200 m in the AS during late southwest monsoon (Below).

3.3.2.6 AOU vs. Major/Minor nutrients and Fe:C rates

AOU is the parameter that provides insight into the extent of remineralization in the water column. AOU is estimated by subtracting the measured dissolved oxygen from saturated dissolved oxygen values. The resultant is the oxygen left over in the water column once the waters are last in touch with the surface or used for the degradation of sinking organic matter by the organisms. The extent of remineralization process can also be understood with the help of major nutrients. The nutrients nitrate and phosphate are best tracers to identify the remineralization activity.

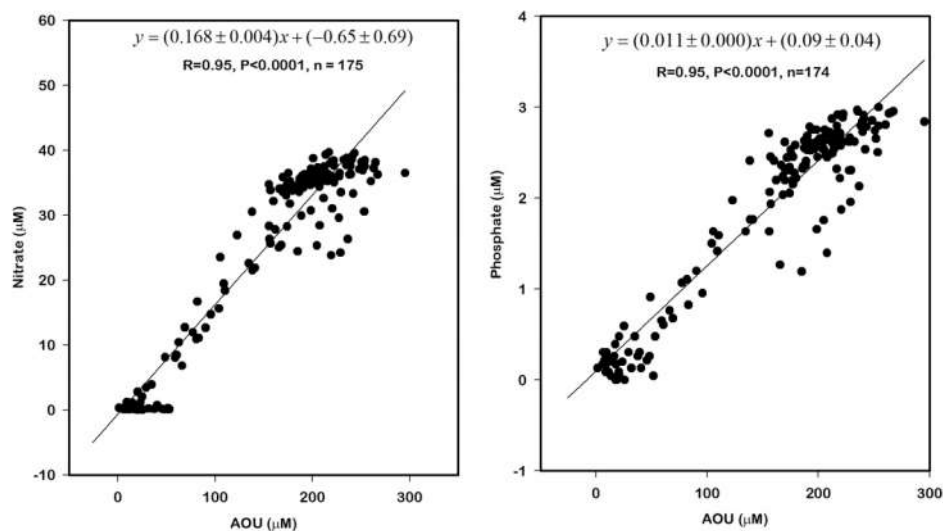


Figure 3.32: AOU vs. nitrate and phosphate relation in the study region.

In the regions where intense OMZ are present Nitrate cannot be used to know the remineralization due to its denitrification and annamox processes in the water column. Therefore, in that case phosphate can be used which, unlike nitrate, doesn't undergo any other processes in the OMZ. The Figure 3.32 shows the scatter plots between AOU vs. N and P in the water column along the study region. A good linear significant relation is observed between AOU and major nutrients (N and P). The observed slopes are close to the Redfield ratios as expected in the open ocean regions. Sengupta et al. (1976) studied the relation between DO and major nutrients in the Northwestern Indian Ocean. The observed relation between AOU and major nutrients in this study is very consistent with the published data of Sengupta et al. (1976). The DFe data is plotted against the AOU values in the study region to find the extent of remineralization.

The data is separated in to two sets, one with intense OMZ region stations and others sampled south of 10° N. As expected, the correlation is not that significant in the rest of the stations compared to AS due to the less remineralization and scavenging of Fe. This is evident from the slopes of AOU vs. DFe in the plot (Figures 3.33). The slope of the AOU vs. DFe in the AS where intense OMZ occurs yielded a high slope compared to remaining stations suggesting that remineralization is the dominant process in the northern stations compared to southern stations (Figure 3.34).

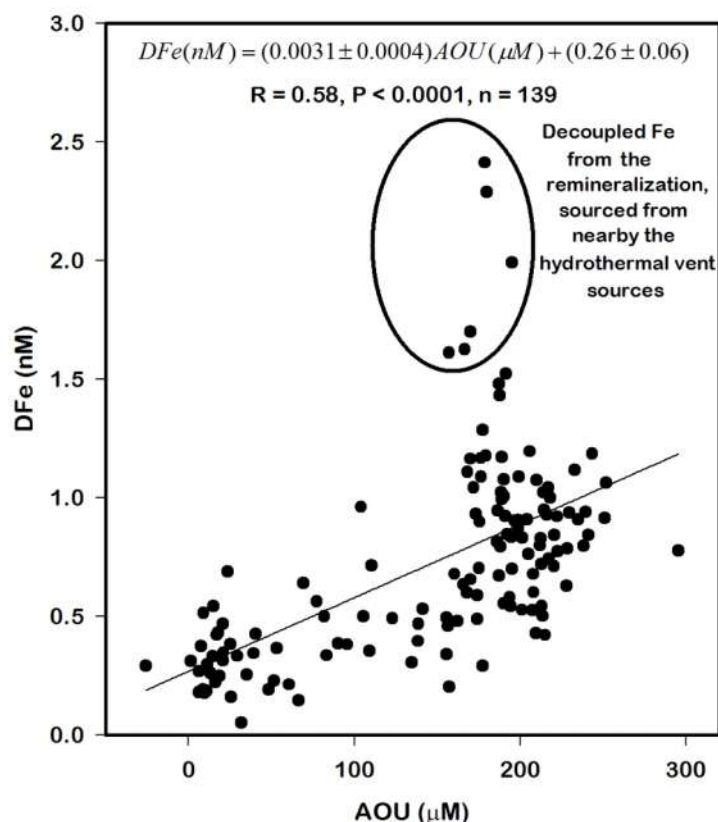


Figure 3.33: AOU vs. DFe scatter plot in the stations of SK-312 other than Northern AS.

As discussed in the earlier section, hydrothermal vents contribute significantly to DFe budget in the region. It is evident clearly from the Figure 3.33 that few of the DFe are decoupled from the remineralized signal and are sourced from the hydrothermal vents in the Indian Ocean. A very strong and significant relation is observed in the stations of the Arabian Sea. Fe:C regeneration ratios estimated in the present data set is based on AOU measurements and an $O_2 : C_{org}$ ratio of 1.4 ± 0.1 (Laws 1991; Anderson, 1995) as discussed in the previous section (3.2.2.6). These Fe:C estimations are valid only in the regions where water masses with low scavenging rates are present. DFe and AOU data in the depth range between 100 to 1000 m are correlated in this region to calculate Fe:C rates.

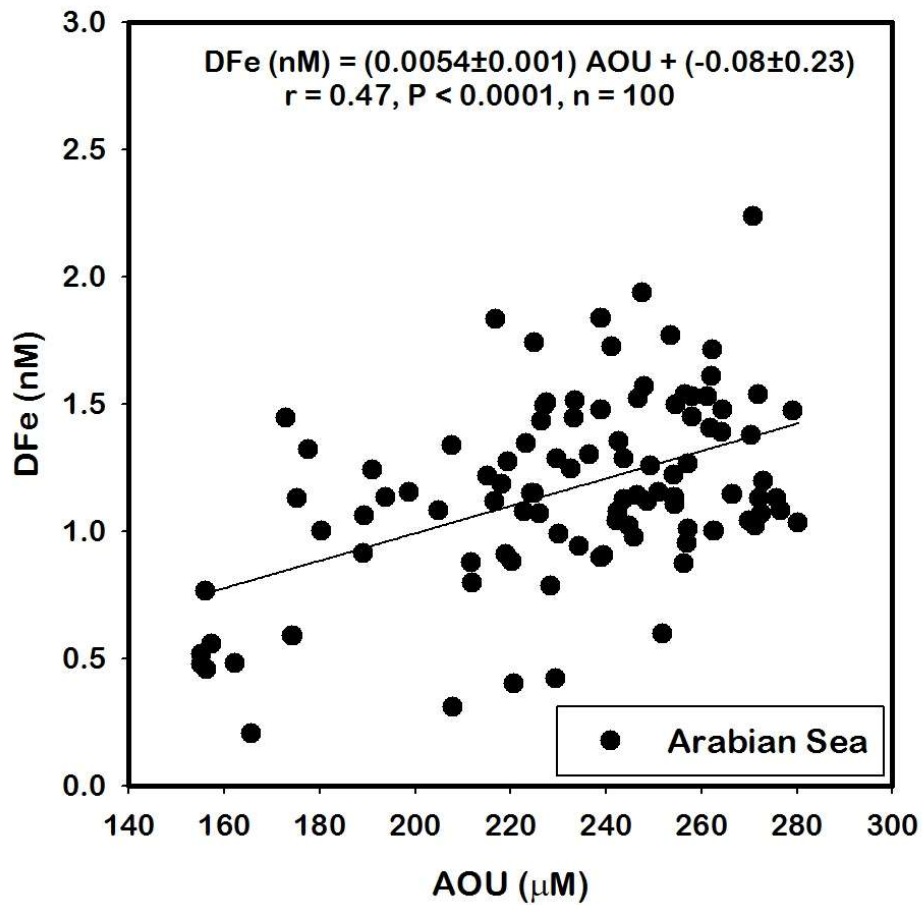


Figure 3.34: DFe vs. AOU scatter plot in the Arabian Sea. Data includes all the stations sampled during SK-312 and SK-324.

The AOU derived Fe:C rate estimated is $7.56 \pm 1.93 \mu\text{mol/mol}$ for the AS and for the western subtropical Indian Ocean the ratio is $4.34 \pm 0.86 \mu\text{mol/mol}$ which is similar to the values obtained in the eastern subtropical Indian Ocean stations. Stations from both the cruises SK-312 and SK-324 are considered for calculating AS Fe:C rates. The estimated Fe:C ratios in the AS is higher than the rates observed for the BoB, Andaman Sea and the subtropical Indian Ocean and implies an overall spatial/regional difference in the availability of DFe and uptake ratios of phytoplankton community.

3.3.2.7 *Fe as a limiting nutrient in the Arabian Sea and the subtropical Indian Ocean*

The term Fe* is already defined in the section 3.2.2.7. A similar calculation has been done for regions in the Arabian Sea and western subtropical Indian Ocean. The cruises data of SK-312 and SK-324 has been used to obtain Fe* section plot that covering the regions of AS and western subtropical Indian Ocean. The AOU vs. Nutrients shows the strong correlations in this region depicting the remineralization is the dominant process in the water column (Figure 3.32). The Figure 3.35 shows the plot between phosphate and DFe in the depth interval of 150 to 1000 m in the water column. The slope obtained for this region is 0.27 ± 0.06 with an intercept of 0.47 ± 0.16 . The slope of the plot 0.27 is taken as $R_{Fe:P}$ and calculated Fe* in the region using the equation

$$Fe^* = DFe \text{ (nM)} - (R_{Fe:P}) * (\text{Phosphate})$$

The obtained $R_{Fe:P}$ value of 0.27 ± 0.06 are used in the above-mentioned Fe* equation to identify the positive and negative Fe* values in the Arabian Sea and subtropical Indian Ocean to identify the potentially growth limiting regions of Fe over phosphate. Fe* section plot along the cruises SK-312 and SK-324 are displayed in the Figure 3.36. A contour line of zero separates the positive Fe* from the negative Fe* in the Figure 3.36 to identify Fe limited regions. Like the BoB and the eastern subtropical Indian Ocean the deeper waters has shown negative Fe* values in the western Arabian Sea and western subtropical Indian Ocean. Positive Fe* values are observed in the regions where hydrothermal derived vent signal is observed. In addition, central and eastern AS also displays positive Fe* values along the SK-312 and SK-324 sections (Figure 3.36). Atmospheric deposition and organic complexation in the intermediate waters together with perennial OMZ waters makes central and eastern Arabian Sea as a Fe replete region. Studies (Measures and Vink, 1999; Moffett et al., 2015) found Fe depleted conditions along the west coast of AS off Oman (west coast of the AS) during post southwest monsoon. Measures et al. (1999) suggested Fe limited region at one single station (S1 in their study) which is very close to the west coast of AS using $NO_3:Fe$ ratios. Experiments done in the waters of the western

AS during the late southwest monsoon period suggests the presence of HNLC conditions (Moffett et al., 2015; Naqvi et al., 2010).

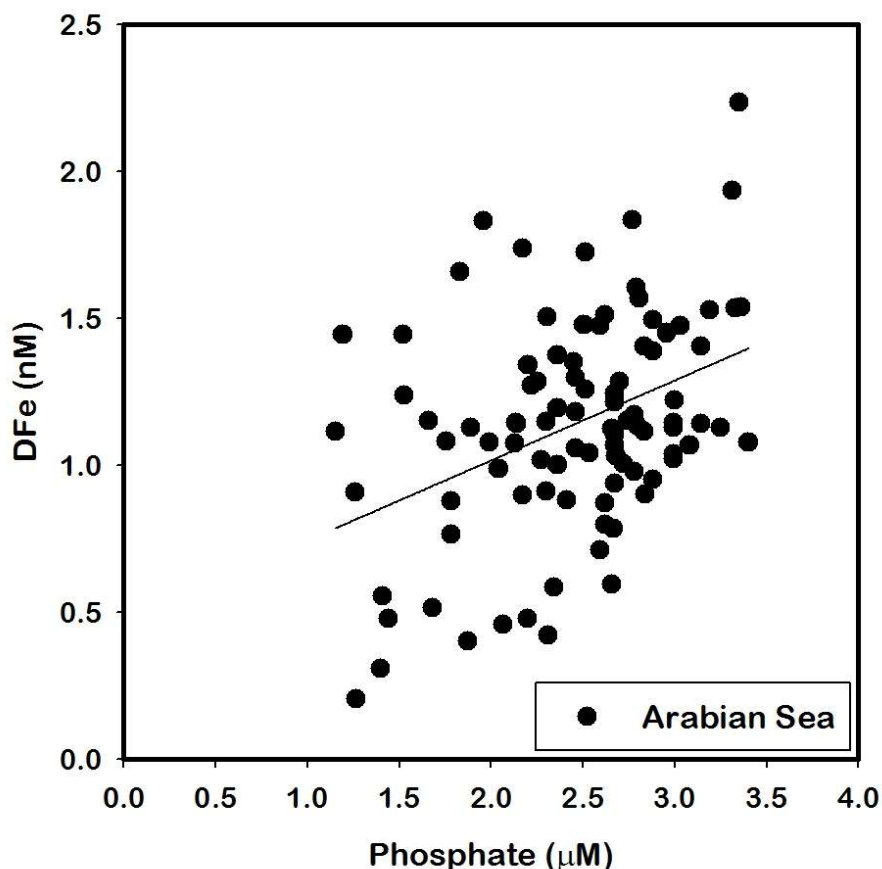


Figure 3.35: DFe vs. Phosphate scatter plot in the western and central Arabian Sea stations of the cruises SK-312 and SK-324. Data taken for the depths between 100 - 1000 m.

The DFe concentrations observed in this study is comparable with their DFe values in the stations close to western AS. Negative Fe^* values have seen along the western AS as moving towards the western part of the AS from the intense OMZ of the central AS and upwelling region of eastern AS which supports the earlier studies. The subsurface waters in the western AS region clearly shows negative Fe^* values that means less Fe for the biological consumption of P over Fe. This region strongly upwells during southwest monsoon period and brings subsurface waters to the surface. Figure 3.36 shows negative Fe^* waters below

subsurface waters along western AS and once these waters upwells to the surface the region will be depletion of DFe. The Fe^* plot along the western AS is the direct evidence from our study for Fe limitation in this region during late southwest monsoon period. Fe addition experiments along the west coast of the AS during remaining seasons have to be done to better understand the HNLC feature in this region.

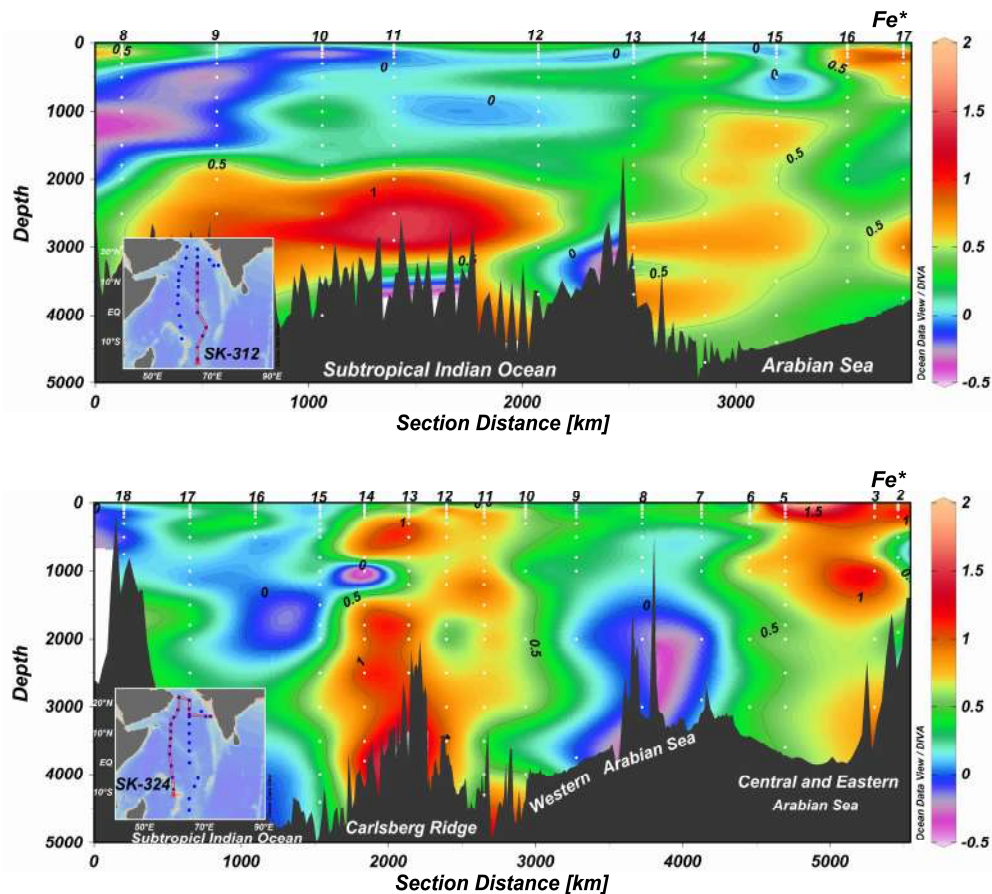


Figure 3.36: Section plot of Fe^* along the stations sampled during SK-312 and SK-324 in the Arabian Sea and subtropical Indian Ocean.

3.4 DFe distributions – The Bay of Bengal vs. The Arabian Sea

The unique geographical location of the northern Indian Ocean comprises of two basins namely the Bay of Bengal and the Arabian Sea with distinctive hydrographic parameters even though situated at the similar latitudes. The

productivity, sources and internal cycling are completely different with respect to each other that reflected in the DFe distributions also and are summarized below:

1. Seasonal variation of DFe concentrations in the surface waters of the AS is found mostly linked to monsoon generated upwelling that brings changes in the plankton community whereas in the BoB, surface DFe values are mostly governed by the riverine input and dust deposition.
2. Particulate flux seems to be contributing to the intermediate waters of the BoB whereas respiration of organic matter degradation is the major source contributing to the intermediate waters of the AS.
3. Remineralization is the dominant process in both the basins but it is higher in the AS compared to the BoB that also reflected in the higher Fe:C rates in the AS.
4. Scavenging of DFe is observed in the waters of BoB below 1000 m whereas in the AS the scavenging is not observed. This may be due to the presence of organic complexes in the deeper waters of the AS.
5. Both the basins show DFe input from continental shelves and margins.
6. The tracer Fe* shows parts of the BoB below 1000 m are deficit of DFe over phosphate whereas similar tracer in the AS shows replete conditions of Fe in the central and eastern AS and deplete conditions in the western AS and subtropical Indian Ocean.

3.5 DFe in the Indian Ocean compared to the Atlantic and the Pacific Oceans

Studies in the global ocean for DFe suggest that multiple sources are contributing for the iron in the contemporary oceans (Boyd and Ellwood, 2010). Surface oceanic regions in the proximity of atmospheric sources, Fe profile shows the scavenged type distribution. Regions like Arabian Sea, North Atlantic Ocean shows high DFe values in the surface waters due to dust deposition that enhances the soluble Fe through photo reduction. In addition, episodic dust variations brought changes in the Fe concentrations in the surface waters of the dust prone regions of the global ocean (Gao et al., 2001). Upwelling regions are the major source for DFe as observed in the Peru and California upwelling regions (Bruland et al., 2005; Hutchins and Bruland, 1998). These regions are characterized by the

presence of intense OMZ due to the high productivity induced by upwelling. Studies in these regions suggest that much of the DFe exist in +2 oxidation state that coincides with the secondary nitrite maxima supported by the dominance of organic complexation (Vedamati et al., 2014; Kondo and Moffett, 2015). The Arabian Sea, which shows similar characteristics as of Peru upwelling region, consists of intense OMZ in the water column and intense upwelling seen along the coast of western and eastern Arabian Sea. Similar enrichment of Fe and secondary nitrite maxima were also seen in this basin along with seasonal limitation of Iron for productivity ((Moffett et al., 2015; Naqvi et al., 2010, this study). DFe concentrations show enrichment in the regions where riverine sources are dominant. The major source for DFe in the West Atlantic Ocean between 5° N and 20° N is the proximity of the river Amazon that is the largest contributor of huge fresh water flux in this region. Study in this region suggests that remineralization of the organic and particulate matter such as Fe oxyhydroxide from the riverine input are the dominant sources (Rijkenberg et al., 2014). Similar DFe concentrations and remineralization processes are also observed at the proximity of the rivers Ganga-Brahmaputra, Irrawaddy and Salween rivers situated to the north of the Bay of Bengal. Studies in the Atlantic and Pacific oceans (Bennett et al., 2008; Ellwood et al., 2018; Resing et al., 2015) highlighted the role of Fe from the hydrothermal derived input to several thousands of kilometers from the non buoyant plumes that stabilizes against scavenging along the isopycnal lines due to organic complexation. Similar long range transport of Fe has been observed in the deeper waters of the stations sampled across the ridges in the Indian Ocean suggesting the similar process dominating in these deeper waters. Iron from submarine sources in the Pacific Ocean (Guieu et al., 2018) has highlighted the role of volcanic ash on the Fe cycle. Similar studies have not been done in this region. Trench region of the Indian Ocean highlighted converging plates as a source for DFe to deeper waters in the basin, which is the typical characteristic that observed in the Indian Ocean.

3.4 Summary and Conclusions

The DFe over the full water column of the Indian Ocean comprising of the AS, the BoB, and the Andaman Sea was studied. The N-S decreasing gradient in the surface DFe concentrations suggests the role of riverine particles and dust deposition. Clear indication for the supply of DFe from the continental shelves of the stations near to the west coast of India has been seen. Sub-surface maxima in the stations south of 5° N was absent compared to the stations in the Northern Indian Ocean. The sub-surface maxima in the low oxygen waters of Northern Indian Ocean could be due to the re-mineralization of organic matter along with the release of DFe from Fe-Mn hydroxide coatings of the particulate matter supplied by rivers like Ganga-Brahmaputra, Salween, and Irrawaddy. Hydrothermal vents supply a significant amount of DFe to the water column in the Indian Ocean. In addition, a strong DFe supply has been observed in the vicinity of the subduction zone in the Java Trench region. DFe concentrations measured in the deeper waters along the stations of Trench region are higher by a factor of 4 compared to the global average deeper value for DFe. Fe:C remineralization rates of 5.74 ± 3.06 $\mu\text{mol/mol}$ in the Andaman Sea, 5.88 ± 2.65 $\mu\text{mol/mol}$ in the BoB, 3.92 ± 0.83 $\mu\text{mol/mol}$ in eastern Indian Ocean and 8.96 ± 3.85 $\mu\text{mol/mol}$ in the east coastal AS, 7.56 ± 1.93 $\mu\text{mol/mol}$ for AS and 4.34 ± 0.86 $\mu\text{mol/mol}$ for western Indian Ocean is observed. The impact of Fe dissolution is much higher in the OMZ waters of the AS, Andaman Sea, and BoB. Other than organic matter re-mineralization, it is evident from Fe* distribution that external sources such as atmospheric deposition, continental shelf, hydrothermal vent sources, subduction source and particulate material from rivers are contributing to DFe pool in the intermediate waters of the BoB, the Andaman Sea and the Indian Ocean. Some parts of the BoB, Andaman Sea and eastern and western subtropical Indian Ocean show negative Fe* values implies Fe limitation over phosphate consumption. Similar Fe* section plot in the eastern and central AS does not displays any negative Fe* portions in the AS. Interestingly Fe* displays negative values along the western AS during post southwest monsoon. The negative Fe* values observed in the western AS are confirming the Fe limitation during late southwest monsoon period.

Annexure 1: DFe data along with the hydrographic parameters

Stn. – Station, Lat. – Latitude, Long. – Longitude, D – Depth, NA – Not Available

DFe – Dissolved Iron, N* - Nitrite, P – Phosphate, Si – Silicate, N – Nitrate,

DO – Dissolved Oxygen, S – Salinity, T – Temperature, Fluor. – Fluorescence

Cruise	Stn.	Lat.	Long.	D (m)	DFe (nM)	N* (µM)	P(µM)	Si (µM)	N (µM)	DO (µM)	S (PSU)	T (°C)	Fluor.
SK-304A	1	13.71	73.26	2	0.705	0.02	0.13	0.92	0.11	206.70	NA	29.24	0.25
SK-304A	1	13.71	73.26	50	0.556	0.04	0.35	0.92	3.98	188.20	35.42	28.51	0.29
SK-304A	1	13.71	73.26	100	0.928	0.10	1.10	6.08	11.23	82.10	36.26	24.70	0.30
SK-304A	1	13.71	73.26	200	1.825	0.04	2.29	24.70	23.75	5.10	35.24	15.40	0.29
SK-304A	1	13.71	73.26	300	1.630	0.14	2.56	29.92	27.96	5.00	35.23	12.94	0.29
SK-304A	1	13.71	73.26	370	1.473	0.04	2.69	32.27	28.21	8.40	35.25	12.29	0.29
SK-304A	1	13.71	73.26	550	1.799	0.08	2.82	42.88	31.57	NA	35.29	11.21	0.29
SK-304A	1	13.71	73.26	747	2.308	0.02	2.87	55.26	30.16	10.70	35.00	9.74	0.29
SK-304A	2	12.39	74.16	2	0.658	0.02	0.02	1.54	0.36	212.00	34.68	29.46	0.30
SK-304A	2	12.39	74.16	50	0.329	0.02	0.04	2.32	0.71	184.80	35.74	29.32	0.23
SK-304A	2	12.39	74.16	100	0.480	0.04	0.18	1.95	0.71	163.20	36.49	28.30	0.59
SK-304A	2	12.39	74.16	150	1.427	0.04	1.89	18.46	22.71	13.90	35.58	18.91	0.29
SK-304A	2	12.39	74.16	200	1.598	0.12	2.21	26.24	26.26	25.60	35.48	14.36	0.15
SK-304A	2	12.39	74.16	300	1.426	0.03	2.48	21.40	27.66	6.50	35.48	12.40	0.15
SK-304A	2	12.39	74.16	400	1.442	0.04	2.32	34.31	29.06	13.50	35.53	11.69	0.15
SK-304A	2	12.39	74.16	500	1.645	0.02	2.50	46.10	29.55	6.50	35.53	11.05	0.15
SK-304A	2	12.39	74.16	625	2.281	0.03	2.52	55.85	31.30	25.20	35.54	10.24	0.15
SK-304A	4	5.00	80.00	5	0.325	0.04	0.16	2.12	0.05	208.64	34.06	29.60	0.15
SK-304A	4	5.00	80.00	10	0.475	0.05	0.00	2.09	0.13	212.32	34.05	29.59	0.15
SK-304A	4	5.00	80.00	25	0.272	0.05	0.04	2.15	0.31	210.47	34.49	29.73	0.15

Chapter 4

Distributions of dissolved Zinc in the Indian Ocean

4.1 Introduction

Zinc (Zn) involves in several metabolic processes in the marine organisms (Sinoir et al., 2012; Vallee and Auld, 1990) due to its vital function as a co-factor for proteins and metallo enzymes. Studies have shown that low concentrations of Zn regulate the community structure, composition and uptake of carbon which in turn may limit the phytoplankton growth (Morel et al., 1994; Tortell et al., 2000; Sunda and Huntsman, 1995; Shaked et al., 2006; Sunda and Huntsman, 1992; Sunda, 2012). Laboratory based culture experiments have shown that Zn may act as a limiting nutrient (Anderson et al., 1978; Brand et al., 1983; Christina et al., 2000; Tortell and Price, 1996).

Unlike Fe, open ocean experiments for Zn are very scarce. On the contrary, some studies examined the impact of Zn limitation on phytoplankton communities and have observed less effects on community structure (Coale, 1991; Coale et al., 2003; Cochlan et al., 2002; Crawford et al., 2003; Franck et al., 2003; Jakuba et al., 2012). In some oligotrophic regions characterized by low silicate concentrations, additions of Zn to seawater resulted in very small/no increase in chlorophyll with substantial changes in the diatom community (Leblanc et al., 2005). However, only about 1 – 3% of the total amount of Zn taken by the diatoms are incorporated in the diatom cells (Ellwood and Hunter, 2000). Furthermore, it has been suggested that ~98% of dissolved Zn concentration in the surface waters are associated with siderophores (*i.e.*, *trace metal binding organic ligands*) (Bruland, 1989; Donat and Bruland, 1990; Bruland and Lohan, 2006; Jakuba et al., 2012). Thus, the bioavailable fraction (*i.e.*, free Zn^{+2} ions and inorganic complexes of Zn) in the surface waters is rather small for the uptake of phytoplankton (Donat and Bruland, 1990; Sunda and Huntsman, 1992). It has been shown that for a typical dissolved Zn concentration of 2-14 pM in seawater, most of which formed organic complexes, limits the growth of the phytoplankton and marine community structure (Ellwood and Van den Berg, 2000; Brand et al., 1983; Sunda and Huntsman, 1992; Sunda and Huntsman, 1995; Shaked et al., 2006; Sinoir et al., 2012).

The Indian Ocean is very different in many aspects compared to other oceanic basins. The most striking differences are (i) It receives atmospheric

Distributions of dissolved Zinc in the Indian Ocean

mineral dust from the nearby arid sources, (ii) Large fresh water influx from perennial rivers in the northeastern side, (iii) Intrusion of Pacific Ocean waters, (iv) Seasonal reversal of monsoons, and (v) The presence of Oxygen minimum zones above 5° N in both northeastern and northwestern parts. All these processes make the study area unique. Several cruises were conducted as a part of GEOTRACES-INDIA programme in the Indian Ocean (Chapter 2). The Zn data generated along the several cruises in the Indian Ocean as a part of GEOTRACES India programme are shown in Figure 4.1.

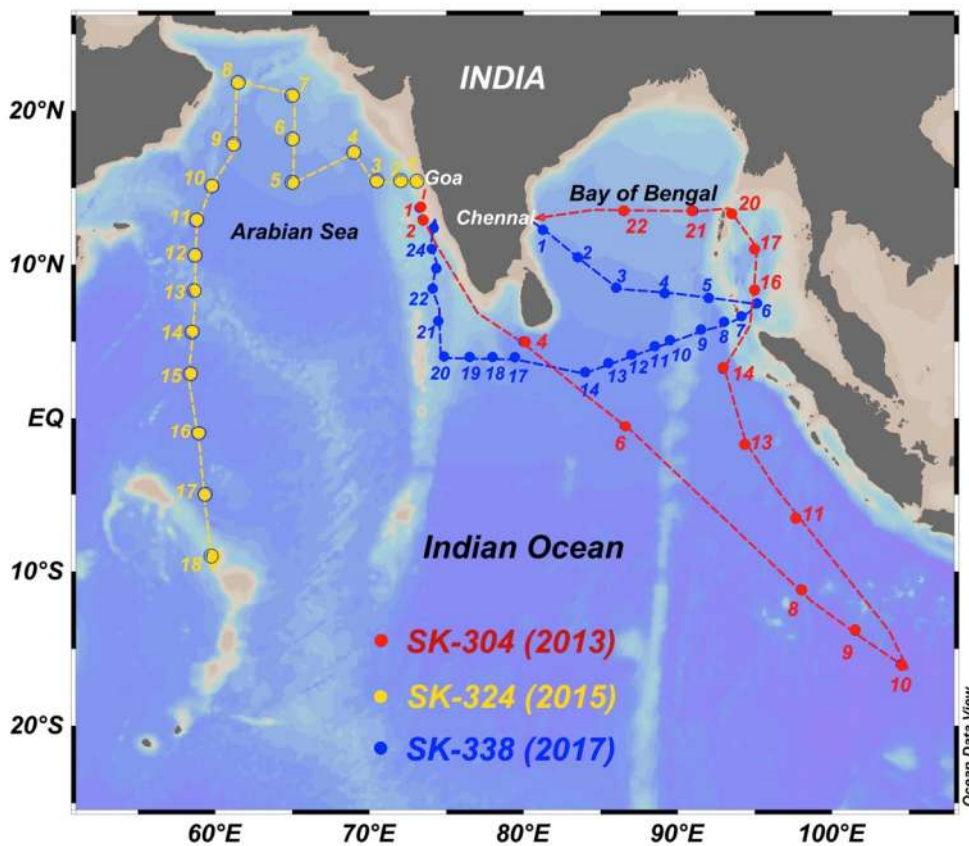


Figure 4.1: Locations of the stations sampled during SK-304, SK-324 and SK-338 as a part of GEOTRACES-India Programme in the Indian Ocean.

4.2 Results

4.2.1 Hydrographic and macro nutrients distribution

The Indian Ocean is unique basin compared to other oceanic regions due to the seasonal reversal of monsoonal winds in the Northern Indian Ocean, which brings lot of nutrients to the surface waters due to upwelling that further enhances the productivity in the basin. Within the Northern Indian Ocean, the AS and the BoB that are situated at the similar geographical location shows contrasting behavior in their hydrographic properties due to the differences in the huge fresh water runoff in to their respective basins. In addition, thermocline of the AS is characterized by the high salinity waters from the Persian Gulf waters (PGW) and Red Sea waters (RSW) in the depth range of 200-300 m and 650-800 m respectively (You & Tomczak, 1993). The origin of the source waters for PGW and RSW are Persian Gulf and Gulf of Aden. The surface waters of AS have high salinity compared to BoB surface waters. The surface waters of AS are termed as Arabian Sea high saline waters (ASHSW). These waters formed during wintertime due to the cooling of surface waters by the continental winds blowing from the continent. The progression of these ASHSW further south (below Equator) is hampered by the summer and winter monsoon currents (Kumar and Prasad, 1999). In contrast, surface waters of BoB are less saline due to the large fresh water influx into the bay. The proximity of the rivers in the North of the BoB makes surface values of salinities 2-3 less than surface waters of AS. Due to the reversal of monsoonal winds, ASHSW can traced in BoB during summer monsoon and low surface saline BoB waters can be seen in the AS during winter time. Mostly the bottom waters of the Northern Indian Ocean contain Antarctic bottom waters (AABW) (Goswami et al., 2014; Singh et al., 2012). Below thermocline, waters are termed as North Indian deep waters (NIDW) in the depth range of 1000 - 1800 m. Between NIDW and AABW, waters are termed as modified North Atlantic deep waters (MNADW). The stations sampled in the Indian Ocean below equator are not affected by the seasonal reversal atmospheric forcing as such in the Northern Indian Ocean.

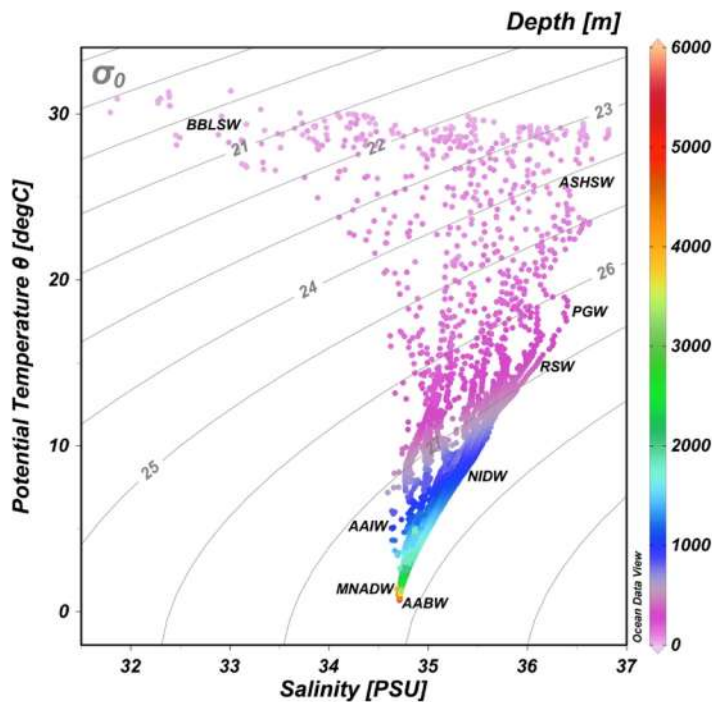


Figure 4.2: Different water masses present in the study region based on Temperature-Salinity data. BBSW-Bay of Bengal less saline waters, ASHSW-Arabian Sea high Saline waters, PGW-Persian Gulf waters, RSW-Red sea waters, NIDW-North Indian deep waters, AAIW- Antarctic intermediate waters, MNADW-Modified North Atlantic deep waters, AABW-Antarctic Bottom waters.

Between 15° S to 20° S, Indonesian Through Flow waters enters into Indian Ocean, these waters form during their transit through Indonesian islands from the Pacific Ocean. These waters are relatively less saline and high in temperature. The circulation and ventilation in the region is documented by previous studies (You, 2000, 1997; You and Tomczak, 1993). Using available literature and Temperature-Salinity data different water masses present in the study region is displayed in the Figure 4.2. The other hydrographic parameter, which characterizes the Indian Ocean from the other oceanic basins, is the presence of perennial oxygen minimum zone (OMZ) in the Northern Indian Ocean waters (Morrison et al., 1999; Paulmier and Ruiz-pino, 2009). The south equatorial current located at the 15° S divides the poorly ventilated thermocline waters of northern Indian Ocean from the waters having rich in DO of south Indian sub tropical gyre.

Distributions of dissolved Zinc in the Indian Ocean

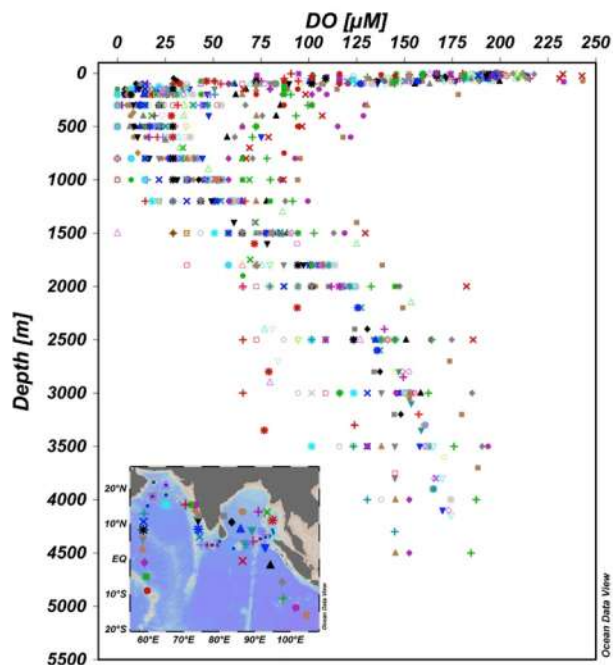


Figure 4.3: The vertical profiles of dissolved oxygen in the sampled region. Decrease in the Oxygen concentrations ($< 50 \mu\text{M}$) observed in the subsurface waters of 100-1000 m while entering into the Northern Indian Ocean.

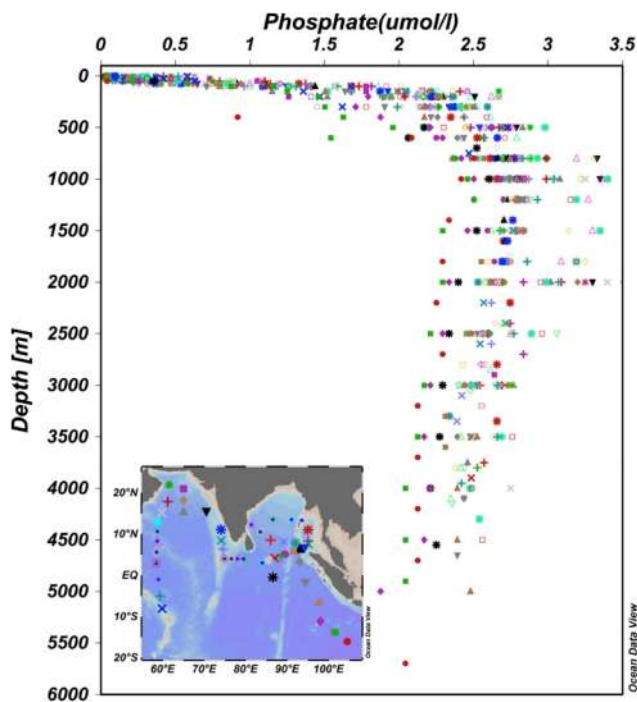


Figure 4.4: Vertical profiles of phosphate from the study region.

A clear decrease in the dissolved oxygen (DO) values as moving from the subtropical gyre to strong atmospheric forcing dominated region of Northern Indian Ocean is observed (Fig. 4.3).

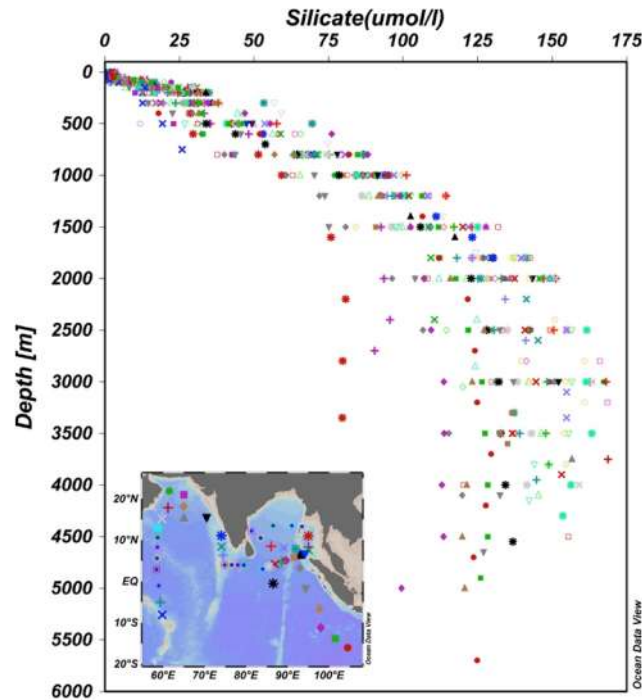


Figure 4.5: Vertical profiles of silicate from the study region.

The basic hydrographic parameters such as dissolved oxygen (DO), phosphate (P) and silicate (Si) are discussed in the Chapter 3. For the sake of understanding and comparing with the Zn data along the SK-304, SK-324 and SK-338 the vertical profiles are shown again in this chapter. The vertical profiles of DO in the study region are shown in the Figure 4.3. A clear distinction in the DO profiles are observed in the depth interval of 100 - 1000 m of the Indian Ocean and Northern Indian Ocean stations. Suboxic condition is prevalent in the subsurface waters of the Northern Indian Ocean. Seasonal anoxia is reported along the west coast of India during summer monsoon (Naqvi et al., 2000; Naqvi

et al., 2006). The vertical profiles of silicate and phosphate are displayed in the Figures 4.4 and 4.5.

4.2.2 Dissolved Zinc distributions

Vertical profiles of DZn in the study region show nutrient type behavior with relatively lower concentrations in the surface waters compared to subsequent deeper layers of the water column (Figure 4.6). The average concentration of DZn obtained in the Indian Ocean including Northern Indian Ocean (BoB, AS and Andaman Sea) is 4.25 ± 2.92 nM (n=730, 1σ). The Zn concentrations in top 50 m water depth in the region obtained is 1.17 ± 0.60 nM, n=142. Intermediate waters between 100 - 1000 m, Zn concentrations observed are 2.92 ± 1.27 nM, n=305. Average Zn concentrations in deeper waters (> 1000 m) of Indian Ocean is 7.68 ± 1.57 nM, n=223. Highest Zn concentrations (~ 14 nM) are observed at the deeper samples of station SK-338/1 close to east coast of India. In addition to this enrichment in the deeper waters, Zn concentrations of $\sim 11-12$ nM are observed at few other stations. DZn data generated in the study region is listed in tables 4.1 to 4.4.

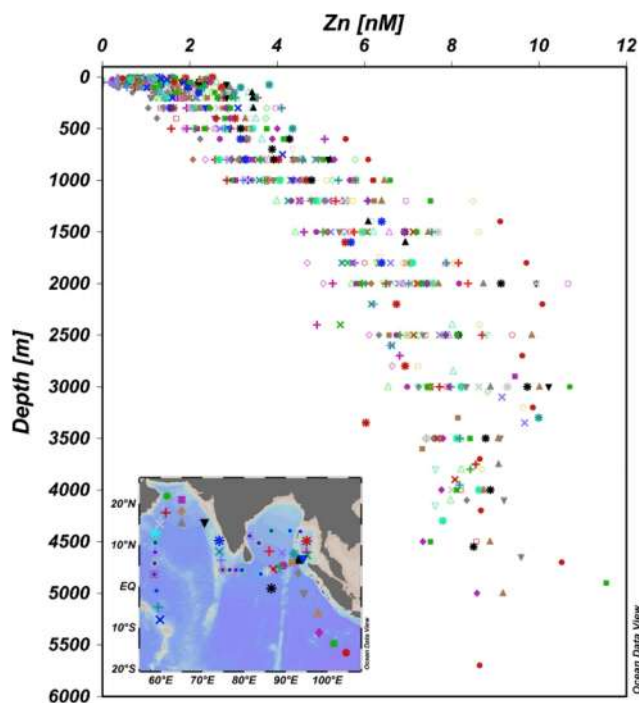


Figure 4.6: Vertical profiles of DZn from the study region with typical nutrient type behavior.

Distributions of dissolved Zinc in the Indian Ocean

Table 4.1: DZn data in Bay of Bengal

Bay of Bengal						
S.No	Cruise	Station	Latitude	Longitude	Depth (m)	Zn (nM)
1	SK-304B	21	13.498	91.002	10	2.422
2	SK-304B	21	13.498	91.002	25	2.354
3	SK-304B	21	13.498	91.002	50	2.516
4	SK-304B	21	13.498	91.002	75	2.830
5	SK-304B	21	13.498	91.002	100	2.788
6	SK-304B	21	13.498	91.002	150	3.349
7	SK-304B	21	13.498	91.002	200	3.077
8	SK-304B	21	13.498	91.002	300	3.426
9	SK-304B	21	13.498	91.002	400	3.521
10	SK-304B	21	13.498	91.002	600	3.655
11	SK-304B	21	13.498	91.002	800	4.515
12	SK-304B	21	13.498	91.002	1000	4.763
13	SK-304B	21	13.498	91.002	1500	6.212
14	SK-304B	21	13.498	91.002	2000	7.332
15	SK-304B	21	13.498	91.002	2400	8.012
16	SK-304B	21	13.498	91.002	2850	8.032
17	SK-304B	22	13.500	86.503	25	1.840
18	SK-304B	22	13.500	86.503	50	2.614
19	SK-304B	22	13.500	86.503	100	2.204
20	SK-304B	22	13.500	86.503	150	2.507
21	SK-304B	22	13.500	86.503	200	2.359
22	SK-304B	22	13.500	86.503	300	3.763
23	SK-304B	22	13.500	86.503	400	3.748
24	SK-304B	22	13.500	86.503	600	3.884
25	SK-304B	22	13.500	86.503	800	5.792
26	SK-304B	22	13.500	86.503	1000	5.278
27	SK-304B	22	13.500	86.503	1500	5.996
28	SK-304B	22	13.500	86.503	2000	6.721
29	SK-304B	22	13.500	86.503	2500	8.154
30	SK-304B	22	13.500	86.503	3050	8.826
31	SK338	1	12.266	81.250	2	0.660
32	SK338	1	12.266	81.250	50	1.992
33	SK338	1	12.266	81.250	100	1.816
34	SK338	1	12.266	81.250	200	1.987
35	SK338	1	12.266	81.250	300	3.977
36	SK338	1	12.266	81.250	600	4.305
37	SK338	1	12.266	81.250	1200	6.953
38	SK338	1	12.266	81.250	2000	10.665
39	SK338	1	12.266	81.250	2800	14.703
40	SK338	1	12.266	81.250	3200	14.893

Distributions of dissolved Zinc in the Indian Ocean

Indian Ocean						
S.No	Cruise	Station	Latitude	Longitude	Depth (m)	Zn (nM)
130	SK-324	17	-5.000	59.350	200	3.049
131	SK-324	17	-5.000	59.350	300	4.099
132	SK-324	17	-5.000	59.350	500	2.811
133	SK-324	17	-5.000	59.350	800	4.579
134	SK-324	17	-5.000	59.350	1000	5.402
135	SK-324	17	-5.000	59.350	1200	6.067
136	SK-324	17	-5.000	59.350	1500	7.545
137	SK-324	17	-5.000	59.350	1800	7.877
138	SK-324	17	-5.000	59.350	2000	7.013
139	SK-324	17	-5.000	59.350	2500	7.852
140	SK-324	17	-5.000	59.350	3000	7.976
141	SK-324	17	-5.000	59.350	3500	8.185
142	SK-324	17	-5.000	59.350	3950	8.179
143	SK-324	18	-8.096	59.806	5	1.689
144	SK-324	18	-8.096	59.806	15	1.399
145	SK-324	18	-8.096	59.806	25	1.544
146	SK-324	18	-8.096	59.806	50	1.970
147	SK-324	18	-8.096	59.806	100	1.315
148	SK-324	18	-8.096	59.806	150	1.874
149	SK-324	18	-8.096	59.806	200	1.842
150	SK-324	18	-8.096	59.806	500	2.788
151	SK-324	18	-8.096	59.806	750	4.645

4.2.3 Zinc vs. Major nutrients (Nitrate, Phosphate and Silicate) Relationship

The vertical profiles of major nutrients Phosphate and Silicate are shown in the Figure 4.4 and 4.5. In the surface ocean waters Nitrate, Phosphate and Silicate are bio limiting and shows lower concentrations in the euphotic zone. In the Indian Ocean, nitrate and phosphate show much shallower regeneration compared to silicate and zinc. This is due to their involvement in the soft tissues of the organic matter and during the degradation of the organic matter these nutrients released back in to the water column. However, despite the involvement of zinc in the soft tissues (Ellwood and Hunter, 2000), it does not correlate well with the nutrients nitrate and phosphate. Interestingly it correlates with the silicate which involves in the frustules formation and has greater regeneration depth compared to nitrate and phosphate. Nitrate is generally not used as a tracer to identify the remineralization process due to their involvement in the

nitrification/denitrification processes in the OMZ waters. However, phosphate can be used as a best tracer for the re-mineralization processes and can compare with the AOU. However, the Zn-P relationship and its kink between contemporary vertical profiles are explained in the section 4.3.8. In the other case Zn and Si in the global oceans are tightly correlated (Janssen and Cullen, 2015; Kim et al., 2017, 2015b; Lohan et al., 2002; Obata et al., 2017; Vu and Sohrin, 2003; Wyatt et al., 2014). Consistent to these observations vertical profiles of Zn and Si in the Indian Ocean correlate significantly. The vertical plots of DZn and silicate of all the stations sampled in the marginal and open ocean waters of Indian Ocean along the cruise tracks SK-304, SK-324 and SK-338 are shown in the Figure 4.5 and 4.6. The black and white lines over the section plots represent the concentration contours for DZn and silicate respectively. A strong and significant correlation is observed between DZn and silicate in the study region. The global Zn vs. Si ratio in the various oceans is close to 0.059. Interestingly, distinct ratios are observed in the basin. The slope obtained for the stations sampled between Equator and 20°S is similar to that of the global ocean. The ratio is consistent with those reported by Gosnell et al. (2012) and Vu & Sohrin (2003) in the Indian Ocean and higher compared to those obtained by Kim et al (2015) and Morley et al. (1993) in the Northern Indian Ocean and the Andaman Sea. The observed ratio for the Northern Indian Ocean is significantly lower compared to global average ratio for Zn vs. Si (GEOTRACES IDP 2014).

4.3 Discussion

4.3.1 Dissolved Zinc in the surface and intermediate waters

DZn concentrations in the top 100 m in the study region consisting of BoB, AS, Andaman Sea and Indian Ocean are 1.26 ± 0.78 nM (n=76), 1.24 ± 0.54 nM (n=83), 1.44 ± 0.81 nM (n=22) and 1.44 ± 0.52 nM (n=30) respectively. The reported values are consistent with the previous studies in the region. The average DZn concentrations for the top 100 m reported by Morley et al. (1993) was 1.36 ± 1.01 nM (n=25) in the southwestern Indian Ocean. Vu & Sohrin (2013) reported DZn concentrations in the Indian Ocean as a part of GEOTRACES-Japan

programme. Their average DZn concentrations in top 100 m water are 1.19 ± 0.43 nM (n=4) in BoB (ER-2) and 0.66 ± 0.44 nM (n=12) in AS (ER-5, ER-6, ER-7). Study of Kim et al. (2015) in BoB for one profile in BoB reported DZn concentration of 0.74 ± 0.29 nM (n=5). The DZn values in the region (21° N to 10° S) are higher by an order of magnitude compared to those reported by Gosnell et al. (2012) in the Indian Ocean (along the zonal transect of 30° S) which is considered as an oligotrophic region. The higher concentrations of DZn in the study region could be due to the proximity of arid landmasses in the Northern side that can be a huge source for Zn. In addition, upwelling of subsurface waters during monsoon seasons is the characteristic of the basin. The observed photic zone concentrations for DZn are not significantly different in the BoB, AS, Andaman Sea and Indian Ocean south of equator unlike Fe where huge spatial variability has seen in the Indian Ocean waters (Chinni et al., 2018). Impact of the biological control on the DZn in the Indian Ocean is not obvious as despite having higher productivity, the Arabian Sea has similar DZn as the BoB and the oligotrophic waters of the Indian Ocean. Alternatively, various dominant sources of Zn in the region are obliterating the biological control. Rivers situated at the northern and northeastern part of the Indian Ocean could be another important source for Zn. The Ganga-Brahmaputra, Irrawaddy, Salween and rivers along the east coast of India are world's third largest contributor of sediment to the Bay (Milliman and Meade, 1983; Robinson et al., 2007). However, studies indicate that 99% of the trace metals brought by the rivers are removed within the estuaries by flocculation. The riverine impact on the open ocean waters, hence, may not be the dominant. The reported values for AS in this study is higher by a factor of two compared to Vu and Sohrin (2013) study sampled during November-January period of 2009. The range obtained by Vu and Sohrin (2013) is limited to central AS (three profiles). However, in the present study samples consists of Eastern, Central and Western AS stations. Within the AS, there exists a perennial denitrifying zone in the central AS. Monsoonal winds bring changes in the biogeochemical properties in the water column. For example, seasonal anoxia is observed in the eastern AS along the west coast of India after southwest monsoon season (Naqvi et al., 2000). Naqvi et al. (2010) suggested that during post-

southwest monsoon, the western AS acts as a HNLC (High Nutrient Low Chlorophyll) region. Therefore, the high mean values and large spread in observed data represent the entire spatial variation of the AS in the top 100 m.

The average DZn concentration in the intermediate waters (100 -1000 m) in BoB is 3.17 ± 1.08 nM (n=80), AS is 2.95 ± 1.12 nM (n=88), Andaman Sea is 3.24 ± 1.14 nM (n=14) and Indian Ocean is 3.57 ± 1.44 (n=53). These values are consistent with those reported by Kim et al. (2015) 2.58 ± 1.04 nM and Vu and Sohrin (2013) 3.22 ± 1.04 nM, n=6 for the intermediate waters. In the intermediate waters of Northern Indian Ocean (comprises of BoB, AS and Andaman Sea), Zn concentrations varies from ~2-4 nM where as in the Indian Ocean intermediate waters, it enriches up to ~6 nM. In the northern stations monotonous behavior in the Zn profile is seen whereas little increasing trend in the Indian Ocean stations is observed. Overall, average DZn is 2.82 ± 1.18 (nM) in the Northern Indian Ocean and in the Indian Ocean it is 3.35 ± 1.52 (nM). Average DZn concentrations in the Northern Indian Ocean is relatively lower compared to that of the Indian Ocean, their ranges, however, are overlapping. Comparison of DZn variations in the region with respect to major nutrients (either nitrate, silicate and phosphate) could bring new insight in DZn biogeochemistry (See the later discussion 4.3).

4.3.2 Dissolved Zinc in the deep waters

The NICW, NIDW, MNADW and AABW are the dominant water masses in the Indian Ocean and Northern Indian Ocean below ~1500 m. The average DZn concentrations noticed are 5.86 ± 0.70 nM (n=29), 7.23 ± 1.84 nM (n=95), 7.50 ± 1.71 nM (n=103), 8.15 ± 1.25 nM (n=68) in the Andaman Sea, BoB, AS and Indian Ocean respectively. The observed values are consistent to the study of Vu and Sohrin (2013), 8.38 ± 1.02 nM (ER-9) in the Indian Ocean, 7.62 ± 1.97 nM (ER-2) in BoB and 8.21 ± 2.18 nM in AS (ER-5/6/7). The lower concentrations observed in the deeper waters of Andaman Sea is due to the exchange of its deeper waters with intermediate waters (~1000 - 1200 m) of BoB across the 10° Prepares channel (Nozaki and Alibo, 2003). These features can also be seen in the basic parameters data temperature, salinity, DO and major nutrients, silicate and

Distributions of dissolved Zinc in the Indian Ocean

phosphate. These observations are consistent with the previous study of Kim et al. (2015) for DZn distributions.

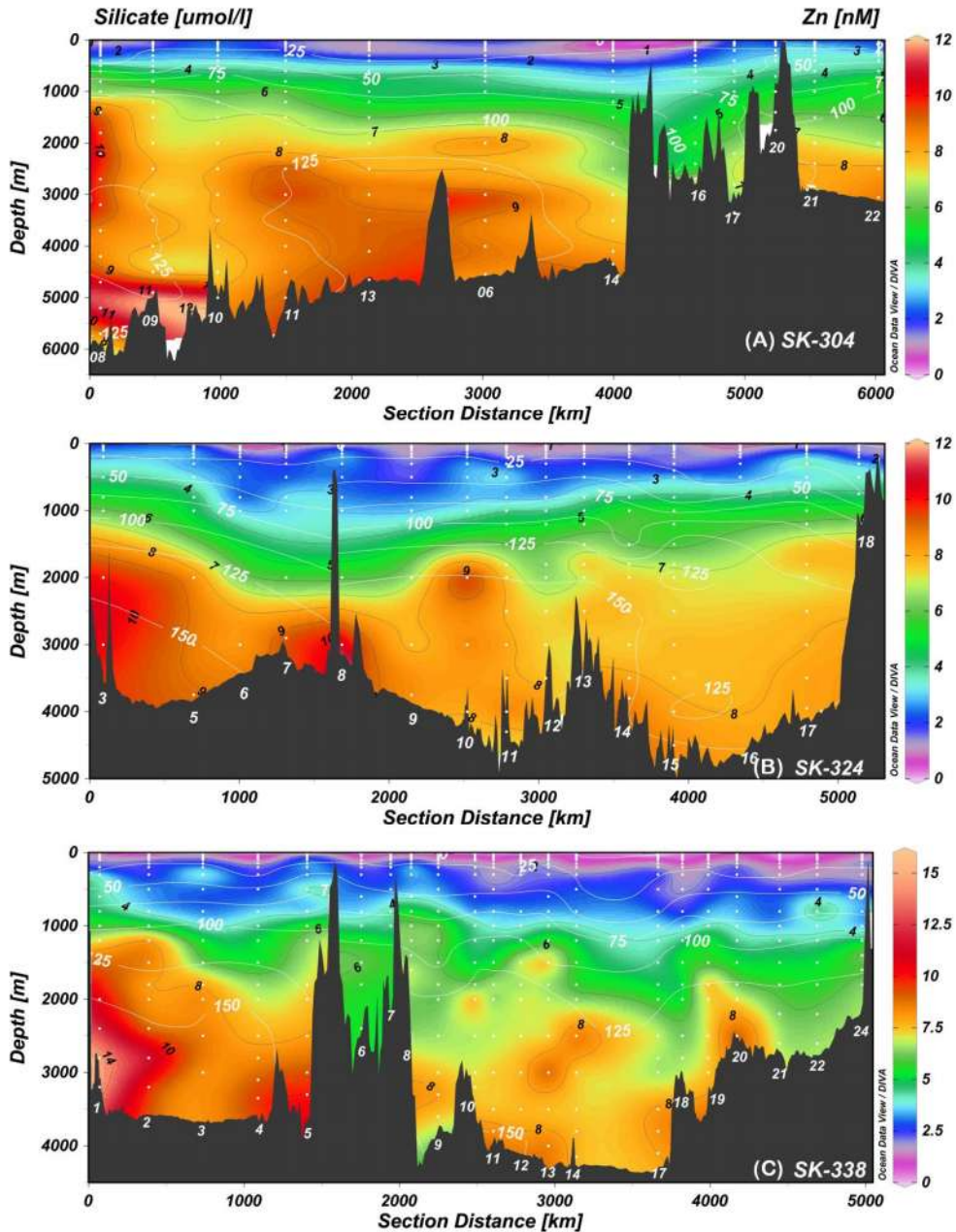


Figure 4.7: Section plots of DZn with black contours mentioning the Zn concentrations overlying with silicate contours (White in color) during (A) SK-304 (B) SK-324, and (C) SK-338 cruises.

Similar observation with respect to the DFe concentrations is also observed (Chinni et al., 2018). Enrichment in the DZn concentrations seen at few stations in the deeper waters of the region could be due to the release of Zn from biogenic rich sediments. The deeper samples of stations SK-338/1 and SK-338/2 are enriched in DZn and are associated with Si enrichment (Figure 4.7). The continuous increase of DZn and Si with depth suggests that biogenic rich sediments can be an important source for Zn in the deeper waters. The high concentrations found at these two locations have not observed in the other deeper samples. The hydrothermal vents are reported as a significant source of trace metals in the deeper waters (Resing et al., 2015; Wu et al., 2011). Nishioka et al. (2013) have identified that hydrothermal vents situated at the Central Indian Ridge system is a significant source for DFe in the deeper waters of Indian Ocean. The hydrothermal derived Fe gets transported thousands of kilometers in deeper waters. This thesis (Chapter 3) also reports enrichment in DFe along the hydrothermal ridges in the Indian Ocean. Roshan et al. (2016) found long-range transport of Zn from the hydrothermally derived input as a source for deeper waters of tropical South Pacific. However, the similar enrichment for the DZn in the deeper waters has not been found in the study region negating the hydrothermal vents as a significant source for the DZn in the Indian Ocean.

Knowledge of the past distributions and circulation of the deep waters has been derived using ($\delta^{13}\text{C}$), Cd/Ca and Ba/Ca of the benthic foraminifera shells (Boyle and Keigwin, 1982; Curry and Lohmann, 1982; Sarnthein et al., 1994). Owing to large (10 fold) difference in DZn between deeper layers of north Atlantic and north Pacific Oceans, Zn/Ca in the foraminifera could serve as a better sensitive tracer of deep waters compared to Cd/Ca (Marchitto et al., 2000). In this context, the Zn concentrations in the deeper waters are crucial to decipher the circulation patterns of deeper layers. In the present study, the deeper waters (>1000 m) Zn/Si relation is $0.060[\text{Si}] + 0.26$ which is greater than the global deep water Zn/Si relation of $0.052[\text{Si}] + 0.79$ (Marchitto et al., 2000). Larger data sets of Zn/Si in the deeper waters throughout the globe are required to better fingerprint the circulation patterns.

4.3.3 Dissolved Zinc and Silicate Relationship

4.3.3.1 Northeastern Indian Ocean

Available data of DZn and Si in the global oceans display a strong positive correlation. It is believed that diatoms in the seawater take silicate for making their frustules. The strong relation between Zn and silicate suggests that Zn is consumed during the frustule formation. However, Elwood and Hunter (2000), has shown that diatoms consume only 1-3% of the total Zn uptake. In the contemporary oceans, Zn shows similar trend of concentration and regeneration length scales as those of silicate which gives the impression that Zn is taken up by the diatoms for the frustule formation and regenerated in the deeper waters due to their dissolution. Nevertheless, recent studies revealed that Zn has been uptaken by biology indicating its incorporation with the organic tissues which gets re-mineralized in the deeper waters. In such case, its behavior should be similar to the phosphate instead of Si but it shows the opposite.

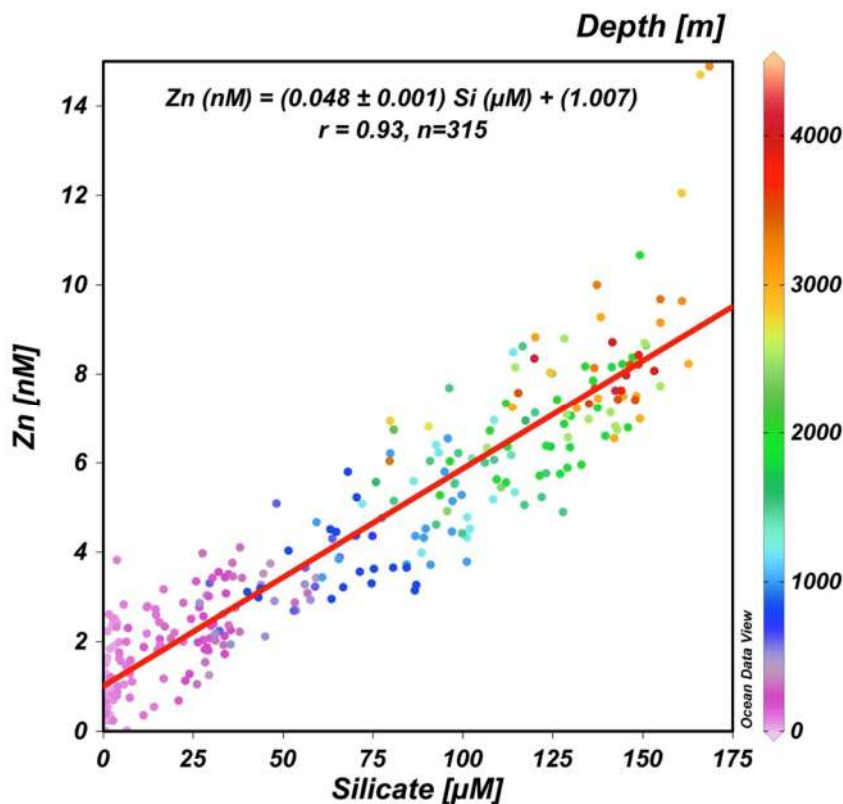


Figure 4.8: Scatter plot between silicate and dissolved Zinc.

It is a matter of debate among chemical oceanographers that “why does DZn show close relation with Si rather than with phosphate”?

A strong and linear correlation has been observed between silicate and zinc in the Northeastern Indian Ocean (Figure. 4.8). The relation observed here is consistent to the previous studies in the Indian Ocean (Saager et al., 1992; Morley et al., 1993; Kim et al., 2015). This is reflected by the similar trend of DZn and silicates in the section profiles (Figure 4.7). Even though the observed correlation between Zn and Si is consistent to the previous studies, a different slope for the Zn and Si in the study region has been observed compared to the studies of Gosnell et al. (2012) and Vu and Sohrin, (2013).

4.3.3.2 Northwestern Indian Ocean

The section plots of Zn and Si in the Figure 4.7, suggests their similar behavior and co-variation in the water column of the study region. Strong relationship (Figure 4.9) between Zn and Si is observed in the northwestern Indian Ocean similar to the studies in the other oceanic environments (Bruland and Franks, 1983; Martin et al., 1990; Lohan et al., 2002; Ellwood, 2008; Croot et al., 2011).

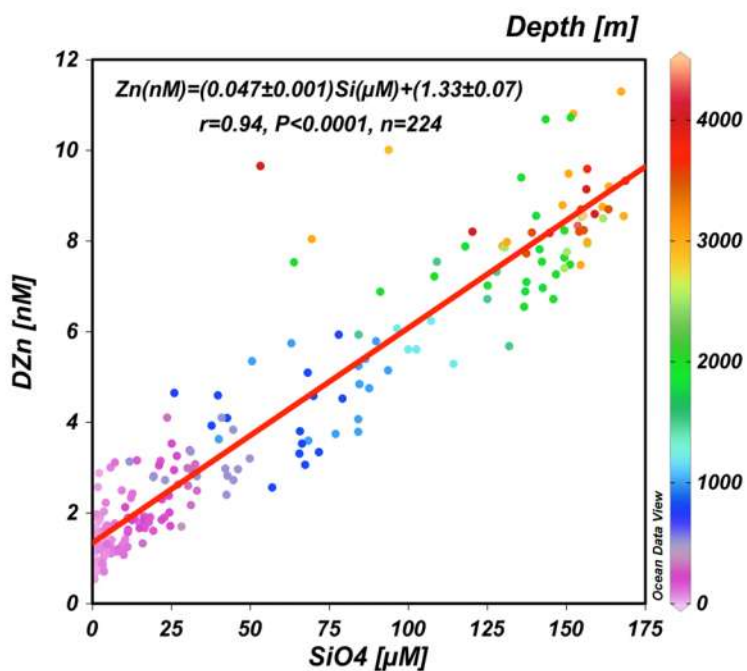


Figure 4.9: Scatter plot for Zn and Si in the Northwestern Indian Ocean.

By compiling the entire data set of Zn and Si in the region, a significant relation, $Zn \text{ (nM)} = (0.047) Si + 1.33$, $r = 0.94$, $n = 224$ was observed.

4.3.4 Comparison of Zinc-Silicate Relationship in the study region with the global ocean

In the present study distinct Zn:Si ratios are observed in the Indian Ocean. The relationship for the Northern Indian Ocean is $Zn \text{ (nM)} = (0.047) Si + (0.94 \pm 0.05)$, $r=0.94$ ($n=575$) (Figure 4.10) whereas for the Indian Ocean correlation is $Zn \text{ (nM)} = (0.057 \pm 0.001) Si + (1.23 \pm 0.11)$, $r=0.96$ ($n=141$) (Figure 4.11). A ratio of 0.065 observed for South Atlantic (Wyatt et al., 2014) and 0.077 for Southern Ocean (Ellwood, 2008).

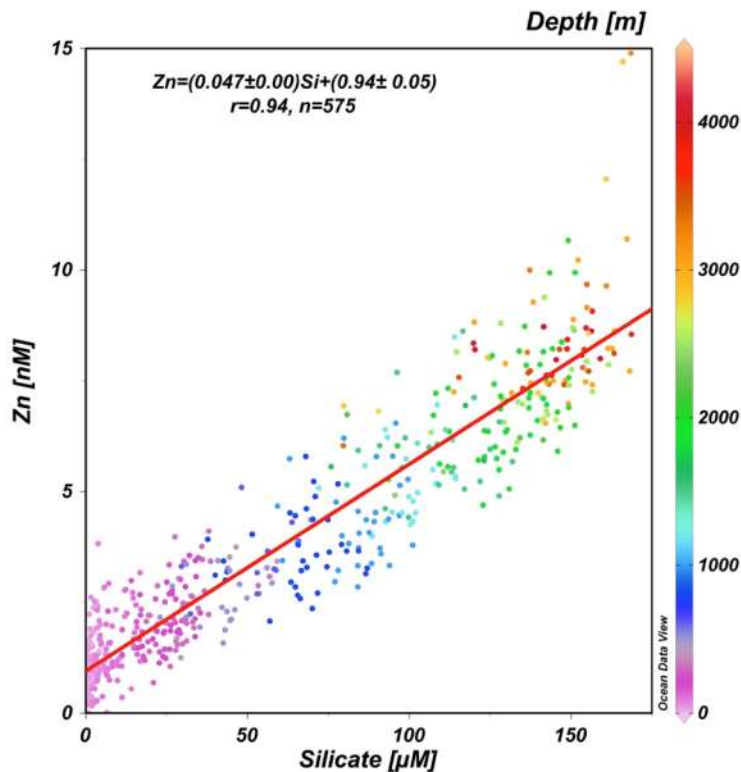


Figure 4.10: The Linear correlation between DZn and silicate in the Northern Indian Ocean stations.

The ratio (0.057 ± 0.001) for the Indian Ocean in the present study is consistent to the ratio (0.059 ± 0.04) reported in the study of Gosnell et al. (2012) and close to the global average Zn:Si ratio (0.059) (GEOTRACES IDP 2014). Interestingly,

Distributions of dissolved Zinc in the Indian Ocean

ratio of 0.047 observed for the Northern Indian Ocean is significantly lower compared to global average Zn:Si ratio and with respect to Indian Ocean (Figure 4.10).

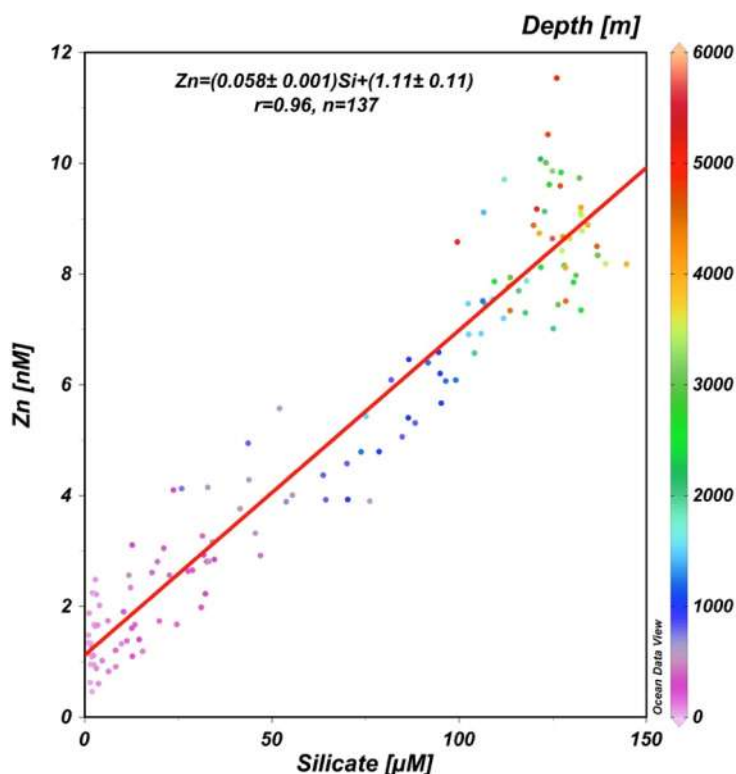


Figure 4.11: The Linear correlation between DZn and Silicate in the stations south of Equator. The observed relation is close to the global average for Zn vs. Si ratio.

The reasons for the observed lower ratio in the Northern Indian Ocean could be due to either increment in the silicate source in the water column that enhances the Si concentrations, which could lead to the observed low ratios, or processes effecting the removal of Zinc from the water column. The Zn:Si ratios in the intermediate and deeper waters are mostly governed by their uptake in the surface waters and re-mineralization in the subsequent deeper waters. The observed lower ratios could be due to either decoupling in the intermediate or/and deeper waters. Overall, the ratios for the deeper waters below 1000 m in Indian Ocean and Northern Indian Ocean are close to and greater than global average ratio. Therefore, the observed lower ratio in the region is due to the variation in the

intermediate waters due to decrease in the Zn/Si ratios. The reason for this mechanistic link between Zn and Si is still unclear. Vance et al. (2017) explained that the observed closeness of Zn-Si globally is coupled with the biogeochemical cycles of Zn and Si in the Southern ocean. In addition to this mechanistic link coupled through Southern Ocean results from this study suggests there could be an effect of OMZ on the Zn biogeochemical cycle.

4.3.5 Zinc vs. Silicate relationship in the oxygen minimum zone waters of the Bay of Bengal, the Andaman Sea and the Arabian Sea

The global Zn–Si ratio in the water column is not a fixed value. The ratio changes in the water column depending on the local hydrographic settings. In the present study distinct slopes has been observed between Zn-Si ratio in the Indian Ocean samples collected south of equator and north of equator comprises of various basins like the Andaman Sea, the Arabian Sea and the Bay of Bengal. The Zn/Si ratios in the stations sampled south of equator is in agreement with the global Zn-Si ratio of 0.059 (GEOTRACES IDP 2014 data). The stations north of equator shows significantly distinct slopes compared to global value for Zn-Si ratio. In the study area, the northern stations of the Indian Ocean, the Andaman Sea, the AS and the BoB are low in O₂ values in the depth range between 100 – 1000 m. The OMZ in the BoB is less intense than the Arabian Sea, which is situated at the same geographical location. The BoB receives more precipitation and less evaporation with huge fresh water supply from rivers which make the surface waters more static and thereby inhibiting the upwelling/mixing of nutrients to the surface waters further reducing the production in these waters. Sample depths between 100 – 1000m were low in DO, which are less than 50µM. Northwestern Indian Ocean, the Arabian Sea, is characterized by the presence to perennial Oxygen Minimum Zone (OMZ) in its intermediate water column. Data set of Zn and Si of intermediate and deeper water with DO content > 50 µM and < 50 µM are plotted separately to analyze the impact of low oxygen on DZn in the Northern Indian Ocean. It is observed that slope for Zn vs. Si in deeper waters (O₂> 50 µM) is close to the global average data whereas intermediate waters (O₂<

50 μM) having lower slope for Zn/Si compared to global data. In the above-mentioned OMZ stations, Zn/Si ratio is much lower (Almost half) compared to global average in all the regions of the Northern Indian Ocean (Figure 4.12 & 4.13). Studies done in the Subarctic Pacific Ocean region (Janssen et al., 2014; Janssen and Cullen, 2015) have invoked and attributed this low slope between Zn and Si to the specific removal process that maybe happening in the low O_2 waters. Sulfide precipitation has been proposed as a mechanism for the removal of cadmium and zinc in the low oxygen waters (Janssen et al., 2014; Janssen and Cullen, 2015). Similar lower ratio of Zn to Si in the OMZ waters in the Subarctic Pacific Ocean waters with respect to the global average value was observed and proposed the formation of sulfide particles in the OMZ which are acting as a removal process for Zn and Cd. These sulphides are highly stable and do not break easily once they form in the water column (Luther et al., 1999).

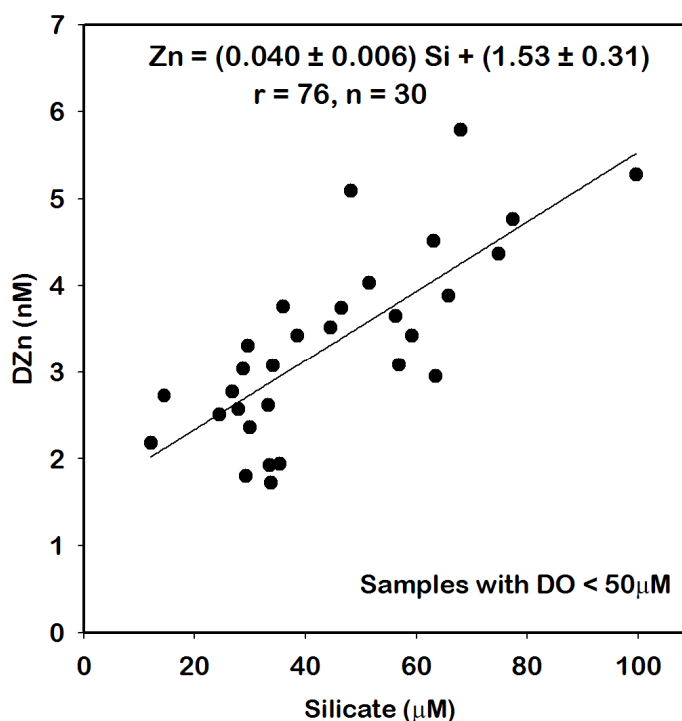


Figure 4.12: Zn vs. Si in the oxygen minimum zone waters of the BoB and the Andaman Sea

It is evident from the plots 4.12 and 4.13 that Zn is definitely lower in the intermediate waters compared to the deeper and surface values with respect to silicate. As mentioned in the above section that either Zn may be precipitating from the water column or preformed low Zn may be transported by the water masses or may be getting advected from the continental shelves/margins, which needed to be addressed. To attribute the in-situ precipitation of ZnS in the water column, sinking particulate matter has to be studied in the water column to ensure

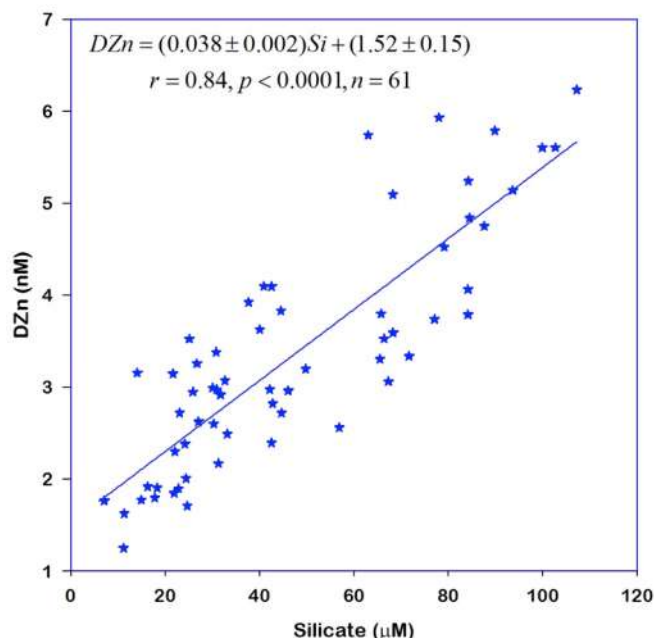


Figure 4.13: Zn vs. Si scatter plots in the oxygen minimum zone waters of the Arabian Sea.

the presence of Zn sulfides. In the present scenario of persistent decline in the oxygen values in the water column of the world oceans (Whitney et al., 2007; Keeling et al., 2010; Stramma et al., 2010; Falkowski et al., 2011), it is vital to understand this mechanism. If this process of Zn removal continues persistently in OMZ, the upwelling prominent regions will be face deficit for Zinc for primary productivity.

4.3.6 Effect of Oxygen minimum zone on the Zn cycle

In the study area, intermediate waters of the Northern Indian Ocean (Andaman Sea, Arabian Sea and BoB) are low in DO in the depth range between 100 – 1000 m. Seasonal anoxia has also been observed in the Northern Indian

Ocean. The observed ratio in the OMZ waters of the Northern Indian Oceans is $Zn \text{ (nM)} = (0.033 \pm 0.002) Si \text{ (}\mu\text{M)}$, $r=0.73$ ($n=187$) (Figure 4.14). The observed ratio is half of the global ratio and this lower ratio in the OMZ waters leads to the lower ratio observed in the Northern Indian Ocean compared to stations south of Equator as well as global ratio. It has also been observed that ratio in the depth interval of 100-1000 m in the stations south of equator are significantly higher compared to Northern Indian Ocean in 100-1000 m depth range. Recent studies observed lower Zn-Si ratio in some of the water columns where DO values are less than $50 \mu\text{M}$. When compared to the global Zn-Si ratio, lower ratios of Zn/Si, 0.033 – 0.045 in the oxygen deficient zones (ODZs) are observed (Janssen and Cullen 2015) similar to what is observed here.

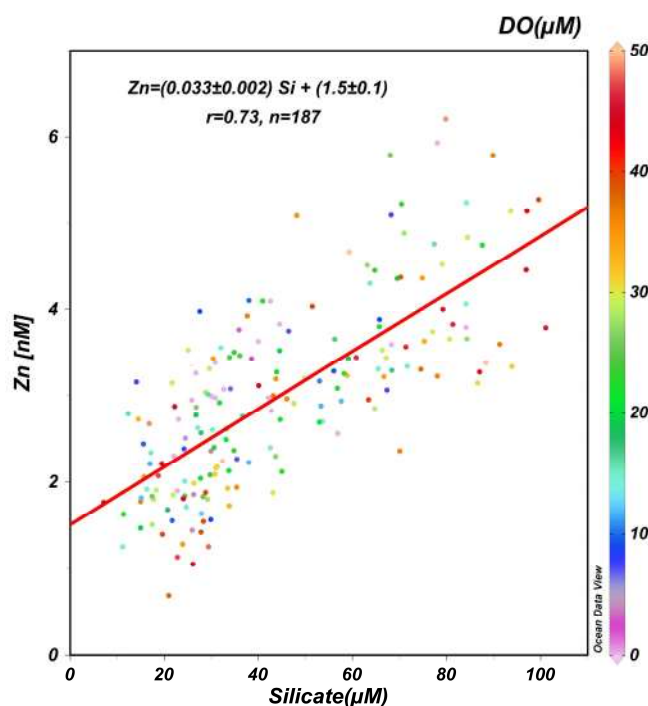


Figure 4.14: Zn vs. Si relationship in the oxygen minimum zone waters of the Northern Indian Ocean. The observed slope is half of the global average Zn vs. Si ratio.

Based on the observations it is proposed that as water masses progress to the OMZ region of Northern Indian Ocean side from the southern side, Zn is

being lost preferentially with respect to the Si or else the observed signal could be due to the water masses, which are already having low Zn and Si. It is already evident from the above sections that ratios noticed in the south of Equator are close to the global ratio. Therefore, the observed lower ratios could be due to the effect of OMZ in the Northern Indian Ocean or water masses in the intermediate depths. The similar lower values also observed in the intermediate waters of the BoB and Andaman Sea. There is no Zn data available for the source regions of RSW and PGW to compare with the present data set in the OMZ region. However, studies in the Black Sea (Anoxic) have shown the Zn removal from the water column as sulfide precipitates. Based on the large data set of DZn and Si in the Northern Indian Ocean with lower Zn/Si ratio in OMZ compared to the that of south of equatorial Indian Ocean and global ocean, it is quite likely that Zn is being removed in the oxygen deficient waters of the Northern Indian Ocean.

4.3.7 Zn vs. Si in the deeper waters of Northern Indian Ocean

DO values below 1000 m depth noticeably increased beyond threshold values and their average concentration below 1000 m is $117.42 \pm 37.17 \mu\text{M}$.

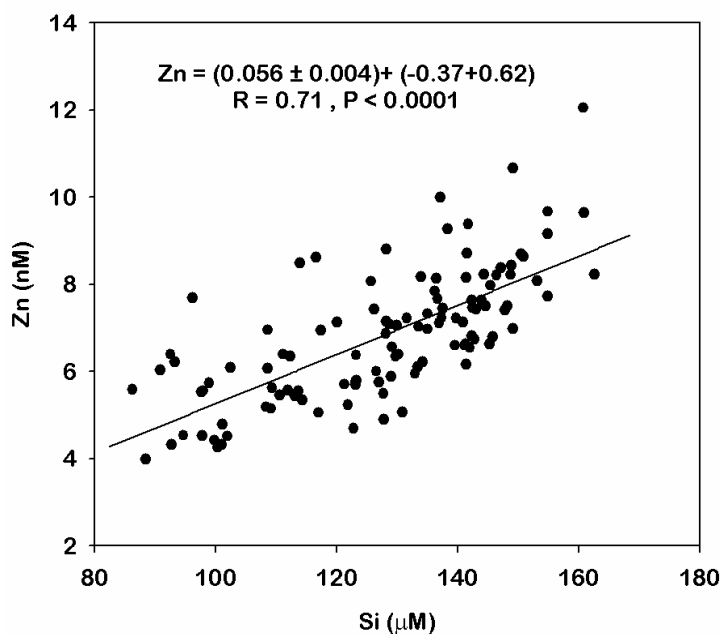


Figure 4.15: Scatter plot of Zn vs. Si in the deeper waters of the Northern Indian Ocean.

The silicate concentrations in the deeper waters are above $90 \mu\text{M}$. The scatter plot between Zn and Si for the deeper waters is shown in the Figure. 4.15. Interestingly the slope observed between Zn and Si for the waters below 1000 m matches with the global Zn:Si ratio which is not the case for the intermediate waters where oxygen values falls below the threshold limits.

4.3.8 Dissolved Zinc and Phosphate Relationship in the Indian Ocean

Figure 4.16, shows the plot between Zn and phosphate in the study region. A kink is observed between Zn vs. P at phosphate concentrations of $\sim 1.5 \mu\text{M}$ corresponding to depth of 75 to 100 m. It is suggested that Zn uptake by phytoplankton involves in organic tissues rather than the frustule formation.

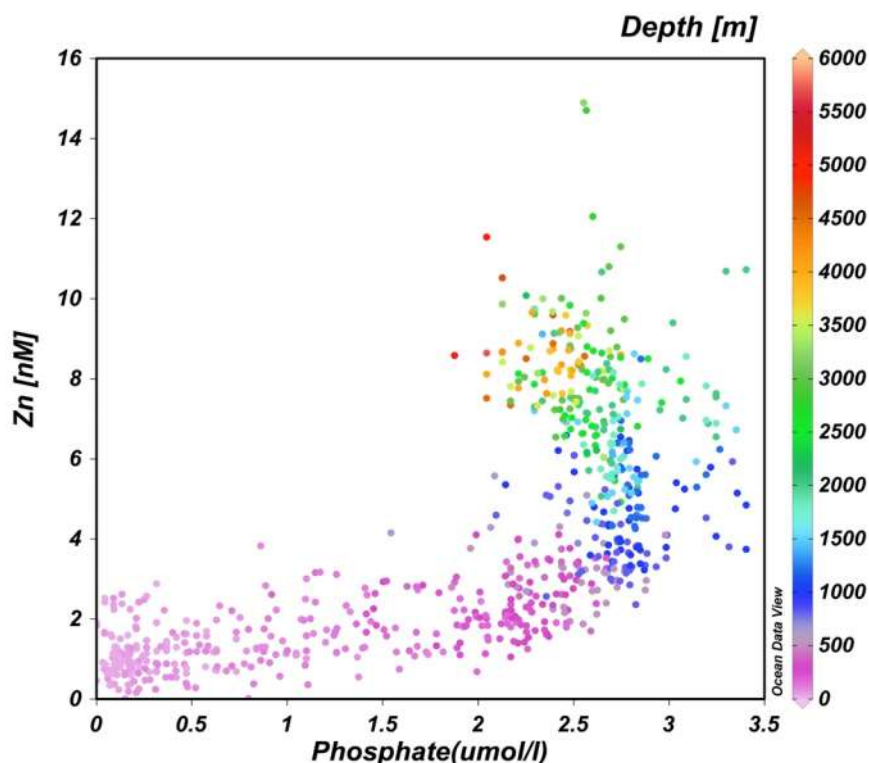


Figure 4.16: Scatter plot between Zn and Phosphate in the Indian Ocean waters.

Therefore, regeneration length scales for Zn should match with the P and not with Si if it involves in the soft tissues and Zn-P plots should be linear. However, in the contemporary oceans, contrast behavior is observed i.e., Zn vs. P scatter plots are not linear. Recent studies highlighted that observed close relation

with the Si but not with the P are lies in the Southern Ocean Zn-Si-P biogeochemical cycles. These correlations between Zn-P and Zn-Si have challenged oceanographers for the last four decades due to the absence of mechanistic understanding of this above-mentioned behavior of Zn with respect to Si and phosphate. A very recent study (de Souza et al., 2018) has explained this mechanistic link using ocean general circulation model and a box-model ensemble. These model results suggest that there exists a different biogeochemical regime for Zn-P at high and low latitudes. The observed Zn-Si tight correlation and Zn- P kink is due to its biogeochemical cycling coupled through the Southern Ocean. This similar behavior also observed for cadmium and P (Middag et al., 2018) and suggested that this analogous behavior may also show for other trace metals through the Southern Ocean.

4.3.9 Comparison of Zn distributions in the Indian Ocean with the Atlantic and Pacific Oceans

Zn concentrations reported in the Indian Ocean lies in between the Atlantic and Pacific Oceans (Vance et al., 2017). Zn cycle in the Atlantic and Pacific Oceans shows nutrient type profile similar to the Indian Ocean that shows surface low due to the biology and increment in the deeper waters due to the remineralization. The lowest Zn concentrations were reported in South Atlantic Ocean so far (Wyatt et al., 2014). There exists a strong correlation between Zn and Si in the Atlantic and Pacific Oceans similar to the observations in the Indian Ocean. Distinct Zn to Si ratios observed within the intra and inter basin implies the huge spatial variability in the phytoplankton community that uptake Zn including processes controlling the Zn cycle (Janssen and Cullen, 2015; Kim et al., 2017; Roshan and Wu, 2015; Wyatt et al., 2014). Hydrothermal input of Zinc near to the Mid Atlantic Ridge and tropical south Pacific Ocean were found with little/high distal effects (Roshan et al., 2016; Roshan and Wu, 2015). Similar distal effects of Zn may be seen along the central Indian Ridge and South western Indian Ridge in the Indian Ocean where it is seen in case of Fe. Zn results in the OMZ water column of the Indian Ocean and the Sub Arctic North Pacific Ocean shows similar Zn vs. Si slopes with the samples having DO < 50 μ M suggesting

that there may be a scavenging of Zn in these deficit waters as observed in the Sub Arctic Pacific Ocean. Studying particulate matter in these deficit waters could explain the scavenging of Zn in these regions. Sedimentary sources near to the continental boundaries are found to be significant source for Zn in the Atlantic and the Pacific Oceans. Similar sources have been found in the Indian Ocean also in the stations close to the east coast of Indian sub continent. The kink observed between Zn and P in the Indian Ocean is consistent the other oceanic basins and this kink arises due to the mechanistic links of Zn that coupled through the Southern Ocean (de Souza et al., 2018).

4.4 Summary and Conclusions

A total of 48 vertical profiles are sampled and analyzed for DZn in the Indian Ocean comprising of the Bay of Bengal, the Arabian Sea, the Andaman Sea and the Indian Ocean samples. Overall, DZn shows nutrient type profile in the present study region. A strong and significant correlation between Zn and silicate and kink between Zn and P in the Indian Ocean is due to the coupled biogeochemical cycling of Zn through Southern Ocean. Overall, Zn vs. Si ratio of 0.047 is observed in the study region from 48 profiles. Distinct slopes for Zn vs. Si is observed when data is separated based on the hydrographic parameter dissolved Oxygen. The Andaman sea, the Arabian Sea and the Bay of Bengal show a ratio which are significantly lower compared to the global average slope of Zn vs. Si of 0.064 whilst Zn vs. Si in the stations south of Equator displays a ratio of 0.057 consistent to the global value. Interestingly deeper samples of BoB, Arabian Sea and Andaman Sea are comparable to the global average data. The lower slopes obtained in the BoB, AS and Andaman Sea are due to the relatively lower DZn in the intermediate waters suggesting Zn removal from the oxygen minimum zone waters. Despite the coupled Zn biogeochemical cycling through Southern Ocean local biogeochemistry of the Northern Indian Ocean having unique features such as oxygen deficiency in the intermediate water column with respect to other oceanic basins influence the Zn cycle in the northern Indian Ocean significantly.

Chapter 5
Synthesis and Future Perspectives

The paramount goals of this study are to understand the distributions of bioactive trace elements, iron (Fe) and zinc (Zn) in the Indian Ocean waters in terms of their sources, sinks and internal cycling. The stated objectives are achieved through establishing clean sampling system and sampling protocols, fabricating sensitive flow injection system and clean sampling of seawater with full depth vertical profiles at an unprecedented resolution conducted in the Indian Ocean (21° N to 28° S) from several cruises between 2013 to 2017. The Indian Ocean is least explored basin for trace element biogeochemical cycles. This study highlights the distributions of Fe and Zn with high-resolution data providing a primary understanding on their sources, sinks and internal cycling in the Indian Ocean. The significant highlights of these results are summarized below.

5.1 Summary

5.1.1 Establishment of clean sampling protocols and sensitive flow injection methods

The trace elements in seawater especially Fe and Zn are more prone to contamination owing to their availability in low concentration from sub nanomolar to picomolar levels in seawater and metallic nature of onboard sampling gear. Regular seawater sampling techniques are not enough to sample these bioactive trace metals. First challenge in this study is sampling the seawater for trace metal studies without any contamination. This is achieved by procuring and establishing clean sampling system comprising the trace metal clean CTD, Teflon coated sampling bottles, epoxy coated rosette, Kevlar conducting cable, non-metallic winch system and clean (class 1000) van. The trace metal rosette was lowered by using a Kevlar cable which is a non-metallic wire having high tensile strength. Sampling and measurement quality have been ascertained intensively and rigorously by comparing Fe and Zn data with available reference materials and cross-over stations of other GEOTRACES group.

Rapid, sensitive and online methods are very important to measure bioactive trace metals to better understand their sources and internal cycling by avoiding contamination during storage and transfer. In this thesis, sensitive semi-automatic flow injection methods to determine sub nM to pM level concentrations of Fe and Zn in the seawater is established. Fe flow injection system established

in the lab is based on the chemiluminescence detection. The method detects Fe (III) in the sample. Briefly, seawater samples were preconcentrated on AF Chelate 650 M, IDA resin to retain the Fe in the seawater by avoiding the seawater matrix at a pH of 3.9 ± 0.1 . The procedural blank for this method is < 60 pM with a precision of within 5%. The detection limit (3 times the standard deviation of the blank) for this method is 0.06 nM. Zn flow injection system established in the lab is based on the fluorometric detection. Seawater samples were pre-concentrated on the IDA resin to retain the Zn and to remove the interfering ions at a pH of 5.1 ± 0.1 . The procedural blank for the Zn method established in the lab is 0.67 nM with a precision of < 10 %.

These established methods to measure low concentration of Fe and Zn in the seawater has been checked by measuring reference standards provided by the GEOTRACES community. The advantage of these established methods is online data production within hours of sampling with an optimal precision and accuracy.

5.1.2 Sources/sinks influencing the DFe and DZn cycling

Huge varieties of sources are contributing to the Fe and Zn biogeochemical cycles in the Indian Ocean. Particulate matter from the riverine sources, atmospheric dust deposition, upwelling along the western and eastern AS, eddies in the BoB, re-mineralization in the Oxygen minimum zone waters of the BoB and the AS are the major sources of DFe and DZn in the Northern Indian Ocean. In addition, shelf sediments and sediment resuspension also found as sources for Fe and Zn. Lateral advection of Fe signal from hydrothermal vent sources to the deeper waters of the Indian Ocean and subduction process also found significant source contributors to the Fe in the seawater. Influences of these sources on their internal cycling are briefed in the following sections.

5.1.2.1 Distributions of dissolved DFe and DZn in the Northern Indian Ocean

DFe profiles from the northern Indian Ocean comprise of the BoB, the Andaman Sea and the AS shows hybrid type profile. Surface concentrations of DFe shows meridional gradient from north to south in the BoB due to the atmospheric supply except in some locations where presence of eddies effecting DFe concentrations locally. Vertical profiles from the BoB imply that continental

shelves and margins are significant source contributors for the DFe. Intermediate waters of BoB are rich in DFe (~ 1.2 nM) due to remineralization from the sinking organic matter and/or particulate matter from the riverine sources. This conclusion is further strengthened by the significant correlation between AOU and DFe in the intermediate waters. The poor ventilation, huge supply of particulate matter from rivers enhances the enrichment of DFe in the intermediate waters of the BoB. Scavenging process dominates in the deeper waters of the BoB. This intermediate increment is faded out slowly as moving southwards towards equator which is consistent to dissolved oxygen. The Andaman Sea also shows similar enrichment in the intermediate waters. DFe is low in the surface waters of the central AS, which increases below the MLD and in the deeper waters (as high as ~ 1 nM). Perennial OMZ, upwelling during summer monsoon and supply of dust from the nearby desert regions are responsible for such profiles. In the western AS, relatively lower values are observed for DFe during post southwest monsoon compared to DFe values at central and eastern AS. In addition, DFe in the coastal stations sampled near west coast of India highlights the important role of continental shelf and margins in contributing to the DFe budget. Stations sampled at the Carlsberg ridge imply DFe input from some unknown hydrothermal vent sources. Distinct Fe:C remineralization rates are observed for the AS, the BoB, the Andaman Sea and for the coastal AS implying the huge spatial variability in the availability and uptake ratios in the surface waters together with different contributing sources.

DZn shows typical nutrient type profile in the BoB, the AS and the Andaman Sea. The significant result observed in all the basins of northern Indian Ocean is the tight correlation of Zn and Si in the study region. The observed slope in the northern Indian Ocean is slightly lower compared to the global Zn – Si relationship. Zn – Si slope of the OMZ waters of the BoB and the AS reveals that Zn is being removed from the water column relative to Si, which could be due to the formation of Zn sulfides in the OMZ. Significant exchange of the deeper waters of Andaman Sea with the intermediate waters of the BoB is evident from the vertical plots of Zn as well as with the hydrographic parameters and Zn – Si

scatter plots. Sediment re-suspension also seems to be a significant source contributor to the DZn in the deeper waters along the east coast of India.

5.1.2.2 Distributions of DFe and DZn in the equatorial and south of equator Indian Ocean

Significant difference in the vertical profiles of DFe is observed between the Northern Indian Ocean and the equatorial and south of equator Indian Ocean. Surface concentrations of DFe are very low in the Indian Ocean stations due to the lack of dust from the arid landmasses. Intermediate maxima have not been observed in these stations. Some of the deeper samples of the stations sampled near the Java trench region are enriched in DFe, by a factor of four compared to global deep water value for DFe. This study highlights that converging plate boundaries could be a significant source of DFe. In addition, some of the stations sampled near the South western and central Indian ridges reveal hydrothermal vents are significant sources of DFe in the deeper waters of the Indian Ocean. DFe concentrations observed in the deeper waters near to these vent locations are as high as ~ 27 nM. Section plots display the transport of these enriched DFe in deeper waters towards Northern Indian Ocean.

The DZn vertical profiles show no much difference compared to the profiles obtained in the Northern Indian Ocean except in the Zn vs. Si slopes. Zn vs. Si in the entire water column of the Indian Ocean are close to the global value clearly emphasizing the role of OMZ on the Zn cycle in the Indian Ocean. Unlike, DFe deeper waters enrichment seen in the trench region is not seen in the DZn case. Hydrothermal derived inputs does not seems to be a significant source for DZn in the Indian Ocean unlike for DFe.

5.2 Future Perspectives

High resolution data of DFe and DZn in this thesis gives a primary level of understanding on their distributions in the Indian Ocean. The overview on different sources, sinks and internal cycling for DFe and DZn in this study helps future studies to better interpret the link between biogeochemical cycles of Fe and Zn with respect to carbon cycle and hence their impact on climate change through

modeled studies. The findings of this thesis addresses few interesting scientific problems needed for future studies which are mentioned below

(i) In this thesis, total dissolved concentrations for DFe is presented. Total DFe comprises of soluble and colloidal fractions, which represents the 99 % of Fe binding with the organic complexes. To address this issue, studies of different size fractions of Fe are required. Very limited information of colloidal and soluble Fe is available in the Indian Ocean. This issue needs to be addressed.

(ii) The oxygen minimum zones in the study region shows high DFe values in the intermediate waters where DO values are low. At a circum neutral pH of seawater Fe is highly unstable and should be removed from the water column which is not the case in the seawater. This is due to the presence of several organic/inorganic ligands in the seawater column, which binds with the Fe in the seawater and further decreases the scavenging process. These processes can be evident clearly only by studying the speciation of Fe and identifying different types of ligand classes and their stability constants.

(iii) Contribution of different sources and their influence on DFe has been identified in the thesis. For the complete understanding and fingerprinting the type of sources/processes contributing/happening in the water column can be achieved only through isotopic studies. To the best of our knowledge there is no single study existed for the isotopic composition information for the Fe in the Indian Ocean.

(iv) This thesis work results show the strong correlation of Zn vs. Si in the water column. The lower slope between Zn vs. Si in the Indian Ocean compared to the other oceanic basins could be due to the presence of OMZ in the Northern Indian Ocean. Results of the work suggest that OMZ might be acting as a sink for the DZn in the intermediate waters. This implication is drawn by comparing simple linear regression plots between Zn vs. Si in the deeper waters and intermediate waters. This can be concluded by further studying the particulate matter in the OMZ waters for the presence of sulfide particles.

(v) The DZn speciation, size fractionation and their isotopic composition studies in the Indian Ocean will provide complete understanding on the

biogeochemical cycle of Zn in the seawater. There is no single data on the Zn isotopic composition and size fractionation studies in the Indian Ocean water samples so far. In future, research in these directions will enhance our knowledge on marine Zn cycle.

References

- Abadie, C., Lacan, F., Radic, A., Pradoux, C., Poitrasson, F., 2017. Iron isotopes reveal distinct dissolved iron sources and pathways in the intermediate versus deep Southern Ocean. *Proceedings of the National Academy of Sciences*, 114(5), 858-863.
- Anderson, M. A., Morel, F. M. M., & Guillard, R. R. L. (1978). Growth limitation of a coastal diatom by low zinc ion activity. *Nature*, 276(5683), 70-71.
- Anderson, L.A., 1995. On the hydrogen and oxygen content of marine phytoplankton. *Deep Sea Research Part I: Oceanographic Research Papers*, 42(9), 1675-1680.
- Aumont, O., Ethe, C., Tagliabue, A., Bopp, L., & Gehlen, M., 2015. PISCES-v2: an ocean biogeochemical model for carbon and ecosystem studies. *Geoscientific Model Development Discussions*, 8(2).
- Bange, H.W., Naqvi, S.W.A., Codispoti, L.A., 2005. The nitrogen cycle in the Arabian Sea. *Progress in Oceanography*, 65(2), 145-158.
- Banase, K. (1959). On upwelling and bottom-trawling off the southwest coast of India. *Journal of the Marine Biological Association of India*, 1(1), 33-49.
- Barbeau, K. (2006). Photochemistry of organic iron (III) complexing ligands in oceanic systems. *Photochemistry and Photobiology*, 82(6), 1505-1516.
- Basu, A. R., Jacobsen, S. B., Poreda, R. J., Dowling, C. B., Aggarwal, P. K., 2001. Large groundwater strontium flux to the oceans from the Bengal Basin and the marine strontium isotope record. *Science*, 293(5534), 1470-1473.
- Beal, L.M., De Ruijter, W.P., Biastoch, A. and Zahn, R., 2011. On the role of the Agulhas system in ocean circulation and climate. *Nature*, 472(7344), 429-436.
- Bennett, S.A., Achterberg, E.P., Connelly, D.P., Statham, P.J., Fones, G.R., German, C.R., 2008. The distribution and stabilisation of dissolved Fe in deep sea hydrothermal plumes. *Earth Planet. Sci. Lett.*
- Bergquist, B.A. and Boyle, E.A.C.G., 2006. Dissolved iron in the tropical and subtropical Atlantic Ocean. *Global Biogeochemical Cycles*, 20(1)
- Bird, M.I., Robinson, R.A.J., Oo, N.W., Aye, M.M., Lu, X.X., Higgitt, D.L., Swe,

- A., Tun, T., Win, S.L., Aye, K.S. and Win, K.M.M., 2008. A preliminary estimate of organic carbon transport by the Ayeyarwady (Irrawaddy) and Thanlwin (Salween) Rivers of Myanmar. *Quaternary International*, 186(1), 113-122.
- Blain, S., Sarthou, G., Laan, P., 2008. Distribution of dissolved iron during the natural iron-fertilization experiment KEOPS (Kerguelen Plateau, Southern Ocean). *Deep Sea Research Part II: Topical Studies in Oceanography*, 55(5), 594-605.
- Boyd, P.W., Watson, A.J., Law, C.S., Abraham, E.R., Trull, T., Murdoch, R., Bakker, D.C., Bowie, A.R., Buesseler, K.O., Chang, H. and Charette, M., 2000. A mesoscale phytoplankton bloom in the polar Southern Ocean stimulated by iron fertilization. *Nature*, 407(6805), 695-702.
- Boyd, P. W., Jickells, T., Law, C. S., Blain, S., Boyle, E. A., Buesseler, K. O., & Harvey, M., 2007. Mesoscale iron enrichment experiments 1993-2005: Synthesis and future directions. *science*, 315(5812), 612-617.
- Boyd, P.W. and Ellwood, M.J., 2010. The biogeochemical cycle of iron in the ocean. *Nature Geoscience*, 3 (10), 675-682.
- Boyle, E. and Edmond, J.M., 1975. Copper in surface waters south of New Zealand. *Nature*, 253(5487): 107-109.
- Boyle, E.A. and Keigwin, L.D., 1982. Deep circulation of the North Atlantic over the last 200,000 years: Geochemical evidence. *Science*, 218 (4574): 784-787.
- Boyle, E.A., 1988. Cadmium: Chemical tracer of deepwater paleoceanography. *Paleoceanography*, 3(4): 471-489.
- Brand, L.E., Sunda, W.G. and Guillard, R.R.L., 1983. Limitation of marine phytoplankton reproductive rates by zinc, manganese, and iron. *Limnology and Oceanography*, 28(6): 1182-1198.
- Bruland, K.W., 1989. Complexation of zinc by natural organic ligands in the central North Pacific. *Limnology and Oceanography*, 34(2): 269-285.
- Bruland, Kenneth W., John R. Donut, and David A. Hutchins., 1991. "Interactive influences of bioactive trace metals on biological production in oceanic waters." *Limnology and Oceanography* 36.8: 1555-1577.

- Bruland, K.W., Rue, E.L., Smith, G.J., DiTullio, G.R., 2005. Iron, macro nutrients and diatom in the Peru upwelling regime: brown and blue waters of Peru. *Mar. Chem.* 93, 81–103.
- Bruland, K.W. and Lohan, M.C., 2006. Controls of trace metals in seawater. *The oceans and marine geochemistry*. Elsevier: 23-47.
- Bruland, K. W., Middag, R. and Lohan, M. C. (2013) Controls of Trace Metals in Seawater In, Mottl, Michael J. and Elderfield, Henry (eds.) *Treatise on Geochemistry: Second Edition*. Philadelphia, USA, Saunders, Elsevier Inc. pp. 19-51. (doi:10.1016/B978-0-08-095975-7.00602-1).
- Chester, R., Berry, A. S., & Murphy, K. J. T. (1991). The distributions of particulate atmospheric trace metals and mineral aerosols over the Indian Ocean. *Marine Chemistry*, 34(3-4), 261-290.
- Christina, L., Hutchins, D.A., Brzezinski, M.A. and Zhang, Y., 2000. Effects of iron and zinc deficiency on elemental composition and silica production by diatoms. *Marine Ecology Progress Series*, 195: 71-79.
- Clemens, S. C., Kuhnt, W., LeVay, L. J., Anand, P., Ando, T., Bartol, M., & Hathorne, E. C. 2016. Expedition 353 summary. Clemens, SC, Kuhnt, W., LeVay, LJ, and the Expedition, 353.
- Coale, K.H., 1991. Effects of iron, manganese, copper, and zinc enrichments on productivity and biomass in the subarctic Pacific. *Limnology and Oceanography*, 36(8): 1851-1864.
- Coale, K.H., Fitzwater, S.E., Gordon, R.M., Johnson, K.S. and Barber, R.T., 1996. Control of community growth and export production by upwelled iron in the equatorial Pacific Ocean. *Nature*, 379 (6566): 621-624.
- Coale, K.H., Wang, X., Tanner, S.J. and Johnson, K.S., 2003. Phytoplankton growth and biological response to iron and zinc addition in the Ross Sea and Antarctic Circumpolar Current along 170 W. *Deep Sea Research Part II: Topical Studies in Oceanography*, 50(3): 635-653.
- Cochlan, W.P., Bronk, D.A. and Coale, K.H., 2002. Trace metals and nitrogenous nutrition of Antarctic phytoplankton: experimental observations in the Ross Sea. *Deep Sea Research Part II: Topical Studies in Oceanography*, 49(16): 3365-3390.

- Crawford, D.W. et al., 2003. Influence of zinc and iron enrichments on phytoplankton growth in the northeastern subarctic Pacific. *Limnology and Oceanography*, 48(4): 1583-1600.
- Cronan, D.S., Tooms, J., 1969. The geochemistry of manganese nodules and associated pelagic deposits from the Pacific and Indian Oceans. *Deep sea Res.* 16, 335–359.
- Croot, P. L., Bowie, A. R., Frew, R. D., Maldonado, M. T., Hall, J. A., Safi, K. A., ... & Law, C. S. (2001). Retention of dissolved iron and Fe II in an iron induced Southern Ocean phytoplankton bloom. *Geophysical Research Letters*, 28(18), 3425-3428.
- Croot, P. L., & Laan, P. (2002). Continuous shipboard determination of Fe (II) in polar waters using flow injection analysis with chemiluminescence detection. *Analytica Chimica Acta*, 466(2), 261-273.
- Curry, W.B. and Lohmann, G.P., 1982. Carbon isotopic changes in benthic foraminifera from the western South Atlantic: Reconstruction of glacial abyssal circulation patterns. *Quaternary Research*, 18(2): 218-235.
- Cutter, G.A. and Bruland, K.W., 2012. Rapid and noncontaminating sampling system for trace elements in global ocean surveys. *Limnol. Oceanogr. Methods*, 10(6): 425-436.
- Damodararao, K., Singh, S. K., Rai, V. K., Ramaswamy, V., & Rao, P. S. (2016). Lithology, Monsoon and Sea-Surface Current Control on Provenance, Dispersal and Deposition of Sediments over the Andaman Continental Shelf. *Frontiers in Marine Science*, 3, 118.
- De Baar, H.J., Timmermans, K.R., Laan, P., De Porto, H.H., Ober, S., Blom, J.J., Bakker, M.C., Schilling, J., Sarthou, G., Smit, M.G., Klunder, M., 2008. Titan: A new facility for ultraclean sampling of trace elements and isotopes in the deep oceans in the international Geotraces program. *Marine Chemistry*, 111(1), 4-21.
- De Jong, J.T.M., Den Das, J., Bathmann, U., Stoll, M.H.C., Kattner, G., Nolting, R.F., De Baar, H.J.W., 1998. Dissolved iron at subnanomolar levels in the Southern Ocean as determined by ship-board analysis. *Analytica Chimica Acta*, 377(2), 113-124.

- de Souza, G.F., Khatiwala, S.P., Hain, M.P., Little, S.H., Vance, D., 2018. On the origin of the marine zinc–silicon correlation. *Earth Planet. Sci. Lett.* 492, 22–34. doi:10.1016/j.epsl.2018.03.050
- Dileep Kumar, Y.-H. Li (1996). Spreading of water masses and regeneration of silica and ^{226}Ra in the Indian Ocean. *Deep Sea Res. Part II*, 43, pp. 83-110.
- Donat, J.R. and Bruland, K.W., 1990. A comparison of two voltammetric techniques for determining zinc speciation in Northeast Pacific Ocean waters. *Marine Chemistry*, 28(4): 301-323.
- Duce Robert A. , Tindale Neil W. , (1991). Atmospheric transport of iron and its deposition in the ocean, *Limnology and Oceanography*, 36, doi: 10.4319/lo.1991.36.8.1715.
- Dutta, K., Bhushan, R. and Somayajulu, B.L.K., 2007. Rapid vertical mixing rates in deep waters of the Andaman Basin. *Science of the Total Environment*, 384(1): 401-408.
- Ellwood, M.J. and Hunter, K.A., 2000. The incorporation of zinc and iron into the frustule of the marine diatom *Thalassiosira pseudonana*. *Limnology and Oceanography*, 45(7): 1517-1524.
- Ellwood, M.J. and Van den Berg, C.M.G., 2000. Zinc speciation in the northeastern Atlantic Ocean. *Marine Chemistry*, 68(4): 295-306.
- Elrod, V. A., Berelson, W. M., Coale, K. H., & Johnson, K. S., 2004. The flux of iron from continental shelf sediments: A missing source for global budgets. *Geophysical Research Letters*, 31(12).
- Ellwood, M.J., Bowie, A.R., Baker, A., Gault-Ringold, M., Hassler, C., Law, C.S., Maher, W.A., Marriner, A., Nodder, S., Sander, S., Stevens, C., Townsend, A., van der Merwe, P., Woodward, E.M.S., Wuttig, K., Boyd, P.W., 2018. Insights Into the Biogeochemical Cycling of Iron, Nitrate, and Phosphate Across a 5,300 km South Pacific Zonal Section (153°E-150°W). *Global Biogeochem. Cycles*. doi:10.1002/2017GB005736
- Falkowski, P. G., 1997. Evolution of the nitrogen cycle and its influence on the biological sequestration of CO₂ in the ocean. *Nature*, 387(6630), 272.
- Falkowski, P.G. et al., 2011. Ocean deoxygenation: Past, present, and future. *Eos, Transactions American Geophysical Union*, 92(46): 409-410.

- F.A. Schott, J.P. McCreary Jr (2001). The monsoon circulation of the Indian Ocean. *Progressions in Oceanography*, 51, pp. 1-123.
- Franck, V.M., Bruland, K.W., Hutchins, D.A. and Brzezinski, M.A., 2003. Iron and zinc effects on silicic acid and nitrate uptake kinetics in three high-nutrient, low-chlorophyll (HNLC) regions. *Marine Ecology Progress Series*, 252: 15-33.
- Frank, M., Whiteley, N., van de Flierdt, T., Reynolds, B.C. and O'Nions, K., 2006. Nd and Pb isotope evolution of deep water masses in the eastern Indian Ocean during the past 33 Myr. *Chemical Geology*, 226(3), 264-279.
- Frants, M., Holzer, M., DeVries, T. and Matear, R.C.J.G., 2016. Constraints on the global marine iron cycle from a simple inverse model. *Journal of Geophysical Research: Biogeosciences*, 121(1): 28-51.
- Frisch, W., 2014. Morphology Across Convergent Plate Boundaries. In: J. Harff, M. Meschede, S. Petersen and J. Thiede (Editors), *Encyclopedia of Marine Geosciences*. Springer Netherlands, Dordrecht, 1-7. DOI: https://doi.org/10.1007/978-94-007-6644-0_110-1.
- Gallant, R. M., & Von Damm, K. L., 2006. Geochemical controls on hydrothermal fluids from the Kairei and Edmond vent fields, 23–25 S, Central Indian Ridge. *Geochemistry, Geophysics, Geosystems*, 7(6).
- Galy, A., France-Lanord, C., 1999. Weathering processes in the Ganges–Brahmaputra basin and the riverine alkalinity budget. *Chemical Geology*, 159(1), 31-60.
- Galy A., France-Lanord C., 2001. Higher erosion rates in the Himalaya: Geochemical constraints on riverine fluxes. *Geology* 29, 23–26.
- Gamo, T., Nakayama, E., Shitashima, K., Isshiki, K., Obata, H., Okamura, K., Kanayama, S., Oomori, T., Koizumi, T., Matsumoto, S. and Hasumoto, H., 1996. Hydrothermal plumes at the Rodriguez triple junction, Indian ridge. *Earth and Planetary Science Letters*, 142(1-2), 261-270.
- Gamo, T., Chiba, H., Yamanaka, T., Okudaira, T., Hashimoto, J., Tsuchida, S., Ishibashi, J.I., Kataoka, S., Tsunogai, U., Okamura, K. and Sano, Y., 2001. Chemical characteristics of newly discovered black smoker fluids and associated hydrothermal plumes at the Rodriguez Triple Junction, Central

- Indian Ridge. *Earth and Planetary Science Letters*, 193(3), 371-379.
- Gao, Y., Kaufman, Y. J., Tanre, D., Kolber, D., & Falkowski, P. G. (2001). Seasonal Distributions of Aeolian Iron Fluxes to the Global Ocean. *Geophysical Research Letters*.
- Geotraces cook book. (<http://www.geotraces.org/sic/intercalibrate-data/cookbook>)
- Geotraces Science plan, 2006. (<http://www.geotraces.org/science/science-plan>)
- Gledhill, M. and Buck, K.N., 2012. The organic complexation of iron in the marine environment: a review. *The microbial ferrous wheel: iron cycling in terrestrial, freshwater, and marine environments*, 29.
- Goldberg, E.D. and Griffin, J.J., 1970, June. The sediments of the northern Indian Ocean. In *Deep Sea Research and Oceanographic Abstracts* (Vol. 17, No. 3, 513-537). Elsevier.
- Gopalakrishna, V.V., Murty, V.S.N., Sengupta, D., Shenoy, S. and Araligidad, N., 2002. Upper ocean stratification and circulation in the northern Bay of Bengal during southwest monsoon of 1991. *Continental Shelf Research*, 22(5), 791-802.
- Gordon, A.L. et al., 1997. Advection and diffusion of Indonesian throughflow water within the Indian Ocean South Equatorial Current. *Geophysical Research Letters*, 24(21): 2573-2576.
- Gordon, A.L., Susanto, R.D. and Vranes, K., 2003. Cool Indonesian throughflow as a consequence of restricted surface layer flow. *Nature*, 425(6960): 824-828.
- Gosnell, K.J., Landing, W.M. and Milne, A., 2012. Fluorometric detection of total dissolved zinc in the southern Indian Ocean. *Marine Chemistry*, 132: 68-76.
- Goswami, V., Singh, S.K. and Bhushan, R., 2012. Dissolved redox sensitive elements, Re, U and Mo in intense denitrification zone of the Arabian Sea. *Chemical Geology*, 291, 256-268.
- Goswami, V., Singh, S. K., & Bhushan, R. (2014). Impact of water mass mixing and dust deposition on Nd concentration and ^{143}Nd of the Arabian Sea water column. *Geochimica et Cosmochimica Acta*, 145, 30-49.

- Gran, H. H. (1931). On the conditions for the production of plankton in the sea. *Conseil Perm. Internat. pour l'Explor. de la Mer. Rapp. et Proces-Verb.*, 75, 37-46.
- Grand, M. M., Measures, C. I., Hatta, M., Hiscock, W. T., Buck, C. S., Landing, W. M., 2015. Dust deposition in the eastern Indian Ocean: The ocean perspective from Antarctica to the Bay of Bengal. *Global Biogeochemical Cycles*, 29(3), 357-374.
- Grand, M.M., Measures, C.I., Hatta, M., Hiscock, W.T., Landing, W.M., Morton, P.L., Buck, C.S., Barrett, P.M. and Resing, J.A., 2015. Dissolved Fe and Al in the upper 1000 m of the eastern Indian Ocean: A high-resolution transect along 95° E from the Antarctic margin to the Bay of Bengal. *Global Biogeochemical Cycles*, 29(3),375-396.
- Grand, M.M., Chocholou, J., Solich, P. and Measures, C.I., 2016. Determination of trace zinc in seawater by coupling solid phase extraction and fluorescence detection in the Lab-On-Valve format. *Analytica chimica acta*, 923: 45-54.
- Grasshoff, K., Ehrhardt, M. and Kremling, K., 1983. *Methods of Seawater Analysis*.
- Grasshoff, K., M. Ehrhardt, and K. Kremling (Eds.) (1992), *Methods of Seawater Analysis*, 634 pp., Verl. Chem., Weinheim, Germany, doi:10.1002/9783527613984.
- Guieu, C., S. B., C. P., C. M., V., C., K., D., Maes, C., Moutin, T., 2018. Iron from a submarine source impacts the productive layer of the Western Tropical South Pacific (WTSP). *Sci. Rep.* doi:10.1038/s41598-018-27407-z
- Gupta, R. S., Rajagopal, M. D., & Qasim, S. Z. (1976). Relationship between dissolved oxygen and nutrients in the north-western Indian Ocean.
- Gupta, R.S., Moraes, C., George, M.D., Kureishy, T.W., Noronha, R.J. and Fondekar, S.P., 1981. Chemistry & hydrography of the Andaman Sea. *Indian Journal of Marine Sciences*, 10, 228–33.
- Hart, T. J., On the phytoplankton of the south-west Atlantic and the Bellingshausen Sea, 1929-31, *Discovery Rep.*, VIII, 1-268, 1934.
- Hopkinson, B.M. and Barbeau, K.A., 2007. Organic and redox speciation of iron

- in the eastern tropical North Pacific suboxic zone. *Marine Chemistry*, 106(1), 2-17.
- Hutchins, D.A., Bruland, K.W., 1998. Iron-limited diatom growth and Si:N uptake ratios in a coastal upwelling regime. *Lett. to Nat.*
- Ibrahim, M. M., Shaban, S. Y., & Ichikawa, K. (2008). A promising structural zinc enzyme model for CO₂ fixation and calcification. *Tetrahedron Letters*, 49(51), 7303-7306.
- Jakuba, R.W., Saito, M.A., Moffett, J.W. and Xu, Y., 2012. Dissolved zinc in the subarctic North Pacific and Bering Sea: its distribution, speciation, and importance to primary producers. *Global Biogeochemical Cycles*, 26(2).
- Janssen, D.J. et al., 2014. Undocumented water column sink for cadmium in open ocean oxygen-deficient zones. *Proceedings of the National Academy of Sciences*, 111(19): 6888-6893.
- Janssen, D.J. and Cullen, J.T., 2015. Decoupling of zinc and silicic acid in the subarctic northeast Pacific interior. *Marine Chemistry*, 177: 124-133.
- Jeandel, C., Thouron, D., & Fieux, M. (1998). Concentrations and isotopic compositions of neodymium in the eastern Indian Ocean and Indonesian straits. *Geochimica et Cosmochimica Acta*, 62(15), 2597-2607.
- Jickells, T.D., An, Z.S., Andersen, K.K., Baker, A.R., Bergametti, G., Brooks, N., Cao, J.J., Boyd, P.W., Duce, R.A., Hunter, K.A. and Kawahata, H., 2005. Global iron connections between desert dust, ocean biogeochemistry, and climate. *science*, 308(5718), 67-71.
- Johnson, D. A., & Damuth, J. E. (1979). Deep thermohaline flow and current-controlled sedimentation in the Amirante Passage: Western Indian Ocean. *Marine Geology*, 33(1-2), 1-44.
- Johnson, G. C., Warren, B. A., & Olson, D. B. (1991). Flow of bottom water in the Somali Basin. *Deep Sea Research Part A. Oceanographic Research Papers*, 38(6), 637-652.
- Johnson, K.S., Elrod, V., Fitzwater, S., Plant, J., Boyle, E., Bergquist, B., Bruland, K., Aguilar-Islas, A., Buck, K., Lohan, M. and Smith, G.J., 2007. Developing standards for dissolved iron in seawater. *Eos, Transactions American Geophysical Union*, 88(11), 131-132.

- Kawagucci, S., Okamura, K., Kiyota, K., Tsunogai, U., Sano, Y., Tamaki, K. and Gamo, T., 2008. Methane, manganese, and helium-3 in newly discovered hydrothermal plumes over the Central Indian Ridge, 18°–20° S. *Geochemistry, Geophysics, Geosystems*, 9(10).
- Keeling, R.F., Kartzinger, A. and Gruber, N., 2010. Ocean deoxygenation in a warming world. *Marine Science*, 2.
- Khan, P.K., Chakraborty, P.P., 2005. Two-phase opening of Andaman Sea: a new seismotectonic insight. *Earth and Planetary Science Letters*, 229(3), 259-271.
- Kim, T., Obata, H., Gamo, T., 2015. Dissolved Zn and its speciation in the northeastern Indian Ocean and the Andaman Sea. *Frontiers in Marine Science*, 2, 60.
- Klunder, M.B., Laan, P., Middag, R., De Baar, H.J.W. and Van Ooijen, J.C., 2011. Dissolved iron in the Southern Ocean (Atlantic sector). *Deep Sea Research Part II: Topical Studies in Oceanography*, 58(25), 2678-2694.
- Kolla, V., Henderson, L. and Biscaye, P.E., 1976. Clay mineralogy and sedimentation in the western Indian Ocean. In *Deep Sea Research and Oceanographic Abstracts*. 23(10), 949-961.
- Kondo, Y., & Moffett, J. W., 2013. Dissolved Fe (II) in the Arabian Sea oxygen minimum zone and western tropical Indian Ocean during the inter-monsoon period. *Deep Sea Research Part I: Oceanographic Research Papers*, 73, 73-83.
- Kondo, Y., Moffett, J.W., 2015. Iron redox cycling and subsurface offshore transport in the eastern tropical South Pacific oxygen minimum zone. *Mar. Chem.* 168, 95–103.
- Kuma, K., Nishioka, J. and Matsunaga, K., 1996. Controls on iron(III) hydroxide solubility in seawater: The influence of pH and natural organic chelators. *Limnology and Oceanography*, 41(3), 396-407.
- Kumagai, H., Nakamura, K., Toki, T., Morishita, T., Okino, K., Ishibashi, J.I., Tsunogai, U., Kawagucci, S., Gamo, T., Shibuya, T. and Sawaguchi, T., 2008. Geological background of the Kairei and Edmond hydrothermal fields along the Central Indian Ridge: implications of their vent fluids?

- distinct chemistry. *Geofluids*, 8(4), 239-251.
- Kumar, M.D. and Li, Y.H., 1996. Spreading of water masses and regeneration of silica and ^{226}Ra in the Indian Ocean. *Deep Sea Research Part II: Topical Studies in Oceanography*, 43(1),83-110.
- Kumar, A., Sarin, M. M., &Srinivas, B., 2010. Aerosol iron solubility over Bay of Bengal: Role of anthropogenic sources and chemical processing. *Marine Chemistry*, 121(1), 167-175.
- Laws, E.A., 1991.Photosynthetic quotients, new production and net community production in the open ocean.*Deep Sea Research Part A. Oceanographic Research Papers*, 38(1), 143-167.
- Liu, X. and Millero, F.J., 2002.The solubility of iron in seawater.*Marine Chemistry*, 77(1): 43-54.
- Leblanc, K. et al., 2005. Fe and Zn effects on the Si cycle and diatom community structure in two contrasting high and low-silicate HNLC areas. *Deep Sea Research Part I: Oceanographic Research Papers*, 52(10): 1842-1864.
- Lohan, M. C., & Bruland, K. W. (2008). Elevated Fe (II) and dissolved Fe in hypoxic shelf waters off Oregon and Washington: an enhanced source of iron to coastal upwelling regimes. *Environmental science & technology*, 42(17), 6462-6468.
- Luther, G.W., Theberge, S.M. and Rickard, D.T., 1999. Evidence for aqueous clusters as intermediates during zinc sulfide formation. *Geochimica et Cosmochimica Acta*, 63(19): 3159-3169.
- Madhupratap M., Gauns M., Ramaiah N., Prasanna Kumar S., Muraleedharan P. M., de Sousa S. N., Sardessai S. and Muraleedharan U., 2003.Biogeochemistry of the Bay of Bengal: physical, chemical and primary productivity characteristics of the central and western Bay of Bengal during summer monsoon 2001. *Deep Sea Research Part II* 50, 881–896.
- Madhupratap, M., Nair, S. S., Haridas, P., & Padmavati, G. (1990). Response of zooplankton to physical changes in the environment: coastal upwelling along the central west coast of India. *Journal of Coastal Research*, 413-426.

- Maldonado, M. T., & Price, N. M. (2001). Reduction and transport of organically bound iron by *Thalassiosira oceanica* (Bacillariophyceae). *Journal of Phycology*, 37(2), 298-310.
- Mantyla, A. W., & Reid, J. L. (1995). On the origins of deep and bottom waters of the Indian Ocean. *Journal of Geophysical Research: Oceans*, 100(C2), 2417-2439.
- Marchitto, T.M., Curry, W.B. and Oppo, D.W., 2000. Zinc concentrations in benthic foraminifera reflect seawater chemistry. *Paleoceanography*, 15(3): 299-306.
- Martin, J. H., & Fitzwater, S. E. (1988). Iron deficiency limits phytoplankton growth in the north-east Pacific subarctic. *Nature*, 331(6154), 341-343.
- Martin, J.H. and Michael Gordon, R., 1988. Northeast Pacific iron distributions in relation to phytoplankton productivity. *Deep Sea Research Part A. Oceanographic Research Papers*, 35(2): 177-196.
- Martin, J.H., Gordon, R.M., Fitzwater, S. and Broenkow, W.W., 1989. Vertex: phytoplankton/iron studies in the Gulf of Alaska. *Deep Sea Research Part A. Oceanographic Research Papers*, 36(5): 649-680.
- Martin, J.H., 1990. Glacial-interglacial CO₂ change: The Iron Hypothesis. *Paleoceanography*, 5(1): 1-13.
- Martin, J.H., Gordon, M and Fitzwater, S.E., 1991. The case for iron. *Limnology and Oceanography*, 36(8):1793-1802.
- Measures, C.I., Vink, S., 1999. Seasonal variations in the distribution of Fe and Al in the surface waters of the Arabian Sea. *Deep Sea Research Part II: Topical Studies in Oceanography*, 46(8), 1597-1622.
- Middag, R., M.A.C., S., Heuven, V., Bruland W, K., de Baar, H.J.W., 2018. The relationship between cadmium and phosphate in the Atlantic Ocean unravelled. *Earth Planet. Sci. Lett.* 492, 79–88.
- Milliman, J. D., & Meade, R. H., 1983. World-wide delivery of river sediment to the oceans. *The Journal of Geology*, 91(1), 1-21.
- Moffett, J. W., Goepfert, T. J., & Naqvi, S. W. A. (2007). Reduced iron associated with secondary nitrite maxima in the Arabian Sea. *Deep Sea Research Part I: Oceanographic Research Papers*, 54(8), 1341-1349.

- Moffett, J.W., Vedamati, J., Goepfert, T.J., Pratihary, A., Gauns, M., Naqvi, S.W.A., 2015. Biogeochemistry of iron in the Arabian Sea. *Limnology and Oceanography*, 60(5), 1671-1688.
- Moore, J. K., & Doney, S. C., 2007. Iron availability limits the ocean nitrogen inventory stabilizing feedbacks between marine denitrification and nitrogen fixation. *Global Biogeochemical Cycles*, 21(2).
- Morel, F. M. M., Reinfelder, J. R., Roberts, S. B., Chamberlain, C. P., Lee, J. G., & Yee, D. (1994). Zinc and carbon co-limitation of marine phytoplankton. *Nature*, 369(6483), 740-742.
- Morel, F.M. et al., 1994. Zinc and carbon co-limitation of marine-phytoplankton. *Nature*, 369(6483): 740-742.
- Morley, N.H., Statham, P.J. and Burton, J.D., 1993. Dissolved trace metals in the southwestern Indian Ocean. *Deep Sea Research Part I: Oceanographic Research Papers*, 40(5): 1043-1062.
- Murton, B. J., Baker, E. T., Sands, C. M., German, C. R., 2006. Detection of an unusually large hydrothermal event plume above the slow-spreading Carlsberg Ridge: NW Indian Ocean. *Geophysical research letters*, 33(10).
- Murty, V.S.N., Sarma, Y.V.B., Rao, D.P., Murty, C.S., 1992. Water characteristics, mixing and circulation in the Bay of Bengal during southwest monsoon. *Journal of Marine Research*, 50(2), 207-228.
- Nagender Nath, B., Balaram, V., Sudhakar, M., Pluger, W.L., 1992. Rare earth element geochemistry of ferro manganese deposits from the Indian Ocean. *Mar. Chem.* 38, 185–208.
- Naqvi, S.W.A., 1994. Denitrification processes in the Arabian Sea. *Proceedings of the Indian Academy of Sciences — Earth and Planetary Sciences*, 103, 279–300.
- Naqvi, S.W.A., Naik, H., Pratihary, A., D'Souza, W., Narvekar, P.V., Jayakumar, D.A., Devol, A.H., Yoshinari, T. and Saino, T., 2006. Coastal versus open-ocean denitrification in the Arabian Sea. *Biogeosciences*, 3(4), 621-633.
- Nishioka, J., Obata, H., Tsumune, D., 2013. Evidence of an extensive spread of hydrothermal dissolved iron in the Indian Ocean. *Earth and Planetary Science Letters*, 361, 26-33.

- Nishioka, J., Obata, H., 2017. Dissolved iron distribution in the western and central subarctic Pacific: HNLC water formation and biogeochemical processes. *Limnology and Oceanography*.
- Nowicki, J.L., Johnson, K.S., Coale, K.H., Elrod, V.A. and Lieberman, S.H., 1994. Determination of zinc in seawater using flow injection analysis with fluorometric detection. *Analytical Chemistry*, 66(17): 2732-2738.
- Nozaki, Y. and Alibo, D.S., 2003. Importance of vertical geochemical processes in controlling the oceanic profiles of dissolved rare earth elements in the northeastern Indian Ocean. *Earth and Planetary Science Letters*, 205(3): 155-172.
- Obata, H., Karatani, H. and Nakayama, E., 1993. Automated determination of iron in seawater by chelating resin concentration and chemiluminescence detection. *Analytical Chemistry*, 65(11), 1524-1528.
- Okubo, A., Obata, H., Nozaki, Y., Yamamoto, Y. and Minami, H., 2004. 230Th in the Andaman Sea: Rapid deep-sea renewal. *Geophysical Research Letters*, 31(22).
- Parekh, P., Follows, M.J. and Boyle, E.C.G.B., 2004. Modeling the global ocean iron cycle. *Global Biogeochemical Cycles*, 18(1).
- Parekh, P., Follows, M.J. and Boyle, E.A.C.G., 2005. Decoupling of iron and phosphate in the global ocean. *Global Biogeochemical Cycles*, 19(2).
- Prasanna Kumar, S., Muraleedharan, P.M., Prasad, T.G., Gauns, M., Ramaiah, N., De Souza, S.N., Sardesai, S. and Madhupratap, M., 2002. Why is the Bay of Bengal less productive during summer monsoon compared to the Arabian Sea?. *Geophysical Research Letters*, 29(24).
- Qian, S., Arnold, L.G., Martin, V., 2004. Spreading of the Indonesian Throughflow in the Indian Ocean. *Journal of Physical Oceanography*, 34(4), 772-792.
- Raju, K.K., Ramprasad, T., Rao, P.S., Rao, B.R. and Varghese, J., 2004. New insights into the tectonic evolution of the Andaman basin, northeast Indian Ocean. *Earth and Planetary Science Letters*, 221(1), 45-162.
- Ramaswamy, V. and Nair, R.R., 1994. Fluxes of material in the Arabian Sea and Bay of Bengal—sediment trap studies. *Journal of Earth System*

- Science, 103(2),189-210.
- Ramaswamy, V., Gaye, B., Shirodkar, P. V., Rao, P. S., Chivas, A. R., Wheeler, D., Thwin, S., 2008. Distribution and sources of organic carbon, nitrogen and their isotopic signatures in sediments from the Ayeyarwady (Irrawaddy) continental shelf, northern Andaman Sea. *Marine Chemistry*, 111(3), 137-150.
- Rao D. P., Sarma V. V., Rao V. S., Sudhakar U., Gupta G. V. M., 1996. On watermass mixing ratios and regenerated silicon in the Bay of Bengal. *Indian Journal of Marine Sciences*, 25, 56–61.
- Ray, D., Kamesh Raju, K.A., Baker, E.T., Srinivas Rao, A., Mudholkar, A.V., Lupton, J.E., Surya Prakash, L., Gawas, R.B. and Vijaya Kumar, T., 2012. Hydrothermal plumes over the Carlsberg Ridge, Indian Ocean. *Geochemistry, Geophysics, Geosystems*, 13(1).
- Resing, J.A., Sedwick, P.N., German, C.R., Jenkins, W.J., Moffett, J.W., Sohst, B.M. and Tagliabue, A., 2015. Basin-scale transport of hydrothermal dissolved metals across the South Pacific Ocean. *Nature*, 523(7559),200-203.
- Rijkenberg, M.J., Steigenberger, S., Powell, C.F., Haren, H., Patey, M.D., Baker, A.R., Achterberg, E.P., 2012. Fluxes and distribution of dissolved iron in the eastern (sub-) tropical North Atlantic Ocean. *Global Biogeochemical Cycles*, 26(3).
- Rijkenberg, M.J.A., Middag, R., Laan, P., Gerringa, L.J.A., Van Aken, H.M., Schoemann, V., De Jong, J.T.M., De Baar, H.J.W., 2014. The distribution of dissolved iron in the West Atlantic Ocean. *PLoS One* 9, 1–14. doi:10.1371/journal.pone.0101323
- Roshan, S., Wu, J., 2015. Water mass mixing: The dominant control on the zinc distribution in the North Atlantic Ocean. *Global Biogeochem. Cycles* 29, 1060–1074. doi:10.1002/2014GB005026
- Roshan, S., Wu, J., Jenkins, W.J., 2016. Long-range transport of hydrothermal dissolved Zn in the tropical South Pacific. *Mar. Chem.* 183, 25–32. doi:10.1016/j.marchem.2016.05.005
- Rudnicki, M. D., & German, C. R., 2002. Temporal variability of the hydrothermal

- plume above the Kairei vent field, 25 S, Central Indian Ridge. *Geochemistry, Geophysics, Geosystems*, 3(2).
- Saager, P.M., De Baar, H.J.W. and Burkill, P.H., 1989. Manganese and iron in Indian Ocean waters. *Geochimica et Cosmochimica Acta*, 53(9): 2259-2267.
- Sañal, V., Kipp, L. E., Henderson, P. B., van Beek, P., Reyss, J. L., Hammond, D. E., ... & Moore, W. S., 2017. Radium-228 as a tracer of dissolved trace element inputs from the Peruvian continental margin. *Marine Chemistry*.
- Sarin, M. M., Krishnaswami, S., Dilli, K., Somayajulu, B. L. K., & Moore, W. S., 1989. Major ion chemistry of the Ganga-Brahmaputra river system: weathering processes and fluxes to the Bay of Bengal. *Geochimica et cosmochimica acta*, 53(5), 997-1009.
- Saager, P.M., De Baar, H.J.W. and Howland, R.J., 1992. Cd, Zn, Ni and Cu in the Indian Ocean. *Deep Sea Research Part A. Oceanographic Research Papers*, 39(1): 9-35.
- Sarma, V. V. S. S., 2002. An evaluation of physical and biogeochemical processes regulating the oxygen minimum zone in the water column of the Bay of Bengal. *Global biogeochemical cycles*, 16(4).
- Sarma, V.V.S.S., Sridevi, B., Maneesha, K., Sridevi, T., Naidu, S.A., Prasad, V.R., Venkataramana, V., Acharya, T., Bharati, M.D., Subbaiah, C.V. and Kiran, B.S., 2013. Impact of atmospheric and physical forcings on biogeochemical cycling of dissolved oxygen and nutrients in the coastal Bay of Bengal. *Journal of oceanography*, 69(2), 229-243.
- Sarma, V.V.S.S., Rao, G.D., Viswanadham, R., Sherin, C.K., Salisbury, J., Omand, M.M., Mahadevan, A., Murty, V.S.N., Shroyer, E.L., Baumgartner, M. and Stafford, K.M., 2016. Effects of freshwater stratification on nutrients, dissolved oxygen, and phytoplankton in the Bay of Bengal. *Oceanography*, 29(2), 222-231.
- Sastry, J.S., Rao, D.P., Murty, V.S.N., Sarma, Y.V.B., Suryanarayana, A. and Babu, M.T., 1985. Watermass structure in the Bay of Bengal. *Mahasagar*, 18(2), 153-162.

- Sarnthein, M. et al., 1994. Changes in east Atlantic deepwater circulation over the last 30,000 years: Eight time slice reconstructions. *Paleoceanography*, 9(2): 209-267.
- Sastry, J.S. et al., 1985. Watermass structure in the Bay of Bengal. *Mahasagar*, 18(2): 153-162.
- Schlitzer R, 2011 Ocean Data View 4. <http://odv.awi.de> (2011).
- Schott, F.A. and McCreary Jr, J.P., 2001. The monsoon circulation of the Indian Ocean. *Progress in Oceanography*, 51(1): 1-123.
- Selavka, C.M., Jiao, K.S. and Krull, I.S., 1987. Construction and comparison of open tubular reactors for post-column reaction detection in liquid chromatography. *Analytical Chemistry*, 59(17): 2221-2224.
- Sengupta, D., Bharath Raj, G.N. and Shenoi, S.S.C., 2006. Surface freshwater from Bay of Bengal runoff and Indonesian throughflow in the tropical Indian Ocean. *Geophysical Research Letters*, 33(22).
- Shankar, D., Vinayachandran, P.N. and Unnikrishnan, A.S., 2002. The monsoon currents in the north Indian Ocean. *Progress in oceanography*, 52(1): 63-120.
- Shaked, Y., Xu, Y., Leblanc, K. and Morel, F.M.M., 2006. Zinc availability and alkaline phosphatase activity in *Emiliana huxleyi*: Implications for Zn-P co-limitation in the ocean. *Limnology and Oceanography*, 51(1): 299-309.
- Shaked, Y., Kustka, A. B., Morel, F. M., & Erel, Y. (2004). Simultaneous determination of iron reduction and uptake by phytoplankton. *Limnology and Oceanography: methods*, 2(5), 137-145.
- Shetye, S. R., Gouveia, A. D., Shenoi, S. S. C., Sundar, D., Michael, G. S., Almeida, A. M., & Santanam, K. (1990). Hydrography and circulation off the west coast of India during the southwest monsoon 1987. *Journal of Marine Research*, 48(2), 359-378.
- Shankar, D., Vinayachandran, P.N. and Unnikrishnan, A.S., 2002. The monsoon currents in the north Indian Ocean. *Progress in oceanography*, 52(1), 63-120.

- Shenoi, S.S.C., Saji, P.K. and Almeida, A.M., 1999. Near-surface circulation and kinetic energy in the tropical Indian Ocean derived from Lagrangian drifters. *Journal of Marine Research*, 57(6): 885-907.
- Sheth, H. C., Ray, J. S., Bhutani, R., Kumar, A., & Smitha, R. S. (2009). Volcanology and eruptive styles of Barren Island: an active mafic stratovolcano in the Andaman Sea, NE Indian Ocean. *Bulletin of Volcanology*, 71(9), 1021.
- Shetye, S.R., Gouveia, A.D., Shankar, D., Shenoi, S.S.C., Vinayachandran, P.N., Sundar, D., Michael, G.S. and Nampoothiri, G., 1996. Hydrography and circulation in the western Bay of Bengal during the northeast monsoon. *Journal of Geophysical Research: Oceans*, 101(C6), 14011-14025.
- Shetye, S.R. et al., 1996. Hydrography and circulation in the western Bay of Bengal during the northeast monsoon. *Journal of Geophysical Research: Oceans*, 101(C6): 14011-14025.
- ShyamPrasad, M. (2007). Indian exploration for polymetallic nodules in the Central Indian Ocean.
- Singh, S.K., Rai, S.K. and Krishnaswami, S., 2008. Sr and Nd isotopes in river sediments from the Ganga Basin: sediment provenance and spatial variability in physical erosion. *Journal of Geophysical Research: Earth Surface*, 113(F3).
- Sinoir, M., Butler, E. C., Bowie, A. R., Mongin, M., Nesterenko, P. N., & Hassler, C. S. (2012). Zinc marine biogeochemistry in seawater: a review. *Marine and Freshwater Research*, 63(7), 644-657.
- Singh, S.K., Rai, S.K. and Krishnaswami, S., 2008. Sr and Nd isotopes in river sediments from the Ganga Basin: sediment provenance and spatial variability in physical erosion. *Journal of Geophysical Research: Earth Surface*, 113(F3).
- Singh, S.P., Singh, S.K., Goswami, V., Bhushan, R. and Rai, V.K., 2012. Spatial distribution of dissolved neodymium and ϵ Nd in the Bay of Bengal: role of particulate matter and mixing of water masses. *Geochimica et Cosmochimica Acta*, 94, 38-56.
- Singh, S. P., Singh, S. K., Bhushan, R., & Rai, V. K., 2015. Dissolved silicon and

- its isotopes in the water column of the Bay of Bengal: Internal cycling versus lateral transport. *Geochimica et Cosmochimica Acta*, 151, 172-191.
- Sirocko, F., & Sarin, M., 1989. Wind-borne deposits in the northwestern Indian Ocean: Record of Holocene sediments versus modern satellite data. *Paleoclimatology and Paleometeorology: modern and past patterns of global atmospheric transport*, 401-433.
- Smitha, B. R., Sanjeevan, V. N., Vimalkumar, K. G., & Revichandran, C. (2008). On the upwelling off the southern tip and along the west coast of India. *Journal of Coastal Research*, 24(sp3), 95-102.
- Song, Q., Gordon, A.L. and Visbeck, M., 2004. Spreading of the Indonesian Throughflow in the Indian Ocean*. *Journal of Physical Oceanography*, 34(4): 772-792.
- Srinivas, B., Sarin, M.M. and Kumar, A., 2011. Impact of anthropogenic sources on aerosol iron solubility over the Bay of Bengal and the Arabian Sea. *Biogeochemistry*, 110(1): 257-268.
- Srinivasan, A., Top, Z., Schlosser, P., Hohmann, R., Iskandarani, M., Olson, D. B., ... & Jenkins, W. J. (2004). Mantle ^3He distribution and deep circulation in the Indian Ocean. *Journal of Geophysical Research: Oceans*, 109(C6).
- S.S.C. Sheno, S.R. Shetye, A.D. Gouveia, G.S. Michael (1993). Salinity Extrema in the Arabian Sea. *Mitt. Geol.-Palaeont. Inst. Univ. Hamburg SCOPE/UNEP Sonder band*, 76, pp. 37-49.
- Statham, P. J., German, C., & Connelly, D. P., 2005. Iron (II) distribution and oxidation kinetics in hydrothermal plumes at the Kairei and Edmond vent sites, Indian Ocean. *Earth and Planetary Science Letters*, 236(3), 588-596.
- Stramma, L., Schmidtko, S., Levin, L.A. and Johnson, G.C., 2010. Ocean oxygen minima expansions and their biological impacts. *Deep Sea Research Part I: Oceanographic Research Papers*, 57(4): 587-595.
- SubhaAnand, S., Rengarajan, R., Sarma, V.V.S.S., Sudheer, A.K., Bhushan, R. and Singh, S.K., 2017. Spatial variability of upper ocean POC export in the Bay of Bengal and the Indian Ocean determined using particle-reactive ^{234}Th . *Journal of Geophysical Research: Oceans*, 122(5), 3753-3770.

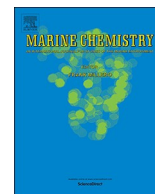
- Sunda, W., 2012. Feedback interactions between trace metal nutrients and phytoplankton in the ocean. *Frontiers in microbiology*, 3: 204.
- Sunda, W.G. and Huntsman, S.A., 1992. Feedback interactions between zinc and phytoplankton in seawater. *Limnology and Oceanography*, 37(1): 25-40.
- Sunda, W.G. and Huntsman, S.A., 1995. Cobalt and zinc interreplacement in marine phytoplankton: biological and geochemical implications. *Limnology and Oceanography*, 40(8): 1404-1417.
- Sunda, W.G. and Huntsman, S.A., 1995. Iron uptake and growth limitation in oceanic and coastal phytoplankton. *Marine Chemistry*, 50(1), 189-206.
- Tagliabue, A., Aumont, O. and Bopp, L.C.G.L., 2014. The impact of different external sources of iron on the global carbon cycle. *Geophysical Research Letters*, 41(3), 920-926.
- Takeda, S., Kamatani, A., Kawanobe, K., 1995. Effects of nitrogen and iron enrichments on phytoplankton communities in the northwestern Indian Ocean. *Marine Chemistry*, 50(1-4), 229-241.
- Tao, C., Lin, J., Guo, S., Chen, Y.J., Wu, G., Han, X., German, C.R., Yoerger, D.R., Zhu, J., Zhou, N. and Su, X., 2004, December. First discovery and investigation of a high-temperature hydrothermal vent field on the ultra-slow spreading Southwest Indian Ridge. In AGU Fall Meeting Abstracts.
- Thi Dieu Vu, H. and Sohrin, Y., 2013. Diverse stoichiometry of dissolved trace metals in the Indian Ocean. *Scientific Reports*, 3, 1745.
- Tomczak, M. and Godfrey, J.S., 2003. *Regional oceanography: an introduction*. Elsevier.
- Tortell, P.D. and Price, N.M., 1996. Cadmium toxicity and zinc limitation in centric diatoms of the genus *Thalassiosira*. *Marine Ecology Progress Series*, 138: 245-254.
- Tortell, P.D., Rau, G.H. and Morel, F.o.M.M., 2000. Inorganic carbon acquisition in coastal Pacific phytoplankton communities. *Limnology and Oceanography*, 45(7): 1485-1500.
- Turner, D.R. and Hunter, K.A., 2001. *The biogeochemistry of iron in seawater*, 6. Wiley Chichester.
- Twining, B.S. and Baines, S.B., 2013. *The trace metal composition of marine*

- phytoplankton. *Annual review of marine science*, 5, 191-215.
- UNESCO.,1993. *Discharge of selected Rivers of the world*, vol.III, 600 pp., Paris.
- Vallee, B.L. and Auld, D.S., 1990. Zinc coordination, function, and structure of zinc enzymes and other proteins. *Biochemistry*, 29(24): 5647-5659.
- Van Dover, C.L., Humphris, S.E., Fornari, D., Cavanaugh, C.M., Collier, R., Goffredi, S.K., Hashimoto, J., Lilley, M.D., Reysenbach, A.L., Shank, T.M., Von Damm, K.L., 2001. Biogeography and ecological setting of Indian Ocean hydrothermal vents. *Science*, 294(5543), 818-823.
- Varkey, M. J., V. S. N. Murty, and A. Suryanarayana.,1996. Physical oceanography of the Bay of Bengal and Andaman Sea, *Oceanogr. Marine Biology.*, 34, 1–70.
- Vedamati, J., Goepfert, T., Mofferr, J.W., 2014. Iron speciation in the eastern tropical South Pacific oxygen minimum zone off Peru. *Limnol. Oceanogr.* 59, 1945–1957.
- Volker, C. and Tagliabue, A., 2015. Modeling organic iron-binding ligands in a three-dimensional biogeochemical ocean model. *Marine Chemistry*, 173, 67-77.
- Waite, T.D., 2001. Thermodynamics of the iron system in seawater. In: Turner, D.R., Hunter, K.A. (Eds.), *Biogeochemistry of Iron in Seawater*. Wiley, West Sussex, England, pp. 291–342.
- Watson, A.J., Bakker, D.C.E., Ridgwell, A.J., Boyd, P.W. and Law, C.S., 2000. Effect of iron supply on Southern Ocean CO₂ uptake and implications for glacial atmospheric CO₂. *Nature*, 407(6805): 730-733.
- Whitney, F.A., Freeland, H.J. and Robert, M., 2007. Persistently declining oxygen levels in the interior waters of the eastern subarctic Pacific. *Progress in oceanography*, 75(2): 179-199.
- Witter, A. E., Lewis, B. L., & Luther III, G. W. (2000). Iron speciation in the Arabian Sea. *Deep Sea Research Part II: Topical Studies in Oceanography*, 47(7), 1517-1539.
- Worsfold, P. J., Lohan, M. C., Ussher, S. J., & Bowie, A. R., 2014. Determination of dissolved iron in seawater: A historical review. *Marine Chemistry*, 166, 25-35.

- Wyatt, N.J. et al., 2014. Biogeochemical cycling of dissolved zinc along the GEOTRACES South Atlantic transect GA10 at 40°S. *Global Biogeochemical Cycles*, 28(1): 44-56.
- Wyrki, K., 1973. *Physical oceanography of the Indian Ocean, The biology of the Indian Ocean*. Springer, pp. 18-36.
- You, Y., 1997. Seasonal variations of thermocline circulation and ventilation in the Indian Ocean. *Journal of Geophysical Research: Oceans*, 102(C5): 10391-10422.
- You, Y., 1998. Intermediate water circulation and ventilation of the Indian Ocean derived from water-mass contributions. *Journal of Marine Research*, 56(5), 1029-1067.
- You, Y., 2000. Implications of the deep circulation and ventilation of the Indian Ocean on the renewal mechanism of North Atlantic Deep Water. *Journal of Geophysical Research: Oceans*, 105(C10): 23895-23926.
- You, Y., Tomczak, M., 1993. Thermocline circulation and ventilation in the Indian Ocean derived from water mass analysis. *Deep Sea Research Part I: Oceanographic Research Papers*, 40(1), 13-56.

List of Publications/Conference Proceedings

- Bikkina, S., Sarin, M.M. and *Venkaresh Chinni*, 2015. Atmospheric ²¹⁰Pb and anthropogenic trace metals in the continental outflow to the Bay of Bengal. **Atmospheric Environment**, 122, pp.737-747.
- *Venkaresh Chinni*, Sunil Kumar Singh, Ravi Bhushan, Rengarajan R, VVS Sarma. Spatial variability in the dissolved iron concentrations in the marginal and open ocean waters of the Indian Ocean. Under Revision, **Marine Chemistry**.
- *Venkaresh Chinni*, Sunil Kumar Singh, Ramaswamy. "Tracking the provenance of rain particulates collected at Goa using Sr-Nd isotopic systematic" delivered at 29th **ISMAS conference** held at parwanoo, Himachal Pradesh, India in 2014.
- Sunil Kumar Singh, *Venkaresh Chinni*, Vineet goswami, Satinder pal Singh. "Trace element biogeochemistry in the Indian Ocean" at 25th **Goldschmidt conference** in Prague, CZ, August 16th – 21st 2015.
- *Venkaresh Chinni*, Sunil Kumar Singh, Ravi Bhushan, Rengarajan. "Dissolved Iron in the Indian Ocean" delivered a talk in **International symposium** on the Indian Ocean held at Goa during 29th November – 04th December 2015.
- *Venkaresh Chinni*, Sunil Kumar Singh, Ravi Bhushan, Rengarajan. "Dissolved Iron in the North-Eastern Indian Ocean" at 26th **Goldschmidt conference** in Yokohama, Japan during 26th June – 1st July 2016.
- Sunil Kumar Singh, *Venkaresh Chinni*, Manan Shah. "A low cost fully automated flow injection system to measure sub nanomolar level concentrations of dissolved iron in seawater" at Thiruvananthapuram, **NSSS conference** held on 09th February 2016.
- *Venkaresh Chinni*, Sunil Kumar Singh. "Distributions of dissolved Zinc from the Geotraces GI-10 transect" delivered a poster and oral talk in 1st **GEOTRACES summer school** held at Brest (France) during August 2017.



Spatial variability in dissolved iron concentrations in the marginal and open waters of the Indian Ocean



Venkatesh Chinni^a, Sunil Kumar Singh^{a,b,*}, Ravi Bhushan^a, R. Rengarajan^a, V.V.S.S. Sarma^c

^a Physical Research Laboratory, Ahmedabad 380009, India

^b CSIR – National Institute of Oceanography, Goa 403004, India

^c CSIR – National Institute of Oceanography, Regional Centre Visakhapatnam, India

ARTICLE INFO

Keywords:

Dissolved Iron
GEOTRACES
Bay of Bengal
Indian Ocean

ABSTRACT

We analyzed 28 full vertical profiles of dissolved iron (DFe) in the Indian Ocean (i.e., between 26°S – 20°N and 72°E – 105°E) during two research expeditions (SK-304: March–May 2013, SK-311: March–April 2014) as part of the GEOTRACES-India programme. Relatively high DFe concentrations in surface waters (≤ 10 m) were observed in the Arabian Sea (AS: 0.68 ± 0.03 nM, $n = 2$) and the Bay of Bengal (BoB: 0.44 ± 0.11 nM, $n = 21$) compared to the stations located south of the equator (0.27 ± 0.16 nM, $n = 17$). Higher DFe in the coastal stations is presumably sourced from the continental shelves. Depth profiles of DFe in the AS, BoB and Andaman Sea showed sub-surface maxima, coinciding with low dissolved oxygen (DO) concentrations. High DFe concentrations in sub-surface waters of the BoB and the Andaman Sea are attributed to desorption of soluble iron from resuspended sediments of the rivers and the remineralization of sinking particulate organic matter. We also observed a significant contribution of DFe from hydrothermal vents situated at the Central Indian ridge and subduction processes along the Java trench to pelagic waters of the Indian Ocean. Fe:C remineralization ratios of 3.92 ± 0.83 , 5.88 ± 2.65 , 8.96 ± 3.85 and 5.74 ± 3.06 $\mu\text{mol/mol}$ were observed in the Indian Ocean, BoB, AS and Andaman Sea, respectively. To assess the surface areas and deep water masses where DFe concentrations potentially limit phytoplankton growth (when reaching the surface) we subtracted the contribution of particulate organic matter remineralization to the DFe pool using the tracer Fe* ($\approx \text{DFe} - R_{\text{Fe,P}}(\text{Phosphate})$). Positive Fe* values in the intermediate waters suggest an external source for DFe, whereas negative Fe* values suggest the absence of such external inputs and/or removal by scavenging processes. Our results contribute to improved understanding of DFe distributions and their coupling with the ocean biogeochemical cycling of carbon and nitrogen in this region.

1. Introduction

Phytoplankton growth (the base of the marine food web) is limited by the availability of the micronutrient Fe in about 30% of the world oceans (Martin and Fitzwater, 1988; Boyd et al., 2007; Boyd and Ellwood, 2010). Fe supply to the surface waters of the oceans influences the biogeochemical cycle of carbon through photosynthesis and, thus, has an impact on the air-sea exchange of CO₂. Additionally, nitrogen fixation in surface waters is often Fe-limited or colimited along with P (Moore et al., 2009; Mills et al., 2004). Although debatable, it has been argued based on the evidence from ice-core and sediment core data sets that aeolian supply of Fe through mineral dust to the Southern Ocean modulated the CO₂ levels in the atmosphere over glacial-interglacial cycles (Martin, 1990; Watson et al., 2000; Pollard et al., 2009; Martínez-García et al., 2011). Major sources of Fe to seawater include

riverine input, continental margin sediments (Lam and Bishop, 2008; Homoky et al., 2012; Lam et al., 2012), hydrothermal vent solutions (Tagliabue et al., 2010; Wu et al., 2011; Nishioka et al., 2013; Resing et al., 2015), extraterrestrial input from meteorites (Johnson, 2001), atmospheric dust (Jickells et al., 2005; Mahowald et al., 2010; Baker and Croot, 2010; Schulz et al., 2012) and anthropogenic pollution sources (Schroth et al., 2009; Sholkovitz et al., 2012).

Despite herculean research efforts on the sources and dynamics of DFe in seawater over the last three decades through major international programmes (e.g., SEAREX, CLIVAR-I, II and GEOTRACES), our understanding about how various factors such as phytoplankton composition, physiological conditions (i.e., oxygen-rich/deficit, grazers, benthic flux, concentration of siderophores), geographical variability in the dust/pollution sources and their impact govern the distribution of DFe is still limited. The global biogeochemical cycle of Fe can be better

* Corresponding author.

E-mail addresses: sunil@nio.org, sunil@prl.res.in (S.K. Singh).

<https://doi.org/10.1016/j.marchem.2018.11.007>

Received 26 February 2018; Received in revised form 1 November 2018; Accepted 12 November 2018

Available online 14 November 2018

0304-4203/ © 2018 Elsevier B.V. All rights reserved.

understood by increasing the ocean-wide DFe data set and evaluating the geographical distribution of sources, sinks and internal cycling. Such studies will be crucial for geochemical models in understanding the biogeochemical cycling of carbon in seawater (Parekh et al., 2004; Tagliabue et al., 2014; Aumont et al., 2015; Volker and Tagliabue, 2015; Frants et al., 2016).

Under the international GEOTRACES programme, the Atlantic and the Pacific Oceans have been sampled and studied in detail for dissolved trace element biogeochemistry. In contrast, very limited surface sampling and depth profiling from the Indian Ocean hinders our understanding on the sources, sinks and internal cycling of Fe in this region. The first vertical profile of DFe in the Indian Ocean was reported by Saager et al. (1989). With the advent of new clean sampling systems and measurement protocols for dissolved trace elements in the ocean, subsequent studies continued to investigate DFe distributions in the Indian Ocean (Takeda et al., 1995; Measures and Vink, 1999; Moffett et al., 2007; Kondo and Moffett, 2013; Nishioka et al., 2013; Vu Thi Dieu and Sohrin, 2013; Grand et al., 2015a,b). In this study, as a part of the GEOTRACES – India programme, 28 full vertical profiles for DFe were collected, spanning the BoB, coastal AS, Andaman Sea and the Indian Ocean during March–May 2013 and March–April 2014 (Fig. 1) to investigate the sources of DFe and the processes governing DFe distributions in this region.

2. Study area

In the present study, seawater samples from various depths at 28 stations in the Indian Ocean were collected encompassing an area between latitudes 26°S to 20°N and longitudes 72°E to 105°E. These samples include various sub-basins such as the BoB, the AS, and the Andaman Sea of the Indian Ocean. Unlike the Atlantic and Pacific Oceans, the Indian Ocean is land-locked in the north and is characterized by the seasonal reversal of monsoonal winds and surface currents. In general, the northern Indian Ocean is more productive compared to

the equatorial and southern Indian Ocean. Several factors are responsible for the relatively high primary productivity in the northern Indian Ocean. These include eddies, coastal upwelling processes, atmospheric dust input from adjacent arid landmasses that together influence the biogeochemistry of the Indian Ocean. However, the two limbs of the northern Indian Ocean, the BoB and the AS (Fig. 1) differ significantly in terms of fresh water influx, primary productivity, the extent of the oxygen minimum zone (OMZ), hydrothermal sources as well as water-mass circulation.

2.1. The Bay of Bengal

The BoB, between latitudes 5–21°N and 80–90°E, experiences both summer and winter monsoons every year during the periods June – September and November – January respectively, which causes changes in the surface circulation and local hydrography. A number of rivers – the Ganga, the Brahmaputra, the Godavari, the Krishna etc., drain into the BoB and supply $\sim 1.6 \times 10^{12} \text{ m}^3$ freshwater (UNESCO, 1993) and $\sim 1.4 \times 10^9$ tons of suspended load annually making it one of the oceanic basins receiving very high flux of continental materials (Milliman and Meade, 1983; Sarin et al., 1989; Galy and France-Lanord, 1999, 2001; Basu et al., 2001; Singh et al., 2008). The fresh water input leads to stratification in the surface BoB and inhibits the vertical mixing (Shetye et al., 1996; Prasanna Kumar et al., 2002; Gopalakrishna et al., 2002; Madhupratap et al., 2003). However, the stratification is often disrupted by the formation of eddies (Prasanna Kumar et al., 2002; Sarma et al., 2016).

2.2. The Arabian Sea

The Arabian Sea (AS) in the northwestern part of the Indian Ocean is situated at the same geographical latitude as the BoB and shares similar atmospheric forcing and seasonal reversal of monsoons. The AS is one of the most productive regions in the world Ocean and receives

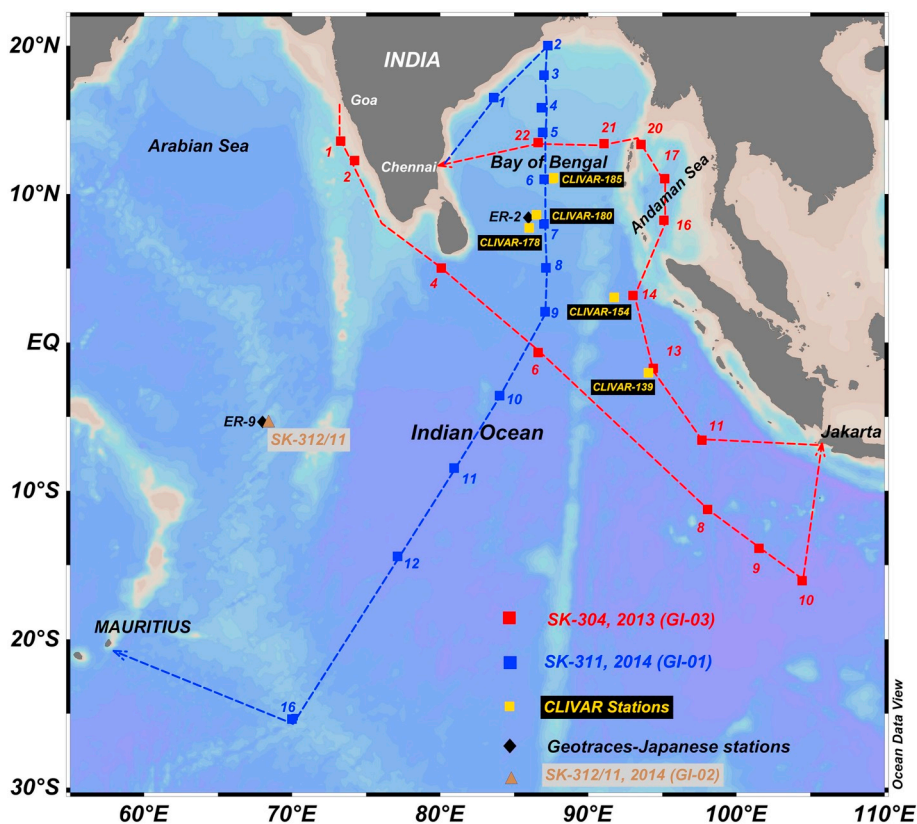


Fig. 1. Map showing the sampling locations in the Indian Ocean during SK-304 (GI-03) in 2013 and SK-311 (GI-01) in 2014 as part of the GEOTRACES-INDIA programme onboard ORV Sagar Kanya. Selected stations of the Japanese GEOTRACES ER-9, ER-2 sampled in 2009, CLIVAR stations 139,154,178,180,185 sampled in 2007 and GEOTRACES-India station SK-312/11 (GI-02) sampled in 2014 in the Indian Ocean are also shown in the figure. Ocean data view 4 software is used for plotting all the colour contours in this and successive figures (Schlitzer, 2017) (For interpretation of the references to color in this figure legend, the reader is referred to the web version of this article.).

Table 1

List of analyzed seawater reference samples for DFe along with their consensus and reported values (from this study).

S.No	STD name	Consensus value	Reported value	n
1	GS	0.546 ± 0.046	0.547 ± 0.041	22
2	GD	1.00 ± 0.10	0.96 ± 0.07	7
3	SAFe D ₂	0.93 ± 0.02	0.95 ± 0.04	14
4	SAFe D ₁	0.67 ± 0.04	0.65 ± 0.04	6

Note that the consensus values are in nmol/Kg and the reported values are in nM. The reported errors are 1 σ .

$\sim 1.7 \times 10^{11} \text{ m}^3$ of water and $\sim 5 \times 10^8$ tons (pre-damming) of sediments annually from rivers along with a huge supply of atmospheric mineral dust ($\sim 1 \times 10^8$ tons per year) from nearby deserts (Goldberg and Griffin, 1970; Kolla et al., 1976; Sirocko and Sarnthein, 1989; Ramaswamy and Nair, 1994; Goswami et al., 2012). The AS is also characterized by the occurrence of an intense OMZ in the water column

where anoxic conditions can be seen along the west coast of India during late summer and autumn (Naqvi, 1994; Naqvi et al., 2006; Bange et al., 2005).

2.3. The Andaman Sea

The Andaman Sea is located in the northeastern part of the Indian Ocean extending from Myanmar in the north to Sumatra in the south and from the Andaman-Nicobar Islands in the west to the Malay Peninsula in the east. The average water column depth of the Andaman Sea is ~ 1100 m. In the north, the basin receives fresh water from the Irrawaddy and the Salween rivers. Horizontal ventilation of the Andaman Sea is restricted from the BoB by the Andaman-Nicobar Islands. Exchange of water from the BoB is mainly through the “Ten Degree Channel” with a sill depth of ~ 800 m and through the Great Channel in the south with a sill depth of ~ 1400 m (Gupta et al., 1981; Nozaki and Alibo, 2003; Raju et al., 2004). Biogeochemistry in this

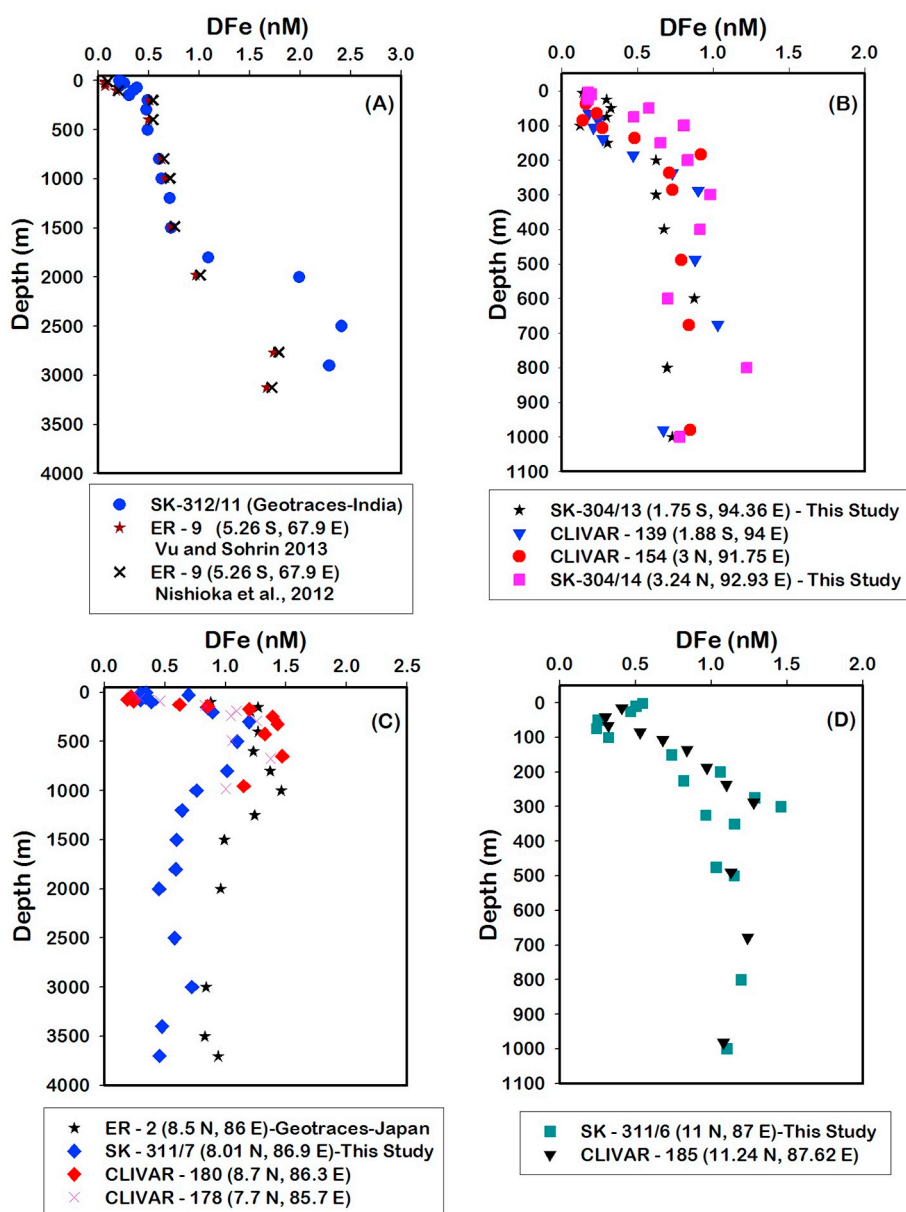


Fig. 2. (A) Comparison of DFe data at the cross-over station between the present study, Nishioka et al. (2013) and Vu Thi Dieu and Sohrin, 2013. (B) Comparison of DFe data among nearby stations of the present study and Grand et al., 2015b. (C) Comparison of DFe data of the Bay of Bengal region among the present study, Vu Thi Dieu and Sohrin, 2013, and Grand et al., 2015b and (D) Top 1000 m comparison of the Bay of Bengal profiles between Grand et al., 2015b and the present study.

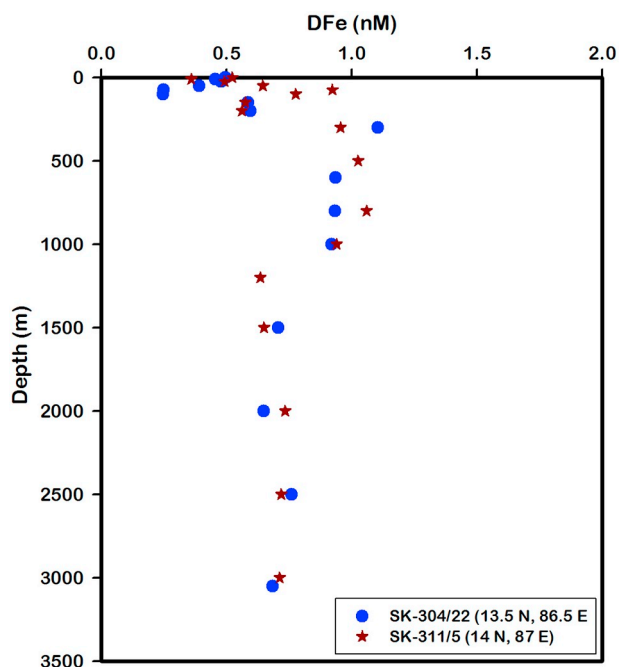


Fig. 3. Comparison of DFe data from two nearby stations in this study (SK-304/22 and SK-311/5). Sampling for SK-304/22 station was done on 6th May 2013 and Sampling for SK-311/5 station was done on 31st March 2014.

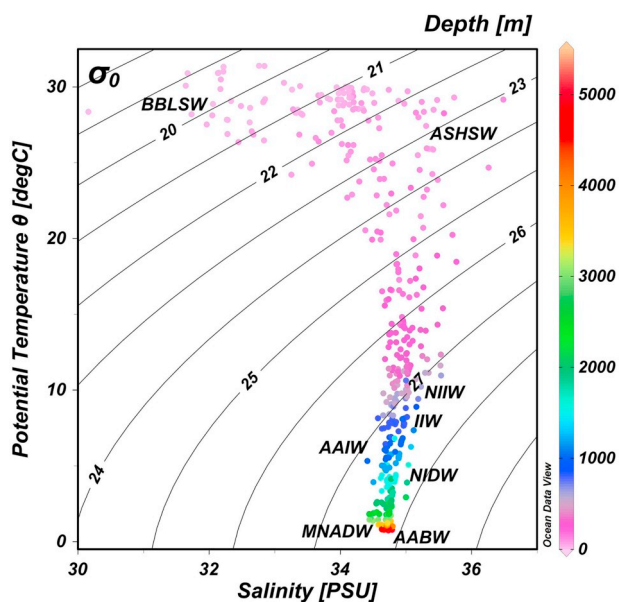


Fig. 4. Salinity vs. potential temperature with isopycnal lines for all the stations of the SK – 304 and SK-311 cruises. BBSW – Bay of Bengal less saline waters, ASHSW Arabian Sea high saline waters, NIIW – North Indian Intermediate waters, IIW – Indonesian Intermediate through flow waters, AAIW – Antarctic intermediate waters, NIDW – North Indian deep waters, AABW – Antarctic bottom waters and MNADW – Modified North Atlantic deep waters.

basin could be influenced by an active subduction zone (Khan and Chakraborty, 2005) and submarine volcanoes (Sheth et al., 2009).

2.4. The Indian Ocean

Compared to the AS and the BoB, the Indian Ocean is oligotrophic in nature due to a lower/negligible supply of nutrients from atmospheric deposition, rivers and no influence from the seasonal reversal of the

monsoonal winds. Additionally, the Indian Ocean receives Pacific Ocean waters via the Indonesian Through Flow (ITF), (You and Tomczak, 1993) between 5°S to 15°S latitude along the Indonesian Islands and transports surface waters to the southern Atlantic Ocean through the Agulhas current (Beal et al., 2011). The Indian Ocean region south of the equator receives far less atmospheric dust and riverine input compared to the northern Indian Ocean but the presence of submarine ridges like the Central Indian Ridge, the Southwest Indian Ridge, and the Carlsberg Ridge makes the Indian Ocean a potentially very large reservoir for trace metals in the deeper waters. The region contains several active hydrothermal vent fields (Van Dover et al., 2001). A recent study reported input from hydrothermal vent fields in the deeper waters of the Indian Ocean for the bioactive trace metals Fe and Mn (Nishioka et al., 2013). In addition, long-range transport of this vent-derived input was seen up to 1000's of kilometers from the sources (Nishioka et al., 2013). This is consistent with a similar study in the South Pacific Ocean that reported lateral transport of DFe over 4500 km from the vent sources (Resing et al., 2015).

2.5. Water masses and circulation

Numerous studies have been carried out in the Indian Ocean to characterize the water masses and their circulation patterns (Wyrtki, 1973; Sastry et al., 1985; Murty et al., 1992; Kumar and Li, 1996; Rao et al., 1996; Varkey et al., 1996; You and Tomczak, 1993; You, 1997, 1998, 2000; Tomczak and Godfrey, 2003; Schott and McCreary Jr, 2001; Frank et al., 2006; Singh et al., 2012; Goswami et al., 2014). Antarctic Bottom Water (AABW) occupies the bottom layers in the Indian Ocean, and may extend up to the northern BoB and the AS. In the northern Indian Ocean, the bottom waters are termed Circumpolar Deep Waters (CDW) mainly due to the mixing of deep waters and bottom waters while intruding into the BoB and AS (You and Tomczak, 1993). Above these bottom waters, Indian deep waters (IDW) occupy the depth range of 1500–3000 m at the Equator and in the northern Indian Ocean. The Indian Ocean also receives upper ocean waters from the Pacific Ocean through the Indonesian Through Flow (ITF) (Qian et al., 2004). These ITF waters are modified while passing by the Indonesian islands and can be traced between 10°S and 15°S (Frank et al., 2006; Clemens et al., 2016). These waters move further along the equator towards the Somali basin and enter the AS with the Somali current during the onset of the southwest monsoon. Antarctic Intermediate Water (AAIW) is relatively less saline compared to the overlying and underlying waters and occupies the depth range from 800 to 1100 m (You, 1998). Northern Indian Intermediate water (NIIW) occupies the majority of thermocline in the northern Indian Ocean (You and Tomczak, 1993; You, 1997), which is an aged form of Indian Central Water. The thermocline of the BoB contains the oldest central water of the northern Indian Ocean (You and Tomczak, 1993).

The salinity of surface waters in the northern BoB is generally low due to a large fresh water influx from the Ganga-Brahmaputra river system. These waters are termed Bay of Bengal Less Saline Waters (BBSW). In contrast, salinity of the surface waters of the AS is higher due to excess evaporation over precipitation and less riverine supply. The upper surface layers in the AS are termed Arabian Sea High Salinity Waters (ASHSW). In addition, the AS contains high saline waters in the depth range between 300 and 800 m originating from two marginal seas; the Persian Gulf Waters (PGW) and the Red Sea Waters (RSW). The seasonal reversal of monsoonal winds brings high salinity surface waters into the BoB during the summer monsoon and less saline waters from the BoB to the AS during the winter monsoon. The surface waters of the Andaman Sea are less saline due to large fresh water supply from the Irrawaddy and the Salween rivers. Deeper depths of the Andaman Sea are filled with central waters from the BoB, flowing across the Ten Degree Channel.

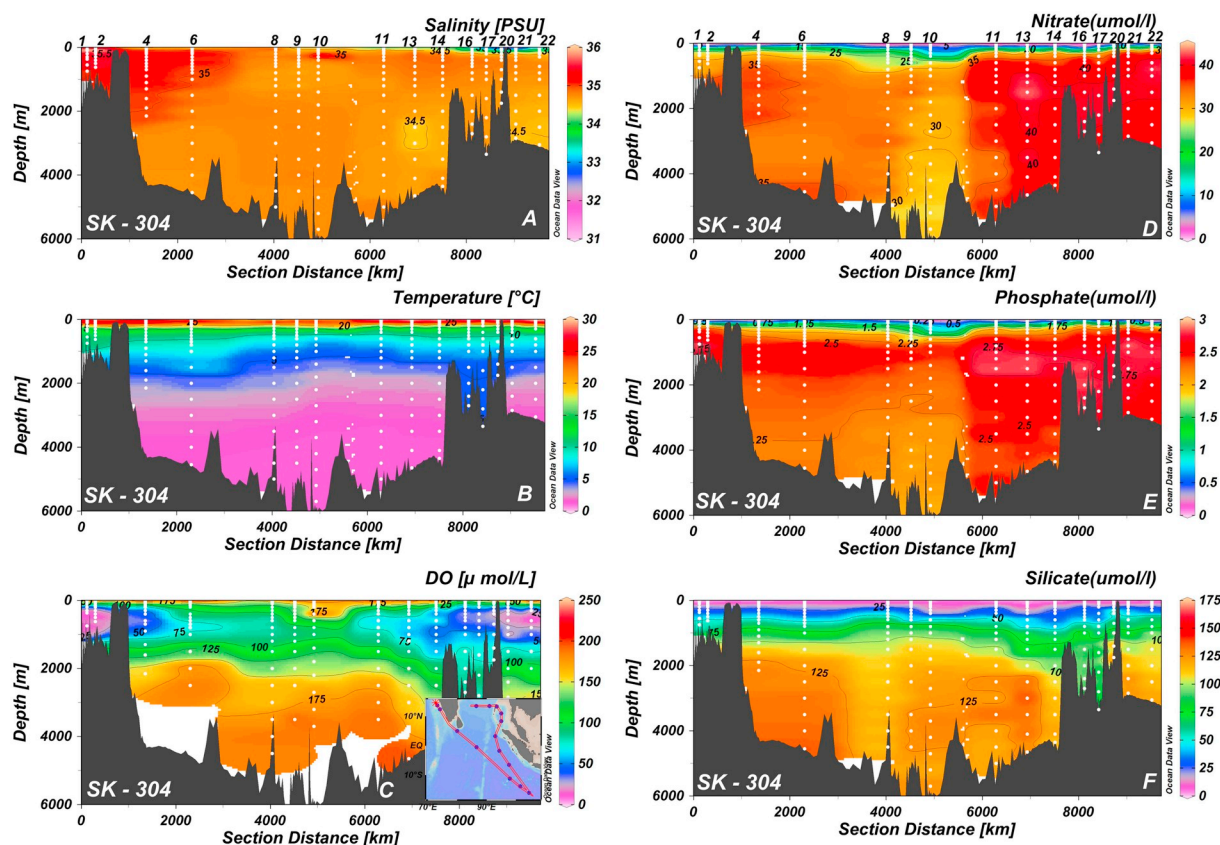


Fig. 5. Section plots for hydrographic parameters from the SK-304 cruise. (A) salinity, (B) temperature, (C) dissolved oxygen, (D) nitrate (E) phosphate, and (F) silicate. Station numbers are shown along the top of the figure. The cruise started from Goa towards Jakarta and was completed at Chennai.

3. Material and methods

3.1. Sampling

Seawater samples for trace metals were collected in the BoB, Andaman Sea, AS and the Indian Ocean on two cruises onboard ORV Sagar Kanya during the spring inter-monsoon periods of 2013 (SK-304/GI-03) and 2014 (SK-311/GI-01) under the GEOTRACES-India programme. A total of 15 full-depth vertical profiles were collected on the SK-304 (GI-03) cruise during March 5–May 6, 2013 starting from Goa and continuing towards the eastern Indian Ocean up to 16°S, 104.46°E. Further sampling was carried out in the northern Indian Ocean (Andaman Sea, BoB) and the cruise terminated at Chennai (Fig. 1). A total of 13 full-depth vertical profiles were collected on the SK-311 cruise during March 26–April 19, 2014, starting from Chennai, moving towards the northern BoB up to ~20°N and then covered a meridional section along 87°E to the southern BoB and parts of the Indian Ocean before reaching Mauritius (Fig. 1). The SK-312 (GI – 02) cruise from Mauritius to Goa during April to May 2014 was a continuation of the SK-311 cruise. During cruise SK-312, the GEOTRACES-Japanese station ER-9 was reoccupied as a cross-over station (SK-312/11) for inter-comparison purposes. Samples were collected using a “trace metal clean” CTD-Rosette system (SEA-BIRD SCIENTIFIC, USA) connected to a Kevlar conducting cable. Samples were collected using 12 L Niskin-X bottles. Upon recovery of the CTD unit on deck, the sampling bottles were taken into a trace metal clean lab (SILHOUETTE STEEL LTD.) for filtration and sub sampling. Salinity, temperature, dissolved oxygen and fluorescence were measured in-situ using sensors attached to the CTD Rosette. The Niskin-X bottle is pressurized using a low overpressure (5 psi) of filtered compressed air. Seawater was filtered through 0.2 μm pore size PALL AcroPak™-500 capsule filters. Each seawater sample was collected directly into a pre-washed 1 L bottle. The 1 L bottles were

rinsed with Milli-Q® water (Millipore, with $R > 18.2 \text{ M}\Omega \text{ cm}^{-1}$) and an alkaline cleaning solution (Extran® MA 01, Merck), then rinsed 3 times with Milli-Q® water, and stored in purified 2 N HCl for 2 weeks. After two weeks, the bottles were rinsed with Milli-Q® water, and the bottles were soaked in a purified ~1 N HNO₃ bath for 1 week. After the soaking period, the bottles were rinsed with Milli-Q® water again and stored in double polyethylene bags until they were used. The purified HCl and HNO₃ for the bottle cleaning were prepared by distilling analytical grade HCl (Merck) and analytical grade HNO₃ (Merck) in a quartz acid distillation system, followed by redistilling in a Savillex DST-1000 acid purification system, and finally diluted with Milli-Q® water to the target concentrations. Before subsample collection in the 1 L bottles, the bottles were rinsed profusely with the corresponding seawater. The 1 L bottles used during the GI-03 cruise were made of high-density polyethylene (TARSONS) while those used on the GI-01 cruise were made of low-density polyethylene (TARSONS). After collection, seawater samples were acidified with ultrapure hydrochloric acid (Fisher Scientific) under class –100 flow bench (Air clean systems) in the trace metal clean lab. The final concentration of HCl was 0.024 M in the seawater sample.

3.2. Basic parameters and major nutrients

Unfiltered seawater samples were collected from the Niskin-X bottles for major nutrients (nitrate, nitrite, silicate and phosphate) and analyzed within 24 h of sampling following standard colorimetric procedures (Grasshoff et al., 1992) using a UV–Visible spectrophotometer (Shimadzu, Model UV-1800). Briefly, major nutrients in the seawater were measured as follows. Phosphate in seawater was allowed to react with acidified ammonium molybdate to yield the phosphomolybdate complex which was reduced using ascorbic acid in the presence of antimonyl ions leading to the formation of phosphomolybdenum blue

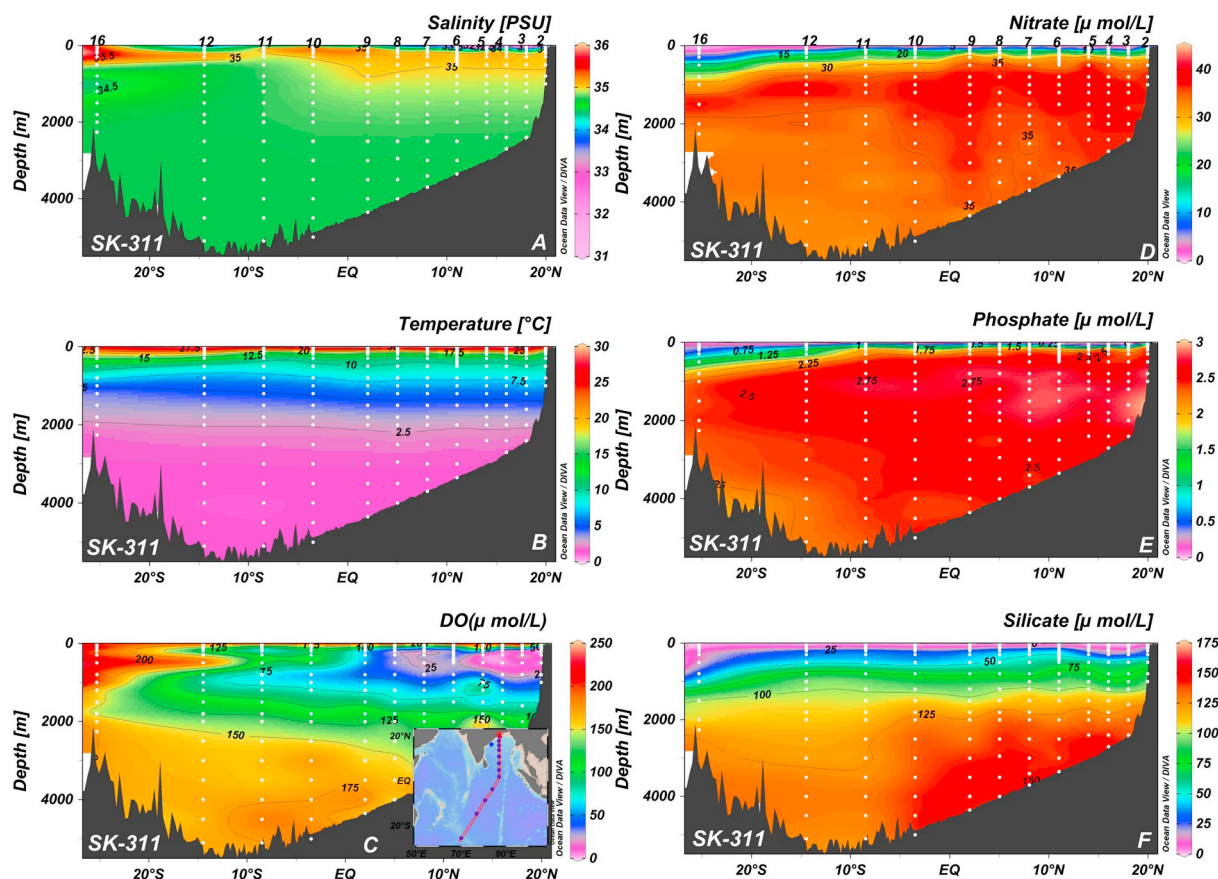


Fig. 6. Section plots for hydrographic parameters from the SK-311 cruise. (A) salinity, (B) temperature, (C) dissolved oxygen, (D) nitrate (E) phosphate, and (F) silicate. Station numbers are shown along the top of the figure. The cruise started from Chennai and was completed at Mauritius.

complex. The absorbance of this complex was measured at 880 nm. Silicate samples were treated with ammonium molybdate under acidic conditions to form the yellow silicomolybdic acid, which was reduced to the silicomolybdenum blue complex with ascorbic acid. Absorbance of this complex was measured at 810 nm. Nitrate was reduced to nitrite using a cadmium-mercury amalgam column and then complexed with sulphaniilamide and N (1-naphthyl) Ethylene diamine to form the azo dye. The absorbance of this dye was measured at 543 nm. Nitrite was measured using the same chemistry but without the cadmium-mercury amalgam column reduction step.

The analytical precision for nitrate, nitrite, phosphate and silicate are ± 0.02 , ± 0.02 , ± 0.01 and ± 0.02 $\mu\text{mol/L}$ respectively. The accuracy of the nutrient data was evaluated by comparing with the cross-over station, ER-9 (GEOTRACES-Japanese station) re-occupied during the GI-02 cruise (SK-312/11) in the AS (see Supplementary Fig. 1). Samples for dissolved oxygen (DO) were collected in glass bottles and analyzed using the Winkler method. All DO samples were analyzed within 6 h of sample collection.

3.3. Analysis of dissolved iron

The samples from the SK-304 (GI-03) and SK-311 (GI-01) cruises were analyzed for DFe within a year from collection. Aliquots were taken from the 11 subsample bottles into 60 ml wide mouth LDPE bottles for DFe analysis. The 60 ml wide mouth LDPE bottles were pre-cleaned following GEOTRACES protocols (GEOTRACES cookbook version 1.0, 2010; <http://www.geotraces.org/sic/intercalibrate-data/cookbook>) inside a class-100 laminar flow bench. These 60 ml aliquots were analyzed for DFe using a flow injection system with chemiluminescence detection as described by Obata et al. (1993), De Jong et al. (1998), De Baar et al. (2008) and Klunder et al. (2011). All

reagent bottles and samples were kept inside a class-100 non-metallic horizontal laminar flow bench. An eight channel peristaltic pump (GILSON MINIPULS) was used for the manifold tubing (Fisher Scientific). The white-white coded PVC tubing (1.02 mm ID) was used for the elution, H_2O_2 , NH_4OH , and luminol channels. Violet – Violet PVC coded tubing (2.02 mm ID) was used for the rinse and sample channels, and Yellow-Orange coded PVC tubing was used for the buffer channel. All other tubing was made of PTFE (0.8 mm ID). A 60 μl aliquot of 1% H_2O_2 (Merck Suprapur®) was added to each 60 ml seawater sample 1 h before the start of analysis to ensure that the DFe was in the Fe(III) oxidation state. Seawater samples were pre-concentrated on TOYOPEARL®AF-Chelate 650 M resin (Tosoh, Bioscience) at a pH of ~ 4.0 for 120 s using online buffering with an ammonium acetate buffer prepared from ultrapure acetic acid (Fisher Scientific) and ultrapure ammonium hydroxide (Fisher Scientific). A 4 cm long Teflon column (custom made, 2.5 mm ID) with a capacity of ~ 200 μl of resin was used for pre-concentrating DFe from the seawater samples. An inline-tapered column (2 cm, Global FIA) was used for removing the blank contribution from the buffer solution. After pre-concentration, the column was rinsed with ultra pure water ($R > 18.2$ $\text{M}\Omega\cdot\text{cm}$; Merck Millipore) containing the trace metal cartridge for 60 s to remove any loosely bound major ions. To elute the retained DFe from the column, 0.4N HCl (Merck Suprapur®) was used. A stock luminol solution was prepared by mixing 540 mg luminol (Sigma Aldrich) and 1000 mg KOH (Sigma Aldrich) in 30 ml UHP water. The luminol working solution was prepared by taking 3 ml of the stock solution in 11 UHP water. To this working luminol solution, TETA (Triethylenetetramine) (Sigma Aldrich) was added and the final concentration of TETA in the solution was 0.7 mM. The eluent mixes with 0.96 N NH_4OH , 0.35 N H_2O_2 and the working luminol solution and passes through a 5 m long mixing coil which is kept inside a water bath of constant temperature (35 °C with a precision of ± 0.1 °C,

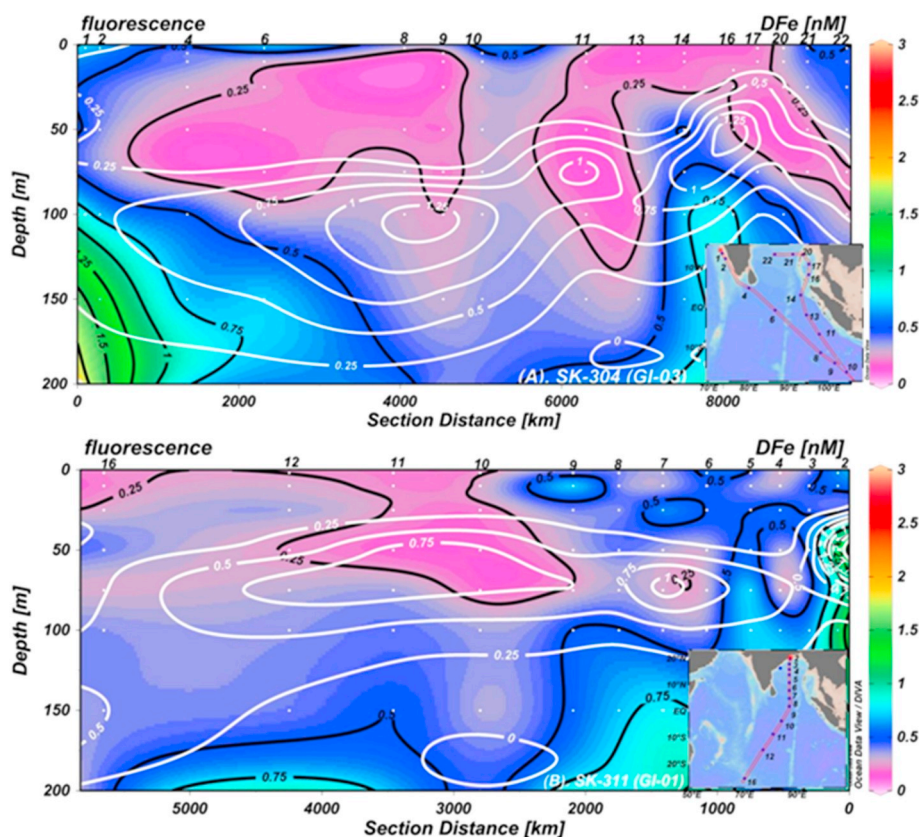


Fig. 7. Section plots for DFe in the upper 200 m with overlying fluorescence contour lines (White colour) (A). cruise SK-304 (GI-03) and (B). cruise SK-311 (GI-01). Black contours represent DFe concentrations. Deepening of the fluorescence peak can be seen moving from north to south. The unit for fluorescence is $\mu\text{g Chla L}^{-1}$.

Cole Parmer) before injecting into a photon counting head (Hamamatsu, Model - H8259–01). The mixing coils were knitted as described by Selavka et al. (1987). Schematics of the method are presented in Supplementary Figs. 2, 3 and 4. LabVIEW software was used for valve operation and signal reading from the photon counting head.

The DFe analysis was calibrated using an ICP Fe standard. A 1000 ppm single element Fe standard (Merck, Certipur®) was used as the primary standard. Intermediate standards were prepared using UHP water acidified to 0.024 M HCl. Working standards were prepared fresh every day in low Fe seawater, also acidified to 0.024 M HCl. A five-point calibration was done during every analysis. The procedural blank was measured by running UHP water as a sample for 2 min. The blank was 0.04 ± 0.02 nM ($n = 3$) and the detection limit (three times the standard deviation of the UHP water) was 0.06 nM. One analytical cycle took 500 s. The accuracy and precision of the DFe analysis were monitored by measuring SAFe and GEOTRACES standards during the analysis of SK-304 and SK-311 samples. The reported and consensus DFe values for the reference standards namely GEOTRACES Surface (GS), GEOTRACES deeper (GD), SAFe (Sampling and analysis of Iron) D₁ and SAFe D₂ are listed in Table 1 and indicate very good accuracy and precision. In addition to these reference standards, one sample was reanalyzed with each sample batch. The coefficient of variation for these replicate analyses was $\sim 4\%$.

3.3.1. Validation of DFe data with cross-over/nearby stations in the study region

To document the validity of the clean sampling system and the DFe analysis, station ER-9 (5.26°S 67.9°E) sampled in 2009 by the Japanese GEOTRACES programme (Nishioka et al., 2013; Vu Thi Dieu and Sohrin, 2013) was re-occupied as a cross-over station during the SK-312 cruise. The DFe data obtained in this study compare quite well with those from station ER-9, despite a five year interval between the cruises

(Fig. 2A). Differences in the DFe data between the two studies for three samples below 2000 m depth could be due to the temporal variations in the hydrothermal plume signal from the nearby ridge system with an active vent field. In the absence of ^3He or CH_4 data from each cruise, this hypothesis could not be confirmed. However, comparison of the hydrographic and nutrient data at this crossover station confirmed the presence of the same water masses during both studies, emphasizing that there could be temporal variations in the DFe plume signal.

Some of the stations occupied during the SK-304 and SK-311 cruises were located close to some CLIVAR stations (sampled only to 1000 m) and a Japanese GEOTRACES station (Fig. 1). Stations SK-304/13 (1.75°N, 94.36°E) and SK-304/14 (3.24°N, 92.93°E) were located near CLIVAR station 139 (1.88°S, 94°E) and CLIVAR station 154 (3°N, 91.75°E) and the DFe concentrations between them compare well (Fig. 2B). The DFe profiles at some stations of the SK-311 cruise in the BoB, which are close to the published data of Vu Thi Dieu and Sohrin (2013) and Grand et al. (2015b) (Fig. 2C, D) compare well. In this study, DFe is marginally lower in the deeper samples (> 1000 m) compared to those of Vu Thi Dieu and Sohrin, (2013; Fig. 2C). The T and S data from stations ER-2 and SK-311/7 suggest similar water masses and hence the lower DFe in this study could have arisen from seasonal variations in the authogenic/detrital particle fluxes and the associated remineralisation of DFe as has been observed in the case of dissolved Nd in the BoB (Singh et al., 2012; Yu et al., 2017). Sinking particle fluxes during the post-monsoon period are higher than during the pre-monsoon period (November vs April).

3.3.1.1. Intra-comparison of DFe data between the SK304 and SK311 cruises. The stations SK-304/22 and SK-311/5 sampled during the GI-03 and GI-01 cruises were located very close to each other in the BoB. The DFe data obtained from these two nearby stations were compared to validate the internal consistency of the sampling and measurement

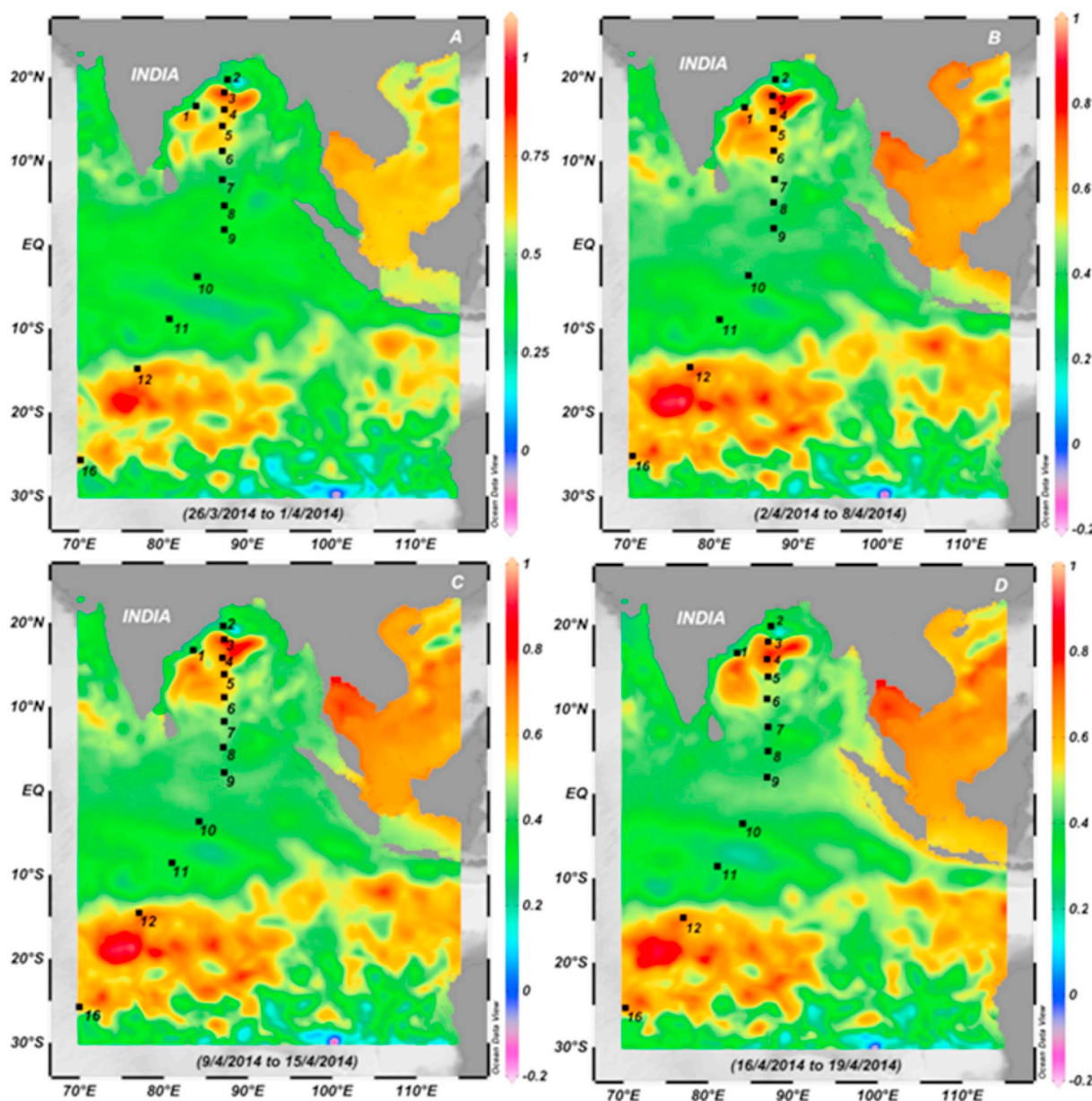


Fig. 8. Sea surface height (SSH) plots during the SK-311 sampling period. The data reveal the presence of a warm core eddy in the Bay of Bengal close to 18°N. SSH data was obtained from CMEMS (COPERNICUS MARINE ENVIRONMENT MONITORING SERVICE).

techniques. Both cruises were done during the spring intermonsoon period approximately one year apart. The vertical profiles of DFe for SK-304/22 and SK-311/5 correlate well except for variations in the surface values (Fig. 3). Variations in the surface values were also observed in the salinity and temperature profiles between SK-304/22 and SK-311/5.

4. Results

4.1. Hydrographic and major nutrient distributions

The different water masses present in the region of this study are shown in Fig. 4 using a potential temperature-Salinity (T-S) diagram. Section plots for salinity, temperature, dissolved oxygen (DO), and major nutrients nitrate, phosphate, and silicate are shown in Figs. 5 and 6. The fluorescence maximum is quite high in the northernmost BoB near the mouth of the Ganga River, and decreased slightly from ~50 m at station SK-311/2 to ~90 m at station SK-311/7 (Fig. 7). Further

deepening of the fluorescence peak was observed moving from the equator to the southern stations (to 120 m at station SK-311/16). A similar north-to-south deepening on the fluorescence maximum was also seen on cruise SK-304 (Fig. 7).

4.1.1. The Arabian Sea

The two stations in the Arabian Sea, SK-304/01 and SK-304/02 (Fig. 1) with water column depth of < 800 m were located close to the west coast of India. The surface waters of this region are characterized by ASHSW, with salinity ~3–4 units higher compared to the northern BoB (Fig. 5A), due to the excess evaporation over precipitation and less influence of fresh water supply (Kumar and Prasad, 1999). The presence of ASHSW, which forms at northern latitudes in the AS, was not found at the southern AS stations due to the North Equatorial current (NEC) and other equatorial currents. The sub-surface waters with high salinity were seen as far as station SK-304/06 (0.53°S, 86.55°E). The dissolved oxygen (DO) shows surface maxima (> 200 μM) at both stations SK-304/1 and SK-304/2 (Fig. 5C). Hypoxic conditions, with DO

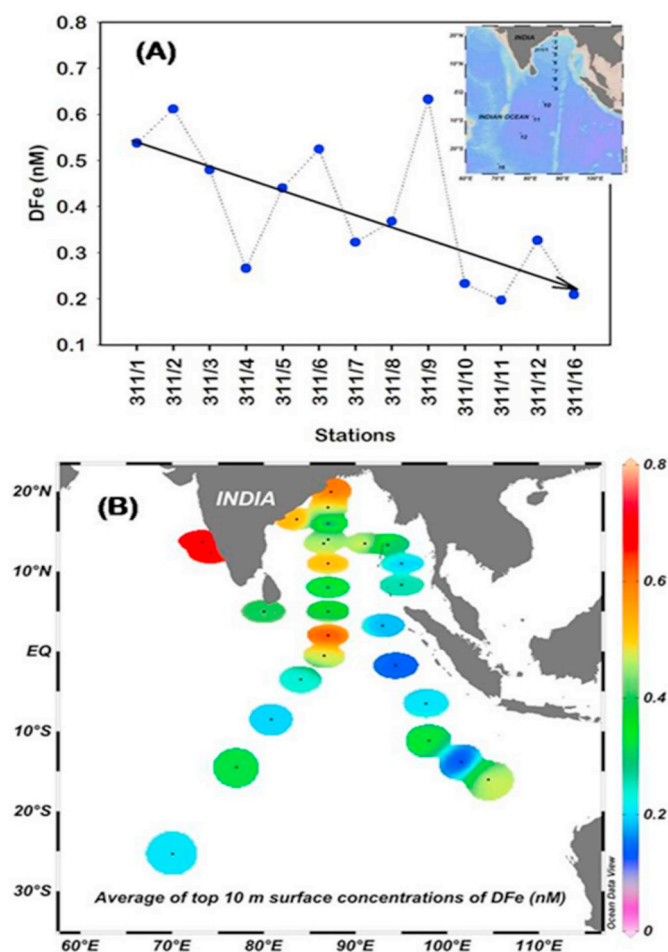


Fig. 9. The surface (average of top 10 m) DFe concentrations in the study region (SK-304 and SK-311). (A) A N-S decreasing trend in DFe (SK – 311) can be seen in the Bay of Bengal. (B) the spatial distribution of surface (top 10 m) DFe concentrations in the entire study region.

from 5 to 25 μM , were observed at these two stations from below 100 m to the bottom, while DO increased in subsurface waters moving farther south. DO values ranged from ~ 12 to $< 50 \mu\text{M}$ at station SK-304/4 between 100 and 1000 m. This station is located near to the zone where oxygen rich waters from the southern Indian Ocean mix with oxygen deficient waters of the Northern Indian Ocean (Fig. 5C). The fluorescence started to increase at 75 m at stations SK-304/1 and SK-304/2 (Fig. 7A). The nutricline starts at 50 m at stations SK-304/01 and SK-304/02. At 50 m nitrate, phosphate and silicate were 3.98, 0.35 and 0.92 μM respectively and at 100 m these values were 11.23, 1.10 and 6.08 μM . Nitrate and phosphate reached a maximum of $\sim 32 \mu\text{M}$ and $\sim 3 \mu\text{M}$ whereas silicate reached a maximum of 56 μM close to the bottom (Fig. 5F).

4.1.2. The Bay of Bengal

The SK-304/21, SK-304/22 and SK-311/1 to SK-311/8 stations were sampled in the BoB. The surface salinities at stations sampled in the BoB (Fig. 6A) were quite low due to the large fresh water influx from rivers that causes the stratification in the upper layers (Gopalakrishna et al., 2002; Sengupta et al., 2006). The less saline waters and stratification were more pronounced at the stations north of 10°N. The dissolved oxygen values were higher at the surface at all of the stations in the BoB. Below 100 m, an OMZ was observed in the northern BoB (Fig. 6C). The primary factors controlling the OMZ in the BoB are the strong vertical stratification and the poor ventilation (Sarma, 2002), which gets intensified in the northern BoB due to the freshwater input (Sarma

et al., 2013; Singh et al., 2012). The OMZ in the intermediate water column of the BoB was observed up to 5°N. The thermocline in the northern bay is shallower compared to the southern bay. Deepening of the thermocline at SK-311/3 was observed compared to neighboring stations. The Sea Surface Height (SSH) plots for SK-311 (Fig. 8) indicate the presence of a mesoscale anticyclonic (warm core) eddy in the northern BoB during cruise SK-311 in 2014, and station SK-311/3 was clearly impacted by this eddy. The nitrate and phosphate concentrations were very low in the top 50 m (Fig. 6D, E) where as the silicate concentrations were relatively higher in the BoB due to riverine input (Fig. 6F).

4.1.3. The Andaman Sea

Stations SK-304/16, SK-304/17 and SK-304/20 were sampled in the Andaman Sea, which is separated from the BoB by the Andaman-Nicobar Islands. The surface salinities in the Andaman basin were quite low (< 33) due to the presence of the Irrawady/Salween Rivers on the northern side of the Andaman Sea. The nitrate and phosphate concentrations were also low in the surface waters compared to the silicate values. The nutricline started at 45 m. Below the oxycline, DO values decreased with depth and to lower than 25 μM . Anoxic conditions (DO $\sim 0 \mu\text{M}$) was not observed at these stations. The hydrographic and nutrient data in the Andaman Sea below 1200 m depth were relatively constant and these deeper values coincide with the values of the BoB in the depth interval of 1000–1200 m. The Andaman Sea exchanges its deeper waters with the intermediate waters of the BoB through the Ten Degree Channel (Nozaki and Alibo, 2003). High vertical mixing rates have been reported in the deeper waters of Andaman Sea (Dutta et al., 2007; Okubo et al., 2004). Similar features in the hydrographic and nutrient parameters were also reported by Kim et al. (2015) in the Andaman Sea.

4.1.4. The Indian ocean

The Indian Ocean south of the equator is an oligotrophic region and the primary production is low compared to the northern Indian Ocean (Subha Anand et al., 2017). The surface salinity was 33.975 at station (SK-311/10) near the equatorial Indian Ocean with a southward increasing trend to 35.197 at SK-311/16. The salinity contours indicate the intrusion of Pacific Ocean waters via the Indonesian Through Flow at stations SK-304/08, SK-304/09 and SK-304/10 (Fig. 5A). More saline waters were observed from the surface to 300 m (35.197 at the surface to 35.566 at 300 m) in the Indian Ocean at 25.3°S. Below 300 m, Antarctic Intermediate Water (AAIW) with lower salinity (34.967 to 34.413) was observed in the depth range of 500 to 1000 m (Fig. 4). The DO values were relatively higher in the depths between 100 and 1000 m in the Indian Ocean stations south of equator compared to the stations located in the BoB (north of equator). The influence of water masses with higher oxygen values can be seen up to 13°S. At station SK-311/16, deepening of the nutricline depth of nitrate, phosphate and silicate was observed (Fig. 6D, E and F).

4.2. Dissolved iron

The overall DFe concentrations in this study ranged from 0.11 nM to 2.61 nM with a mean value of $0.69 \pm 0.37 \text{ nM}$ ($n = 500$). This average concentration of DFe does not include the 20.86 nM DFe concentration observed at 2260 m at station SK-311/16, which we attribute to hydrothermally-derived Fe input (see discussion below). The DFe profiles in coastal areas of the AS and BoB deviated from nutrient-type profiles. Vertical profiles of DFe in other locations clearly show nutrient type behavior with surface minima and increasing concentrations with depth. The surface (average of $\leq 10 \text{ m}$) concentrations of DFe in the study region are shown in Fig. 9. Surface DFe in the BoB displayed a north – south decreasing trend with relatively higher concentrations in the north except at stations SK-311/6 and SK-311/9. The low surface value of DFe at station SK-311/4 could be due to the impact of the

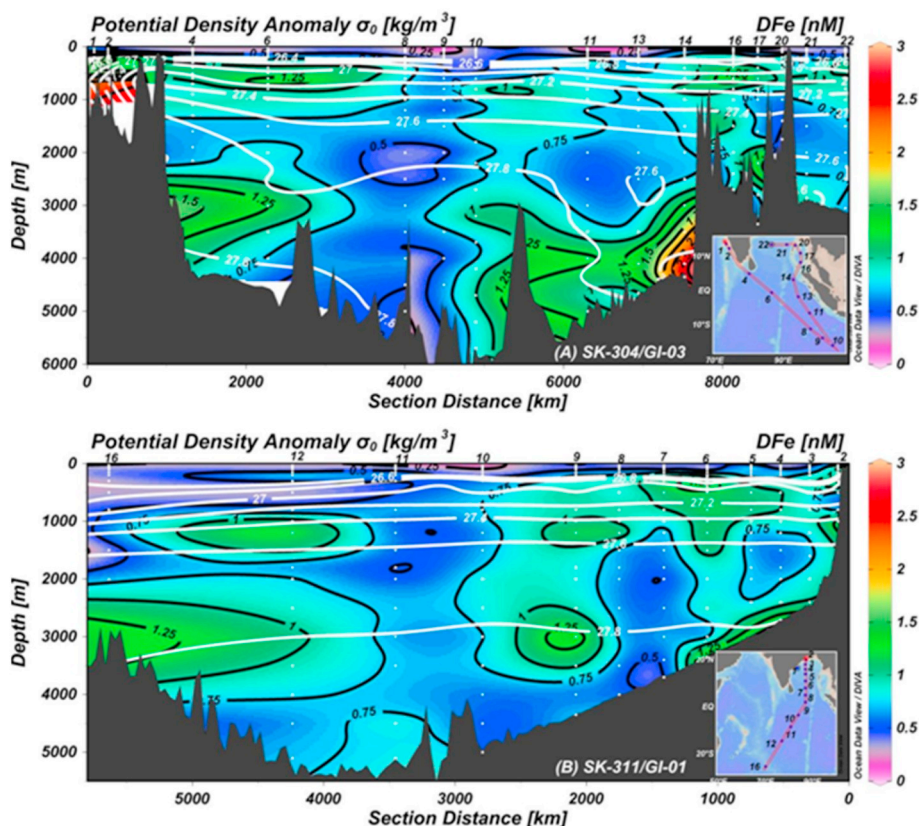


Fig. 10. Sections of DFe profiles with overlying potential density anomaly contour lines (White colour). (A) cruise SK-304 (GI-03) and (B) cruise SK-311 (GI-01). High DFe concentrations were found near coastal stations of the Arabian Sea, intermediate waters of the Bay of Bengal, and the Andaman Sea and deeper samples near the Java trench.

anticyclonic eddy. Intermediate waters between 100 and 1000 m in the BoB, from the north to 5°N were rich in DFe (Figs. 10 and 11). Sub-surface DFe maxima were also seen at the Andaman Sea stations. The DFe in the intermediate waters (100–1000 m) averaged 0.95 ± 0.22 nM ($n = 76$) for the BoB, 0.90 ± 0.24 nM ($n = 21$) for the Andaman Sea, and 0.61 ± 0.28 nM ($n = 79$) for the Indian Ocean, respectively. This enrichment was not seen in the stations south of 5°N. The concentrations of DFe at the coastal AS stations (water depth ≤ 800 m) were also quite high (~ 2.3 nM, Fig. 11A), presumably due to input from the shelf/slope sediments. The average concentrations of DFe for the deeper waters (> 1000 m) were 0.77 ± 0.24 nM ($n = 66$) in the BoB, 0.83 ± 0.27 nM ($n = 11$) in the Andaman Sea and 0.75 ± 0.23 nM ($n = 78$) in the Indian Ocean (excluding the 20.86 nM value for the 2260 m sample at SK-311/16). The deeper samples from stations SK-304/11, SK-304/13 and SK-304/14 along the Java trench region were also elevated in DFe, especially at SK-304/14 where the samples below 4000 m were 2.61 nM.

5. Discussion

5.1. DFe distributions

The sections of the DFe from cruises SK-304 and SK-311 are shown in Fig. 10. DFe concentrations in the Indian Ocean from this study averaged $\sim 0.69 \pm 0.37$ nM ($n = 500$). It is also discernible from the DFe sections in the top 200 m of the water column (Fig. 7) that the peak in fluorescence somewhat coincides with low DFe concentrations, especially at stations south of the equator. This relationship was not observed in the DFe profiles from stations located close to the coast (SK-304/1, SK-304/2, SK-311/2, and SK-311/3) which were presumably impacted by DFe sourced from the sediments (in the AS) and from riverine particles (in the BoB). In addition to the presence of different water masses in each basin (section 4.1) other variable processes such as re-mineralization of particulate organic matter, dissolution of

atmospheric dust, release from reducing shelf and slope sediments, and input from hydrothermal vents and subduction sources likely affected the distribution of DFe in the study region. These impacts on the DFe profiles are discussed basin-by-basin in the following sections.

5.1.1. The Coastal Arabian Sea

The Arabian Sea (AS) is characterized by an intense denitrifying zone in the open waters (a perennial process) along with seasonally anoxic conditions in the inner and mid shelf waters off the west coast of India during the late southwest monsoon and autumn seasons (Gupta et al., 2016; Naqvi et al., 2000, 2006). Upwelling in the eastern AS brings nutrient rich sub-surface waters to the euphotic zone and, thereby, enhances the productivity in the region. The vertical distributions of DFe in the AS water column at SK-304/1 and 304/2 did not follow the typical nutrient type behavior (Fig. 11a). Both profiles showed minima between 50 and 100 m, slight maxima at ~ 200 m and slight minima around ~ 400 m, followed by an increase towards the bottom. The minima from 50 to 100 m are slightly above the fluorescence maxima (Fig. 7A), but may be due to phytoplankton uptake. The maxima at 200 m and the minima at 400 m are presumably due to a variable combination of regeneration from sinking organic matter and release from the reducing shelf and slope sediments. The increase in DFe concentrations from ~ 1.4 – 1.8 nM in the depth range (i.e., 100–400 m) to ~ 2.3 nM in the bottom waters (650–747 m) is also consistent with some combination of these two processes. These high DFe concentrations in the intermediate and deep waters could then be transported laterally towards the open ocean. Recent studies have highlighted the role of continental margins as a significant source for dissolved trace metals (Elrod et al., 2004; Rijkenberg et al., 2012; Sanial et al., 2017). More sampling along the west coast of India is needed to quantify the DFe fluxes from organic matter oxidation and from the reducing shelf and slope sediments along the west coast of India.

The concentrations of DFe in the waters of the coastal AS (i.e., SK-304/1, water column depth 747 m and SK-304/2, water column depth

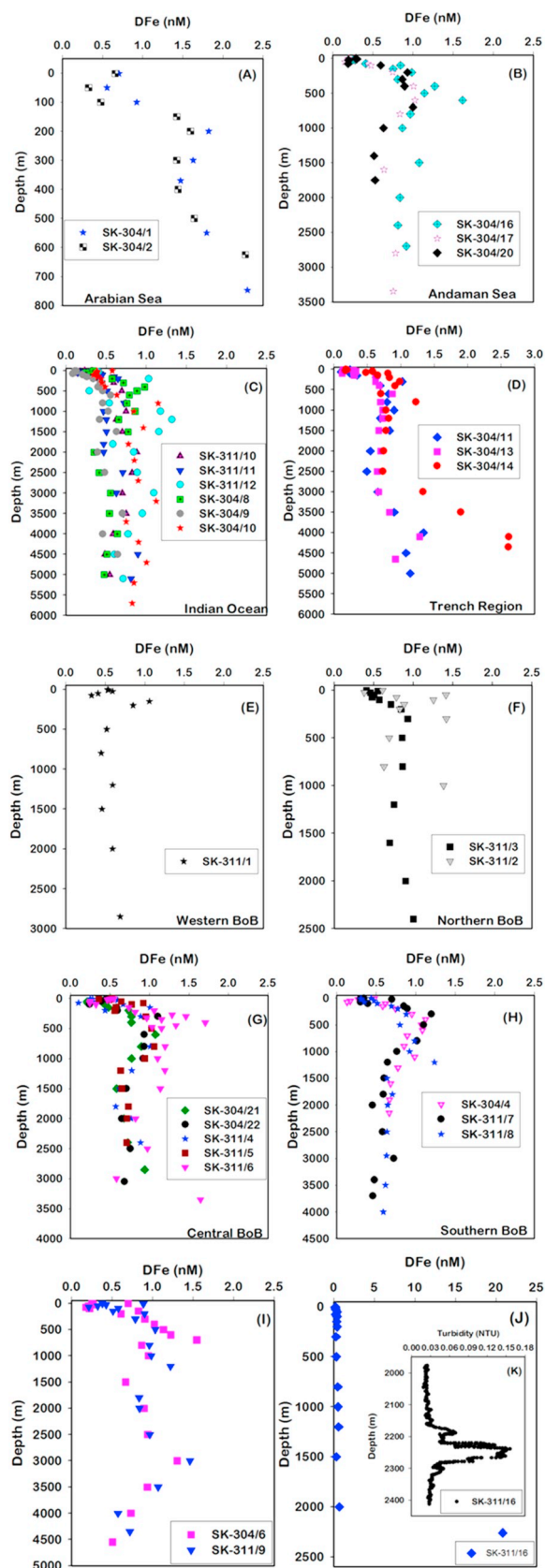


Fig. 11. Vertical profiles of DFe from this study. (A) Coastal Arabian Sea, (B) Andaman Sea, (C) Indian Ocean, (D) Java Trench Region, (E) Northwestern Bay of Bengal, (F) Northern Bay of Bengal, (G) Central Bay of Bengal, (H) Southern Bay of Bengal, (I) Near Equator stations, (J) station SK-311/16 sampled near the Triple junction region and enclosed fig. (K) displaying turbidity data at station SK-311/16 between 2000 and 2400 m. Turbidity data was obtained from a transmissometer mounted on the ship's hydrographic CTD.

650 m) are compared with the published data from nearby stations from Nishioka et al. (2013) and Moffett et al. (2015) as a function of density in Supplementary Fig. 5. The surface DFe concentrations at our stations are relatively higher compared to those reported by Nishioka et al. (2013) whereas the sub-surface DFe concentrations are comparable with open ocean AS values (Supplementary Fig. 5).

5.1.2. The Bay of Bengal

The vertical profiles of DFe in the BoB region are shown in the Fig. 11E, F, G and H. The DFe concentrations in the surface waters of the BoB displayed a decreasing N-S trend (Fig. 9). High DFe (~ 0.615 nM) was observed in the surface waters at station SK-311/2, which is located close to the mouth of the Ganga-Brahmaputra (GB) River system. In contrast, relatively low DFe (~ 0.344 nM) was observed in the surface waters at the southern end of the BoB (SK-311/6 and SK-311/7). The high surface DFe values north of equator in the BoB is consistent with a previous study (Grand et al., 2015b) although the decreasing trend of surface DFe was not as evident in the present study compared to the trend reported by Grand et al. (2015b). This may be due to the presence of eddies in the BoB (Fig. 8). However, a more detailed seasonal study is needed to understand the role of eddies on micronutrients in the BoB. The correlation observed between surface DFe and DAL in the BoB indicates the role of atmospheric deposition and/or riverine sediments in controlling their abundances north of the equator (Grand et al., 2015b). Previous studies have emphasized that the surface waters of the BoB receive anthropogenically processed mineral dust (with more soluble aerosol Fe) from nearby arid landmasses during continental outflow (Kumar et al., 2010; Srinivas et al., 2011).

The sub-surface (between 50 and 200 m) enrichment of DFe was observed in the stations SK-311/1 and SK-311/2. This sub-surface DFe maximum (~ 1 nM at station SK-311/1) is not as prominent as seen at station SK-311/2. The magnitude of riverine particles received at station SK-311/2 was high compared to station SK-311/1. Station SK-311/2 is situated at the mouth of GB River system whereas SK-311/1 is situated in the northwestern BoB proximal to the monsoonal rivers Godavari, Krishna etc. The river discharge during the sampling time of SK-311/1 was low from the Godavari, Krishna etc., compared to discharge received from the GB river system at station SK-311/2. The GB river system alone supplies 133×10^9 mol/yr dissolved silica to the world oceans from riverine input (Sarin et al., 1989; Singh et al., 2015). The large flux of terrestrial sediments supplied by the GB river system could be an important source of DFe to the sub-surface waters of the northern BoB.

In addition, a high export flux of organic matter was observed at station SK-311/1, although with low primary production and Subha Anand et al., (2017) observed high POC values during the same cruise at this station. The high export of particulate organic carbon at station SK-311/1 suggests that DFe may be getting scavenged from the water column.

We observed low DO values (≤ 25 μ M) at stations SK-311/2 to SK-311/8 (5° N) in the BoB between 150 and 1000 m. Such low oxygen levels were not observed further to the south. The poor ventilation of waters in this region associated with the surface stratification in the upper layer makes DO low in the intermediate waters of the BoB (Sarma, 2002; Sarma et al., 2016). The section plots of DFe in the BoB (Fig. 10) display high concentration of DFe in the intermediate waters (between 100 and 1000 m) which are associated with low DO levels. Such high DFe concentrations were not seen at stations to the south with relatively higher concentrations of oxygen. These observations emphasize that remineralisation of organic matter along with dissolution of Fe from the sediments are the main sources for high DFe in the intermediate waters of the BoB. Overall, the internal cycling of DFe in the northern BoB is likely to have been affected by processes like the huge suspended/particulate matter discharge from the rivers and remineralization in the OMZ zone along with scavenging (Sarin et al.,

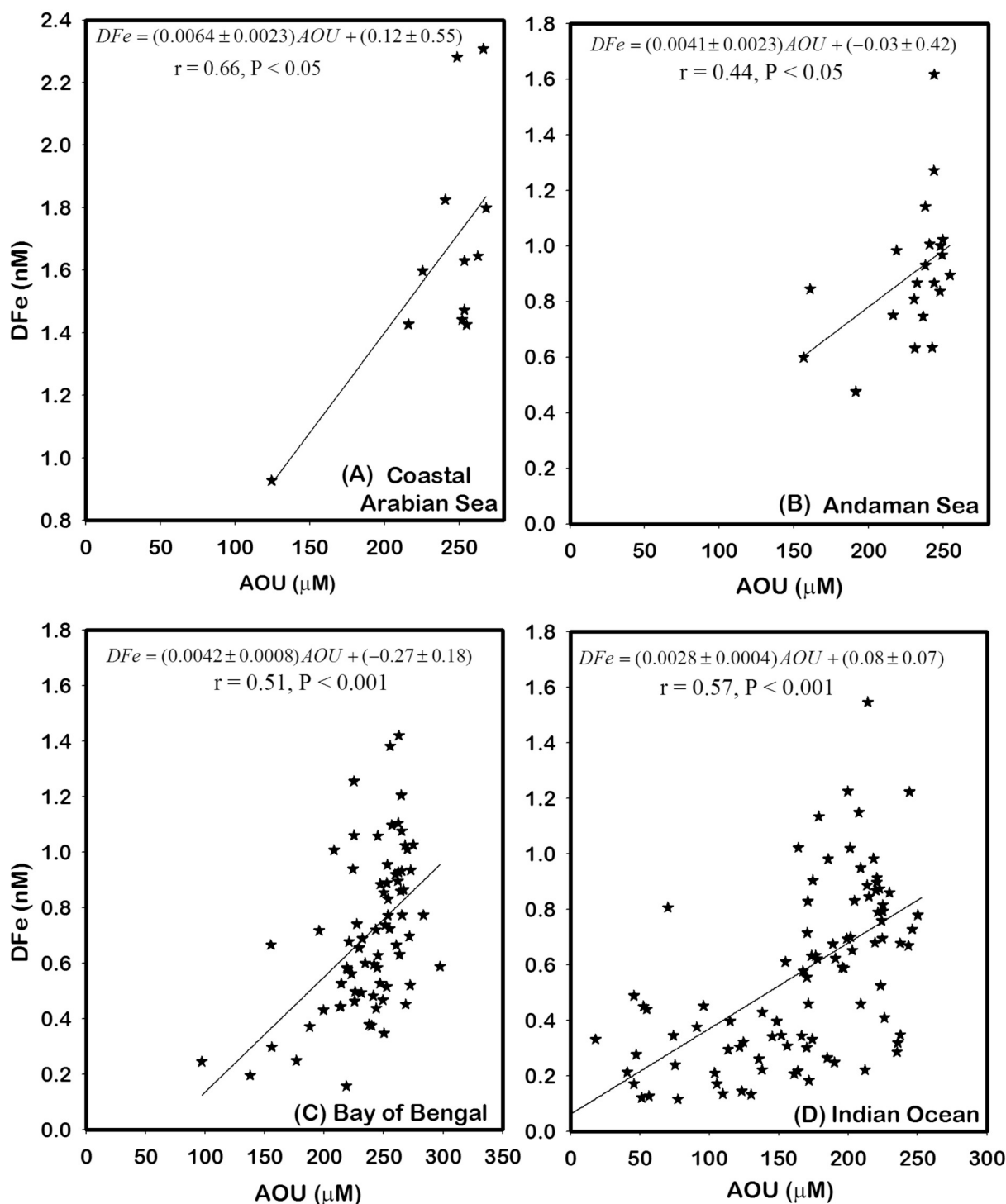


Fig. 12. DFe vs. AOU linear plots in the (A) coastal Arabian Sea, (B) the Andaman Sea, (C) the Bay of Bengal, and (D) the Indian Ocean. The significant relation between AOU and DFe between 100 and 1000 m shows that remineralization in the intermediate water is a source for DFe.

1989; McCreary et al., 1996; Shankar et al., 2002; Singh et al., 2012; Goswami et al., 2014; Yu et al., 2017).

Singh et al. (2012) reported that Antarctica Bottom Water (AABW) dominates the bottom waters of the BoB. The average DFe concentrations for AABW in the BoB for depths > 2700 m was 0.83 ± 0.38 nM ($n = 16$). These bottom waters are overlain by Northern Indian Deep Water (NIDW) and Modified North Atlantic deep waters MNADW in the depth range of 1200 to ~2500 m. The average DFe concentrations of NIDW and MNADW in the BoB was 0.75 ± 0.18 nM ($n = 50$).

5.1.3. The Andaman Sea

Vertical profiles of DFe in the Andaman Sea are displayed in Fig. 11B. The DFe concentrations in the top 25 m in the Andaman Sea averaged $\sim 0.24 \pm 0.04$ nM ($n = 8$). Sub-surface enrichment in the DFe level was observed in the intermediate waters between 100 and 1000 m with an average concentration of 0.90 ± 0.24 nM ($n = 21$). This sub-surface enrichment is attributed to remineralization processes and/or redox cycling in the water column. The Andaman Sea receives a large amount of suspended sediment and particulate organic matter from the Irrawaddy and Salween rivers (Bird et al., 2008; Ramaswamy

Table 2
A comparison of Fe:C ratios from various oceanic basins with the present study.

Location	Fe:C ($\mu\text{mol}/\text{mol}$)	Study
Andaman sea	5.74 ± 3.06	This work
Bay of Bengal	5.88 ± 2.65	This work
Indian Ocean (South of 5°N)	3.92 ± 0.83	This work
Arabian Sea (Coastal)	8.96 ± 3.85	This work
Indian Ocean subtropical gyre	4.1 ± 1.5	Grand et al., 2015a,b
Western North Atlantic	3.4	Rijkenberg et al., 2014
Eastern North Atlantic	4	Rijkenberg et al., 2012
Tropical North Atlantic	11 ± 1.0	Bergquist and Boyle, 2006
Southern Ocean	1.8 ± 0.4	Sunda 1997; Johnson et al., 1997
North Pacific	4.6 ± 2.7	Sunda 1997; Johnson et al., 1997
Southeastern Pacific Ocean	4.2	Fitzsimmons et al., 2016

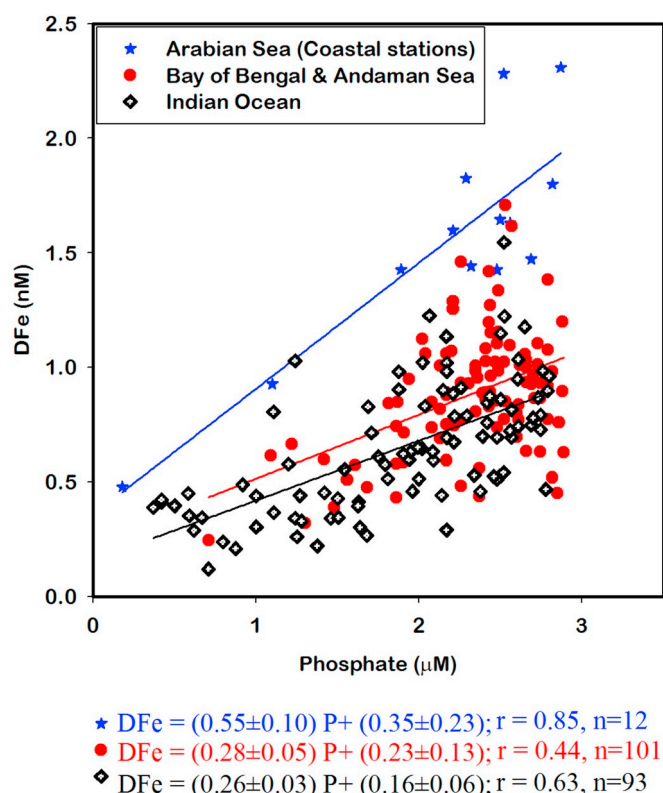


Fig. 13. Correlation between DFe and phosphate at depths of 100–1000 m in the coastal AS, the BoB, the Andaman Sea and the Indian Ocean.

et al., 2008; Damodararao et al., 2016). The DFe concentrations in the Andaman basin below 1200 m water depth centered on 0.83 ± 0.27 nM ($n = 10$). Monotonous behavior in the hydrographic parameters such as salinity, temperature, DO, silicate, phosphate (Figs. 5 and 6) and micronutrient dissolved zinc (Kim et al., 2015) has been observed in the deeper waters of the Andaman basin. The Andaman Sea exchanges waters with the BoB mainly through the Ten Degree Channel, which is deeper (sill depth of ~ 800 m) relative to the Preparis channel on the north side (sill depth of ~ 250 m, Varkey et al., 1996). The ventilation time estimated for the deeper waters of the Andaman Sea is ~ 5 y (Dutta et al., 2007; Okubo et al., 2004). The vertical profiles at SK304/17 and SK304/16, located in the core of the Andaman basin, display monotonous DFe values below 1800 m. This observation suggests low scavenging rates for DFe in deeper waters, potentially due to organic complexation. Since the deeper waters of the Andaman Sea are rapidly exchanged with the intermediate waters of

the BoB, similar organic complexation occurring in the depth interval of 800–1200 m of the BoB should be reflected in the deeper waters of Andaman Sea. We are not aware of any study from the BoB and the Andaman Sea focusing on organic complexation of DFe. However, our inference is based only on five data points of DFe values (i.e., below 1500 m) in the Andaman Sea; high resolution DFe data sets, including data for Fe binding ligands, are required for further understanding.

5.1.4. The Indian Ocean

The DFe at stations sampled in the Indian Ocean (south of 5°N) during SK-304 and SK-311 are shown in Fig. 11C and I. The DFe concentrations are lower in these regions compared to other regions in the northern Indian Ocean (Fig. 10). Sub-surface maxima were not prominent at these stations. Excluded from the section plot is a very high concentration of DFe (20.86 nM) that was observed at 2260 m at station SK-311/16 (Fig. 11J), which is presumably sourced from the hydrothermal vents from a nearby ridge system (a conclusion supported by the turbidity maximum from 2200 to 2300 m; Fig. 11K). Along the central Indian ridge and south-west Indian ridge, the presence of several hydrothermal vents has been reported (Van Dover et al., 2001; Tao et al., 2004; Statham et al., 2005; Kawagucci et al., 2008; Ray et al., 2012; Nishioka et al., 2013). An active hydrothermal vent was also identified over the central Indian ridge segment 12 miles north of the triple junction region (Gamo et al., 1996, 2001). The sampled location in this study (station SK-311/16) is well known for hydrothermal activity and was identified earlier as the Kairie vent field (Rudnicki and German, 2002; Gallant and Von Damm, 2006; Kumagai et al., 2008). Rudnicki and German (2002) observed DFe maxima and the plume particles between 2150 and 2350 m and clear water below 2400 m. The higher DFe concentration observed in this study along with those observed on the Japanese GEOTRACES cruise (Nishioka et al., 2013) in this region suggest a significant supply of DFe into the deeper waters of the southern Indian Ocean from the hydrothermal vents present along the Central Indian Ridge and south-western Indian Ridge. The lateral advection of DFe from the Kairie vent site may be the reason for the observed high concentrations of DFe at SK-311/12 between water depth of 2000 and 3000 m (Fig. 11C). The DFe profiles at stations located closer to the equator (SK-304/6 and SK-311/9) are shown in the Fig. 11I. This location lies in the region where high DO containing waters from the southern Indian Ocean mixes with the poorly ventilated low DO containing waters. These two stations were sampled in the same season but in successive years. In the depth interval of 2500–3000 m, elevated DFe (1.3–1.5 nM) was seen in both profiles along the density anomaly of 27.8 kg m^{-3} (Fig. 10A and B) and could have been sourced from a nearby subduction zone characterized by high DFe (discussed in a later section). High DFe is unlikely to be attributed to sediment release as concentrations of DFe decreased towards the bottom. The average DFe concentrations in AABW (depths > 3000 m) in the Indian Ocean is 0.77 ± 0.24 nM ($n = 26$). Singh et al. (2012) showed that 80–90% of the waters > 3000 m is dominated by AABW in the northern Indian Ocean and this dominant feature is seen up to 12°N.

5.1.5. High DFe along the Java trench

During SK-304B (Second leg of SK-304), three profiles (SK-304/11, 13, 14) were sampled along the Java Trench (Fig. 1), from the eastern to the northern Indian Ocean before entering into the Andaman Sea. The vertical profiles of DFe for these three stations are shown in (Fig. 11D). The surface concentrations were very low in this area compared to other stations in the Indian Ocean. Sub-surface maxima were not observed in these stations unlike in the northern Indian Ocean stations. These locations are characterized neither by low DO nor by river-borne particle fluxes. The average DFe concentration (0.87 ± 0.19 nM, $n = 7$) in the depth range between 100 and 1000 m at station SK-304/14, matches quite well with that of the Andaman Sea (0.90 ± 0.24 nM) indicating that intermediate waters of the Andaman Sea may pass through the Great Channel in the southern direction to the

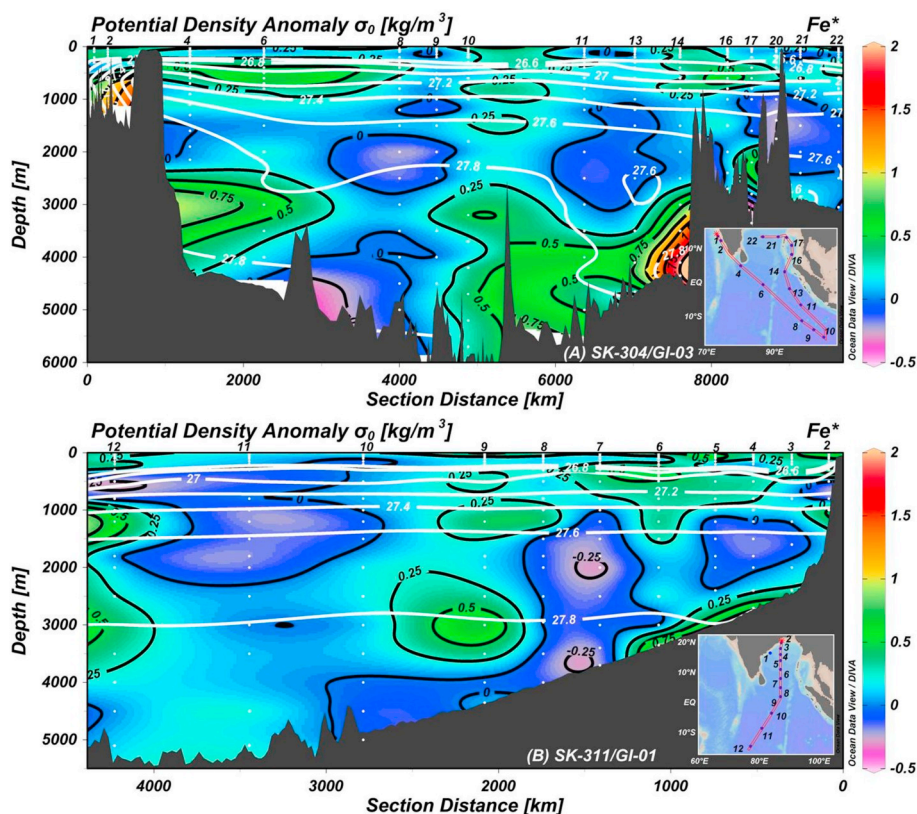


Fig. 14. Section plots of Fe^* with overlying potential density anomaly for (A) cruise SK-304 (GI-03) and (B) cruise SK-311 (GI-01). The black contour line of zero separating the excess Fe^* from deficient Fe^* for both the sections.

equatorial and northeastern Indian Ocean (Varkey et al., 1996). We have compared the DO, Si and P values for these locations. The values reported for DO, Si and P for 304/16 & 17 and 304/14 are not significantly different. The location of SK-304/14 is close to the Great Channel and may receive a DFe signal from 100 to 1000 m depth coming out of the Andaman Sea. The hydrographic parameters (T and S) at 100–1000 m at SK-304/14, SK-304/16 and SK-304/17 were compared and found to be consistent. DFe concentrations at these stations are invariant between depths 1000–2500 m with increase in DFe values below 2500 m, reaching 2.61 nM at station SK-304/14 (Figs. 10A and 11D). The DFe concentration below 4000 m at station SK304/14 (~2.61 nM) is higher by a factor of 4 compared to DFe in deeper waters of the global oceans (Martin et al., 1989; Johnson et al., 2007; Rijkenberg et al., 2014; Worsfold et al., 2014; Nishioka et al., 2013; Abadie et al., 2017) including the Indian Ocean (this study; section 4.2). The lateral advection of higher DFe from station SK-304/14 could be responsible for the high DFe we observed at 3000 m at station SK-311/9 and SK-304/6. This transport of DFe could be mediated by the north-westward transport of AABW along the east side of the Ninety Degree East Ridge (NER), (Frank et al., 2006; Clemens et al., 2016). Fingerprinting of bottom ventilation at the NER is still poorly understood. As suggested by Frank et al. (2006), there may be a possibility of AABW flowing westward across the sills of the NER and may carry the high DFe water from SK-304/14 to station SK-311/9 and SK-304/6. The density anomaly at depth with the high DFe values at station SK-304/14 is 27.6–27.8 $Kg\ m^{-3}$ (Fig. 10) which is quite similar to that observed at 3000 m at station SK-311/9 and station SK-304/6. High DFe was also observed at deeper depths at stations SK-304/11 and SK-304/13 suggesting that the elevated DFe observed at station SK-304/14 is getting advected > 1000 km.

High DFe in the deeper water at the station SK-304/14 is perhaps associated with the subduction boundary along the Java Trench. We are not aware of any other reports of high DFe sourced from a subduction

zone. The high DFe was observed very close to the trench near the subduction boundary (Figs. 1 & 10A). This region is seismically very active and experiences frequent earthquakes due to the convergence of the Indian plate with the Indonesian plate. This convergent plate boundary represents an active continental margin where oceanic lithosphere is being subducted beneath the continental lithosphere without a marine basin behind the volcanic arc; rather the arc is built directly on the adjacent continent (Frisch, 2014). The presence of high DFe in this region is also associated with elevated concentrations of dissolved REEs (our unpublished results), indicating that the fault system could be interacting with subducting seawater and sediment with poly metallic nodules which could act as a source of DFe. If true, this subduction zone source of DFe, quite different from the well-known underwater hydrothermal sources, would represent a unique and previously unrecognized source of DFe to the oceans. Understanding the mechanisms for this proposed new source of DFe, and learning how widespread it might be, will require significant additional research.

5.2. Apparent Fe:C remineralization ratios

Fe:C regeneration ratios estimated from the present data set are based on the linear relationships between DFe and AOU in the range of 100–1000 m depth (Fig. 12) using an $O_2: C_{org}$ molar ratio of 1.4 ± 0.1 , somewhat higher than the standard “Redfield” ratio of $132/106 = 1.25$ (Laws, 1991; Anderson, 1995). Apparent oxygen utilization (AOU = Saturated O_2 concentration (a function of temperature and salinity) minus the observed concentration) represents the amount of oxygen consumed during the aerobic respiration of organic matter. These Fe:C regeneration ratios are valid only in water masses with low DFe scavenging rates, and have been calculated for a variety of ocean basins (Bergquist and Boyle, 2006; Rijkenberg et al., 2014; Grand et al., 2015b and references therein). It is suggested in the studies of Witter et al. (2000), Hopkinson and Barbeau (2007) and Boyd and Ellwood

(2010) that enhanced DFe in OMZs is due to DFe release during organic matter remineralization, which is then stabilized by Fe binding ligands in the solution. In the present study, DFe maxima in the OMZs north of the equator at depths of 100–1000 m suggest that release of Fe from remineralization of particulate organic matter and/or suspended sediment are the dominant processes rather than scavenging.

The calculated Fe:C ratios are $5.88 \pm 2.65 \mu\text{mol/mol}$, $5.74 \pm 3.06 \mu\text{mol/mol}$, $8.96 \pm 3.85 \mu\text{mol/mol}$ and $3.92 \pm 0.83 \mu\text{mol/mol}$ for the BoB, Andaman Sea, AS and the Indian Ocean, respectively. If these estimated Fe:C ratios reflect the stoichiometry of the organic matter sinking from the euphotic zone of the Indian Ocean, BoB, AS and the Andaman Sea, it implies some significant regional differences in the Fe:C uptake ratios of the phytoplankton communities. The estimated Fe:C ratios in the present study are shown in Table 2 along with the Fe:C ratios for other oceanic basins.

5.3. DFe as a limiting nutrient

Fe^* is defined by Parekh et al. (2005) as $\text{Fe}^* = [\text{DFe}] - R_{\text{Fe:P}} \times [\text{PO}_4^{-3}]$ where $R_{\text{Fe:P}}$ represents the average biological uptake ratio of Fe to phosphate. The value $R_{\text{Fe:P}}$ may vary significantly depending on regional differences in the phytoplankton community structure (Sunda and Huntsman, 1995; Twining and Baines, 2013). The term $R_{\text{Fe:P}} \times [\text{PO}_4^{-3}]$ represents the DFe contribution from organic matter remineralization in the water column. Fe^* has been used in oceanic basins like the tropical and subtropical Atlantic Oceans (Bergquist and Boyle, 2006), the western Atlantic Ocean (Rijkenberg et al., 2014), the tropical and subtropical southeastern Pacific Ocean (Blain et al., 2008), and the western and central subarctic Pacific Oceans (Nishioka and Obata, 2017). These studies have used Fe^* to identify waters where DFe is the potentially growth limiting nutrient vs. phosphate ($\text{Fe}^* < 0$) and also to identify waters where external sources for DFe other than organic matter remineralization might be important ($\text{Fe}^* > 0$). The AS stations which were sampled near the west coast of India had an $R_{\text{Fe:P}}$ value of 0.55 ± 0.10 with an intercept of 0.35 ± 0.23 . A $R_{\text{Fe:P}}$ value of 0.28 ± 0.05 was found for the BoB and the Andaman Sea together with an intercept of 0.23 ± 0.13 and the Indian Ocean samples had an $R_{\text{Fe:P}}$ value of 0.26 ± 0.03 with an intercept of 0.16 ± 0.06 (Fig. 13). The positive intercepts indicate excess DFe concentrations relative to phosphate from the remineralization of organic matter. The obtained $R_{\text{Fe:P}}$ values are used in the Fe^* equation to identify waters with positive and negative Fe^* values in the study region. The $R_{\text{Fe:P}}$ for data in the previously published study of Grand et al. (2015b) was also calculated to compare with the present study, yielding a value of 0.32 ± 0.07 with an intercept of 0.22 ± 0.18 for the BoB and a ratio of 0.30 ± 0.06 with an intercept of 0.09 ± 0.13 for the Indian Ocean, similar to the range of $R_{\text{Fe:P}}$ values estimated in the present study.

A zero contour line (Fig. 14) differentiates waters with excess vs. deficient DFe over phosphate. Positive Fe^* values are observed in the intermediate waters of the northern Indian Ocean and the coastal region of the AS suggesting additional sources for DFe in these waters other than in-situ remineralization. The positive Fe^* values are mostly observed between isopycnal lines of $26.4\text{--}27.2 \text{ Kg m}^{-3}$ which are mostly NIIW (white contour lines of Figs. 14 A and B). Negative Fe^* values in the same density interval of $26.4\text{--}27.2 \text{ Kg m}^{-3}$ (Fig. 14B) were observed south of the equator suggesting that scavenging is important in the oxygen rich waters of oligotrophic Indian Ocean stations and/or due to inefficient DFe regeneration during organic matter remineralization. The high particulate fluxes from rivers and shelf sediments could be important sources of the additional DFe in the intermediate waters of northern Indian Ocean. In addition to high particle flux and shelf sediments observed in the northern Indian Ocean, positive Fe^* values observed in some regions of the Indian Ocean (south of equator) could be attributed to external sources such as hydrothermal vents and subduction regions as discussed earlier. Interestingly,

negative Fe^* values are observed in the waters of the northern Indian Ocean below 1200 m. A recent study of Subha Anand et al. (2017) mentioned that export fluxes, based on particle reactive ^{234}Th measurements of sinking organic matter, are very low in the BoB due to remineralization in the sub-surface waters. Since the export of organic carbon is less due to shallow remineralization (which generally happens between 100 and 1000 m) in the BoB, export of DFe from the surface water to intermediate/deep waters may also be low. Therefore, negative Fe^* values (Fig. 14A and B) observed in the deeper waters of northern Indian Ocean could be due to less Fe export from the upper water column and scavenging of preformed and regenerated DFe in the deeper water column.

6. Conclusion

The DFe concentrations over the full water column of the Indian Ocean including the AS, the BoB, the Andaman Sea, and the southern Indian Ocean were measured. The overall N–S decreasing gradient in the surface DFe concentrations suggests the role of riverine particles and dust deposition as important sources in the surface waters of northern Indian Ocean. Clear indication for the supply of DFe from the shelf and slope sediments near the west coast of India was observed. Sub-surface DFe maxima at stations south of 5°N were absent compared to the stations in the northern Indian Ocean. The sub-surface maxima in the low oxygen waters of the northern Indian Ocean could be due to the re-mineralization of organic matter along with the release of DFe from shelf and slope sediments. Hydrothermal vents seem to supply a significant amount of DFe to the water column in the southern Indian Ocean and there is a need to quantify those fluxes to the deeper waters of Indian Ocean. In addition, a strong DFe supply has been observed in the vicinity of the subduction zone along the Java Trench region. DFe concentrations measured in the deeper waters along the Trench region are higher by a factor of 4 compared to the global average deep water values for DFe. This suggests that DFe release during subduction processes may be a previously unrecognized source of DFe to the water column, and demands further study. Fe:C remineralization ratios were calculated for the AS, the Andaman Sea, the BoB, and the open waters of the Indian Ocean. The impact of DFe release from particle and sediments was significant in the OMZs of the AS, Andaman Sea, and BoB. In addition to organic matter re-mineralization, it is evident from the Fe^* distribution that external sources other than remineralization are contributing to the DFe pool in the northern region of this study.

Acknowledgements

This work has been done with the support from Ministry of Earth Sciences - INDIA. We thank the Captains of SK-304, SK-311 ORV Sagar Kanya and the entire crew for their kind cooperation during all operations onboard. We also thank cruise participants of SK-304 and SK-311 for providing help in sample collection and processing onboard. Our sincere thanks are due to Prof. Christopher Measures from the University of Hawaii, and Prof. Maeve Lohan and Dr. Angela Milne from the University of Plymouth for their extraordinary support during the establishment of the flow injection system for DFe measurements. We also thank Prof. Greg Cutter from Old Dominion University and Prof. Christopher Measures for helping in establishing the clean sampling system in India. We sincerely thank Mr. Manan Shah for automation of FIAS. Seawater reference standards were provided by Prof. Kenneth Bruland, University of California, Santa Cruz (USA) (<https://websites.pmc.ucsc.edu/~kbruland/GeotracesSaFe/kwbGeotracesSaFe.html>). Authors are thankful to the Associate Editor and two anonymous reviewers for their constructive comments and reviews which helped improve the manuscript significantly. Sea Surface height information was taken from CMEMS (COPERNICUS MARINE ENVIRONMENT MONITORING SERVICE).

Appendix A. Supplementary data

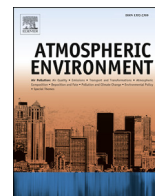
Supplementary data to this article can be found online at <https://doi.org/10.1016/j.marchem.2018.11.007>.

References

- Abadie, C., Lacan, F., Radic, A., Pradoux, C., Poitras, F., 2017. Iron isotopes reveal distinct dissolved iron sources and pathways in the intermediate versus deep Southern Ocean. *Proc. Natl. Acad. Sci.* 114 (5), 858–863.
- Anderson, L.A., 1995. On the hydrogen and oxygen content of marine phytoplankton. *Deep-Sea Res. I Oceanogr. Res. Pap.* 42 (9), 1675–1680.
- Amundt, O., Ethe, C., Tagliabue, A., Bopp, L., Gehlen, M., 2015. PISCES-v2: an ocean biogeochemical model for carbon and ecosystem studies. *Geosci. Model Dev. Discuss.* 8 (2).
- Baker, A.R., Croot, P.L., 2010. Atmospheric and marine controls on aerosol iron solubility in seawater. *Mar. Chem.* 120 (1–4), 4–13.
- Bange, H.W., Naqvi, S.W.A., Codispoti, L.A., 2005. The nitrogen cycle in the Arabian Sea. *Prog. Oceanogr.* 65 (2), 145–158.
- Basu, A.R., Jacobsen, S.B., Poreda, R.J., Dowling, C.B., Aggarwal, P.K., 2001. Large groundwater strontium flux to the oceans from the Bengal Basin and the marine strontium isotope record. *Science* 293 (5534), 1470–1473.
- Beal, L.M., De Ruijter, W.P., Biastoch, A., Zahn, R., 2011. On the role of the Agulhas system in ocean circulation and climate. *Nature* 472 (7344), 429–436.
- Bergquist, B.A., Boyle, E.A.C.G., 2006. Dissolved iron in the tropical and subtropical Atlantic Ocean. *Glob. Biogeochem. Cycles* (1), 20.
- Bird, M.I., Robinson, R.A.J., Oo, N.W., Aye, M.M., Lu, X.X., Higgitt, D.L., Swe, A., Tun, T., Win, S.L., Aye, K.S., Win, K.M.M., 2008. A preliminary estimate of organic carbon transport by the Ayeyarwady (Irrawaddy) and Thanlwin (Salween) Rivers of Myanmar. *Quat. Int.* 186 (1), 113–122.
- Blain, S., Sarthou, G., Laan, P., 2008. Distribution of dissolved iron during the natural iron-fertilization experiment KEOPS (Kerguelen Plateau, Southern Ocean). *Deep-Sea Res. II Top. Stud. Oceanogr.* 55 (5), 594–605.
- Boyd, P.W., Ellwood, M.J., 2010. The biogeochemical cycle of iron in the ocean. *Nat. Geosci.* 3 (10), 675–682.
- Boyd, P.W., Jickells, T., Law, C.S., Blain, S., Boyle, E.A., Buesseler, K.O., Coale, K.H., Cullen, J.J., De Baar, H.J., Follows, M., Harvey, M., 2007. Mesoscale iron enrichment experiments 1993–2005: synthesis and future directions. *Science* 315 (5812), 612–617.
- Clemens, S.C., Kuhnert, W., Levay, L.J., Anand, P., Ando, T., Bartol, M., Bolton, C.T., Ding, X., Gariboldi, K., Giosan, L., Hathorne, E.C., 2016. Indian Monsoon Rainfall. Expedition 353 summary. In: *Proceedings of the International Ocean Discovery Program*, pp. 353.
- Damodaran, K., Singh, S.K., Rai, V.K., Ramaswamy, V., Rao, P.S., 2016. Lithology, monsoon and sea-surface current control on provenance, dispersal and deposition of sediments over the andaman continental shelf. *Front. Mar. Sci.* 3, 118.
- De Baar, H.J., Timmermans, K.R., Laan, P., De Porto, H.H., Ober, S., Blom, J.J., Bakker, M.C., Schilling, J., Sarthou, G., Smit, M.G., Klunder, M., 2008. Titan: a new facility for ultraclean sampling of trace elements and isotopes in the deep oceans in the international Geotraces program. *Mar. Chem.* 111 (1), 4–21.
- De Jong, J.T.M., Den Das, J., Bathmann, U., Stoll, M.H.C., Kattner, G., Nolting, R.F., De Baar, H.J.W., 1998. Dissolved iron at subnanomolar levels in the Southern Ocean as determined by ship-board analysis. *Anal. Chim. Acta* 377 (2), 113–124.
- Dutta, K., Bhushan, R., Somayajulu, B.L.K., 2007. Rapid vertical mixing rates in deep waters of the Andaman Basin. *Sci. Total Environ.* 384 (1), 401–408.
- Elrod, V.A., Berelson, W.M., Coale, K.H., Johnson, K.S., 2004. The flux of iron from continental shelf sediments: a missing source for global budgets. *Geophys. Res. Lett.* (12), 31.
- Fitzsimmons, J.N., Conway, T.M., John, S.G., Boyle, E.A., 2016. Dissolved iron and iron isotopes in the Southeastern Pacific Ocean. *Glob. Biogeochem. Cycles* 30, 1372–1395. <https://doi.org/10.1002/2015GB005357>.
- Frank, M., Whiteley, N., van de Fliedert, T., Reynolds, B.C., O’Nions, K., 2006. Nd and Pb isotope evolution of deep water masses in the eastern Indian Ocean during the past 33 Myr. *Chem. Geol.* 226 (3), 264–279.
- Frants, M., Holzer, M., Devries, T., Matear, R.C.J.G., 2016. Constraints on the global marine iron cycle from a simple inverse model. *J. Geophys. Res. Biogeosci.* 121 (1), 28–51.
- Frisch, W., 2014. Morphology across convergent plate boundaries. In: Harff, J., Meschede, M., Petersen, S., Thiede, J. (Eds.), *Encyclopedia of Marine Geosciences*. Springer Netherlands, Dordrecht, pp. 1–7. https://doi.org/10.1007/978-94-007-6644-0_110-1.
- Gallant, R.M., Von Damm, K.L., 2006. Geochemical controls on hydrothermal fluids from the Kairei and Edmond vent fields, 23–25 S, Central Indian Ridge. *Geochem. Geophys. Geosyst.* 7 (6).
- Galy, A., France-Lanord, C., 1999. Weathering processes in the Ganges–Brahmaputra basin and the riverine alkalinity budget. *Chem. Geol.* 159 (1), 31–60.
- Galy, A., France-Lanord, C., 2001. Higher erosion rates in the Himalaya: geochemical constraints on riverine fluxes. *Geology* 29, 23–26.
- Gamo, T., Nakayama, E., Shitashima, K., Isshiki, K., Obata, H., Okamura, K., Kanayama, S., Oomori, T., Koizumi, T., Matsumoto, S., Hasumoto, H., 1996. Hydrothermal plumes at the Rodriguez triple junction, Indian ridge. *Earth Planet. Sci. Lett.* 142 (1–2), 261–270.
- Gamo, T., Chiba, H., Yamanaka, T., Okudaira, T., Hashimoto, J., Tsuchida, S., Ishibashi, J.I., Kataoka, S., Tsunogai, U., Okamura, K., Sano, Y., 2001. Chemical characteristics of newly discovered black smoker fluids and associated hydrothermal plumes at the Rodriguez Triple Junction, Central Indian Ridge. *Earth Planet. Sci. Lett.* 193 (3), 371–379.
- Goldberg, E.D., Griffin, J.J., 1970. The sediments of the northern Indian Ocean. *Deep-Sea Res. Oceanogr. Abstr.* 17 (3), 513–537 (Elsevier).
- Gopalakrishna, V.V., Murty, V.S.N., Sengupta, D., Shenoy, S., Araligid, N., 2002. Upper Ocean stratification and circulation in the northern Bay of Bengal during southwest monsoon of 1991. *Cont. Shelf Res.* 22 (5), 791–802.
- Goswami, V., Singh, S.K., Bhushan, R., 2012. Dissolved redox sensitive elements, Re, U and Mo in intense denitrification zone of the Arabian Sea. *Chem. Geol.* 291, 256–268.
- Goswami, V., Singh, S.K., Bhushan, R., 2014. Impact of water mass mixing and dust deposition on Nd concentration and ϵ Nd of the Arabian Sea water column. *Geochim. Cosmochim. Acta* 145, 30–49.
- Grand, M.M., Measures, C.I., Hattala, M., Hiscock, W.T., Buck, C.S., Landing, W.M., 2015a. Dust deposition in the eastern Indian Ocean: the ocean perspective from Antarctica to the Bay of Bengal. *Glob. Biogeochem. Cycles* 29 (3), 357–374.
- Grand, M.M., Measures, C.I., Hattala, M., Hiscock, W.T., Landing, W.M., Morton, P.L., Buck, C.S., Barrett, P.M., Resing, J.A., 2015b. Dissolved Fe and Al in the upper 1000 m of the eastern Indian Ocean: a high-resolution transect along 95° E from the Antarctic margin to the Bay of Bengal. *Glob. Biogeochem. Cycles* 29 (3), 375–396.
- Grasshoff, K., Ehrhardt, M., Kremling, K. (Eds.), 1992. *Methods of Seawater Analysis*. Verl. Chem, Weinheim, Germany. <https://doi.org/10.1002/9783527613984>. 634 pp.
- Gupta, R.S., Moraes, C., George, M.D., Kureishy, T.W., Noronha, R.J., Fondecarr, S.P., 1981. Chemistry and hydrography of the Andaman Sea. *Indian J. Mar. Sci.* 10, 228–233.
- Gupta, G.V.M., Sudheesh, V., Sudharma, K.V., Saravanan, N., Dhanya, V., Dhanya, K.R., Lakshmi, G., Sudhakar, M., Naqvi, S.W.A., 2016. Evolution to decay of upwelling and associated biogeochemistry over the southeastern Arabian Sea shelf. *J. Geophys. Res. Biogeosci.* 1–17. <https://doi.org/10.1002/2015JG003163>.
- Homoky, W.B., Severmann, S., McManus, J., Berelson, W.M., Riedel, T.E., Statham, P.J., Mills, R.A., 2012. Dissolved oxygen and suspended particles regulate the benthic flux of iron from continental margins. *Mar. Chem.* 134, 59–70.
- Hopkinson, B.M., Barbeau, K.A., 2007. Organic and redox speciation of iron in the eastern tropical North Pacific suboxic zone. *Mar. Chem.* 106 (1), 2–17.
- Jickells, T.D., An, Z.S., Andersen, K.K., Baker, A.R., Bergametti, G., Brooks, N., Cao, J.J., Boyd, P.W., Duce, R.A., Hunter, K.A., Kawahata, H., 2005. Global iron connections between desert dust, ocean biogeochemistry, and climate. *Science* 308 (5718), 67–71.
- Johnson, K., 2001. Iron supply and demand in the upper ocean: is extraterrestrial dust a significant source of bioavailable iron? *Glob. Biogeochem. Cycles* 15 (1), 61–63.
- Johnson, K.S., Elrod, V., Fitzwater, S., Plant, J., Boyle, E., Bergquist, B., Bruland, K., Aguilar-Islas, A., Buck, K., Lohan, M., Smith, G.J., 2007. Developing standards for dissolved iron in seawater. *EOS Trans. Am. Geophys. Union* 88 (11), 131–132.
- Johnson, K.S., Michael Gordon, R., Coale, K.H., 1997. What controls dissolved iron concentrations in the world ocean? *Mar. Chem.* 57, 137–161. [https://doi.org/10.1016/S0304-4203\(97\)00043-1](https://doi.org/10.1016/S0304-4203(97)00043-1).
- Kawagucci, S., Okamura, K., Kiyota, K., Tsunogai, U., Sano, Y., Tamaki, K., Gamo, T., 2008. Methane, manganese, and helium-3 in newly discovered hydrothermal plumes over the Central Indian Ridge, 18°–20° S. *Geochem. Geophys. Geosyst.* 9 (10).
- Khan, P.K., Chakraborty, P.P., 2005. Two-phase opening of Andaman Sea: a new seismotectonic insight. *Earth Planet. Sci. Lett.* 229 (3), 259–271.
- Kim, T., Obata, H., Gamo, T., 2015. Dissolved Zn and its speciation in the northeastern Indian Ocean and the Andaman Sea. *Front. Mar. Sci.* 2, 60.
- Klunder, M.B., Laan, P., Middag, R., De Baar, H.J.W., Van Ooijen, J.C., 2011. Dissolved iron in the Southern Ocean (Atlantic sector). *Deep-Sea Res. II Top. Stud. Oceanogr.* 58 (25), 2678–2694.
- Kolla, V., Henderson, L., Biscaye, P.E., 1976. Clay mineralogy and sedimentation in the western Indian Ocean. *Deep-Sea Res. Oceanogr. Abstr.* 23 (10), 949–961.
- Kondo, Y., Moffett, J.W., 2013. Dissolved Fe (II) in the Arabian Sea oxygen minimum zone and western tropical Indian Ocean during the inter-monsoon period. In: *Deep Sea Research Part I: Oceanographic Research Papers*. Vol. 73. pp. 73–83.
- Kumagai, H., Nakamura, K., Toki, T., Morishita, T., Okino, K., Ishibashi, J.I., Tsunogai, U., Kawagucci, S., Gamo, T., Shibuya, T., Sawaguchi, T., 2008. Geological background of the Kairei and Edmond hydrothermal fields along the Central Indian Ridge: implications of their vent fluids’ distinct chemistry. *Geofluids* 8 (4), 239–251.
- Kumar, M.D., Li, Y.H., 1996. Spreading of water masses and regeneration of silica and 226 Ra in the Indian Ocean. *Deep-Sea Res. II Top. Stud. Oceanogr.* 43 (1), 83–110.
- Kumar, S.P., Prasad, T.G., 1999. Formation and spreading of Arabian Sea high-salinity water mass. *J. Geophys. Res. Oceans* 104 (C1), 1455–1464.
- Kumar, A., Sarin, M.M., Srinivas, B., 2010. Aerosol iron solubility over Bay of Bengal: role of anthropogenic sources and chemical processing. *Mar. Chem.* 121 (1), 167–175.
- Lam, P.J., Bishop, J.K., 2008. The continental margin is a key source of iron to the HNLC North Pacific Ocean. *Geophys. Res. Lett.* 35 (7).
- Lam, P.J., Ohnemus, D.C., Marcus, M.A., 2012. The speciation of marine particulate iron adjacent to active and passive continental margins. *Geochim. Cosmochim. Acta* 80, 108–124.
- Laws, E.A., 1991. Photosynthetic quotients, new production and net community production in the open ocean. *Deep-Sea Res.* 1 38 (1), 143–167.
- Madhupratap, M., Gauns, M., Ramaiah, N., Prasanna Kumar, S., Muraleedharan, P.M., de Sousa, S.N., Sardesai, S., Muraleedharan, U., 2003. Biogeochemistry of the Bay of Bengal: physical, chemical and primary productivity characteristics of the central and western Bay of Bengal during summer monsoon 2001. *Deep-Sea Res. II* 50, 881–896.
- Mahowald, N.M., Kloster, S., Engelstaedter, S., Moore, J.K., Mukhopadhyay, S., McConnell, J.R., Albani, S., Doney, S.C., Bhattacharya, A., Curran, M.A.J., Flanner, M.G., 2010. Observed 20th century desert dust variability: impact on climate and biogeochemistry. *Atmos. Chem. Phys.* 10 (22), 10875–10893.

- Martin, J.H., 1990. Glacial-interglacial CO₂ change: the iron hypothesis. *Paleoceanography* 5 (1), 1–13.
- Martin, J.H., Fitzwater, S.E., 1988. Iron deficiency limits phytoplankton growth in the north-east Pacific subarctic. *Nature* 331 (6154), 341–343.
- Martin, J.H., Gordon, R.M., Fitzwater, S., Broenkow, W.W., 1989. Vertex: phytoplankton/iron studies in the Gulf of Alaska. *Deep-Sea Res.* I 36 (5), 649–680.
- Martínez-García, A., Rosell-Melé, A., Jaccard, S.L., Geibert, W., Sigman, D.M., Haug, G.H., 2011. Southern Ocean dust–climate coupling over the past four million years. *Nature* 476 (7360), 312.
- Mccreary, J.P., Han, W., Shankar, D., Shetye, S.R., 1996. Dynamics of the East India coastal current 2. Numerical solutions. *J. Geophys. Res.* 101, 13993–14010.
- Measures, C.I., Vink, S., 1999. Seasonal variations in the distribution of Fe and Al in the surface waters of the Arabian Sea. *Deep-Sea Res.* II Top. Stud. Oceanogr. 46 (8), 1597–1622.
- Milliman, J.D., Meade, R.H., 1983. World-wide delivery of river sediment to the oceans. *J. Geol.* 91 (1), 1–21.
- Mills, M.M., Ridame, C., Davey, M., La Roche, J., Geider, R.J., 2004. Iron and phosphorus co-limit nitrogen fixation in the eastern tropical North Atlantic. *Nature* 429 (6989), 292.
- Moffett, J.W., Goepfert, T.J., Naqvi, S.W.A., 2007. Reduced iron associated with secondary nitrite maxima in the Arabian Sea. *Deep-Sea Res.* I Oceanogr. Res. Pap. 54 (8), 1341–1349.
- Moffett, J.W., Vedamati, J., Goepfert, T.J., Pratihary, A., Gauns, M., Naqvi, S.W.A., 2015. Biogeochemistry of iron in the Arabian Sea. *Limnol. Oceanogr.* 60 (5), 1671–1688.
- Moore, C.M., Mills, M.M., Achterberg, E.P., Geider, R.J., Laroche, J., Lucas, M.I., McDonagh, E.L., Pan, X., Poulton, A.J., Rijkenberg, M.J., Suggett, D.J., 2009. Large-scale distribution of Atlantic nitrogen fixation controlled by iron availability. *Nat. Geosci.* 2 (12), 867.
- Murty, V.S.N., Sarma, Y.V.B., Rao, D.P., Murty, C.S., 1992. Water characteristics, mixing and circulation in the Bay of Bengal during southwest monsoon. *J. Mar. Res.* 50 (2), 207–228.
- Naqvi, S.W.A., 1994. Denitrification processes in the Arabian Sea. In: *Proceedings of the Indian Academy of Sciences — Earth and Planetary Sciences.* vol. 103. pp. 279–300.
- Naqvi, S.W.A., Jayakumar, D.A., Narvekar, P.V., Naik, H., Sarma, V.V.S.S., D'Souza, W., Joseph, S., George, M.D., 2000. Increased marine production of N₂O due to intensifying anoxia on the Indian continental shelf. *Nature* 408, 346–349. <https://doi.org/10.1038/35042551>.
- Naqvi, S.W.A., Naik, H., Pratihary, A., D'Souza, W., Narvekar, P.V., Jayakumar, D.A., Devol, A.H., Yoshinari, T., Saino, T., 2006. Coastal versus open-ocean denitrification in the Arabian Sea. *Biogeosciences* 3 (4), 621–633.
- Nishioka, J., Obata, H., 2017. Dissolved iron distribution in the western and central subarctic Pacific: HNLC water formation and biogeochemical processes. *Limnol. Oceanogr.* 62 (5), 2004–2022.
- Nishioka, J., Obata, H., Tsumune, D., 2013. Evidence of an extensive spread of hydrothermal dissolved iron in the Indian Ocean. *Earth Planet. Sci. Lett.* 361, 26–33.
- Nozaki, Y., Ailbo, D.S., 2003. Importance of vertical geochemical processes in controlling the oceanic profiles of dissolved rare earth elements in the northeastern Indian Ocean. *Earth Planet. Sci. Lett.* 205 (3), 155–172.
- Obata, H., Karatani, H., Nakayama, E., 1993. Automated determination of iron in seawater by chelating resin concentration and chemiluminescence detection. *Anal. Chem.* 65 (11), 1524–1528.
- Okubo, A., Obata, H., Nozaki, Y., Yamamoto, Y., Minami, H., 2004. 230Th in the Andaman Sea: rapid deep-sea renewal. *Geophys. Res. Lett.* 31, 1–5. <https://doi.org/10.1029/2004GL020226>.
- Parekh, P., Follows, M.J., Boyle, E.C.G.B., 2004. Modeling the global ocean iron cycle. *Glob. Biogeochem. Cycles* 18 (1).
- Parekh, P., Follows, M.J., Boyle, E.A.C.G., 2005. Decoupling of iron and phosphate in the global ocean. *Glob. Biogeochem. Cycles* 19 (2).
- Pollard, R.T., Salter, I., Sanders, R.J., Lucas, M.I., Moore, C.M., Mills, R.A., Statham, P.J., Allen, J.T., Baker, A.R., Bakker, D.C., Charette, M.A., 2009. Southern Ocean deep-water carbon export enhanced by natural iron fertilization. *Nature* 457 (7229), 577.
- Prasanna Kumar, S., Muraliedharan, P.M., Prasad, T.G., Gauns, M., Ramaiah, N., De Souza, S.N., Sardesai, S., Madhupratap, M., 2002. Why is the Bay of Bengal less productive during summer monsoon compared to the Arabian Sea? *Geophys. Res. Lett.* 29 (24).
- Qian, S., Arnold, L.G., Martin, V., 2004. Spreading of the Indonesian Throughflow in the Indian Ocean. *J. Phys. Oceanogr.* 34 (4), 772–792.
- Raju, K.K., Ramprasad, T., Rao, P.S., Rao, B.R., Varghese, J., 2004. New insights into the tectonic evolution of the Andaman basin, Northeast Indian Ocean. *Earth Planet. Sci. Lett.* 221 (1), 45–162.
- Ramaswamy, V., Nair, R.R., 1994. Fluxes of material in the Arabian Sea and Bay of Bengal sediment trap studies. *J. Earth Syst. Sci.* 103 (2), 189–210.
- Ramaswamy, V., Gaye, B., Shirodkar, P.V., Rao, P.S., Chivas, A.R., Wheeler, D., Thwin, S., 2008. Distribution and sources of organic carbon, nitrogen and their isotopic signatures in sediments from the Ayeyarwady (Irrawaddy) continental shelf, northern Andaman Sea. *Mar. Chem.* 111 (3), 137–150.
- Rao, D.P., Sarma, V.V., Rao, V.S., Sudhakar, U., Gupta, G.V.M., 1996. On watermass mixing ratios and regenerated silicon in the Bay of Bengal. *Indian J. Mar. Sci.* 25, 56–61.
- Ray, D., Kamesh Raju, K.A., Baker, E.T., Srinivas Rao, A., Mudholkar, A.V., Lupton, J.E., Surya Prakash, L., Gawas, R.B., Vijaya Kumar, T., 2012. Hydrothermal plumes over the Carlsberg Ridge, Indian Ocean. *Geochim. Geophys. Geosyst.* 13 (1).
- Resing, J.A., Sedwick, P.N., German, C.R., Jenkins, W.J., Moffett, J.W., Soth, B.M., Tagliabue, A., 2015. Basin-scale transport of hydrothermal dissolved metals across the South Pacific Ocean. *Nature* 523 (7559), 200–203.
- Rijkenberg, M.J., Steigenberger, S., Powell, C.F., Haren, H., Patey, M.D., Baker, A.R., Achterberg, E.P., 2012. Fluxes and distribution of dissolved iron in the eastern (sub-tropical) North Atlantic Ocean. *Glob. Biogeochem. Cycles* 26 (3).
- Rijkenberg, M.J.A., Middag, R., Laan, P., Gerringa, L.J.A., Van Aken, H.M., Schoemann, V., De Jong, J.T.M., De Baar, H.J.W., 2014. The distribution of dissolved iron in the West Atlantic Ocean. *PLoS One* 9, 1–14. <https://doi.org/10.1371/journal.pone.0101323>.
- Rudnicki, M.D., German, C.R., 2002. Temporal variability of the hydrothermal plume above the Kairei vent field, 25 S, Central Indian Ridge. *Geochim. Geophys. (2)*, 3 Geosystems.
- Saager, P.M., De Baar, H.J.W., Burkill, P.H., 1989. Manganese and iron in Indian Ocean waters. *Geochim. Cosmochim. Acta* 53 (9), 2259–2267.
- Sanial, V., Kipp, L.E., Henderson, P.B., van Beek, P., Reys, J.L., Hammond, D.E., Hawco, N.J., Saito, M.A., Resing, J.A., Sedwick, P., Moore, W.S., 2017. Radium-228 as a tracer of dissolved trace element inputs from the Peruvian continental margin. *Mar. Chem.* 201, 20–34.
- Sarin, M.M., Krishnaswami, S., Dilli, K., Somayajulu, B.L.K., Moore, W.S., 1989. Major ion chemistry of the Ganga-Brahmaputra river system: weathering processes and fluxes to the Bay of Bengal. *Geochim. Cosmochim. Acta* 53 (5), 997–1009.
- Sarma, V.V.S.S., 2002. An evaluation of physical and biogeochemical processes regulating the oxygen minimum zone in the water column of the Bay of Bengal. *Glob. Biogeochem. Cycles* 16 (4).
- Sarma, V.V.S.S., Sridevi, B., Maneesha, K., Sridevi, T., Naidu, S.A., Prasad, V.R., Venkatarmana, V., Acharya, T., Bharati, M.D., Subbaiah, C.V., Kiran, B.S., 2013. Impact of atmospheric and physical forcings on biogeochemical cycling of dissolved oxygen and nutrients in the coastal Bay of Bengal. *J. Oceanogr.* 69 (2), 229–243.
- Sarma, V.V.S.S., Rao, G.D., Viswanadham, R., Sherin, C.K., Salisbury, J., Omand, M.M., Mahadevan, A., Murty, V.S.N., Shroyer, E.L., Baumgartner, M., Stafford, K.M., 2016. Effects of freshwater stratification on nutrients, dissolved oxygen, and phytoplankton in the Bay of Bengal. *Oceanography* 29 (2), 222–231.
- Sastry, J.S., Rao, D.P., Murty, V.S.N., Sarma, Y.V.B., Suryanarayana, A., Babu, M.T., 1985. Watermass structure in the Bay of Bengal. *Mahasagar* 18 (2), 153–162.
- Schlitzer, R., 2017. *Ocean Data View*. odv.awi.de.
- Schott, F.A., McCreary Jr., J.P., 2001. The monsoon circulation of the Indian Ocean. *Prog. Oceanogr.* 51 (1), 1–123.
- Schroth, A.W., Crusius, J., Sholkovitz, E.R., Bostick, B.C., 2009. Iron solubility driven by speciation in dust sources to the ocean. *Nat. Geosci.* 2 (5), 337.
- Schulz, M., Prospero, J.M., Baker, A.R., Dentener, F., Ickes, L., Liss, P.S., Mahowald, N.M., Nickovic, S., Garcia-Pando, C.P., Rodriguez, S., Sarin, M., 2012. Atmospheric transport and deposition of mineral dust to the ocean: implications for research needs. *Environ. Sci. Technol.* 46 (19), 10390–10404.
- Selavka, C.M., Jiao, K.S., Krull, I.S., 1987. Construction and comparison of open tubular reactors for post-column reaction detection in liquid chromatography. *Anal. Chem.* 59 (17), 2221–2224.
- Sengupta, D., Bharath Raj, G.N., Shenoi, S.S.C., 2006. Surface freshwater from Bay of Bengal runoff and Indonesian throughflow in the tropical Indian Ocean. *Geophys. Res. Lett.* 33 (22).
- Shankar, D., Vinayachandran, P.N., Unnikrishnan, A.S., 2002. The monsoon currents in the north Indian Ocean. *Prog. Oceanogr.* 52 (1), 63–120.
- Sheth, H.C., Ray, J.S., Bhutani, R., Kumar, A., Smitha, R.S., 2009. Volcanology and eruptive styles of Barren Island: an active mafic stratovolcano in the Andaman Sea, NE Indian Ocean. *Bull. Volcanol.* 71 (9), 1021.
- Shetye, S.R., Gouveia, A.D., Shankar, D., Shenoi, S.S.C., Vinayachandran, P.N., Sundar, D., Michael, G.S., Nampoothiri, G., 1996. Hydrography and circulation in the western Bay of Bengal during the northeast monsoon. *J. Geophys. Res.* Oceans 101 (C6), 14011–14025.
- Sholkovitz, E.R., Sedwick, P.N., Church, T.M., Baker, A.R., Powell, C.F., 2012. Fractional solubility of aerosol iron: synthesis of a global-scale data set. *Geochim. Cosmochim. Acta* 89, 173–189.
- Singh, S.K., Rai, S.K., Krishnaswami, S., 2008. Sr and Nd isotopes in river sediments from the Ganga Basin: sediment provenance and spatial variability in physical erosion. *J. Geophys. Res.* Earth Surf. (F3), 113.
- Singh, S.P., Singh, S.K., Goswami, V., Bhushan, R., Rai, V.K., 2012. Spatial distribution of dissolved neodymium and ¹⁴Nd in the Bay of Bengal: role of particulate matter and mixing of water masses. *Geochim. Cosmochim. Acta* 94, 38–56.
- Singh, S.P., Singh, S.K., Bhushan, R., Rai, V.K., 2015. Dissolved silicon and its isotopes in the water column of the Bay of Bengal: internal cycling versus lateral transport. *Geochim. Cosmochim. Acta* 151, 172–191.
- Sirocko, F., Sarin, M., 1989. Wind-borne deposits in the northwestern Indian Ocean: record of Holocene sediments versus modern satellite data. In: *Paleoclimatology and Paleometeorology: Modern and Past Patterns of Global Atmospheric Transport*, pp. 401–433.
- Srinivas, B., Sarin, M.M., Kumar, A., 2011. Impact of anthropogenic sources on aerosol iron solubility over the Bay of Bengal and the Arabian Sea. *Biogeochemistry* 110 (1), 257–268.
- Statham, P.J., German, C., Connelly, D.P., 2005. Iron (II) distribution and oxidation kinetics in hydrothermal plumes at the Kairei and Edmond vent sites, Indian Ocean. *Earth Planet. Sci. Lett.* 236 (3), 588–596.
- Subha Anand, S., Rengarajan, R., Sarma, V.V.S.S., Sudheer, A.K., Bhushan, R., Singh, S.K., 2017. Spatial variability of upper ocean POC export in the Bay of Bengal and the Indian Ocean determined using particle-reactive 234Th. *J. Geophys. Res.* Oceans 122 (5), 3753–3770.
- Sunda, W.G., 1997. Control of dissolved iron concentrations in the world ocean: A comment. *Mar. Chem.* 57, 169–172. [https://doi.org/10.1016/S0304-4203\(97\)00045-5](https://doi.org/10.1016/S0304-4203(97)00045-5).
- Sunda, W.G., Huntsman, S.A., 1995. Iron uptake and growth limitation in oceanic and coastal phytoplankton. *Mar. Chem.* 50 (1), 189–206.

- Tagliabue, A., Bopp, L., Dutay, J.C., Bowie, A.R., Chever, F., Jean-Baptiste, P., Bucciarelli, E., Lannuzel, D., Remenyi, T., Sarthou, G., Aumont, O., 2010. Hydrothermal contribution to the oceanic dissolved iron inventory. *Nat. Geosci.* 3 (4), 252.
- Tagliabue, A., Aumont, O., Bopp, L.C.G.L., 2014. The impact of different external sources of iron on the global carbon cycle. *Geophys. Res. Lett.* 41 (3), 920–926.
- Takeda, S., Kamatani, A., Kawanobe, K., 1995. Effects of nitrogen and iron enrichments on phytoplankton communities in the northwestern Indian Ocean. *Mar. Chem.* 50 (1–4), 229–241.
- Tao, C., Lin, J., Guo, S., Chen, Y.J., Wu, G., Han, X., German, C.R., Yoerger, D.R., Zhu, J., Zhou, N., Su, X., 2004, December. First discovery and investigation of a high-temperature hydrothermal vent field on the ultra-slow spreading Southwest Indian Ridge. In: AGU Fall Meeting Abstracts.
- Tomczak, M., Godfrey, J.S., 2003. *Regional Oceanography: An Introduction*. Elsevier.
- Twining, B.S., Baines, S.B., 2013. The trace metal composition of marine phytoplankton. *Annu. Rev. Mar. Sci.* 5, 191–215.
- UNESCO, 1993. *Discharge of Selected Rivers of the World*. vol. III (600 pp., Paris).
- Van Dover, C.L., Humphris, S.E., Fornari, D., Cavanaugh, C.M., Collier, R., Goffredi, S.K., Hashimoto, J., Lilley, M.D., Reysenbach, A.L., Shank, T.M., Von Damm, K.L., 2001. Biogeography and ecological setting of Indian Ocean hydrothermal vents. *Science* 294 (5543), 818–823.
- Varkey, M.J., Murty, V.S.N., Suryanarayana, A., 1996. In: Ansell, A.D. (Ed.), *Physical Oceanography of the Bay of Bengal and Andaman Sea*. Oceanography and Marine Biology: An Annual Review. vol. 34. UCL Press, pp. 1–70.
- Volker, C., Tagliabue, A., 2015. Modeling organic iron-binding ligands in a three-dimensional biogeochemical ocean model. *Mar. Chem.* 173, 67–77.
- Vu Thi Dieu, H., Sohrin, Y., 2013. Diverse stoichiometry of dissolved trace metals in the Indian Ocean. *Sci. Rep.* 3, 1745.
- Watson, A.J., Bakker, D.C.E., Ridgwell, A.J., Boyd, P.W., Law, C.S., 2000. Effect of iron supply on Southern Ocean CO₂ uptake and implications for glacial atmospheric CO₂. *Nature* 407 (6805), 730–733.
- Witter, A.E., Lewis, B.L., Luther III, G.W., 2000. Iron speciation in the Arabian Sea. *Deep-Sea Res. II Top. Stud. Oceanogr.* 47 (7), 1517–1539.
- Worsfold, P.J., Lohan, M.C., Ussher, S.J., Bowie, A.R., 2014. Determination of dissolved iron in seawater: a historical review. *Mar. Chem.* 166, 25–35.
- Wu, J., Wells, M.L., Rember, R., 2011. Dissolved iron anomaly in the deep tropical–subtropical Pacific: evidence for long-range transport of hydrothermal iron. *Geochim. Cosmochim. Acta* 75 (2), 460–468.
- Wyrtki, K., 1973. Physical oceanography of the Indian Ocean. In: *The Biology of the Indian Ocean*, pp. 18–36.
- You, Y., 1997. Seasonal variations of thermocline circulation and ventilation in the Indian Ocean. *J. Geophys. Res. Oceans* 102 (C5), 10391–10422.
- You, Y., 1998. Intermediate water circulation and ventilation of the Indian Ocean derived from water-mass contributions. *J. Mar. Res.* 56 (5), 1029–1067.
- You, Y., 2000. Implications of the deep circulation and ventilation of the Indian Ocean on the renewal mechanism of North Atlantic Deep Water. *J. Geophys. Res. Oceans* 105 (C10), 23895–23926.
- You, Y., Tomczak, M., 1993. Thermocline circulation and ventilation in the Indian Ocean derived from water mass analysis. *Deep-Sea Res. I Oceanogr. Res. Pap.* 40 (1), 13–56.
- Yu, Z., Colin, C., Meynadier, L., Douville, E., Dapoigny, A., Reverdin, G., Wu, Q., Wan, S., Song, L., Xu, Z., Bassinot, F., 2017. Seasonal variations in dissolved neodymium isotope composition in the Bay of Bengal. *Earth Planet. Sci. Lett.* 479, 310–321. <https://doi.org/10.1016/j.epsl.2017.09.022>.



Atmospheric ^{210}Pb and anthropogenic trace metals in the continental outflow to the Bay of Bengal



Srinivas Bikkina, M.M. Sarin*, Venkatesh Chinni

Physical Research Laboratory, Ahmedabad 380009, India

HIGHLIGHTS

- First study on atmospheric ^{210}Pb in continental outflow to the Bay of Bengal.
- Aerosol ^{210}Pb activity is considerably higher than model results in literature.
- Heavy metal concentrations in outflow are similar to those over Bay of Bengal.
- High enrichment factors of metals raises the issue of aerosol toxicity in outflow.

ARTICLE INFO

Article history:

Received 16 July 2015

Received in revised form

13 October 2015

Accepted 15 October 2015

Available online 19 October 2015

Keywords:

Aerosols

Trace metals

Pb210

Indo-Gangetic Plain

Bay of Bengal

Ocean biogeochemistry

ABSTRACT

Atmospheric ^{210}Pb and trace metals (Pb, Cd, Cu, Mn, Cr, Co, Ni and Zn) have been studied in fine mode aerosols ($\text{PM}_{2.5}$) from a sampling site (Kharagpur: 22.3°N , 87.3°E) in the Indo-Gangetic Plain (IGP) during the continental outflow (November–March) to the Bay of Bengal (BoB). The aerosol ^{210}Pb activity (1.3 – 6.6 mBq m^{-3}) is significantly high in the wintertime (December–January) compared to model based data in the literature. The cause for higher ^{210}Pb activity is attributed to enhanced ^{222}Rn emanation from Alluvium in the IGP as well as lower boundary layer height. The trace metal concentrations (in ng m^{-3}) also exhibit pronounced temporal variability (Pb: 8 – 296 , Mn: 8 – 568 , Cr: 4.5 – 33 , Cu: 2.1 – 29.3 , Ni: 2.3 – 14.3 , Co: 0.5 – 1.6 and Cd: 1 – 29.5) and are of comparable magnitude with those documented over the BoB (Srinivas and Sarin, 2013b), suggesting dominant impact of IGP-outflow on marine atmospheric boundary layer. The enrichment factors (EF_{crust}) of Pb, Cd, Cu, Mn, Cr, Co and Ni in $\text{PM}_{2.5}$, relative to upper continental crust, varied as 105 – 1561 , 1265 – 24006 , 13 – 87 , 3 – 99 , 7 – 27 , 3 – 19 and 9 – 27 , respectively. Significant linear relationship among trace metals and chemical species (non-sea-salt- K^+ , nss-SO_4^{2-} and EC) emphasizes their anthropogenic source. The high concentrations and EF_{crust} of Pb, Cd and Cu, together with residence time of $\text{PM}_{2.5}$ (2 – 13 days, assessed from ^{210}Pb) in the IGP-outflow has implications to increase in the aerosol toxicity and their impact on biogeochemistry of ocean surface waters via air-sea deposition.

© 2015 Elsevier Ltd. All rights reserved.

1. Introduction

The atmospheric transport of mineral dust from continents to the open ocean has been recognized as an important source of trace metals via air-sea deposition (Duce et al., 1991; Jickells et al., 2005) and their subsequent impact on biogeochemical cycles and carbon sequestration in the upper ocean (de Leeuw et al., 2014; Mahowald,

2011; Schulz et al., 2012). Several investigations in the past have assessed their sources, transport and deposition fluxes to the global ocean (Mahowald et al., 2005; Tegen and Fung, 1994). However, these fluxes need reassessment in the present-day scenario of growing anthropogenic component of trace metals vis-à-vis that associated with mineral dust, particularly in the polluted continental outflows (e.g. from south Asia to the Indian Ocean; from East Asia to the North Pacific and North Africa/America to the North Atlantic).

The impact of anthropogenic trace metals (Cu, Pb) on ocean surface biogeochemistry (such as changes in ecosystem response and alteration in plankton species) has been highlighted by Paytan

* Corresponding author. Geosciences Division Physical Research Laboratory, Ahmedabad, 380009, India.

E-mail address: sarin@prl.res.in (M.M. Sarin).

et al. (2009). Moreover, growing level of evidence from marginal seas that include Bay of Bengal (Echegoyen et al., 2014; Grand et al., 2015; Paytan et al., 2009; Vu and Sohrin, 2013), South- and East-China Sea (Guo et al., 2014; Hsu et al., 2010; Xu et al., 2014), Sea of Japan (Kang et al., 2011) and Mediterranean Sea (Liger et al., 2014), suggest enhanced air-sea deposition of heavy metals to the surface waters. However, studies focusing on air-borne trace metals from south Asia during the continental outflow are rather limited in the literature (Balasubramanian et al., 2013; Siefert et al., 1999; Srinivas and Sarin, 2013b). Some of them have emphasized the need for reassessment of atmospheric abundances of mineral dust and anthropogenic component of trace metals to the Northern Indian Ocean (comprising of Bay of Bengal and Arabian Sea) in a changing climate scenario in south Asia.

In this context, earlier studies have documented the impact of atmospheric outflow from the Indo-Gangetic Plain (IGP) on chemical composition of aerosols over the Bay of Bengal during the late NE-monsoon (December–March) (Srinivas et al., 2011, 2014 and references therein). The IGP, one of the most dynamic regions in northern India and northbound by the Himalayas, is characterized by rapidly growing anthropogenic emissions (viz., fossil-fuel combustion, biomass/bio-fuel burning and industrial activities). Furthermore, regional soils in the IGP are characterized by Alluvium derived from weathering products of rivers draining through southern slopes of Himalaya. Due to rapid industrialization, urbanization and large-scale agricultural activities in the IGP, episodes of haze and fog conditions are wide-spread during the wintertime (Ram et al., 2012 and references therein). Under favourable meteorological conditions during the late NE-monsoon, downwind long-range transport of atmospheric pollutants and mineral dust enter into the marine atmospheric boundary layer (MABL) of the Bay of Bengal.

The Bay of Bengal (BoB), characterized as low nutrient chlorophyll system (LNLC) (Paytan et al., 2009), is influenced by wide-spread anthropogenic sources compared to the Arabian Sea during the late NE-monsoon. The optical and chemical properties of aerosols within the MABL of BoB have been well studied (Kedia et al., 2010; Kumar et al., 2008; Nair et al., 2013; Srinivas and Sarin, 2013a; Srinivas et al., 2011). Although Srinivas and Sarin (2013b) have investigated the sources/transport pathways of atmospheric trace metals to the BoB, their inferences are largely based on air mass back trajectories and chemical composition of aerosols within the MABL obtained during different cruises (March–April 2006 and January 2009). The study reported in this manuscript aims to assess the atmospheric abundances of trace metals over the IGP representing the continental outflow to the BoB with a view to assess their sources, long-range transport and air-sea deposition. With this objective, aerosol sampling was carried out from a continental site (Kharagpur: 22.3°N, 87.3°E), a few kilometers away from the northwest-coast of BoB.

2. Materials and methods

2.1. PM_{2.5} collection & analysis

For this study, PM_{2.5} samples (N = 46) were collected (from November 2009 to March 2010) on pre-combusted (at 450 °C) tisuquartz filters (PALLFLEX[®]™, 8" × 10") using a high-volume air sampler (HVS, Thermo-Anderson Inc., flow rate: 1.13 m³ min⁻¹). Each sample was collected by continuously operating the HVS for ~22 h. For further details of sample collection and chemical composition of PM_{2.5} with respect to water-soluble inorganic ions (Na⁺, NH₄⁺, K⁺, Mg²⁺, Ca²⁺, Cl⁻, NO₃⁻ and SO₄²⁻) carbonaceous species (EC, OC, WSOC) and crustal elements (Al, Fe, Ca and Mg),

reference is made to our earlier publication (Srinivas et al., 2014).

An aliquot of aerosol filter (4–5 circular punches of 2.0 cm dia.) was digested in Teflon distilled HF and HNO₃ acids in a microwave digestion system (Milestone Inc.). After digestion, solutions were suitably diluted to 18.0 ml with Milli-Q water (specific resistivity ≈ 18.2 MΩ-cm) and stored in pre-cleaned 30 ml polypropylene bottles. The acid extracts were used for the measurement of Pb, Cd, Cu, Mn, Cr, Co and Ni on Q-ICP-MS (Thermo X-series II). For further details of analytical protocol for filter digestion and analysis on Q-ICP-MS, reference is made to our earlier publication (Srinivas and Sarin, 2013b). Along with samples, blank filters were also digested and measured for trace metals. The trace metal concentrations reported in this study were suitably corrected for blanks. To check the analytical accuracy of the measurements, a standard reference material (USGS rock standard, ~0.4224 g of W1 basalt) was digested along with aerosol samples and analysed for crustal metals (Al, Ca, Fe and Mg), which shows good agreement with the certified values (within 10%) (Srinivas and Sarin, 2013b). Based on repeat analyses of samples and standards, the overall analytical precision is better than 6% for Pb, Cd, Cu, Mn and 10% for Cr, Co, Ni and Zn.

For assaying ²¹⁰Pb activity, one-fourth filter aliquot (PM_{2.5} sample) was packed in a plastic vial and placed inside a coaxial well of high-purity Germanium (HPGe) detector. Specific details regarding sample preparation and radioactive counting system are described by Rastogi and Sarin (2013). The energy scale on multi-channel analyser was calibrated with respect to photon peaks at 1173 keV and 1332 keV from a Co-60 source. The ²¹⁰Pb activity, with 4.05% gamma yield, was assessed based on counts under 46.5 keV energy region. The counting efficiency of HPGe detector was ascertained using ²³⁸U spike solution of known concentration (with pre-calibrated ²¹⁰Pb activity) loaded on 1/4th tisuquartz filter and packed similar to the sample filter (keeping similar geometry). The overall propagated errors regarding the measurement of ²¹⁰Pb activity were within 10%.

2.2. Air-mass back trajectories (AMBTs)

In order to ascertain the source regions/transport pathways of chemical constituents that dominate the composition of PM_{2.5} at the study site (Kharagpur), air-mass back trajectory analysis was performed for the sampling days. Five-day isentropic AMBTs were computed at an arrival height of 500 m using hybrid single particle lagrangian integrated trajectory model (HYSPLIT, Version 4.0; (Draxler and Rolph, 2009 and references therein; Draxler et al., 2012) from the NOAA (National Oceanic Aeronautic and Administration) air resources laboratory. The GDAS archived meteorological parameters from the NCEP-reanalysis datasets have been used as input files for the HYSPLIT model. Overall, the AMBT cluster during sampling days reveal the impact of long-range atmospheric transport from the upwind source regions in the IGP to the sampling site (Kharagpur).

In order to be consistent with our earlier study (Srinivas et al., 2014), we have split the sampling days from November 2009 to March 2010 into three categories, viz., pre-NE-monsoon (November 2009), NE-monsoon (December 2009–February 2010) and post-NE-monsoon (March 2010). It is relevant to state that the impact of continental air masses from the IGP on MABL of the BoB is more dominant during the wintertime (January) compared to spring-post-NE-monsoon (March–April) (Srinivas and Sarin, 2013b and references therein). A similar trend in the seasonal variability with respect to chemical composition of PM_{2.5} has been documented from the sampling site during the continental outflow (November 2009–March 2010) to the BoB (Srinivas and Sarin, 2014; Srinivas et al., 2014)).

2.3. Cluster analysis

Cluster analysis is a powerful tool to trace the potential source regions of atmospheric constituents based on similarities in the air mass circulation (Abdalmogith and Harrison, 2005). Furthermore, due to inherent uncertainties in meteorological datasets and analysis errors, transport pathway of air masses based on individual trajectories may not be very reliable to apportion the source regions (Wang et al., 2010). As an alternate, clustering of AMBTs over a receptor site through statistical analysis has been proposed as an effective way to assess the potential sources of ambient particulate matter (Borge et al., 2007; Stohl, 1998). The underlying principle of cluster analysis is to reduce the variability among trajectories within a cluster and to enlarge the variability among various clusters by considering the horizontal moving speed and direction of air masses. In this study, cluster analysis was performed for the sampling days through PC-based HYSPLIT graphical user interface (GUI, downloaded from the URL, <http://ready.arl.noaa.gov/HYSPLIT.php>) and using the meteorological (NCEP/NCAR reanalysis) datasets from the archived model outputs (Kim et al., 2005). The cluster analysis results are interpreted in terms of varying source strength of atmospheric outflow from the IGP to the BoB during three sampling time periods (November 2009; December 2009–February 2010 and March 2010) (see Fig. 1).

3. Results and discussion

3.1. Temporal variability of trace metals

The concentration of trace metals show pronounced temporal variability during the study period (November 2009–March 2010; Fig. 2). It is noteworthy that concentrations of Mn ($190 \pm 156 \text{ ng m}^{-3}$) and Pb ($121 \pm 72 \text{ ng m}^{-3}$) are considerably high compared to other trace metals. Further, the concentrations of Mn and Pb varied almost two orders of magnitude, variation ranging from 8 to 568 ng m^{-3} and 8–296 ng m^{-3} , respectively. In contrast, other trace metals exhibit variability by one order of magnitude, their range correspond to 5–33 ng m^{-3} ($12 \pm 6 \text{ ng m}^{-3}$) for Cr, 2–29 ng m^{-3} ($8 \pm 5 \text{ ng m}^{-3}$) for Cu, and 2–14 ng m^{-3} ($6 \pm 3 \text{ ng m}^{-3}$) for Ni. Similar temporal trends were observed for Mn and Cr, suggesting their common anthropogenic source. In this study, concentration of Co is lower ($0.5\text{--}1.6 \text{ ng m}^{-3}$; $\sim 1.0 \pm 0.2 \text{ ng m}^{-3}$) than other trace metals. Although Cd showed large variability ($1\text{--}30 \text{ ng m}^{-3}$), the mean atmospheric concentration is found to be somewhat lower than other trace metals (except Co). It is also evident from Fig. 2 that temporal variability of Cd is relatively less significant. Likewise, the temporal trends of Cu and to some extent Ni show small temporal variability in the IGP-outflow, quite similar to the temporal of Pb and Cu.

As the concentrations of trace metals from anthropogenic sources may be over-estimated due to their contribution from mineral dust, we have investigated the temporal variability based on mass ratios normalized with Al (Fig. 3). A close similarity in the temporal trends are noteworthy for Pb/Al, Cu/Al, and Cd/Al, suggesting their common source. These heavy metals enter the atmosphere through high temperature combustion processes such as emission from coal-fired power plants (Reddy et al., 2005). A number of coal-fired power plants in the eastern part of the Indo-Gangetic Plain (Nair et al., 2007) could serve as a dominant source for the atmospheric abundances of trace metals in the atmospheric outflow to the BoB. In this context, recent studies have documented heavy metal concentrations (Cr, Mn, Pb, Cu, Ni and Co) in the fly ash from coal fired power plants (Agrawal et al., 2010; Sushil and Batra, 2006). A similar temporal variability in Mn/Al, Cr/Al, Co/Al and Ni/Al ratios (Fig. 3) suggests their common source

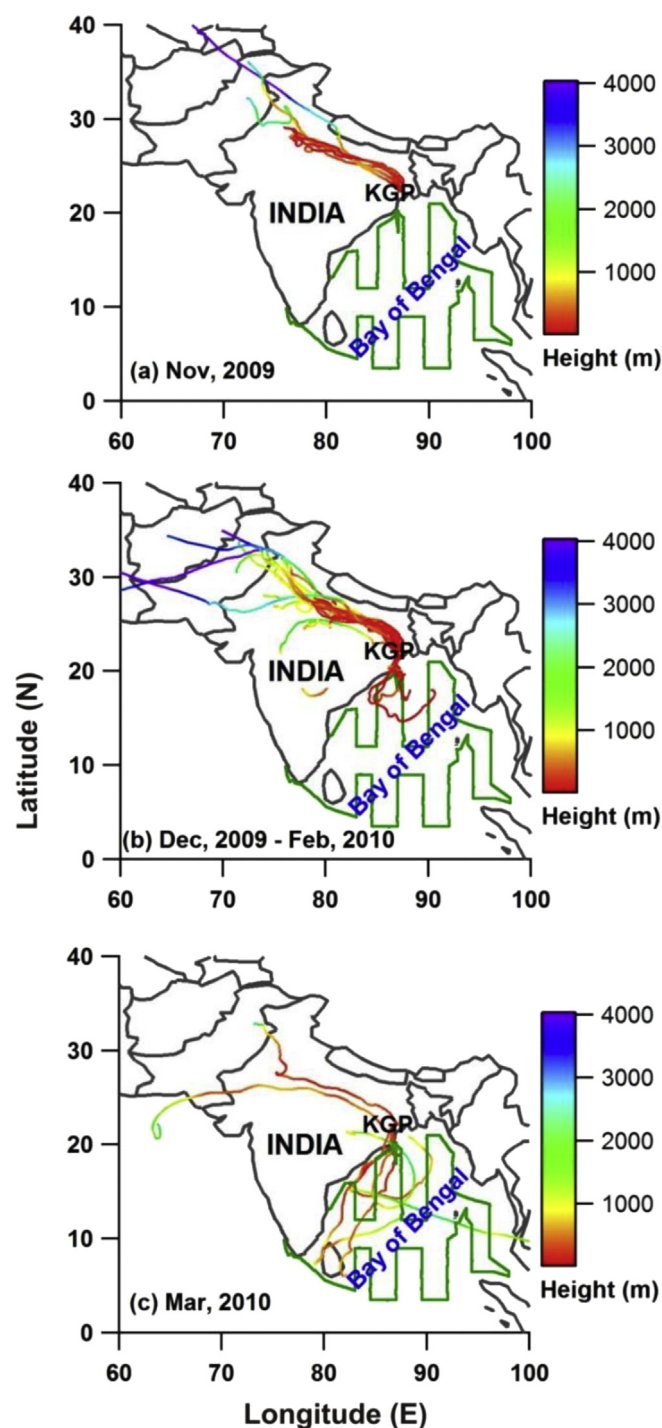


Fig. 1. Downwind sampling site (Kharagpur referred as KGP) in the Indo-Gangetic Plain and air mass back trajectories (AMBTs) for the three sampling periods: (a) November 2009, (b) December 2009–February 2010 and (c) March 2010. Also shown is a cruise track conducted in the Bay of Bengal in January 2009.

and/or transport pathway from upwind sources in the IGP.

A statistical summary of trace metals concentrations for the three sampling time periods (November 2009; December 2009–February 2010; March 2010) is described in Table 1. In addition, the temporal variability of mean atmospheric concentrations of trace metals during these three sampling periods is shown in Fig. 4. From this figure, it is noteworthy that higher concentrations of trace metals (except Pb, Cu and Ni) in winter

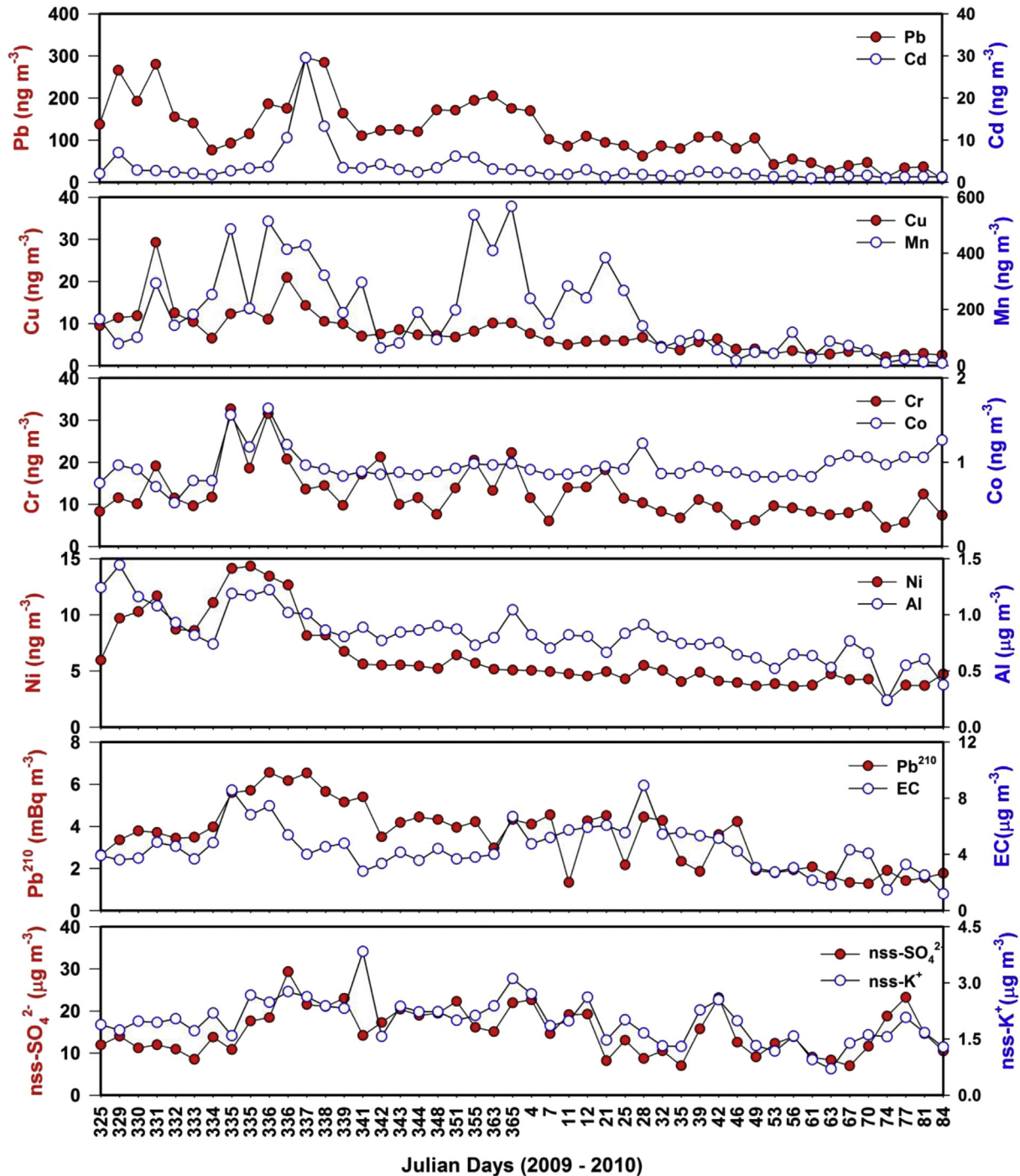


Fig. 2. Temporal variability in the atmospheric abundances of trace metals (Pb, Cd, Cu, Mn, Cr, Co and Ni), ^{210}Pb activity (this study) in $\text{PM}_{2.5}$ from the Indo-Gangetic Plain outflow to the Bay of Bengal. Data for chemical constituents (Al, elemental carbon (EC), nss-SO_4^{2-} and K^+) is from (Srinivas et al., 2014).

months (December 2009–February 2010) compared to those in preceding and subsequent sampling time periods (November 2009 and March 2010, respectively). The shallow atmospheric boundary layer height (~ 700 m; (Nair et al., 2007)) during the wintertime could result in efficient trapping of ground-based emissions to a lower height compared to pre- and post-NE-monsoon and, therefore, explains high concentrations of metals during December 2009–February 2010.

A similar seasonal pattern is also noteworthy for other anthropogenic chemical species such as EC, nss-SO_4^{2-} , and nss-K^+ (Fig. 4).

In contrast, a notable decreasing trend in the mass concentrations is observed for Pb, Cu and Ni during November 2009–March 2010 (Fig. 4). However, this feature is consistent with the temporal trend of Al reported by Srinivas et al. (2014). With these observations, we argue that the observed decrease in mean concentrations of Pb, Cu and Ni (Table 1) over the study site (Kharagpur) is associated with the long-range atmospheric transport of mineral dust. Although emitted from anthropogenic sources, these heavy metals are attached to mineral dust via condensation in the atmosphere. Srinivas et al. (2014) have documented a substantial decrease in

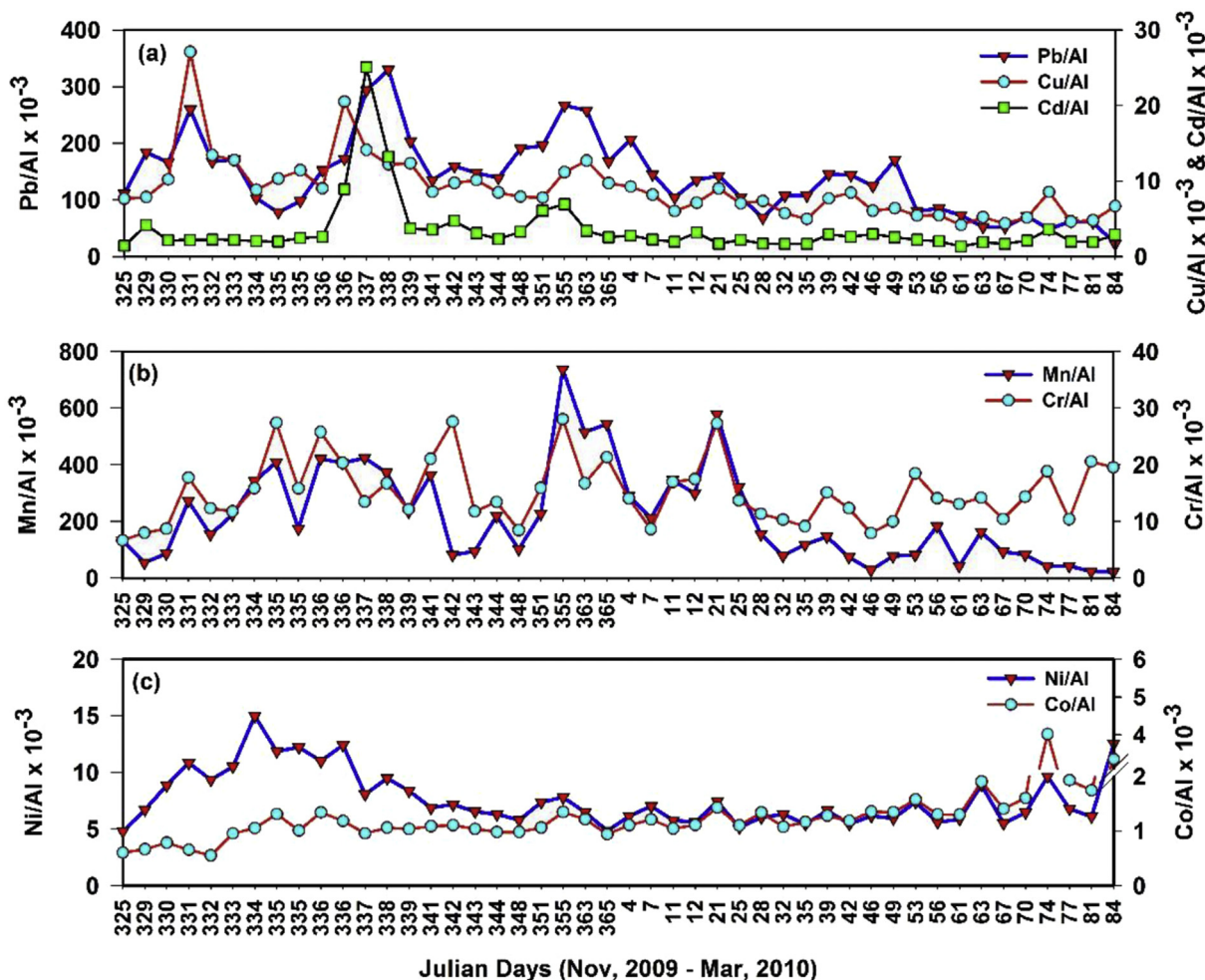


Fig. 3. Temporal variability in atmospheric abundances of trace metals (this study) normalized with Al in $PM_{2.5}$ sampled from the Indo-Gangetic Plain during November 2009–March 2010. Data for Al is from Srinivas and Sarin, 2014.

Table 1

Statistical summary of trace metal concentrations ($ng\ m^{-3}$) and ^{210}Pb activity ($mBq\ m^{-3}$) in $PM_{2.5}$ in the atmospheric outflow from the Indo-Gangetic Plain outflow. X_a and X_g refer to arithmetic and geometric mean concentration, respectively.

Element	Nov 2009 (N = 7)	Dec 2009–Feb 2010 (N = 31)	Mar 2010 (N = 8)
	Range (X_a , X_g & median)		
Pb	76–280 (178, 165, 155)	42–296 (132, 120, 110)	8–47 (31, 27, 35)
Cd	2.1–7.0 (3.0, 2.7, 2.4)	1.3–29.5 (4.2, 3.0, 2.7)	1.0–1.6 (1.3, 1.3, 1.3)
Cu	6.5–29.3 (13.1, 11.8, 11.4)	2.8–20.9 (7.8, 7.0, 7.1)	2.1–3.4 (2.8, 2.7, 2.7)
Mn	78–294 (174, 158, 165)	18–568 (233, 172, 198)	8–87 (37, 26, 25)
Cr	8–19 (12, 11, 4)	5–33 (14, 12, 12)	4.5–12.4 (7.9, 7.6, 7.7)
Co	0.5–1.0 (0.8, 0.8, 0.8)	0.8–1.6 (1.0, 1.0, 0.9)	0.8–1.3 (1.0, 1.0, 1.1)
Ni	6–12 (9, 9, 10)	3.6–14.3 (6.3, 5.8, 5.1)	2.3–4.7 (3.9, 3.8, 4.0)
^{210}Pb	2.6–5.6 (3.8, 3.7, 3.5)	1.3–6.6 (4.0, 3.6, 4.2)	1.3–1.9 (1.6, 1.6, 1.6)

mineral dust concentration in $PM_{2.5}$ (assessed based on Al abundance), sampled from Kharagpur during November 2009–March 2010. It is also relevant to state that the samples collected in pre NE-monsoon overlap with the time period of open biomass burning emissions in the IGP (October–November) during which significant amount of dust is injected into the atmosphere. A comparison of trace metal concentrations from this study with other geographical locations in south and south-east Asia is presented in Table 2. It is implicit from Table 2 that heavy metal concentrations from IGP are somewhat lower than those reported over Southeast Asian regions such as Beijing, Taiwan and Vietnam and are consistent with that

documented over Japan.

Furthermore, multiple linear regression analysis with chemical constituents ($nss-SO_4^{2-}$, $nss-K^+$, etc.) provide insight of the possible sources of trace metals in the atmospheric outflow from the Indo-Gangetic Plain. The Pearson's correlation coefficient matrix computed for all three sampling periods (Table S1 in the supporting information) shows significant correlation among Pb, Cd, and Cu, suggesting their common anthropogenic source. Likewise, correlation of heavy metals with Al (Table S1) indicate their condensation on mineral dust in the continental outflow. Although significant correlations were observed among other trace metals

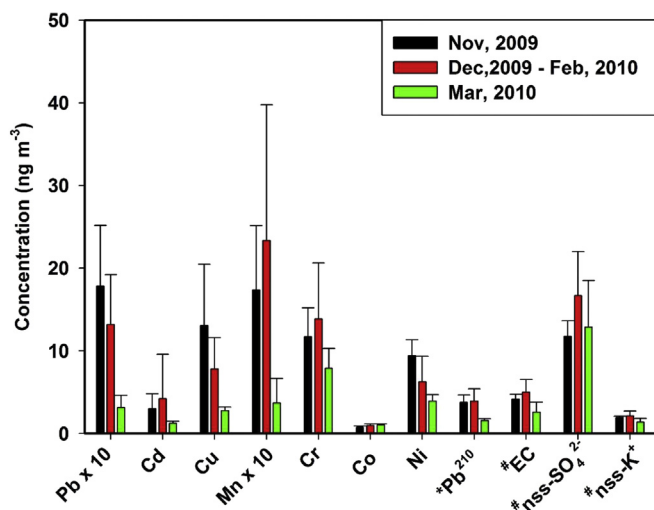


Fig. 4. Comparison of atmospheric concentrations of trace metals (Pb, Cd, Cu, Mn, Cr, Co and Ni), ^{210}Pb and anthropogenic species (EC, nss-SO_4^{2-} and nss-K^+) in $\text{PM}_{2.5}$ during different seasons as sampled from the Indo-Gangetic Plain outflow. # refer to data obtained from Srinivas and Sarin (2014).

(Ni, Cr and Cu), their sources were not well recognised in the literature, suggesting contribution from multiple sources. However, emissions from coal-fired power plants in the IGP is the dominant source of heavy metals (Pb, Cd, Cu, Cr and Mn). Therefore, it is logical to argue that the long-range transport of heavy metals absorbed on mineral dust is evident from their significant linear relationship.

3.2. Source apportionment

Five-day three-hourly isentropic AMBTs at 100 m a.g.l. have been used for the cluster analysis in order to apportion the sources of airborne trace metals over the study site (Kharagpur). We have identified three clusters and their fractional contribution to total air masses transported to the receptor site (Kharagpur located in IGP) are calculated for the three sampling periods (pre-, NE- and post-NE-monsoon). Fig. 5 depicts the mean trajectory paths over the sampling site in IGP for each of these three sampling periods (November 2009; December 2009–February 2010 and March 2010). The maximum contribution comes from cluster one that clearly shows long-range transport from upwind pollution sources in the IGP (Punjab, Haryana, Delhi, Uttar Pradesh, and West Bengal). Among the three sampling periods, the percentage contribution

from cluster one show higher values in the winter (December 2009–February 2010; 84%) compared to pre-NE-monsoon (November 2009; 64%) and post-NE-monsoon (March 2009; 51%). Although the percentage contribution from cluster one and two varied significantly among the three sampling periods, however, no noticeable difference is observed in the transport pathways of air masses to the receptor site (Kharagpur, IGP). A relatively small percentage contribution of air masses from the BoB to the sampling site is also noteworthy during March 2009.

3.3. Diagnostic ratios

The impact of biomass/bio-fuel burning emissions and fossil-fuel combustion sources from the Indo-Gangetic Plain, during the late NE-monsoon (December–March), on the MABL of the Bay of Bengal have been documented in the literature (Gustafsson et al., 2009; Rengarajan et al., 2007; Srinivas et al., 2011)). In order to assess the contribution of anthropogenic sources to airborne trace metals during the continental outflow, we have made use of diagnostic ratios of chemical constituents and their inter-element relationships. A comparison of diagnostic ratios of trace metals in $\text{PM}_{2.5}$ (normalized with EC, nss-SO_4^{2-} and nss-K^+) within the IGP (December 2009–February 2010) and those associated with the IGP-outflow sampled over the BoB (December 2008–January 2009; (Srinivas and Sarin, 2013b)) is presented in Fig. S1. Emissions from coal-fired power plants are dominant source of EC and nss-SO_4^{2-} ; whereas nss-K^+ and significant fraction of EC are contributed from the vegetation burning. Thus, their occurrence in $\text{PM}_{2.5}$ is generally taken as contribution from biomass burning emissions (BBEs) (Andreae, 1983).

The diagnostic ratios (Fig. S1) from study site in the IGP are higher than those documented in the IGP-outflow sampled over the BoB. Although similar wind regimes and same size fraction ($\text{PM}_{2.5}$) have been analysed from the two study regions, differences in diagnostic ratios (Fig. S1) cannot be explained by temporal variability in the source strength. It is likely that differences in the diagnostic ratios (at study site and over the BoB) are influenced by association of heavy metals with fine mode mineral dust (Alluvium), and thus, leading to their efficient removal from the atmosphere during downwind transport.

3.4. Temporal variability of ^{210}Pb and residence time of $\text{PM}_{2.5}$

The ^{210}Pb activity shows pronounced temporal variability (Fig. 2), and ranged from 1.3 to 6.6 mBq m^{-3} ($3.5 \pm 1.5 \text{ mBq m}^{-3}$). The ^{210}Pb activity levels are higher during the pre-NE-monsoon (November 2009: 2.6–5.6 mBq m^{-3} ; Fig. 4) and NE-monsoon

Table 2
Comparison of mean mass concentrations (ng m^{-3}) of trace metals in atmospheric outflow from the Indo-Gangetic Plain with a few studies in the literature.

Region	Pb	Cd	Cu	Mn	Cr	Co	Ni	Reference
Indo-Gangetic Plain	8.4–296 (121)	1.0–29.5 (3.5)	2.1–29.3 (7.7)	8–568 (190)	4.5–32.6 (12.5)	0.5–1.6 (1.0)	2.3–14.3 (6.3)	This study
Bay of Bengal	2.4–41 (21)	0.04–2.0 (0.8)	0.5–7.5 (2)	1–113 (19)	1.0–8.2 (2.6)	0.03–0.3 (0.1)	0.4–4.3 (0.8)	Srinivas and Sarin, 2014
Ahmedabad, India	28–1023	0.1–5.4	2.3–32.8	5.5–226	<1–38.4	–	<1–7.2	Sudheer & Rengarajan, 2012
Tokyo, Japan	125	–	30	–	6.1	–	–	Var et al. (2000)
Vietnam, Ho Chi Minh	146	–	1.3	–	8.6	–	–	Hien et al., 2001
Taiwan, Taichung	574	8.5	199	–	29.3	–	–	Fang et al. (2003)
Ulleung Island (Japan/East Sea)	4.4–35.8 (20)	–	2.8–66.7 (23.5)	–	–	0.04–1.4 (0.3)	0.9–4.6 (2.6)	Kang et al. (2009)
Mediterranean Sea	24.9	0.22	5.9	16.7	2.3	–	–	Koçak et al. (2004)
Gulf of Aqaba	7	0.1	3.4	16.7	3.0	0.3	2.8	Chen et al. (2008)
East China Sea	17	0.5	58	16	3.7	0.25	1.5	Hsu et al. (2010)
Irish Sea	43	–	21	8.4	2.1	0.4	3.0	Chester et al. (2000)
Beijing, China	430	6.8	110	–	19	–	–	Okuda et al., 2004

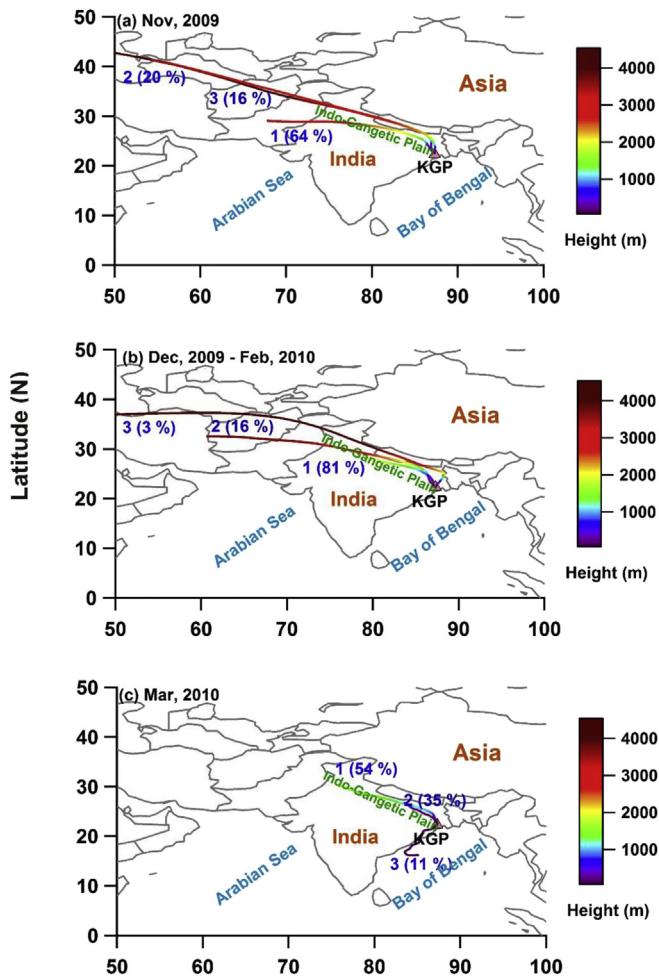


Fig. 5. Cluster analysis performed by PC-based version of HYSPLIT and using GDAS archived datasets. The colour indicates the height of the trajectories. (For interpretation of the references to colour in this figure legend, the reader is referred to the web version of this article.)

(December, 2009–February, 2010; 1.3–6.6 mBq m⁻³; Fig. 4) compared to that in the post NE-monsoon (March 2010: 1.3–1.9 mBq m⁻³; Fig. 4). The seasonal differences (Table 1) are further ascertained from the one-way ANOVA analysis [F (2, 43) = 11.2; P-value < 0.05; N = 46]. The high levels of ²¹⁰Pb activity in November 2009 and December 2009–February 2010 can be attributed to contribution from post-harvest agricultural-waste (from paddy-crop) burning emissions in the IGP during October–November. A supporting argument for this inference comes from our earlier study, documenting similar increase in atmospheric abundances of PM_{2.5}, OC and K⁺ during November 2009 and December 2009–February 2010 due to contribution from biomass burning emissions (Srinivas and Sarin, 2014). Hammer et al. (2007) had interpreted similar temporal trends of ²¹⁰Pb and OC due to their common transport pathways from the source region.

Studies reported in the literature have documented high activity levels of ²¹⁰Pb and its decay product, ²¹⁰Po, in Savannah forest fires and biomass burning plumes (Carvalho, 1995; Lambert et al., 1991; Nho et al., 1996). In this study, it is likely that during crop-residue burning in agricultural fields (and with rise in ambient temperature) could change the soil porosity. Thus, enhanced emanation of

²²²Rn and subsequent decay to ²¹⁰Pb could explain the observed high levels of ²¹⁰Pb activity during November 2009. Although the source strength of agricultural-waste burning emissions significantly decreases during December 2009–February 2010, the accumulation of ²²²Rn under stable atmospheric conditions together with the shallow boundary layer height could result in enhanced ²¹⁰Pb activity in the wintertime (December 2009–February 2010). The seasonal variability of ²¹⁰Pb activity (this study) is also consistent with results reported by Ram and Sarin (2012) from an urban site (Kanpur: 26.5°N and 80.3°E) in the IGP. Therefore, high activity levels of ²¹⁰Pb during the continental outflow from the IGP could be a combination of contribution from biomass burning emissions and the accumulation of ²²²Rn under stable atmospheric conditions.

In order to assess the impact of trace metals on the MABL of BoB, it is important to ascertain the residence time of PM_{2.5} in the atmospheric outflow from the IGP. In this study, we have estimated the mean residence time of PM_{2.5} during the continental outflow to the BoB using environmental radionuclide ²¹⁰Pb. It has been suggested that environmental radionuclides (²¹⁰Pb and ²¹⁰Po) can be used to estimate the residence time of airborne particulates (Baskaran, 2011; Rastogi and Sarin, 2013). In this context, earlier studies have used ²²²Rn–²¹⁰Pb and ²¹⁰Pb–²¹⁰Po pairs to assess the aerosol residence time at various geographical locations (Kim et al., 2000; McNeary and Baskaran, 2007). In this study, ²¹⁰Pb based residence time of PM_{2.5} is estimated similar to the approach of Rastogi and Sarin (2013). The ²¹⁰Pb is a decay product of ²²²Rn emanating continuously from surface soils. Due to the short half-life of ²²²Rn (t_{1/2}–3.8 days), it decays to produce ²¹⁰Pb in the atmosphere, which in turn gets attached to ambient aerosols. Since ²²²Rn fluxes from the soil are relatively well constrained (Rastogi and Sarin, 2013 and references therein), the residence time (τ) of aerosols can be best estimated by measuring the ambient ²¹⁰Pb activity. Under steady state conditions, the production rate of a radionuclide of interest is equal to its decay rate and removal by dry or wet deposition (Rastogi and Sarin, 2013). Under steady state conditions, we have

$$\frac{dN_{Pb-210}}{dt} = \lambda_{Rn-222}N_{Rn-222} - \lambda_{Pb-210}N_{Pb-210} - \lambda_R N_{Pb-210} \quad (1)$$

In this equation, $\lambda_{Rn-222}N_{Rn-222}$ is the production rate of ²¹⁰Pb or activity (A) of ²²²Rn. Likewise, $\lambda_{Pb-210}N_{Pb-210}$ corresponds to decay rate of ²¹⁰Pb in the atmosphere. The term, $\lambda_R N_{Pb-210}$ is the removal rate of ²¹⁰Pb from the atmosphere in which λ_R refer to first order rate constant (= 1/τ_{aero}; where τ_{aero} is the residence time) for the removal of aerosols (i.e., mainly by dry- or wet fall out) to which ²¹⁰Pb gets attached in the atmosphere. Thus, above equation can be transformed as follows after rearranging.

$$\frac{dN_{Pb-210}}{dt} = A_{Rn-222} - A_{Pb-210} - \left(\frac{1}{\tau_{aero}}\right)N_{Pb-210} \quad (2)$$

$$\tau_{aero} = \left(\frac{1}{\lambda_{Pb-210}} \frac{A_{Pb-210}}{A_{Rn-222}}\right) / \left(1 - \frac{A_{Pb-210}}{A_{Rn-222}}\right) \quad (3)$$

Decay constant (λ_{Pb-210}) = ln2/(t_{1/2}–Pb210); t_{1/2} is the half-life of ²¹⁰Pb (22.3 years).

Using Equation (3), we have estimated the residence time based on measured ²¹⁰Pb activity (expressed in milli Becquerel per cubic meter; mBq m⁻³) in PM_{2.5} sampled over IGP during the continental outflow to the BoB. However, Rn²²² activity is adopted from Rastogi and Sarin (2013) as 1.2 atoms cm⁻² sec⁻¹, originally suggested by Turekian et al. (1977).

In Equation (3), A_{Pb-210} refers to activity of ²¹⁰Pb atoms present

in the air for a given columnar height in which aerosol residence time need to be estimated. In this regard, Turekian et al. (1977) have suggested that ^{210}Pb exhibits variability up to an altitude of ~6 km above the ground level and, therefore, can be assumed as uniform for assessing the residence time of aerosols below this height. Since most of the aerosols are confined within the atmospheric boundary layer of IGP during the continental outflow, we have selected 2 km height for estimating the residence time of $\text{PM}_{2.5}$. Based on the measured ^{210}Pb activity, we have estimated the average residence time of $\text{PM}_{2.5}$ over IGP during the continental outflow, which corresponds to 7 days (range: 2–13 days). The temporal variability in the residence time of $\text{PM}_{2.5}$ over IGP is depicted in Fig. S2. The mean residence time of (~7 days) of $\text{PM}_{2.5}$ in the IGP-outflow, thus, indicate the considerable influence of trace metals on surface waters of BoB via air-sea deposition.

3.5. Enrichment factors – biogeochemical significance

We have estimated the enrichment factors (EF_{crust}) to determine which trace metals in the continental outflow originate from the crustal source vis-à-vis their anthropogenic emission. EF_{crust} is obtained by normalizing the mass ratio of metal (M) to Al in $\text{PM}_{2.5}$ with that documented for upper continental crust (UCC; (McLennan, 2001 and references therein)).

$$\text{EF}_{\text{crust}} = \frac{\left(\frac{M}{Al}\right)_{\text{aerosol}}}{\left(\frac{M}{Al}\right)_{\text{UCC}}} \quad (4)$$

Chester et al. (1993) had reported that trace metals with an EF_{crust} greater than 10 are described as anomalously enriched elements (AEE) and less than 10 are referred as non-enriched elements (NEE). It is also implicit that AEEs can have significant contribution from non-crustal origin (or anthropogenic sources).

The EF_{crust} for Pb, Cd, Cu, Mn, Cr, Co and Ni in the IGP-outflow (November 2009–March 2010), varied from 105 to 1561, 1265 to 24006, 13 to 87, 3 to 99, 7 to 27, 3 to 19, and 9 to 27, respectively (Table S2). However, these enrichment factors are comparable with that in the air masses sampled over the BoB originating from the IGP (December 2008–January 2009) (Srinivas and Sarin, 2013b). Fig. 6 depicts the box-whisker plots, showing the comparison of EF_{crust} of trace metals over IGP during November 2009–March 2010 with

IGP-outflow sampled over the BoB during December 2008–January 2009 (Srinivas and Sarin, 2013b)). In Fig. 6, it is noteworthy that the EF_{crust} for Pb, Cd, Cu and Mn show higher values (i.e., >10) in the IGP-outflow and, therefore, considered as AEEs. This observation is also consistent with our earlier finding from the BoB during the continental outflow from IGP (Srinivas and Sarin, 2013b). Overall, the overwhelming contribution of heavy metals from the anthropogenic sources (coal fired power plants, metal smelters and gasoline combustion emissions), over crustal sources, could explain their high EF_{crust} . The enrichment factors for Cr, Co and Ni are significantly lower and, hence, considered as NEEs. These trace metals have significant contribution from the crustal source.

The high EF_{crust} of trace metals in the IGP-outflow suggest significant influence on their biogeochemical cycles in surface waters of BoB. In this context, Echegoyen et al. (2014) reported higher Pb concentration in the Indian Ocean, which is attributed to emissions from south Asia as a consequence of late phasing out of leaded gasoline. Their study also suggests that Pb concentrations in the Indian Ocean are somewhat higher than those reported in the North Atlantic and the North Pacific. Likewise, the Pb concentrations and isotopic composition from the coral reefs reveal contribution from anthropogenic sources over the Indian Ocean (Boyle et al., 2014; Lee et al., 2014). Combining our results (high EF_{Pb} in the IGP-outflow, Table S2) with studies reported in the literature, we suggest that emissions of Pb from South Asia during the continental outflow are responsible for its enhanced concentration in the MABL.

Recent measurements on dissolved trace metals (Al, Fe, Pb, Mn, Co, and Ni) from the North Indian Ocean (Vu and Sohrin, 2013) also reveal significant impact of outflow from south Asia via air-sea deposition. In this context, aerosol toxicity on marine phytoplankton has been emphasized for BoB, which is mainly attributed to the presence of high atmospheric abundances of Cu (Guo et al., 2011; Paytan et al., 2009). In contrast, addition of atmospheric aerosols sampled over the Sargasso Sea to natural phytoplankton assemblages, resulted in enhanced (~10 fold increase) *Synechococcus* spp., population (Mackey et al., 2012). The phytoplankton growth is ascribed to the presence of Co, Mn and Ni in marine aerosols (Mackey et al., 2012). Given this scenario, the observed higher atmospheric abundances of these trace metals (Co, Mn and Ni) and their EF_{crust} in the IGP-outflow (Table S2) suggests the downwind transport and subsequent impact on surface waters of

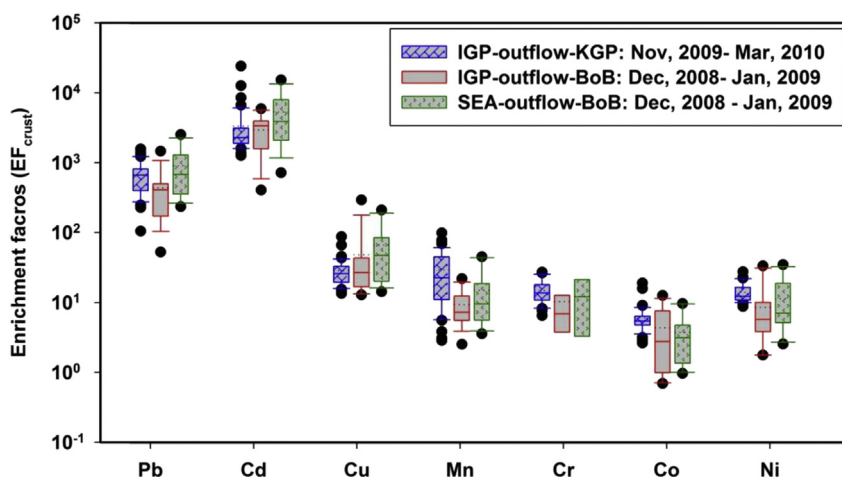


Fig. 6. Box-whiskers for crustal enrichment factors (EF_{crust}), defined as the ratio of mass concentration of metal to Al in aerosols to that documented for upper continental crust (McLennan, 2001), of trace metals (Pb, Cd, Cu, Mn, Cr, Co and Ni) in $\text{PM}_{2.5}$ sampled from the Indo-Gangetic Plain outflow to the Bay of Bengal during November 2009–March 2010. The lower and upper edges of Boxes correspond to 25 and 75 percentile, while the solid and dashed lines in the Box represent median (or 50 percentile) and mean values. The lower and upper whiskers are 5 and 95 percentile, respectively, the black dots are outliers in the data which are <5 and >95 percentile data points.

BoB via air-sea deposition.

3.6. Dry depositional fluxes

Since the mean atmospheric residence time of PM_{2.5} is estimated to be seven days, it is therefore relevant to assess the dry-deposition fluxes over the sampling site in IGP and can be taken as similar to air-sea deposition to the BoB. The dry-deposition fluxes were estimated as atmospheric concentrations of trace metals (C_M) times the dry-deposition velocity (V_d) (Srinivas and Sarin, 2013b and references therein).

$$\text{Dry-deposition flux} = C_M \times V_d \quad (5)$$

The V_d is difficult to constrain and depends on various meteorological parameters such as wind speed, atmospheric stability, relative humidity, terrain roughness, and also particle size etc. All these factors introduce an overall uncertainty of about a factor 2–3 on the estimated deposition fluxes (Duce et al., 1991; Hsu et al., 2010).

Since we have studied the PM_{2.5} fraction, a V_d of 0.1 cm s⁻¹ is used for estimating the deposition fluxes. Since the EF_{crust} of Pb, Cd and Cu are greater 10, these trace metals might have originated from high temperature combustion processes and, therefore, mostly exists in fine mode (Duce et al., 1991; Hsu et al., 2010). However, the chosen V_d (0.1 cm s⁻¹) for these anthropogenic trace metals can be justified owing to their high EF_{crust} . Similar V_d of 0.1 cm s⁻¹ for Pb, Cd, Cu, Mn Cr, Co and Ni have been used elsewhere by several researchers (Chen et al., 2008; Hsu et al., 2010; Srinivas and Sarin, 2013b). A statistical summary for the range, mean and standard deviation of dry-deposition fluxes of trace metals over IGP during Pre-NE-monsoon, NE-monsoon and Post-NE-monsoon is presented in Table S3. It is implicit from Table S3 that air-sea deposition of fine alluvial dust to the BoB (this study), assessed based on Al concentration in PM_{2.5} over IGP, is somewhat higher in Pre-NE-monsoon compared to NE-monsoon or Post-NE-monsoon. As mentioned earlier, a likely explanation for this would be due to dust intrusion during crop-residue burning activity (during October–November) in the IGP.

3.7. Residence time of trace metals in the BoB

Since BoB is influenced by the IGP-outflow, we have estimated the residence time of trace metals (τ) in the surface ocean using their mean atmospheric deposition fluxes from Table S3 and seawater concentrations (C_{sw} , expressed in nmol kg⁻¹) from the recent GEOTRACES Japanese expedition (Vu and Sohrin, 2013). This approach of estimating residence time of trace metals is similar to that described in Srinivas and Sarin (2013b).

$$\text{Residence time of trace metal } (\tau \text{ yrs.}) = C_{\text{sw}} * Z_{\text{mix}} / (f_{\text{dry}} * [\text{F.S.}]_{\text{metal}}) \quad (6)$$

Here, Z_{mix} refers to mixed layer depth in the BoB (~30 m, (Narvekar and Prasanna Kumar, 2006)) and $[\text{F.S.}]_{\text{metal}}$ corresponds to fractional solubility of trace metal in PM_{2.5}. The precipitation events over the BoB during the continental outflow are not significant, based on tropical rainfall measurement mission (TRMM) (Srinivas and Sarin, 2013b). In addition, the chemical composition of marine aerosols during a summer cruise reveal weak continental impact over the BoB (Sarin et al., 2010). Therefore, estimated dry-deposition fluxes of trace metals over IGP (Table S3) represent the total atmospheric deposition to the BoB.

In a previous study, Srinivas and Sarin (2013b) have documented that soluble iron is mainly associated with alluvial mineral dust in the IGP-outflow. Further, the EF_{crust} of Fe from this study (<10; see Table S2) indicate its contribution from crustal source. Therefore, the fractional solubility of trace metals for which EF_{crust} is less than 10 (NEEs) is assumed to be similar to that of mineral dust (~15%; (Srinivas et al., 2014)). In contrast, the trace metals with high EF_{crust} (i.e., AEEs) can have significant contribution from anthropogenic sources. Numerous studies documented high fractional solubility for the trace metals that are of anthropogenic origin (Echegoyen et al., 2014; Schroth et al., 2009; Sholkovitz et al., 2010). Therefore, we have estimated the residence time of trace metals by assuming their fractional solubility as 15% and 100% for natural (or dust) and anthropogenic sources, respectively, are controlling the solubility (see Table 3). Although 100% solubility is unrealistic, it is still considered to estimate the case for the maximum solubility from anthropogenic sources over mineral dust (if it is higher).

The estimated residence time, with mean atmospheric deposition in the IGP-outflow from this study (November 2009–March 2010) and using solubility range of 15–100% for Pb, Cd, Cu and Mn, varied from 3 to 0.3, 45 to 4.5, 284 to 28.4 and 20 to 2.0 yrs, respectively. The uncertainty in the estimation of residence time of trace metals using Equation (6) largely comes from the atmospheric deposition fluxes that have an inherent uncertainty with respect to assumed dry-deposition velocity (i.e., a factor 2–3). Among the trace metals, the residence time of Pb, Cd and Cu are consistent with that documented for the Gulf of Aqaba (Chen et al., 2008) and also with documented for the BoB (Srinivas and Sarin, 2013b). Likewise, the residence time of Mn, Co and Ni in surface waters of the BoB using their mean dry-deposition flux in Table S3 turns to be 30, 89 and 641 yrs, respectively. The reported seawater concentrations of Al, Mn and Co by Vu and Sohrin (2013), show enrichment in the surface waters of BoB, which is attributed to their contribution from atmospheric deposition. On the other hand, their study documented that Fe and Ni are depleted in surface waters of the BoB, which is explained by invoking their uptake by marine phytoplankton and scavenging in the water column (2013).

Table 3

Estimated residence time (τ) of trace metals with respect to dry-deposition fluxes in the outflow from the Indo-Gangetic Plain and seawater concentrations from the Bay of Bengal (Vu and Sohrin, 2013).

Metal	f_{dry} ($\mu\text{g m}^{-2} \text{day}^{-1}$)			C_{sw} (nmol/kg)	τ (yrs)- with min f_{dry}		τ (yrs)- with max f_{dry}		τ (yrs)- with Mean f_{dry}	
	min	max	av		#min	\$max	#min	\$max	#min	\$max
Pb	0.72	25.62	10.49	0.08	46	5	1.3	0.1	3	0.3
Cu	0.18	2.53	0.67	1.50	1058	106	75.3	7.5	284	28.4
Mn	0.7	49.05	16.43	3.00	471	47	6.7	0.7	20	2.0
Cd	0.08	2.55	0.3	0.06	169	17	5.3	0.5	45	4.5
Co	0.04	0.14	0.08	0.04	118	12	33.7	3.4	59	5.9
Ni	0.2	1.24	0.55	2.00	1174	117	189.3	18.9	427	42.7

Note: # and \$ refer to estimated residence time of trace metal by assuming its fraction solubility of 10 and 100% in the dry-deposition.

However, their concentrations in surface waters could be influenced by atmospheric input. By combining our observations (elevated concentrations, high EF_{Crust} , residence time of $PM_{2.5}$ over IGP during the continental outflow) with the literature data, we argue that air-sea deposition of heavy metals from anthropogenic sources can have significant influence on the surface waters of BoB.

4. Conclusions

This study highlights the significance of anthropogenic trace metals and Pb^{210} activity in the continental outflow from Indo-Gangetic Plain to the BoB. During the continental outflow (December–March), measured trace metals and ^{210}Pb activity show pronounced temporal variability. The isentropic air-mass back trajectories (5-day) together with covariability between trace metals and ^{210}Pb suggests their common advective transport from the upwind source regions of IGP. Likewise, significant linear correlation with chemical constituents ($nss-SO_4^{2-}$, $nss-K^+$ and EC) also suggests their anthropogenic nature. The abundances and enrichment factors of Pb, Cd, Cu and Mn (relative to crust) over the IGP and in the IGP-outflow sampled over BoB suggest their non-crustal origin (from anthropogenic sources). The ^{210}Pb based residence time of $PM_{2.5}$ over IGP during the continental outflow to the BoB varied from 2 to 13 days with mean value of about 7 days. The biogeochemical significance of air-sea deposition of heavy metals in the IGP-outflow to the BoB needs further evaluation with coupled ocean-atmosphere models to understand their impact on surface waters.

Acknowledgements

We thank the ISRO-Geosphere and Biosphere Programme (GBP) for financial support. We also thank A. Sarkar and T.K. Dalai for their logistical help in aerosol samples collection at IIT, Kharagpur.

Appendix A. Supplementary data

Supplementary data related to this article can be found at <http://dx.doi.org/10.1016/j.atmosenv.2015.10.044>.

References

- Abdalmogith, S.S., Harrison, R.M., 2005. The use of trajectory cluster analysis to examine the long-range transport of secondary inorganic aerosol in the UK. *Atmos. Environ.* 39, 6686–6695.
- Agrawal, P., Mittal, A., Prakash, R., Kumar, M., Singh, T.B., Tripathi, S.K., 2010. Assessment of contamination of soil due to heavy metals around coal fired thermal power plants at Singrauli region of India. *Bull. Environ. Contam. Toxicol.* 85, 219–223.
- Andreae, M.O., 1983. Soot carbon and excess fine potassium: long-range transport of combustion-derived aerosols. *Science* 220, 1148–1151.
- Balasubramanian, R., Karthikeyan, S., Potter, J., Wurl, O., Durville, C., 2013. Chemical characterization of aerosols in the equatorial atmosphere over the Indian Ocean. *Atmos. Environ.* 78, 268–276.
- Baskaran, M., 2011. Po-210 and Pb-210 as atmospheric tracers and global atmospheric Pb-210 fallout: a review. *J. Environ. Radioact.* 102, 500–513.
- Borge, R., Lumbreras, J., Vardoulakis, S., Kassomenos, P., Rodríguez, E., 2007. Analysis of long-range transport influences on urban PM_{10} using two-stage atmospheric trajectory clusters. *Atmos. Environ.* 41, 4434–4450.
- Boyle, E.A., Lee, J.-M., Echegoyen, Y., Noble, A., Moos, S., Carrasco, G., Zhao, N., Kayser, R., Zhang, J., Gamo, T., 2014. Anthropogenic lead emissions in the ocean. *Oceanography* 69.
- Carvalho, F.P., 1995. Origins and concentrations of ^{222}Rn , ^{210}Pb , ^{210}Bi and ^{210}Po in the surface air at Lisbon, Portugal, at the Atlantic edge of the European continental landmass. *Atmos. Environ.* 29, 1809–1819.
- Chen, Y., Paytan, A., Chase, Z., Measures, C., Beck, A.J., Sañudo-Wilhelmy, S.A., Post, A.F., 2008. Sources and fluxes of atmospheric trace elements to the Gulf of Aqaba, Red Sea. *J. Geophys. Res.* Atmos. (1984–2012) 113.
- Chester, R., et al., 2000. Trace metal chemistry of particulate aerosols from the UK mainland coastal rim of the NE Irish sea. *Atmos. Environ.* 34 (6), 949–958.
- Chester, R., Murphy, K.J.T., Lin, F.J., Berry, A.S., Bradshaw, G.A., Corcoran, P.A., 1993. Factors controlling the solubilities of trace metals from non-remote aerosols deposited to the sea surface by the 'dry' deposition mode. *Mar. Chem.* 42, 107–126.
- de Leeuw, G., Guieu, C., Arneft, A., Bellouin, N., Bopp, L., Boyd, P.W., van der Gon, H.A.D., Desboeufs, K.V., Dulac, F., Facchini, M.C., 2014. Ocean–atmosphere Interactions of Particles, Ocean–Atmosphere Interactions of Gases and Particles. Springer, pp. 171–246.
- Draxler, R., Rolph, G., 2009. HYSPLIT (Hybrid Single-particle Lagrangian Integrated Trajectory) Model Access via NOAA ARL READY Website. NOAA Air Resources Laboratory, Silver Spring, MD, p. 2003.
- Draxler, R., Stunder, B., Rolph, G., Stein, A., Taylor, A., 2012. HYSPLIT 4 User Guide Overview.
- Duce, R., Liss, P., Merrill, J., Atlas, E., Buat-Menard, P., Hicks, B., Miller, J., Prospero, J., Arimoto, R., Church, T., 1991. The atmospheric input of trace species to the world ocean. *Glob. Biogeochem. Cycles* 5, 193–259.
- Echegoyen, Y., Boyle, E.A., Lee, J.-M., Gamo, T., Obata, H., Norisuye, K., 2014. Recent distribution of lead in the Indian Ocean reflects the impact of regional emissions. *Proc. Natl. Acad. Sci.* 111, 15328–15331.
- Fang, Guor-Cheng, et al., 2003. Characterization of particulate, metallic elements of TSP, $PM_{2.5}$ and $PM_{2.5-10}$ aerosols at a farm sampling site in Taiwan, Taichung. *Sci. Total Environ.* 308 (1), 157–166.
- Grand, M.M., Hatta, M., Hiscock, W.T., Buck, C.S., Landing, W.M., 2015. Dust deposition in the eastern Indian Ocean: the ocean perspective from Antarctica to the Bay of Bengal. *Glob. Biogeochem. Cycles* 29, 357–374.
- Guo, C., Yu, J., Ho, T., Chen, B., Wang, L., Song, S., Kong, L., Liu, H., 2011. Dynamics of phytoplankton community structure in the South China Sea in response to the East Asian aerosol input. *Biogeosci. Discuss.* 8, 6637.
- Guo, L., Chen, Y., Wang, F., Meng, X., Xu, Z., Zhuang, G., 2014. Effects of Asian dust on the atmospheric input of trace elements to the East China Sea. *Mar. Chem.* 163, 19–27.
- Gustafsson, Ö., Kruså, M., Zencak, Z., Sheesley, R.J., Granat, L., Engström, E., Praveen, P., Rao, P., Leck, C., Rodhe, H., 2009. Brown clouds over South Asia: biomass or fossil fuel combustion? *Science* 323, 495–498.
- Hammer, S., Wagenbach, D., Preunkert, S., Pio, C., Schlosser, C., Meinhardt, F., 2007. Lead-210 observations within CARBOSOL: a diagnostic tool for assessing the spatiotemporal variability of related chemical aerosol species? *J. Geophys. Res.* Atmos. 112, D23S03.
- Hsu, S.-C., Wong, G.T.F., Gong, G.-C., Shiah, F.-K., Huang, Y.-T., Kao, S.-J., Tsai, F., Candice Lung, S.-C., Lin, F.-J., Lin, I.L., Hung, C.-C., Tseng, C.-M., 2010. Sources, solubility, and dry deposition of aerosol trace elements over the East China Sea. *Mar. Chem.* 120, 116–127.
- Jickells, T., An, Z., Andersen, K.K., Baker, A., Bergametti, G., Brooks, N., Cao, J., Boyd, P., Duce, R., Hunter, K., 2005. Global iron connections between desert dust, ocean biogeochemistry, and climate. *Science* 308, 67–71.
- Kang, J., Choi, M.-S., Yi, H.-I., Song, Y.-H., Lee, D., Cho, J.-H., 2011. A five-year observation of atmospheric metals on Ulleung Island in the East/Japan Sea: temporal variability and source identification. *Atmos. Environ.* 45, 4252–4262.
- Kang, Jeongwon, Choi, Man-Sik, Lee, Chang-Bok, 2009. Atmospheric metal and phosphorus concentrations, inputs, and their biogeochemical significances in the Japan/East Sea. *Sci. Total Environ.* 407 (7), 2270–2284.
- Kedia, S., Ramachandran, S., Kumar, A., Sarin, M., 2010. Spatiotemporal gradients in aerosol radiative forcing and heating rate over Bay of Bengal and Arabian Sea derived on the basis of optical, physical, and chemical properties. *J. Geophys. Res.* Atmos. (1984–2012) 115.
- Kim, G., Hussain, N., Church, T.M., 2000. Excess ^{210}Po in the coastal atmosphere. *Tellus B* 52, 74–80.
- Kim, J., Yoon, S.-C., Jefferson, A., Zaborowski, W., Kang, C.-H., 2005. Air mass characterization and source region analysis for the Gosan super-site, Korea, during the ACE-Asia 2001 field campaign. *Atmos. Environ.* 39, 6513–6523.
- Koçak, M., et al., 2004. Spatio-temporal aerosol trace metal concentrations and sources in the Levantine Basin of the Eastern Mediterranean. *Atmos. Environ.* 38 (14), 2133–2144.
- Kumar, A., Sudheer, A., Sarin, M., 2008. Chemical characteristics of aerosols in MABL of Bay of Bengal and Arabian Sea during spring inter-monsoon: a comparative study. *J. Earth Syst. Sci.* 117, 325–332.
- Lambert, G., LeCloarec, M.-F., Ardouin, B., Bonsang, B., 1991. Long-lived Radon daughters signature of Savanna fires. In: Levine, J.S. (Ed.), *Global Biomass Burning*. The MIT Press, London, pp. 181–184.
- Lee, J.-M., Boyle, E.A., Suci Nurhati, I., Pfeiffer, M., Meltzner, A.J., Suwargadi, B., 2014. Coral-based history of lead and lead isotopes of the surface Indian Ocean since the mid-20th century. *Earth Planet. Sci. Lett.* 398, 37–47.
- Liger, E., Duenas, C., Fernández, M.C., Cañete, S., Gordo, E., Pérez, M., 2014. Atmospheric Deposition Fluxes of Aluminium, Iron and Trace Metals in a Coastal Station on the NW-Alboran Sea (W-Mediterranean).
- Mackey, K.R., Buck, K.N., Casey, J.R., Cid, A., Lomas, M.W., Sohrin, Y., Paytan, A., 2012. Phytoplankton responses to atmospheric metal deposition in the coastal and open-ocean Sargasso Sea. *Front. Microbiol.* 3.
- Mahowald, N., 2011. Aerosol indirect effect on biogeochemical cycles and climate. *Science* 334, 794–796.
- Mahowald, N.M., Baker, A.R., Bergametti, G., Brooks, N., Duce, R.A., Jickells, T.D., Kubilay, N., Prospero, J.M., Tegen, I., 2005. Atmospheric global dust cycle and iron inputs to the ocean. *Glob. Biogeochem. Cycles* 19.
- McLennan, S.M., 2001. Relationships between the trace element composition of sedimentary rocks and upper continental crust. *Geochim. Geophys. Geosyst.* 2.
- McNeary, D., Baskaran, M., 2007. Residence times and temporal variations of ^{210}Po in aerosols and precipitation from southeastern Michigan, United States.

- J. Geophys. Res. Atmos. (1984–2012) 112.
- Nair, V.S., Moorthy, K.K., Alappattu, D.P., Kunhikrishnan, P., George, S., Nair, P.R., Babu, S.S., Abish, B., Satheesh, S., Tripathi, S.N., 2007. Wintertime aerosol characteristics over the Indo-Gangetic Plain (IGP): impacts of local boundary layer processes and long-range transport. *J. Geophys. Res. Atmos.* (1984–2012) 112.
- Nair, V.S., Moorthy, K.K., Babu, S.S., 2013. Influence of continental outflow and ocean biogeochemistry on the distribution of fine and ultrafine particles in the marine atmospheric boundary layer over Arabian Sea and Bay of Bengal. *J. Geophys. Res. Atmos.* 118, 7321–7331.
- Narvekar, J., Prasanna Kumar, S., 2006. Seasonal variability of the mixed layer in the central Bay of Bengal and associated changes in nutrients and chlorophyll. *Deep Sea Res. Part I Oceanogr. Res. Pap.* 53, 820–835.
- Nho, E.Y., Ardouin, B., Le Cloarec, M.F., Ramonet, M., 1996. Origins of 210Po in the atmosphere at lamto, ivory coast: biomass burning and saharan dusts. *Atmos. Environ.* 30, 3705–3714.
- Okuda, Tomoaki, et al., 2004. Daily concentrations of trace metals in aerosols in Beijing, China, determined by using inductively coupled plasma mass spectrometry equipped with laser ablation analysis, and source identification of aerosols. *Sci. Total Environ.* 330 (1), 145–158.
- Paytan, A., Mackey, K.R., Chen, Y., Lima, I.D., Doney, S.C., Mahowald, N., Labiosa, R., Post, A.F., 2009. Toxicity of atmospheric aerosols on marine phytoplankton. *Proc. Natl. Acad. Sci.* 106, 4601–4605.
- Ram, K., Sarin, M., Sudheer, A., Rengarajan, R., 2012. Carbonaceous and secondary inorganic aerosols during wintertime fog and haze over urban sites in the Indo-Gangetic Plain. *Aerosol Air Qual. Res.* 12, 359–370.
- Ram, K., Sarin, M.M., 2012. Atmospheric 210Pb, 210Po and 210Po/210Pb Activity Ratio in Urban Aerosols: Temporal Variability and Impact of Biomass Burning Emission. 2012 64.
- Rastogi, N., Sarin, M., 2013. Temporal variability in residence time of ambient aerosols using environmental 210 Pb. *Curr. Sci.* 105, 1.
- Reddy, M.S., Basha, S., Joshi, H., Jha, B., 2005. Evaluation of the emission characteristics of trace metals from coal and fuel oil fired power plants and their fate during combustion. *J. Hazard. Mater.* 123, 242–249.
- Rengarajan, R., Sarin, M., Sudheer, A., 2007. Carbonaceous and inorganic species in atmospheric aerosols during wintertime over urban and high-altitude sites in North India. *J. Geophys. Res. Atmos.* (1984–2012) 112.
- Sarin, M., Kumar, A., Srinivas, B., Sudheer, A., Rastogi, N., 2010. Anthropogenic sulphate aerosols and large Cl-deficit in marine atmospheric boundary layer of tropical Bay of Bengal. *J. Atmos. Chem.* 66, 1–10.
- Schroth, A.W., Crusius, J., Sholkovitz, E.R., Bostick, B.C., 2009. Iron solubility driven by speciation in dust sources to the ocean. *Nat. Geosci.* 2, 337–340.
- Schulz, M., Prospero, J.M., Baker, A.R., Dentener, F., Ickes, L., Liss, P.S., Mahowald, N.M., Nickovic, S., Garcia-Pando, C.P., Rodríguez, S., 2012. Atmospheric transport and deposition of mineral dust to the ocean: implications for research needs. *Environ. Sci. Technol.* 46, 10390–10404.
- Sholkovitz, E.R., Sedwick, P.N., Church, T.M., 2010. On the fractional solubility of copper in marine aerosols: toxicity of aeolian copper revisited. *Geophys. Res. Lett.* 37.
- Siefert, R.L., Johansen, A.M., Hoffmann, M.R., 1999. Chemical characterization of ambient aerosol collected during the southwest monsoon and intermonsoon seasons over the Arabian Sea: Labile-Fe (II) and other trace metals. *J. Geophys. Res. Atmos.* (1984–2012) 104, 3511–3526.
- Srinivas, B., Sarin, M., 2013a. Atmospheric deposition of N, P and Fe to the Northern Indian Ocean: Implications to C-and N-fixation. *Sci. Total Environ.* 456, 104–114.
- Srinivas, B., Sarin, M., 2013b. Atmospheric dry-deposition of mineral dust and anthropogenic trace metals to the Bay of Bengal. *J. Mar. Syst.* 126, 56–68.
- Srinivas, B., Sarin, M., Kumar, A., 2011. Impact of anthropogenic sources on aerosol iron solubility over the Bay of Bengal and the Arabian Sea. *Biogeochemistry* 110, 257–268.
- Srinivas, B., Sarin, M.M., 2014. PM_{2.5}, EC and OC in atmospheric outflow from the Indo-Gangetic Plain: temporal variability and aerosol organic carbon-to-organic mass conversion factor. *Sci. Total Environ.* 487, 196.
- Srinivas, B., Sarin, M.M., Rengarajan, R., 2014. Atmospheric transport of mineral dust from the Indo-Gangetic Plain: temporal variability, acid processing and iron solubility. *Geochem. Geophys. Geosyst.* <http://dx.doi.org/10.1002/2014GC1005>.
- Stohl, A., 1998. Computation, accuracy and applications of trajectories—A review and bibliography. *Atmos. Environ.* 32, 947–966.
- Sudheer, A.K., Rengarajan, R., 2012. Atmospheric mineral dust and trace metals over urban environment in western India during winter. *Aerosol Air Qual. Res.* 12, 923–933.
- Sushil, S., Batra, V.S., 2006. Analysis of fly ash heavy metal content and disposal in three thermal power plants in India. *Fuel* 85, 2676–2679.
- Tegen, I., Fung, I., 1994. Modeling of mineral dust in the atmosphere: sources, transport, and optical thickness. *J. Geophys. Res. Atmos.* (1984–2012) 99, 22897–22914.
- Turekian, K.Y., Nozaki, Y., Benninger, L.K., 1977. Geochemistry of atmospheric radon and radon products. *Annu. Rev. Earth Planet. Sci.* 5, 227.
- Vu, H.T.D., Sohrin, Y., 2013. Diverse stoichiometry of dissolved trace metals in the Indian Ocean. *Sci. Rep.* 3.
- Wang, F., Chen, D., Cheng, S., Li, J., Li, M., Ren, Z., 2010. Identification of regional atmospheric PM_{2.5} transport pathways using HYSPLIT, MM5-CMAQ and synoptic pressure pattern analysis. *Environ. Model. Softw.* 25, 927–934.
- Xu, W., Yan, W., Zhang, G., Li, J., Miao, L., Huang, W., 2014. Levels and distribution of heavy metals in atmospheric particulate matters over the northern South China Sea. *Environ. Sci. Pollut. Res.* 21, 8774–8781.